Approaches to Photoactivated Cytotoxins

A thesis submitted in partial fulfilment of the requirements for the degree of **Doctor of Philosophy in Chemistry** at the **University of Canterbury**

JANADARI KARIYAWASAM

Supervisor: **Assoc. Prof. Richard M. Hartshron**
University of Canterbury
Christchurch
New Zealand 8041.

2016

Acknowledgements

It gives me immense pleasure in expressing my gratitude to all the people without whom this thesis would not have been possible to accomplish. First and foremost, I would like to acknowledge my supervisor Associate Professor Richard Hartshorn for accepting me into his research group and for his incredible guidance, encouragement and advice over the past few years. Not only the insightful discussions, I immensely value all his suggestions, criticisms to improve my oral and written communication skills in a scientific community, which in turn made me a stronger and more confident person. I am grateful for his patience, support and abundance of ideas throughout the writing of this thesis. This is an honour and privilege to be a part of the Hartshorn group and I will carry the pride lifelong.

My sincere thanks go to my co-supervisor Dr. Jan Wikaira for her scientific advices and long discussions to improve scientific writing skills. Also I would like to extend my gratitude to Dr. Matthew Polson for generously sharing his time and expertise in X–ray crystallography and constructive suggestions offered throughout during the course of my research.

The academic and technical members of the Chemistry Department have been tremendously helpful and thanks to Dr. Marie Squire, Dr. Amelia Albrett for excellent assistance with NMR and mass spectrometry. I also thank all the technical staff, Wayne, Nick, Gill, Laurie, Rob and Danny, for many ways they contributed to this research.

I extend my thanks to Dr. Sally Gaw for her friendly and welcoming nature and for stopping by 832 offices to ask about my family and work. I'm always thankful to Prof. Peter J.Steel for sharing his chemistry knowledge. I'm grateful to Prof Richard Keene for all his support during my visit to Adelaide, Australia for RACI national congress.

Thanks to Nathan Wain from the Learning Skill Centre at the University of Canterbury for the formatting tips.

My special thanks to Dr. Susie Meade for her support and advice for receiving BIC unsupported fee funding and many thanks to Biological Science Department for offering me BIC financial support. I would also like to thank University of Canterbury Student

Association (UCSA) and University of Canterbury financial services for offering me some Dr. Mickles fund during financially difficult situations. Thank you very much Department of Chemistry, University of Canterbury for offering me departmental scholarship for 2015.

Travel grants from the Evans Fund and the New Zealand Institute of Chemistry (NZIC) for attending conferences were very much appreciated.

My special thanks go to the present and past members of the Hartshorn group especially Sally, Maria, Gurpreet and Fatemeh for their friendship and for all the good times we shared together. I would also like to extend my thanks to Fairbank group for their friendship, laughs and also letting me to use their laboratory facilities.

My special thanks to Davey Lim for reading countless pages of this thesis and constructive suggestions throughout the research.

Also my thanks go to Siji for being an amazing friend and her support for proof reading the thesis.

I would like to thank Mr. Nimal Kariyapperuma for his financial support to travel to New Zealand and to start my studies at University of Canterbury.

My deepest thanks go to my parents for their emotional and financial support. Thank you for encouraging me in many ways to come this far in education.

Finally and most importantly I would like to express my deepest thanks to my husband, Lakshman, my children Sonal and Susanne for their love, support and also for being patience with my busy schedule.

Contents

Abstract

Ruthenium(II)-cobalt(III) heterodinuclear systems are of interest as potential photoactivated cytotoxins.

This thesis describes synthetic approaches to the preparation of ruthenium(II)-cobalt(III) heterodinuclear prodrug systems.

The majority of work described in this thesis explores the coordination chemistry of amino alcohol ligands with cobalt(III), and use of the amino alcohol cobalt(III) complexes in safer synthetic approaches to nitrogen mustard complexes.

This thesis presents the successful synthesis and characterisation of twenty four complexes and twenty three X-ray crystal structures.

Twelve different cobalt(III) complexes of 2-((2-aminoethyl)amino)ethanol, **L1**, and its derivatives are presented in chapter 02, including ten that have been characterised by X-ray crystallographic methods. A reaction web has been developed for the interconversion of a number of these complexes.

Chapter 03 presents the successful synthesis of ten new cobalt(III) complexes with series of more complicated amino alcohol ligands, including some that also include zinc(II) or manganese(II). The utilisation of these amino alcohol complexes for the synthesis of potentially bis-alkylating cobalt(III) nitrogen mustard complexes is also discussed, and a total of sixteen X-ray crystallographic studies are presented in this chapter.

The synthesis and characterisation of new ruthenium complexes [Ru(4,4'-dmbpy)$_2$(pytp)]$^{2+}$ and [Ru(4,4'-decbpy)$_2$(pytp)]$^{2+}$ are presented in chapter 04, along

with NMR experiments that examine the synthesis of ruthenium(II)-cobalt(III) complexes.

The chemistry discovered in this project extends the coordination chemistry of these amino alcohol complexes and use of them as precursors for the synthesis of nitrogen mustard complexes with potential for use in photoactivated cytotoxins.

Abbreviations

BET	back electron transfer
bpy	2,2'-bipyridine
decbpy	4,4'-diethoxycarbonyl-2,2'-bipyridine
DMF	dimethylformamide
dmbpy	4,4'-dimethyl-2,2'-bipyridine
DNA	deoxyribonucleic acid
en	ethane-1,2-diamine
ESI-MS	electrospray ionisation mass spectrometry
EtOH	ethanol
gCOSY	gradient correlation spectroscopy
HMBC	heteronuclear multiple-bond correlation spectroscopy
HSQC	heteronuclear single-quantum correlation spectroscopy
HOTf	trifluoromethanesulfonic acid
ISC	Inter system crossing
LMCT	ligand- to- metal charge transfer
LUMO	lowest unoccupied molecular orbital
MeOH	methanol
MLCT	metal-to-ligand charge transfer
NOESY	nuclear overhauser spectroscopy
NMR	nuclear magnetic resonance
OTf	trifluoromethanesulfonate
phen	1,10-phenanthroline
pytp	(3-pyridine-2-yl)-[1,2,4]triazino[5,6-f][1,10]phenanthroline
THF	tetrahydrofuran

TMPS	sodium 3-(trimethylsilyl)-1-propane sulfonate
TOCSY	total correlated spectroscopy
tren	tris(2-aminoethyl)amine

Atom Colour Scheme

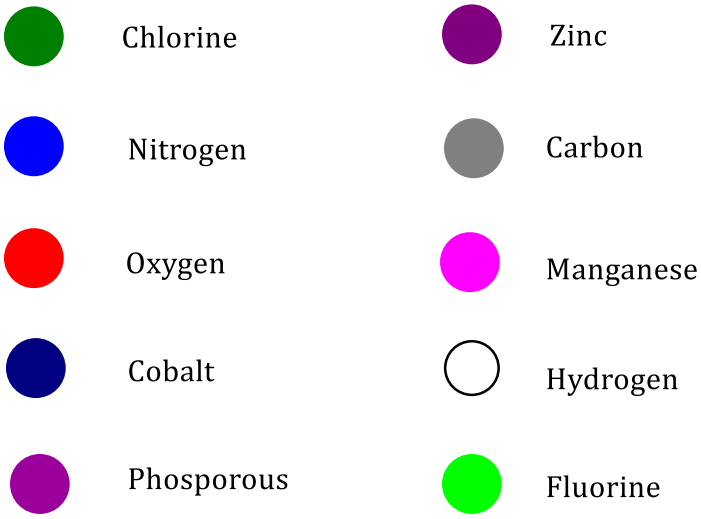

Chapter 01

Introduction

1. Introduction

Cancer is presently a major cause of mortality in developed countries and will become even more so in low-income countries as the global population increases.[1] Although some cancers occur in the young, most are associated with the elderly.[2]

The global burden of cancer continues to increase largely because of the ageing and growth of the world population, alongside an increasing adoption of cancer causing behaviours, particularly smoking in economically developing countries. Based on the GLOBOCAN 2008,[3] about 12.7 million cancer cases and 7.6 million cancer deaths are estimated to have occurred in 2008, of these 56% of the cases and 64% of the deaths occurred in the economically developing countries. Breast cancer is the most frequently diagnosed cancer and the leading cause of cancer death among females, accounting for 23% of the total cancer cases and 14% of the cancer deaths. Lung cancer is the leading cancer site in males, comprising 17% of the total new cancer cases and 23% of the total cancer deaths. According the Ministry of Health, New Zealand reports published in 2016, statistics shows cancer registration rate of 335.7 per 100,000 populations in NZ.[4]

1.1 The beginnings of chemotherapy

This thesis will explore chemistry that may prove useful in the development and synthesis of new anti-cancer drugs. The next sections of this introduction will therefore describe approaches that have been taken in chemotherapy and provide a context for the work that was undertaken in this project.

During a military operation in World War II, some soldiers were accidentally exposed to mustard gas.[5] They were later found to have very low white blood cell counts. While

white blood cells usually regenerate very quickly, cancer cells also divide and grow very quickly. The doctors wondered whether the effect of mustard gas, slowing down the rapid growth of white blood cells, may have the same effect on cancer cell growth.[6] Doctors tried treating patients with advanced lymphomas by injecting them with bis(2-chloroethyl)sulfide, the active chemical compound in "mustard gas". Even though the effect was temporary, the patients did experience a remarkable improvement in their health.[7]

Development of the nitrogen mustard, *N,N*-bis(2-chloroethyl)ethylamine, led research into other nitrogen mustard derivatives such as mustine, *N,N*-bis(2-chloroethyl)-methylamine, that might slow down or stop the division and growth of cancer cells.

It would be another decade before it was discovered that *N,N*-bis(2-chloroethyl)-methylamine works by attaching to the DNA of the cancer cell in a way that prevents the DNA from functioning, leading to cell death.

These findings influenced the researchers to investigate new chemotherapeutic drugs as well as to improve existing drugs. There are more than 100 different types of chemotherapy drugs today which are used to treat many different cancers.

1.1.1 How chemotherapy works

When our cells are damaged or dead, we rapidly produce new ones to replace them. Cell regeneration in our bodies is a meticulously controlled process. Cancer cells have lost the ability to control this regeneration; their reproduction (division and growth) is out of control. This leads to uncontrolled growth of cells and they start to occupy more and more space, until eventually they invade the sites of useful cells. This eventually leads to destruction of normal functional properties of relevant tissues and organs.

Most chemotherapeutic drugs (anti-proliferating drugs) interfere with a cancer cell's ability to divide and reproduce. Chemotherapeutic drugs may be administered into the bloodstream to attack cancer cells throughout the body, or they can be delivered directly to specific cancer sites.

Most chemotherapeutic (anti proliferating) drugs cause cell death by interrupting many cell cycle processes.

Some drugs are less damaging, to the point where the cell is too damaged to divide, but not so damaged that it will die. These drugs are known as cytostatic chemotherapeutic drugs, and examples are tamoxifen or hormone treatments. The effect of these drugs is to stop the growth and spread of the cancer, without necessarily shrinking the cancer.[8]

1.2 Mechanisms of chemotherapeutic agents

One interesting class of chemotherapeutic agents used in cancer therapy is comprised of molecules that interact with DNA. Research in this area has revealed a range of molecules that act as antitumor agents, including groove binders, alkylating agents, and intercalating compounds.[9] The mechanistic features of each drug category are related to their chemical nature or activity. The chemical nature of some of the anticancer drugs in relation to their cytotoxic activity is discussed below.

1.2.1 DNA intercalators as cytotoxic agents

DNA intercalators are flat molecules that insert between planar bases of DNA, without forming covalent bonds. This DNA binding mode was first proposed by Lerman.[10] The only recognized forces that maintain the stability of the DNA intercalated complexes are

Van der Waals, hydrogen bonding, hydrophobic, and/or charge transfer forces[11], [12], [13], [14] however, a frontier orbital interaction has also been suggested.[15]

Intercalation has the effect of lengthening the duplex by around 3 Å per bound drug molecule, causes unwinding of DNA. The degree of unwinding depends on the structure of the intercalating molecule and the site of intercalation.[16] This distortion can prevent replication and transcription by interfering with the action of topoisomerases. Topoisomerase I and II are enzymes that control the changes in DNA structure by catalysing the breaking and re-joining of the phosphodiester backbone of DNA strands during the normal cell cycle.[17], [18]

The stable complex is formed, due to π stacking of flat components of the intercalated drug and the DNA, Figure 1.1 to Figure 1.4. Ellipticine, **1.01**, shown in Figure **1.1**, consists of a planar heterocyclic ring system that intercalates between the base pairs of helical nucleic acids as a possible mode of action.[19] Ellipticine has been observed to interact with DNA and to increase its melting temperature through intercalation. These intercalator drugs interrupt the cell cycle. Therefore intercalators are often more toxic to cancer cells and other rapidly proliferating cells than to normal cells.

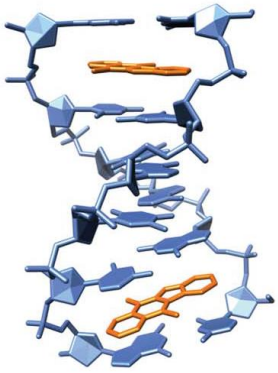

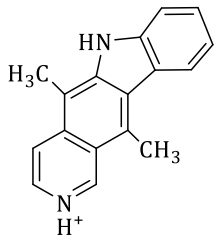

1.01

Figure 1.1. *X-ray crystal structure showing the binding of ellipticine,* ***1.01****, to a DNA oligomer, by intercalation.*[20], [21]

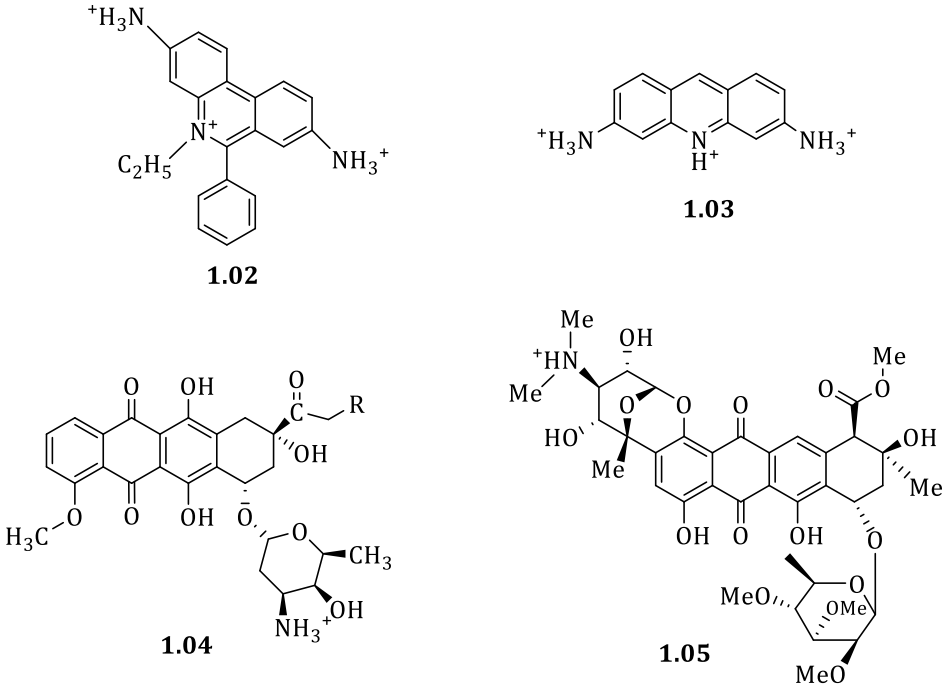

Figure 1.2. *Representative DNA intercalators[22], **1.02**, ethidium, **1.03**, proflavin, **1.04**, R=H; daunomycin, R= OH; adriamycin, **1.05** nogalamycin.*

The compounds shown in Figure 1.2 are some of the organic intercalators. Many DNA intercalating transition metal complexes are also reported in literature, such as those from Barton's group.[23] Some octahedral metallointercalators and metalloinserters shown in Figure 1.3 and Figure 1.4.

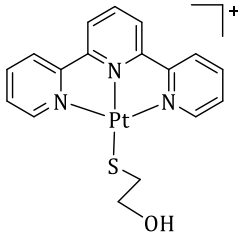

$[Pt(terpy)(HET)]^{+}$

1.06

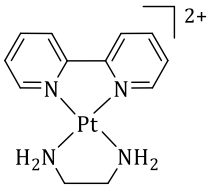

$[Pt(bipy)(en)]^{2+}$

1.07

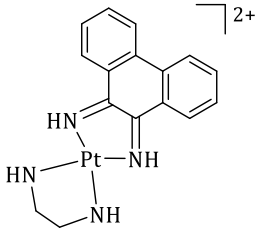

$[Pt(phi)(en)]^{2+}$

1.08

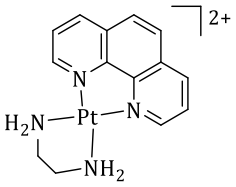

$[Pt(phen)(en)]^{2+}$

1.09

Figure 1.3. *Platinum metallo-intercalators; terpy = 2,2',6',2''-terpyridine; phen = 1,10-phenanthroline; bpy = 2,2'-bipyridine; phi = 9,10-diaminophenanthrene; HET= 2-hydroxyethanethiolate.*

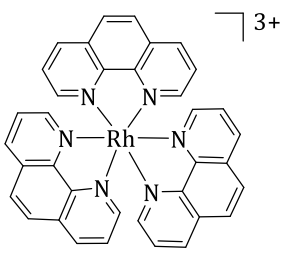

$[Rh(phen)_3]^{3+}$

1.10

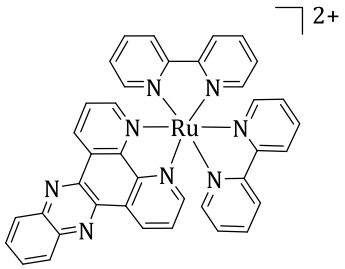

$[Ru(bpy)_2(dppz)]^{2+}$

1.11

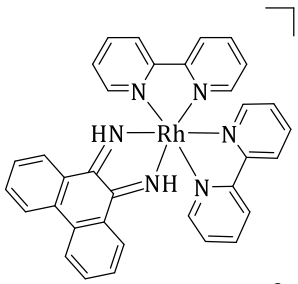

$[Rh(bpy)_2(phi)]^{3+}$

1.12

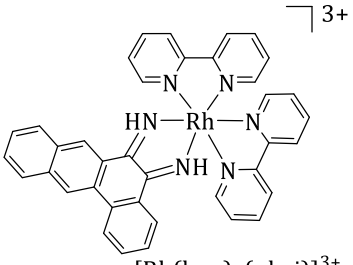

$[Rh(bpy)_2(phzi)]^{3+}$

1.13

Figure 1.4. Octahedral metallointercalators containing planar aromatic ligands: phen, phi, dppz, phzi. dppz = dipyrido[3,2-a:2,3-c]phenazine, phzi = benzo[a]phenazine-5,6-quinonediimine.

Metallointercalators are composed of a metal component and the coordinated flat aromatic ligands as shown in Figure 1.3 and Figure 1.4. The flat aromatic component can intercalate between the nitrogen bases of DNA and lead to cell death.[24], [25], [26], [27]

The Pt(II) complexes containing heterocyclic aromatic ligands, shown in Figure 1.3, binds to DNA duplexes non-covalently, intercalating between the base pairs.[16]

1.2.2 DNA major and minor groove binders

In a detailed analysis of DNA structure, there are two types of grooves that can be seen; the major groove has the nitrogen and oxygen atoms of the base pairs pointing inward toward the helical axis, whereas in the minor groove, the nitrogen and oxygen atoms point outwards as shown in Figure 1.5.

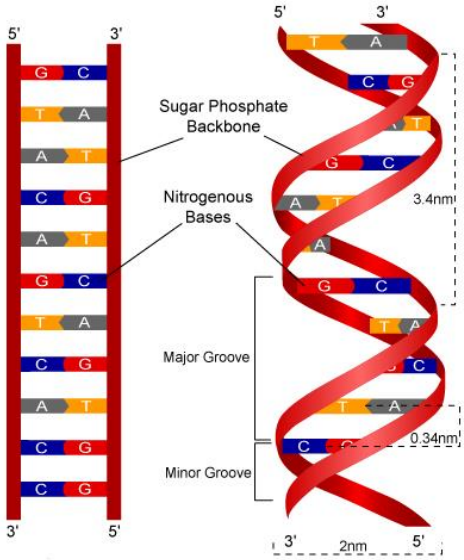

Figure 1.5. *Base pairing of major and minor groove of DNA double helix.*

Minor groove binders of DNA constitute an important class of derivatives in anticancer therapy. These compounds form hydrogen bonds and non-covalent interactions, with DNA[28] through electrostatic and hydrogen bonding interactions, Figure 1.6.[29]

Acetylaminofluorine, **1.14**, is one of the examples for minor grove binders as shown in Figure 1.6. These ligands generally consist of arc shaped, planar and unfused aromatic hydrocarbons with a positive electrostatic potential that attracts them to the negative potential of the minor groove, with the arc matching the curvature of the DNA double helix. The N2 amino group of guanine generally blocks binding of these drugs by steric hindrance but also by widening the minor groove. For these reasons, most minor groove binding drugs are AT-specific.[30]

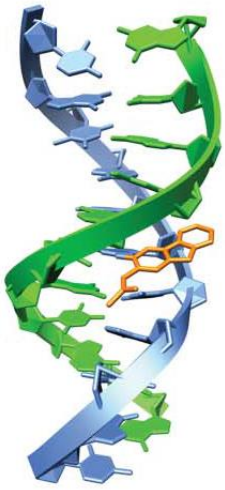

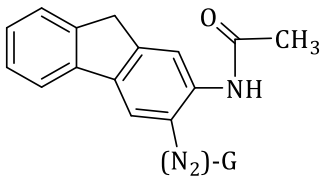

1.14

Figure 1.6. *Acetylaminofluorine , **1.14**, is one of the minor groove binders.[20]*

Hydrogen bonds and Van der Waals contacts are important forces for the interaction of distamycin, netropsin and tallimustin with DNA. These compounds consist of characteristic oligopeptide-pyrrole-carbamoyl frameworks, Figure 1.7. The compounds shown in Figure 1.7 demonstrate a strong preference for adenine-thymine (AT)-rich sequences; containing at least four AT base pairs in the DNA double helix.[31]

Among the minor groove binders shown in Figure 1.7, Tallimustin, **1.17**, is structurally different by having a nitrogen mustard component at one end of the molecule. This

nitrogen mustard component has potential DNA alkylating properties. More detail about DNA alkylating nitrogen mustards can be found in section 1.2.3.1.

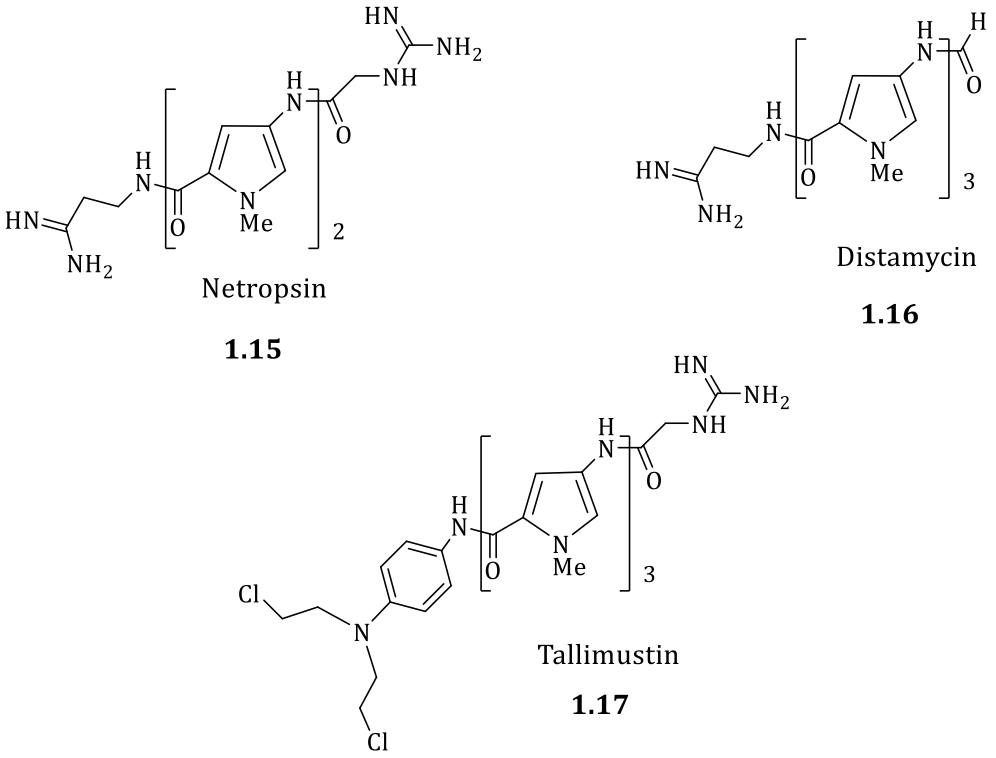

Figure 1.7. *Examples of minor groove binders.*[31]

There are cytotoxic compounds that act as major groove alkylators such as Nitrosourea.[32] But to date, there is no solid evidence about drugs which target direct major-groove binding.[30]

1.2.3 DNA alkylating agents

Alkylating agents comprise a major class of therapeutics used in the treatment of different types of cancers.[33] Alkylating agents are highly reactive molecules that react with nitrogen bases of DNA and ultimately cause cell death.[34] The unwinding of the DNA double helix during the cell cycle facilitates easy access of DNA alkylating agents

and therefore their reaction with DNA base pairs. This means that cells that divide rapidly, such as cancer cells, are more likely to be affected. Unfortunately, due to the nonspecific nature of these DNA alkylating agents, severe side effects can arise where rapid cell division take place under normal conditions (e.g. in hair follicles and the stomach lining).[35]

In oncology, the term alkylating agent refers to any antineoplastic compound that irreversibly binds to a variety of susceptible biomolecules such as nucleic acids, proteins, amino acids, and nucleotides. This covalent interaction mediates cell death through interference with DNA structure and function, inactivation of DNA repair enzymes, or cell membrane damage.

DNA alkylating agents can be mono-functional or bi-functional. Mono-functional agents make adducts with target molecules, while bi-functional agents can form cross-links (inter-or intra-strand), Figure 1.8, in DNA or between DNA and proteins.[36], [37]

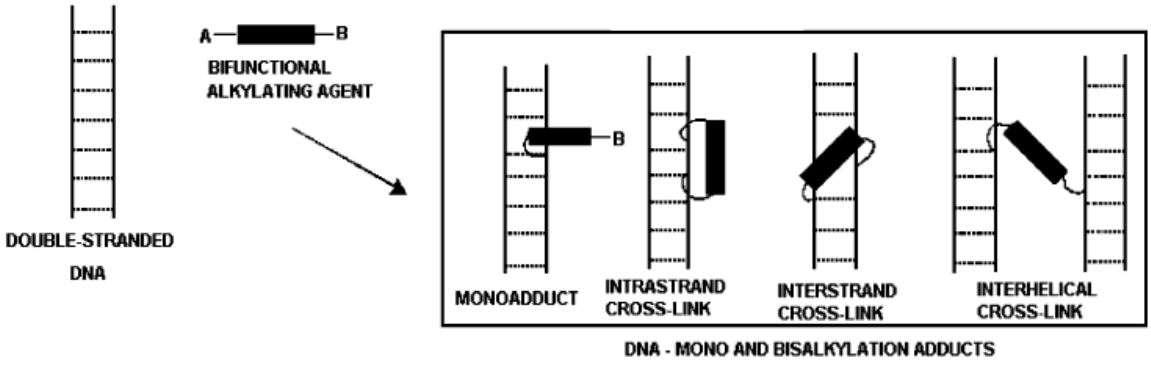

Figure 1.8. *Schematic representation of DNA alkylation by mono- or bi-functional alkylating agents.*[33], [36]

There are preferential sites of alkylation in DNA depending on the nature of the nucleophile and of the alkylating agent.[38], [39], [40] The most frequent sites of base alkylation in DNA are the guanine N7 and O6 positions, adenine N1 and cytosine N3.[39],

[41], [42] Alkylation on other sites such as adenine N6, N7, thymine O2, N3, O4, or cytosine O2 have also been observed, but to a lesser extent, Figure 1.9.[43]

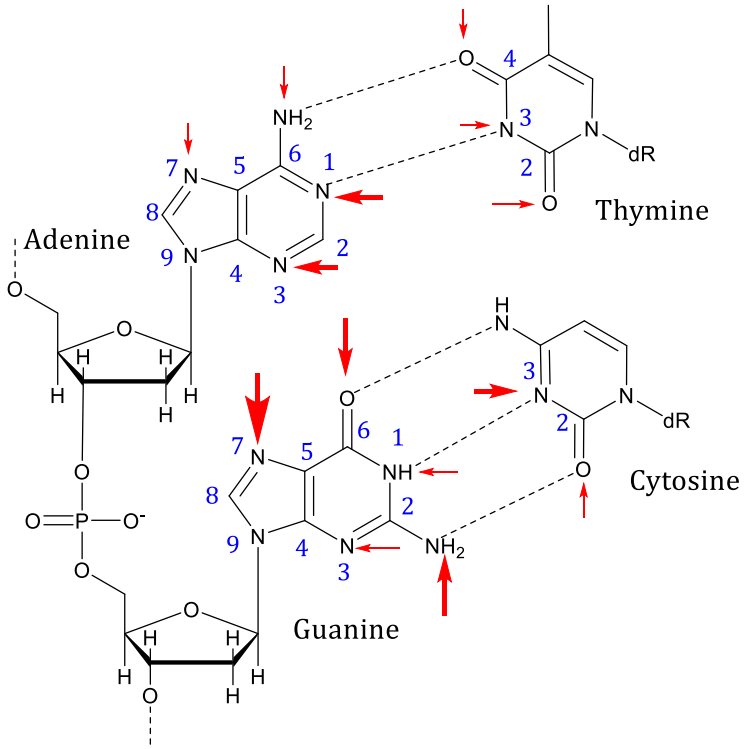

Figure 1.9. *Different sites of base alkylation are shown in red arrows. The size of arrow is roughly proportional to the frequncy of alkylation.*[33]

The alkylation on guanine O6, N1, N2 and thymine O6, N1, N2 or O4 results in stable DNA adducts.[44] Alkylation on other positions leads to chemically unstable adducts that are converted to do DNA damage by opening of the base ring.[40], [44] That is especially the case for the most common base alkylation at guanine N7 position which is readily converted into a 5-alkyl formamidopyrimidine (fapy) by opening of the imidazole ring, Figure 1.10.[45] Similar observations have been reported for adenine N3 alkylation, leading to an abasic site formation.

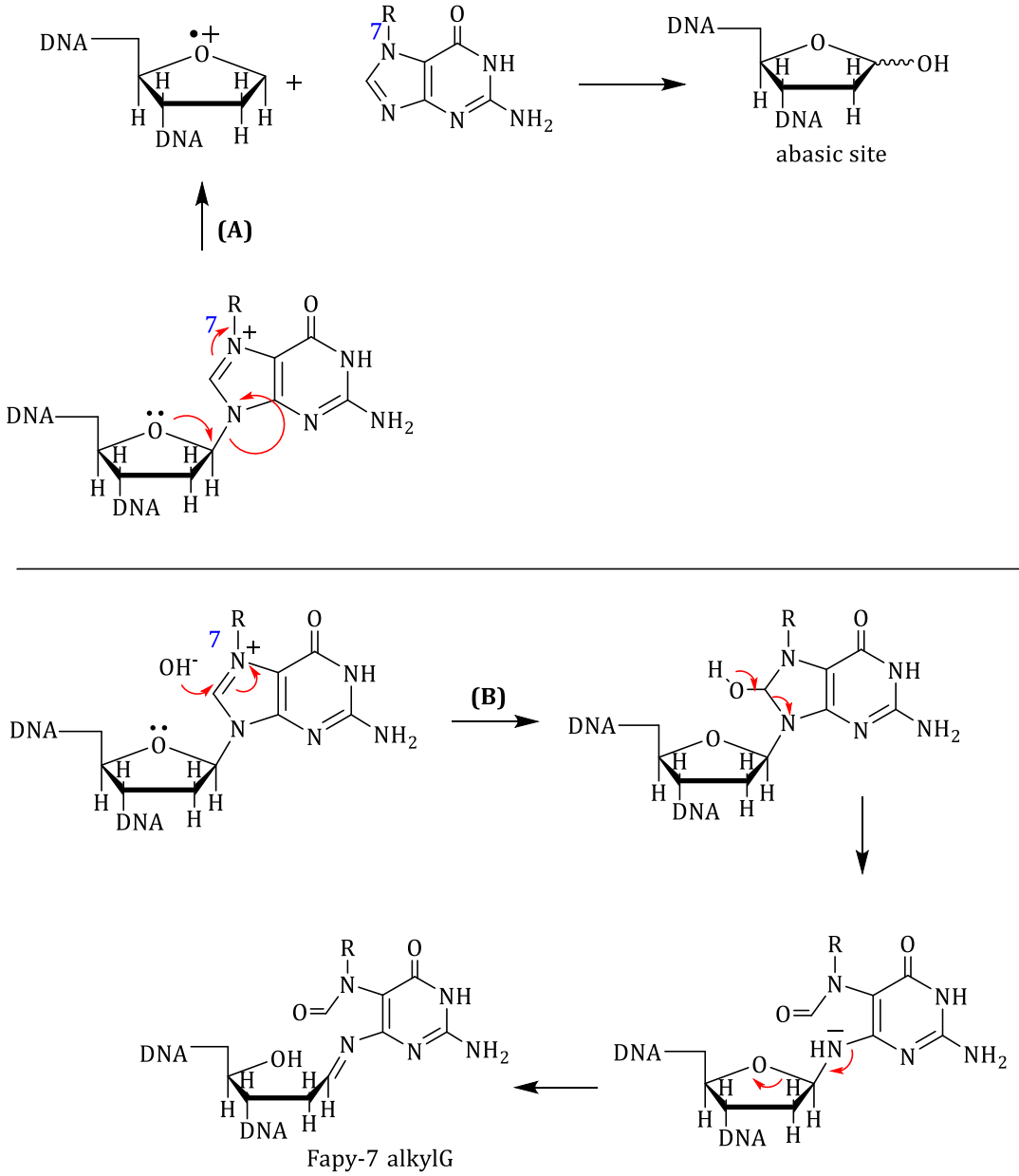

Figure 1.10. *Mechanisms of conversion of N7 alkylated guanine into a cytotoxic DNA lesion.*

(A) Conversion of an abasic site following depurination. This is initiated by the π electron delocalization of N7-C8 double – bond of the imidazole ring (red arrows).

(B) Conversion into 2,6-diamino-4-hydroxy-5N alkyl formamidopyrimidine (Fapy-7alkylG) by hydrolysis of the imidazole ring in basic conditions as an example.

Puyo *et al.*[33] reported seven classes of alkylating agents. The chemical structures of the corresponding compounds are shown below, Figure 1.11.

A Nitrogen mustards

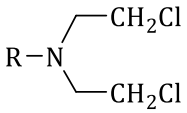

1.18

B Oxazaphosphorines

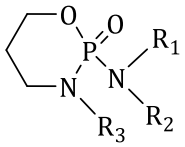

1.19

C Ethylene imines

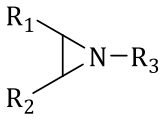

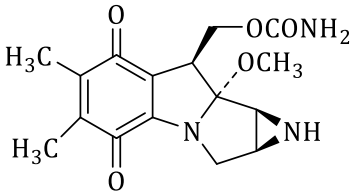

Mitomycin C

1.20

D Nitrosoureas

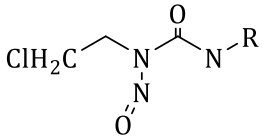

1.21

E Alkyl alkane sulfonates

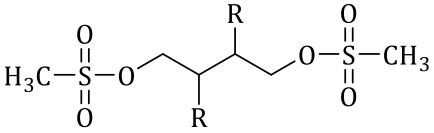

1.22

F Triazenes and hydrazines

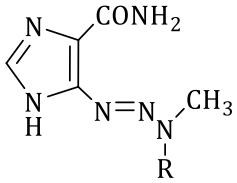

1.23

G Platinum compounds

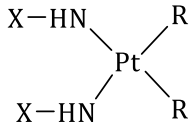

1.24

Figure 1.11. *Seven classes of alkylating agents.*

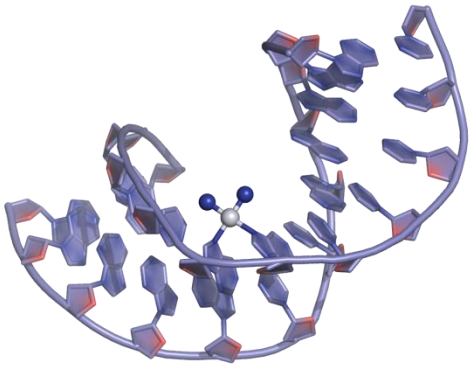

1.25

Figure 1.12. *Intrastrand DNA cross linking cisplatin,* ***1.25****.*

The traditional alkylators such as the nitrogen mustards react with nucleophilic sites in DNA (usually the guanine N7 and O6 positions) through one or more electron-deficient alkyl groups. Both cisplatin, Figure 1.12, and carboplatin, act in a similar way, as they both bind directly through the platinum atom, most commonly to guanine bases. The loss of both the chloride ligands of cisplatin leads to the formation of intra-strand cross-links causing unwinding of the helix, Figure 1.12, preventing transcription, and leading to cell death.

1.2.3.1 Nitrogen mustards as DNA alkylating agents

Mustin, discovered by Gilman and Goodman in 1946, is the first alkylating agent for showing remarkable chemotherapeutic activity in the treatment of lymphomas. Mustin, **1.26** was the first alkylating agent to obtain FDA approval in 1949.[33]

Nitrogen mustards represent the earliest, and perhaps the most extensively studied DNA interstrand cross-linking agents, in Figure 1.13. Mustin **1.26** and chlorambucil **1.27** are two of the most heavily employed clinical anticancer drugs today, along with a number of other mustard based structures.[37, 46]

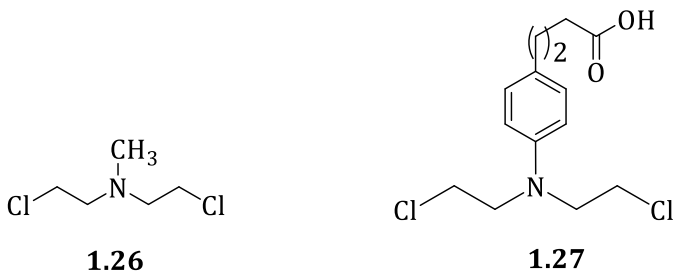

Figure 1.13. *Two clinically important DNA cross-linking nitrogen mustards.*

Mechanism of Action

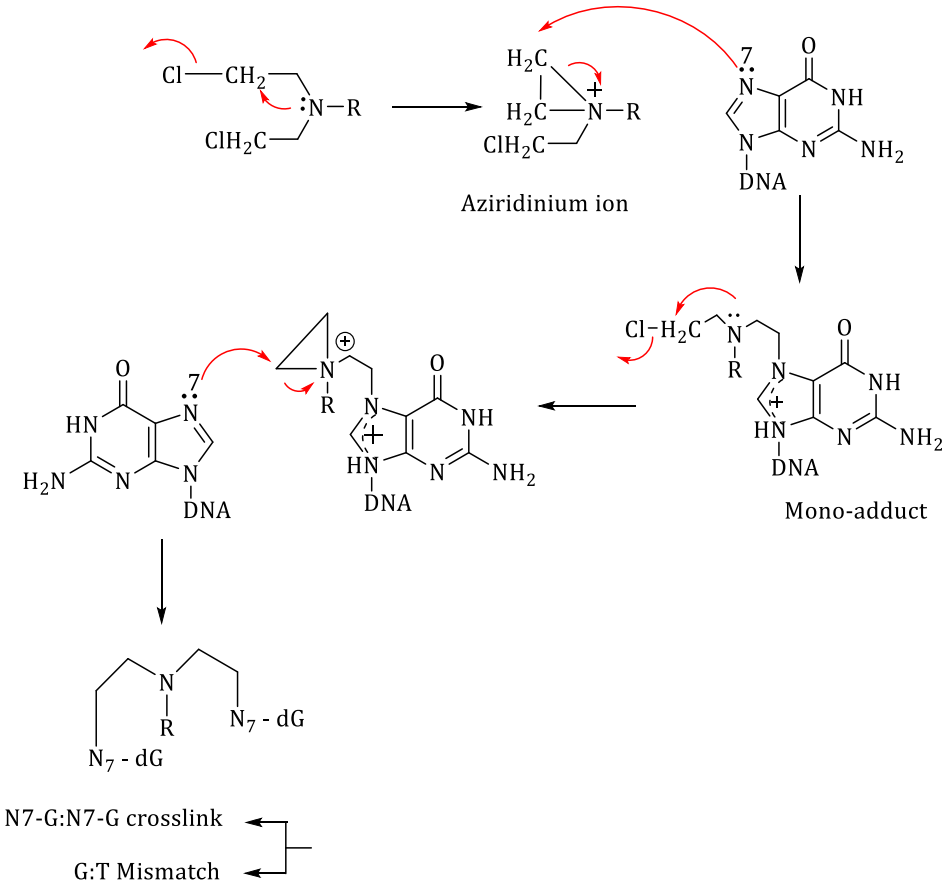

Figure 1.14. *A mechanism for the alkylation of guanine N7 via production of a reactive aziridinium ion. The mono-alkylation product can lead to Alkyl-N7G:T base mispairing or can be the target of a second alkylation leading to N7G-N7G inter-strand cross-links. The chemical structures of R groups are shown below.*

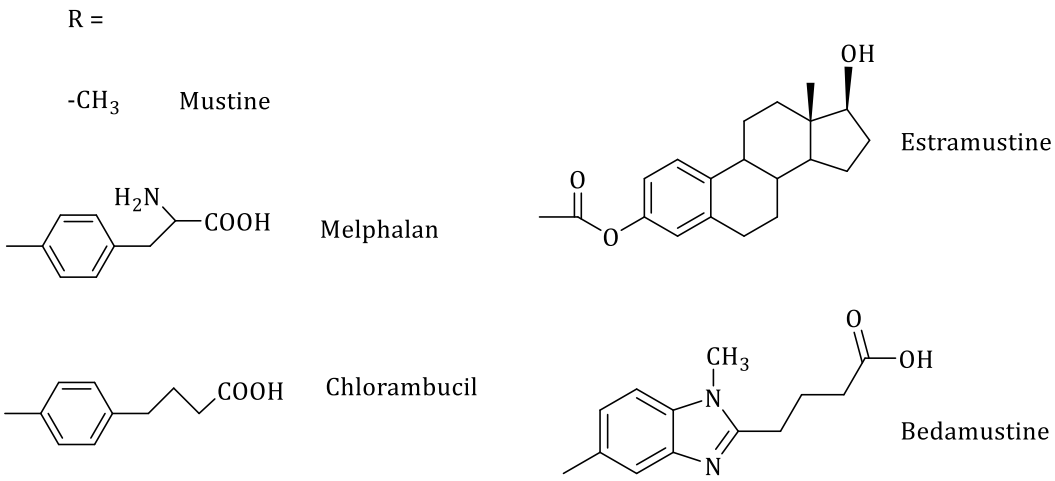

The Figure 1.14 shows the mechanism for the alkylation of DNA by nitrogen mustard compounds. Most nitrogen mustard compounds share a common *N,N*-bis(2-chloroethyl)amino motif that leads to the formation of an aziridinium ion, the electrophilic entity responsible for the establishment of the covalent link with the nucleophilic centre of the base, mainly the guanine N7 and O6 positions.[47] The resulting products of monoalkylation can lead to base mispairing that is potentially mutagenic. Povirk *et al.*[48] reported a wide array of mutations as a result of monoalkylation, including base substitution at both G-C and A-T base pairs.

The DNA cross linking nitrogen mustard compounds show a high degree of cytotoxicity due to their ability to induce DNA interstrand cross links, thereby inhibiting replication.[37], [39]

1.3 Side effects of chemotherapeutic agents

A principal downside of chemotherapeutic drugs is the non-specificity for cancerous cells. When developing novel chemotherapeutic agents a delicate balance between poisoning as many cancer cells as possible while sparing healthy cells is a key factor. The side effects of such chemotherapies also mean that there is a limitation to the number of times, and/or the length of time a treatment can be administered.
It is highly likely that chemotherapy with such anticancer drugs can effectively destroy most cancer cells in the body if sufficiently high doses can be administered for enough time; however this comes at the cost of near total destruction of the body.
Therefore science has been faced with a challenge to find anticancer drugs that are more selective, which minimise their harmful side effects, making these chemotherapeutic drugs more tolerable for the patient.

1.4 Targeted therapies and anticancer drug design

Prodrugs systems are one of the popular treatments to achieve selective activity of the cancer drugs. Prodrugs undergo chemical conversions by metabolic processes to release active drug.

As researchers learn more about other chemical or biochemical markers of cancer cells that cause cancer, they have been able to develop drugs that target these changes, a treatment often called targeted therapy. The targeted therapy drugs are often able to attack cancer cells while doing less damage to normal cells, by exploiting the natural mechanisms of cancer cell activity; the programming that sets them apart from normal,

healthy cells. These drugs tend to have different (and often less severe) side effects than those of standard chemotherapeutic drugs.

Hypoxia selective drugs and photoactivated cytotoxins can be categorised as targeted therapies and are relevant background for this research. The work described in this thesis is mainly about the synthesis of cytotoxic nitrogen mustard compounds attached to the cobalt(III) inert metal centre and attempts to use these cobalt(III) nitrogen mustard compounds in the synthesis of heterodinuclear complexes that may exhibit photoactivated cytotoxicity

1.4.1 Hypoxia selective cytotoxins; classification and mechanism of activation

Tumour hypoxia is the situation where tumour cells have been deprived of oxygen. As a tumour grows, it rapidly outgrows its blood supply, leaving portions of the tumour with regions where the oxygen concentration is significantly lower than in healthy tissues, Figure 1.15. Hypoxic microenvironments in solid tumours are the result of available oxygen being consumed within 70 to 150 μm of tumour vasculature by rapidly proliferating tumour cells, thus limiting the amount of oxygen available to diffuse further into the tumour tissue.[49], [50], [51], [52]

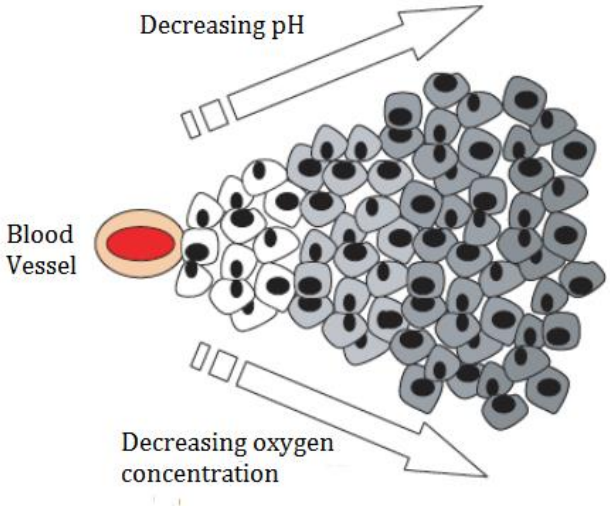

Figure 1.15. *Development of hypoxic region when cells get pushed away from blood vessels.*[53]

The first drug in the hypoxia selective category to enter clinical testing is tirapazamine, **1.28** shown in Figure 1.16.[51],[54] Further information on tumour hypoxia can be found in the review article published by Hockel *et al*.[55]

Treatment of cancer through hypoxia selective prodrugs is an important therapeutic target. This exploits major differences between tumoral and normal tissues. A drug active only to hypoxic cells would be selectively toxic to tumour cells in hypoxic regions.[56], [57] Also, within the tumour, it is the hypoxic cells that develop resistance to standard therapy, due to lack of blood and oxygen supply and therefore by targeting these hypoxic cells, reduce the development of resistance to standard therapy of the tumour as a whole.[51]

Tirapazamine (TPZ) is an excellent substrate for various intracellular reductase enzymes which deliver a single electron to the molecule, thereby producing a free radical intermediate. In the presence of oxygen, this free radical is rapidly oxidised back to the parent molecule with the formation of a superoxide radical. However, in regions

of reduced oxygen concentration, as in the situation with hypoxic cells, this does not occur. Instead, the highly reactive TPZ radical, Figure 1.16, will remove a hydrogen atom from nearby macromolecules, resulting in structural damage. If this nearby molecule is DNA, then the TPZ radical produces both single and double strand breaks leading to cell death.[58]

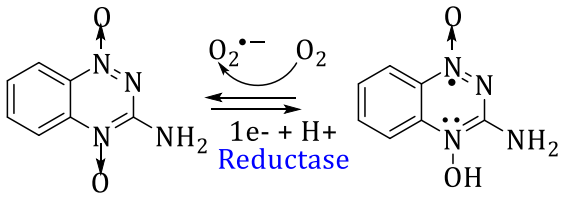

TPZ **1.28** TPZ radical **1.29**

Figure 1.16. *The metabolism of tirapazamine (TPZ) to its free-radical moiety causing preferential toxicity to hypoxic cells by damaging the DNA double helix.*[59], [60], [61]

The bis-*N*-oxide banoxanthrone (AQ4N), shown in Figure 1.17, is another bio-reductive drug which was developed as an analogue of mitoxantrone, Figure 1.18. Similar to other bio-reductive compounds, AQ4N is reductively activated, in this case to AQ4. The reduction product, AQ4, has a high DNA affinity constant which stabilizes the DNA double helix as measured by a large increase in DNA melting temperature.

AQ4N is the only bio-reductive drug entered in to clinical trials. AQ4N targets the topoisomerase which is crucial to cell division.[62]

When AQ4N was tested, in oxic conditions, of 60 tumour cell lines little or no cytotoxicity was observed (IC50 >100 μM).[62] Furthermore, the drug has been shown to have greater toxicity when applied in combination with other chemotherapeutics, and

is, to date, the most promising compound for treatment of hypoxia induced chemo-resistance.[63]

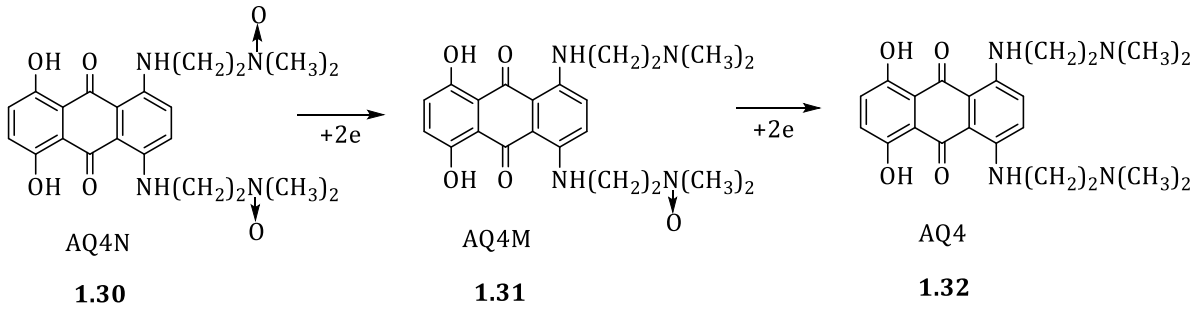

Figure 1.17. *Reductive activation of AQ4N to AQ4.*

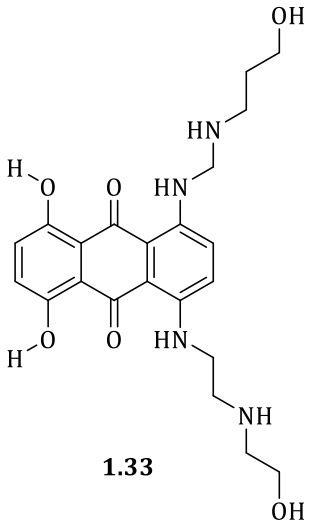

Figure 1.18. *Chemical structure of Mitoxantrone.*

1.4.1.1 Cobalt(III) complexes as hypoxia selective anti-cancer compounds

This concept is based on less toxic compounds which release the corresponding active drug under hypoxic conditions in cancerous tissues.[64] For prodrug activation several cancer targeting mechanisms have been reported, one of which is activation by reduction in the inherently hypoxic tissue found in most solid tumours.[65]

Cobalt(III) compounds have been explored as such bio-reducible prodrugs due to the significant difference in the ligand lability of the two oxidation states.[65], [66] While octahedral d^6 low-spin cobalt(III) complexes are kinetically inert, labile d^7 high-spin cobalt(II)complexes are formed after reduction. In the presence of oxygen, this would immediately lead to re-oxidation; cobalt(II) complexes easily undergo ligand substitution reactions, enabling the release of biologically active ligands.[67] This concept has already been used as a trigger for release of several cytotoxic compounds, such as nitrogen mustards[66] and DNA minor groove alkylator[68] by complexing them to cobalt(III) metal centres.

Karnthaler-Benbakka *et al.*[69] reported the synthesis of a novel epidermal growth factor receptor (EGFR) inhibitor that is specifically activated in malignant tissues. This prodrug strategy is based on the assumption that the intact complexes would be too bulky and, therefore prevent binding of the inhibitor to the ATP binding pocket of the EGFR molecule, Figure 1.19. This enables the selective activation of the drug only after reduction and release in the hypoxic tumour tissue, resulting in reduced systemic toxicity.[69]

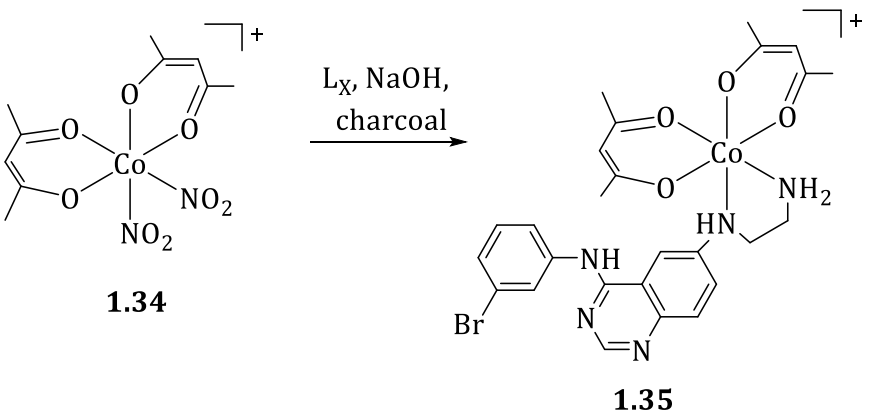

Figure 1.19. *Synthesis of cobalt(III) complex containing quinazoline derivative, shows selective release of ligand under hypoxic conditions.*

Activation of the prodrug, **1.35**, was studied using fluorescence spectroscopy. Karntheler-Benbakka *et al.*[69] reported that the fluorescence was diminished in treated cells with the complex **1.35** under normoxic conditions, suggesting an intact cobalt(III) complex. Under hypoxic conditions, a strong increase of fluorescence was observed in treated cells indicating activation of the prodrug with subsequent ligand release.

Cobalt(III) complexes containing 8-hydroxyquinoline (8-HQ) **1.36**, Figure 1.20 and cyclen based auxiliary ligands were also reported in the literature.[69] Ahn *et al.*[68] synthesised $[Co(III)(cyclen)(azaCBI)]^{2+}$, **1.37**, Figure 1.21 to demonstrate selective release of azaCBI, (1-(chloromethyl)-3-[(5,6,7-pyrolo[3,2-f]quinolin-5-ol), under hypoxic conditions.

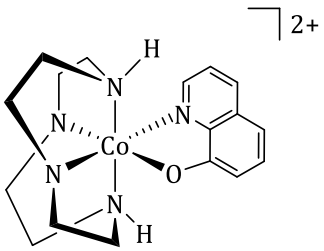

Co(III)(cyclen)(8-HQ)

1.36

Figure 1.20. *Chemical structure of Co(III)(cyclen)(8HQ).*

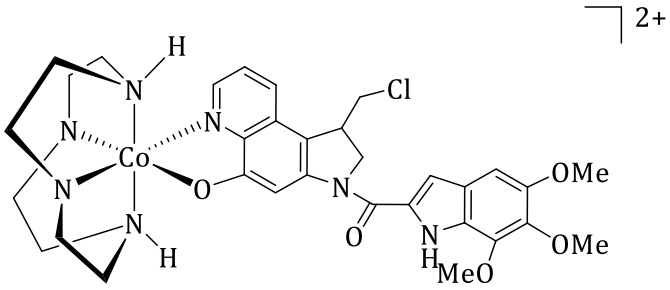

Co(III)(cyclen)(azaCBI)

1.37

Figure 1.21. *Chemical structure of* $[Co(III)(cyclen)(azaCBI.)]^{2+}$

Ahn *et al* studied complex **1.37** to show the release of highly potent azaCBI cytotoxin, by both radiolytic and non-radiolytic pathways under hypoxic conditions.

Investigation of complexes **1.38** and **1.39**, Figure 1.22 was reported by Lu *et al.*[70] The bridging variation is highlighted in red.

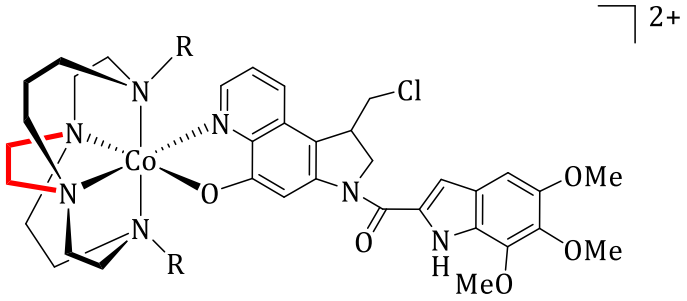

R = H; **1.38**

R = Me; **1.39**

Figure 1.22. *Complex containing N bridged cyclam ligand.*

Synthesis and hypoxia activity of similar cyclam cobalt(III) complexes were also reported by Chang *et al*.[71], [72]

1.4.1.2 Hypoxia selective cobalt(III) complexes with a cytotoxic nitrogen mustard ligand

Nitrogen mustards are well known for their DNA alkylating ability and non-specific toxicity in their active form. One of the strategies to target their cytotoxicity is by using a hypoxia activated cobalt(III) inert metal centre. This is achieved by complexing the nitrogen mustard to the cobalt(III) metal centre.[73]

Coordination of the nitrogen lone pair of the nitrogen mustard to cobalt(III) should supress its toxicity since the electron pair is no longer available to activate the nitrogen mustard by making the highly strained aziridinium ion, Figure 1.14. Such cobalt(III)

complexes are kinetically inert. The nitrogen mustard ligand can then be released following reduction of the cobalt(III) metal centre to a labile cobalt(II) state. The cytotoxic nitrogen mustard will presumably be released by rapid ligand exchange with surrounding water molecules.[74] The activation can be largely confined to regions of hypoxia, hence providing tumour selectivity.[75]

A range of cobalt(III) complexes of nitrogen mustard ligands have been synthesised and investigated for their cytotoxic activity.

Ware *et al.* with his co-workers reported the synthesis and characterisation of range of different cobalt(III) complexes containing nitrogen mustard ligands. Most of the complexes studied by Ware *et al.*, contain *N,N*-bis(2-chloroethyl)ethane-1,2-diamine (DCE), **1.40** or *N,N'*-bis(2-chloroethyl)ethane-1,2-diamine (BCE), **1.41** nitrogen mustard ligands, Figure 1.23.[74]

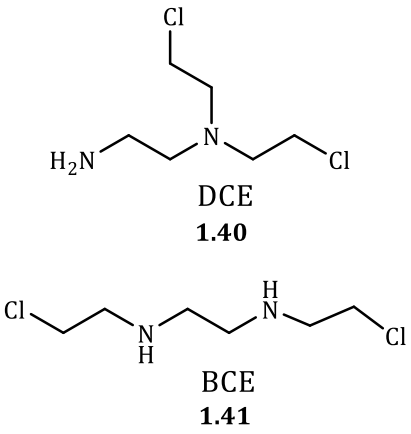

Figure 1.23. *Chemical structure of DCE and BCE nitrogen mustards.*

The other auxiliary ligands around the cobalt(III) centre were modified during different synthetic approaches to tune the reduction potential and kinetic stability of the

complexes as hypoxia selective anticancer drugs. Changing auxiliary ligands resulted in positive, negative and neutral complexes.

To ensure hypoxic selectivity, the reduced cobalt(II) complex containing the nitrogen mustard ligand must be sufficiently stable to allow re-oxidation in oxygenated cells to compete effectively with ligand loss. The kinetic stability of the reduced cobalt(II)complexes were greatly enhanced by coordinated chelating ligands.[74], [76]

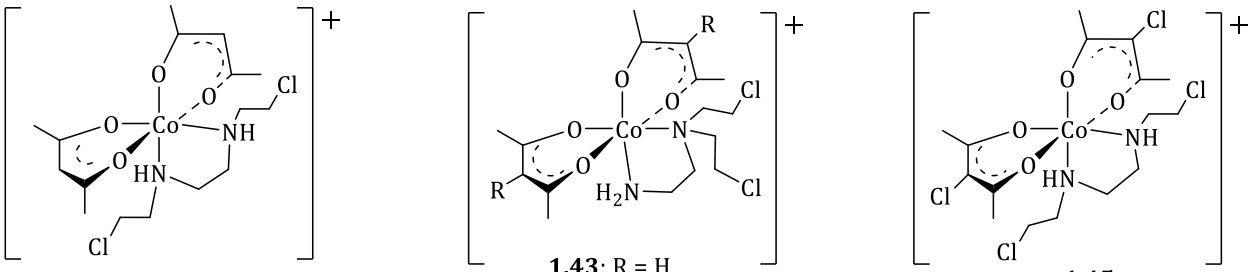

Figure 1.24. *Chemical structures for the complexes with chelating ligands **1.42**, $[Co(acac)_2(BCE)]^+$, **1.43**, $[Co(acac)_2(DCE)]^+$, **1.44**, $[Co(Meacac)_2(DCE)]^+$, **1.45**, $[Co(Clacac)_2(BCE)]^+$ (Claca = 3-chloropentane-2,4-dionato anion).*

The acetylacetonate (acac) ligand was successfully used as a bidentate monoanionic ligand, which coordinates to cobalt(III) through the two oxygen donor atoms to form delocalised chelate rings, Figure 1.24.[77]

Denny *et al.*[77] reported novel cobalt complexes of nitrogen mustard alkylating agents having hypoxia-selective anti-tumour properties.

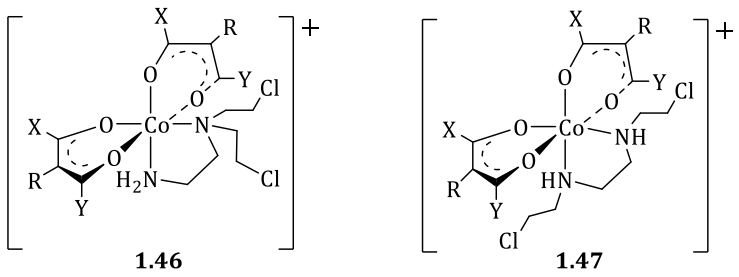

Figure 1.25. *Chemical structures of complex **1.46** and complex **1.47**.*

X =Y= H / lower alkyl (optionally substituted with hydroxyl and / or amino functions) containing from 1 to 6 carbon atoms, phenyl (optionally substituted with Me, OQ, CONHQ, and / or NHCOQ).

R = H, lower alkyl (optionally substituted with hydroxyl and / or amino functions), phenyl (optionally substituted with Me, OQ, CONHQ and / NHCOQ.

Q = lower alkyl (optionally substituted with hydroxyl and / or amino functions) and containing from 1 to 6carbon atoms) or halogen.

Both of the Denny *et al.*[77] and Ware *et al*. research outcomes confirmed that the cytotoxicity of the complexes **1.43, 1.44, 1.45, 1.46** and **1.47** was indeed due to release of the respective nitrogen mustard ligands under hypoxic conditions.[74]

Ware *et al.*[76] further investigated complexes in a similar class with tropolonates (trop) as ancillary ligands, Figure 1.26. Tropolonates are flat molecules when they coordinated to the cobalt(III) centre, and minimises the steric hindrance in complexes with bulky tertiary amine nitrogen mustard ligands.

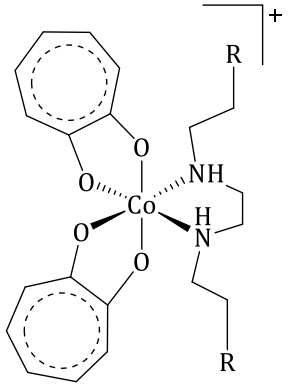

(**1.48**) BCE, R = Cl
(**1.49**) BEE, R = H

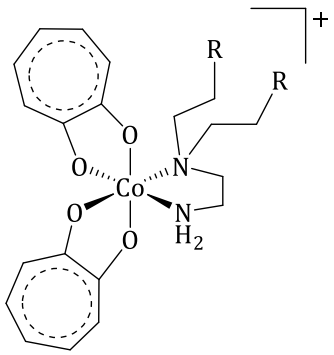

(**1.50**) DCE, R = Cl
(**1.51**) DEE, R = H

Figure 1.26. *Chemicals structures of $[Co(trop)_2(L)]^+$ (L = BCE, BEE, DCE, DEE).*

(BCE = N,N'-bis(2-chloroethyl)ethane-1,2-diamine; DCE = N,N- bis(2-chloroethyl)ethane-1,2-diamine; BEE =N,N'-diethylethane-1,2-diamine; DEE= N,N-diethylethane-1,2-diamine)

The tropolonato complexes have significantly higher reduction potential than the corresponding acac complexes, suggesting more facile cellular reduction. The tropolonato ligands therefore facilitate the cellular reduction of the coordinated cobalt(III) centres hence release of the mustard ligand.

Ware *et al.*[78] also synthesised the cobalt(III) complexes with electron rich sulfur containing dithiocarbamate ligands. The dithiocarbamato (R_2dtc^-) ligand replaced $Racac^-$ as alternative bidentate, monoanionic chelating ligands. These coordinate through two sulfur atoms, and complexes of the formulae $[Co(R_2dtc)_2(DCE)]^+$ retain an overall cationic charge.

The different R substituents tailor properties such as redox potential and lipophilicity of the $[Co(R_2dtc)_2(L)]^+$ complexes. Different alkyl groups with increasing number of carbon atoms (CH_3, $(CH_2)_2$, $(CH_2)_4$) were introduced as different R groups to create hydrophobic character to the complex hence facilitating the easy travelling across the cell membrane.

The sulfur donors on R_2dtc are capable of making a huge difference in electron transfer properties conferred on the cobalt(III)/cobalt(II) couple, Figure 1.27.[78] The coordinated electron rich sulfur donors reduce the reduction potential of cobalt(III)/ cobalt(II) couple. The small size of the four membered chelate rings minimises the steric bulk for tertiary amine nitrogen mustard ligands.

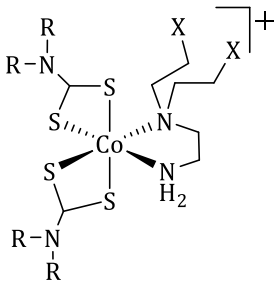

(**1.52**) X = H, R2 = Me_2
(**1.53**) X = H, R_2 - Et_2
(**1.54**) X = H, R_2 = $(CH_2)_4$
(**1.55**) X =Cl, R_2 = Me_2
(**1.56**) X = Cl, R_2 = Et_2

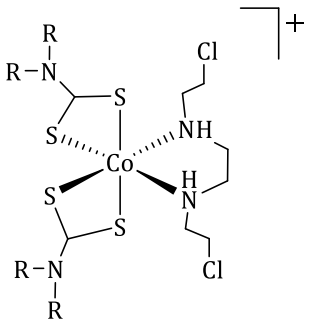

(**1.57**) X = H, R2 = Me_2
(**1.58**) X = Cl, R_2 = $(CH_2)_4$
(**1.59**) X =Cl, R_2 = Me_2

Figure 1.27. *Chemical structures of bis(dialkyl)dithiocabamato)cobalt(III) complexes of BCE and DCE bidentate nitrogen mustard.*

It was also found that the ligands containing sulfur atoms increase the kinetic stability of the complex.[79], [80] Lower potentials were expected for dithiocarbamate systems compared to oxygen donor systems for example $Co(R_2dtc)_3$ and $Co(Racac)_3$.[80]

Cobalt(III) nitrogen mustard complexes containing an overall positive charge have been reported in literature. [73-74], [77-78] Taking different approach for the synthesis, Craig *et al.*[81] reported cobalt(III) DCE complexes containing oxalate(ox) and carbonato ligands, $[Co(ox)_2(DCE)]^-$ and $[Co(CO_3)_2(DCE)]^-$. These were the first DCE complexes to be prepared which bear an overall negative charge, Figure 1.28.[81] These complexes were synthesised to study their properties in relation to the overall negative charge created by oxalate and carbonate ancillary ligands. Possibly the overall negative charge lowers the reduction potential of these complexes.

The ancillary ligands present on the cobalt(III) metal centre are also important to tune the physiologically and chemically important properties of the complex such as cobalt(III) / cobalt(II) reduction potential, overall charge, solubility and hydro-or

lipophilicity. These factors place a major role for entering the prodrug into the biological system and also in releasing the active nitrogen mustard into the target sites.

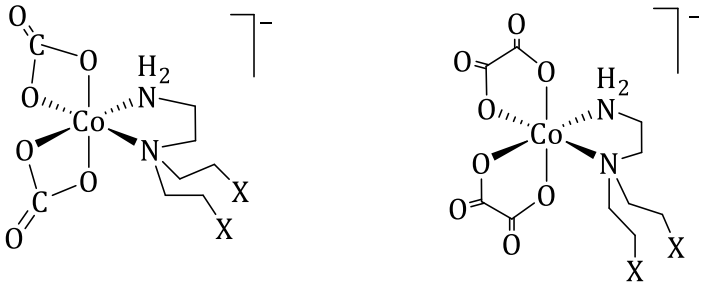

(**1.60**) X = H

(**1.61**) X = Cl

(**1.62**) X = H

(**1.63**) X = Cl

Figure 1.28. *Anionic carbonate and oxalate cobalt(III) nitrogen mustard, DCE and BCE.*

1.4.2 Photo-activated cytotoxins

The fields of phototherapy and inorganic chemotherapy both have long histories. Inorganic photoactivated chemotherapy offers both temporal and spatial control over drug activation and has remarkable potential for the treatment of cancer. Photoactivated cytotoxins (PACT) provide the opportunity for control over when and where a drug is activated, using light energy, and resulting in a greater specificity of drug action. The use of an inactive precursor or "prodrug" is an important strategy in drug targeting.[82], [83]

For biological systems, light is a convenient trigger, as it provides control over the location and timing for the creation of an active agent;[84] and if longer wavelengths are used (visible and near-IR), the light itself is generally not damaging to cells or tissues. Thus, such photo triggered agents can be used in both basic research and for clinical applications.

There is a great deal of interest in the field of photoactivated metal complexes, with a special focus on compounds that damage DNA.[85] Farrer *et al.*[83] reviewed a series of investigations of PACT for cancer treatment using metal complexes; mainly Ti, V, Cr, Mn, Re, Fe, Ru, Os, Co, Rh, Pt and Cu metal complexes.

Aqueous solubility, cell uptake and stability in biological media are common considerations for any potent drug. But photoactivated metal anticancer agents should have additional key features like:

- A large difference between cytotoxicity in the presence and absence of irradiation is desirable in order to limit unwanted side effects, which may also reduce drug efficacy.

- The wavelength of activation preferably lies within a phototherapeutic window of 620-850 nm. This range has the maximum depth penetration into mammalian tissue.[86] However, other wavelengths could prove useful to initiate the desired photochemical reaction. For example, some ruthenium(II) polypyridyl systems have well-established and characterised photochemistry in the 420-450nm range that could be used to demonstrate the potential of photoactivated cytotoxin systems.[83]

Photodynamic therapy (PDT) is more controllable and has the potential to selectively destroy malignant cells while sparing the normal tissues.

PDT elicits phototoxic reactions that selectively destroy tumour cells and spare normal cells.[87], [88]

Hematoporphyrin derivatives have been investigated for the treatment of tumours, which led to the first clinically approved PDT agent, Photofrin, Figure 1.29, for diseases such as bladder cancer.[89]

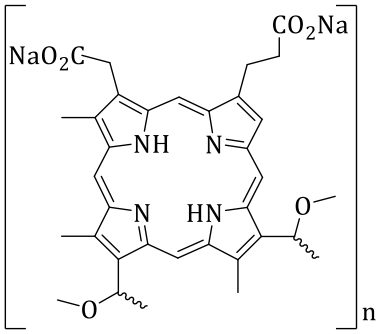

Photofrin n = 1-9

1.64

Figure 1.29. *Molecular structure of Photofrin consists of up to nine monomeric units (shown above) connected via ester linkages.*

Mackowiak *et al.*[90] explained the use of nanoparticles in combination with photosensitizers for targeted drug delivery. Apart from photosensitizing, light energy can be used to activate the drug to furnish the cytotoxic activity. This photosensitizer and nanoparticle prodrug combine system together increases cytotoxicity.

Platinum(II) diamine complexes such as *cis*-platin are effective anticancer drugs, however they also have accompanying side effects. Kasparkova *et al.*[91] investigated the design of platinum complexes with low toxicity that could be photoactivated selectively at the target site. Pt(IV) azide complex *cis,trans*-(Pt(en)(N_3)$_2$(OH)$_2$] **1.65,** Figure 1.30 was unreactive towards DNA until irradiated with light.

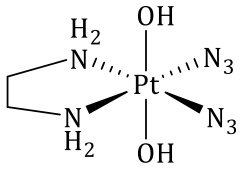

1.65

Figure 1.30. *Chemical structure of [Pt(IV)(en)(N$_3$)$_2$(OH)$_2$].*

Octahedral Pt(IV) complexes are remarkably stable in the dark even in the presence of cellular reducing agents such as glutathione, but readily undergo photoinduced ligand substitution and photoreduction reactions.[92] A number of photoactivated platinum(IV) prodrug systems have been reported in the literature.[93], [94], [95] Karatochwil [96] explored the feasibility of photolyzing the Pt(IV) complex *trans,cis*-[PtCl$_2$I$_2$(en)] to its cytotoxic species by visible light. Further information about Pt(IV) prodrug systems can be read in Balzani *et al.* and Gandioso *et al.* publications. [93, 95, 97-100]

For Pt(IV) to be active, it must first be reduced by biological reductants (e.g. ascorbate or glutathione (GSH)) to the corresponding Pt(II) antitumor agents.[101] Thus Pt(IV) complexes may be considered as inactive prodrugs, some of the Pt(IV) drugs are reported to be hypoxia active.[102]

1.5. Photochemistry of polypyridylruthenium(II) complexes

Polypyridylruthenium(II) systems are probably the most extensively studied class of transition metals complexes in relation to their photochemical properties.[103], [104-106] Polypyridylruthenium(II) complexes are popular for their triplet metal- to-ligand charge transfer (^{3}MLCT) excited state with a relatively long life time at room temperature (~1 μs) and the ability to facilitate easy electron transfer reactions.[107] The

photochemistry of the $[Ru(bpy)_3]^{2+}$ complex can be explained by Jablonski diagram, Figure 1.31.

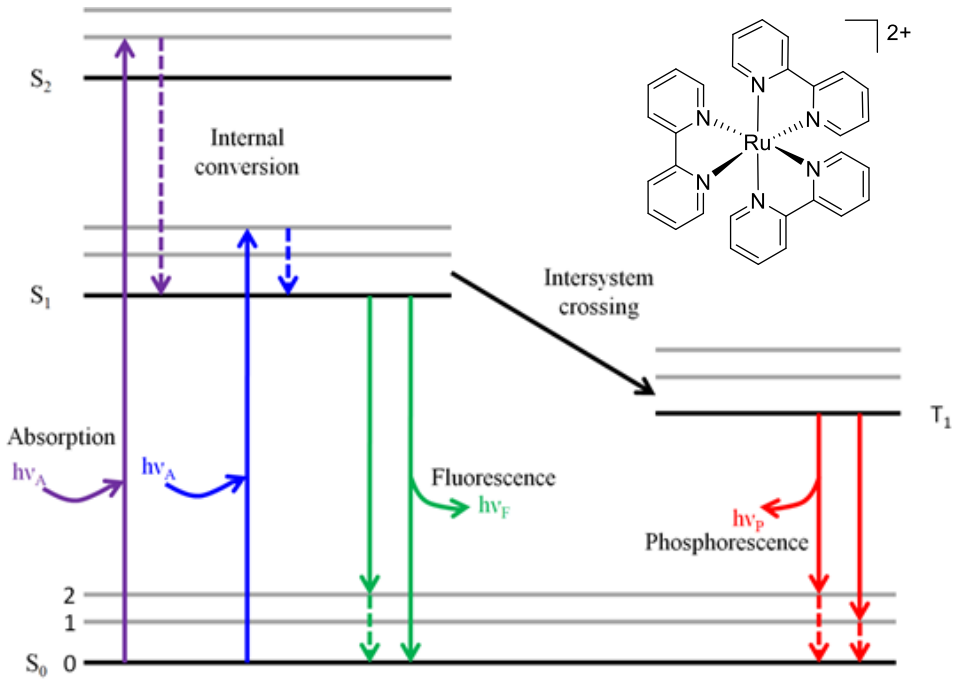

Figure 1.31. *Jablonski diagram, showing various photochemical processes due to the absorption of light by the fluorophore.*

When the electron in lowest energy state received the right energy, the electron is excited from the lowest energy singlet ground state (S_0) to singlet excited state (S_1). By changing the spin state of the electron, the energy of the electron lowers to its triplet (T_1) excited state. The complex shows strong emission from (T_1) state.[108]

Komatsuzaki *et al.*[107] reported the photochemical properties of ruthenium-cobalt and ruthenium-nickel dinuclear complexes. Ruthenium(II) works as a photosensitizer according to previously discussed electronic processes and cobalt(III) and nickel(II) moieties as electronic acceptors. Also, further information on use of photochemistry in

heterodinuclear systems such as Ru/Co, Ru/Rh, Ru/Ir, Ru/Mn and Ru/Pt are reported by Song *et al.*[109]

Photo electronic excitation and electronic transfer of bimetallic systems can be represented with a simple schematic as shown in the Figure 1.32.

.

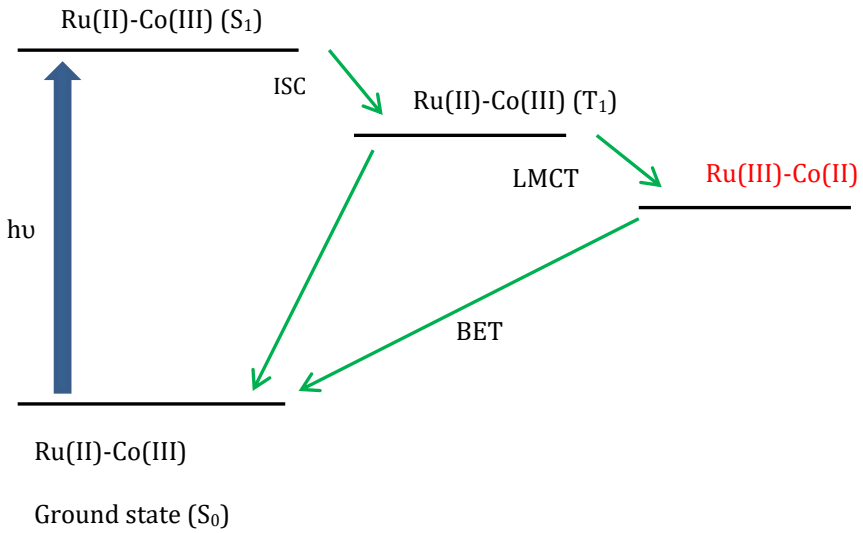

Figure 1.32. *Energy level diagram showing possible electron travel pathways in Ru(II)-Co(III) heterodinuclear complexes.*

The energy diagram contains an extra energy level compared to the $[Ru(bpy)_3]^{2+}$ system. The electron transfers (LMCT) from the bridging ligand to the cobalt(III) causing the reduction of the metal centre. At this stage, rapid exchange of ligands takes place due to the labile nature of cobalt(II) metal centre, and the recovery to the ground state occurs through back electron transfer (BET).[110]

1.6 Ruthenium(II)-cobalt(III) heterodinuclear systems as potential photoactivated cytotoxins.

Holbrook *et al*.[110] reported the photoactivated electron transfer system using a ruthenium(II)-cobalt(III) heterodinuclear complex and we aimed for a similar mechanism to be employed to develop a photoactivated cytotoxic system.

The mechanism of photoinduced ligand release can be explained using the following diagram.

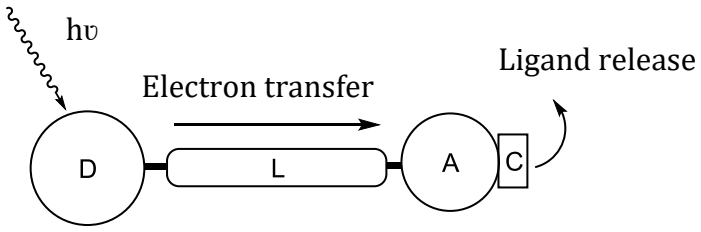

Figure 1.33. *Graphical representation of photo-activated ligand release. Photo-induced electron transfer from donor (D), through linker (L), to acceptor (A) causes cytotoxic ligand (C) release. Polypyridylruthenium(II) system will act as an electron donor system and cobalt(III) complex with coordinated nitrogen mustard will act as an electron acceptor system.*

When polypyridylruthenium(II) complex is irradiated with visible light, it is subsequently oxidised to ruthenium(III) *via* a metal to ligand charge transfer type process. The electron is then transferred through the bridging ligand to the cobalt(III) metal centre, reducing it to cobalt(II). The labile nature of cobalt(II) facilitates the release of the attached cytotoxin, thus forming the basis of light induced drug release for such systems.

Connection of the cobalt(III) centre to a group which can donate an electron upon excitation by an external light source should allow selective release of a cytotoxic molecule at the tumour site using relatively non-invasive techniques.

Our proposal involves using polypyridylruthenium(II) photochemistry to trigger release of a ligand from a cobalt ion.

Such electron transfer reactions have been observed before in Ru-Co systems. [110], [111], [112], [113], [114] Among these, only Downward *et al.* [113], [114] and Holbrook *et al.*[110] have reported subsequent ligand exchange reactions. Ligand release occurs due to the reduction of the cobalt(III) metal centre.[114]

The work reported in this thesis discusses the synthetic strategy of a heterodinuclear metal complex in order to study its photo-activated cytotoxicity. Research work reported here is based on preliminary studies performed by Downward *et al.*[113] It was demonstrated that photo-induced ligand release could be achieved in the model system in Figure 1.34.

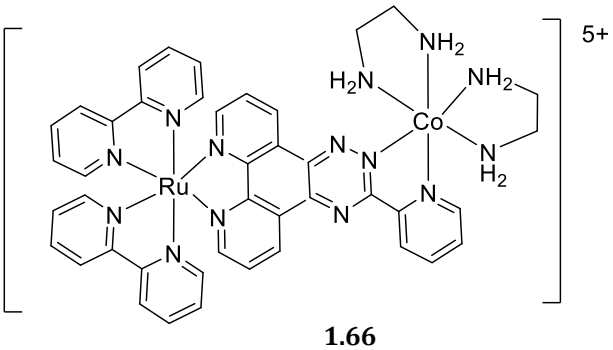

1.66

Figure 1.34. *Ru(II)-Co(III) heterodinuclear model system.*

Upon irradiation the complex **1.66** in 1:1 solvent mixture of D_2O and CH_3CN using white light at room temperature, photo-induced ligand release of the above complex was

observed. The release of the ethane-1,2-diamine ligands was observed by ^{1}H NMR spectroscopy, Figure 1.35.

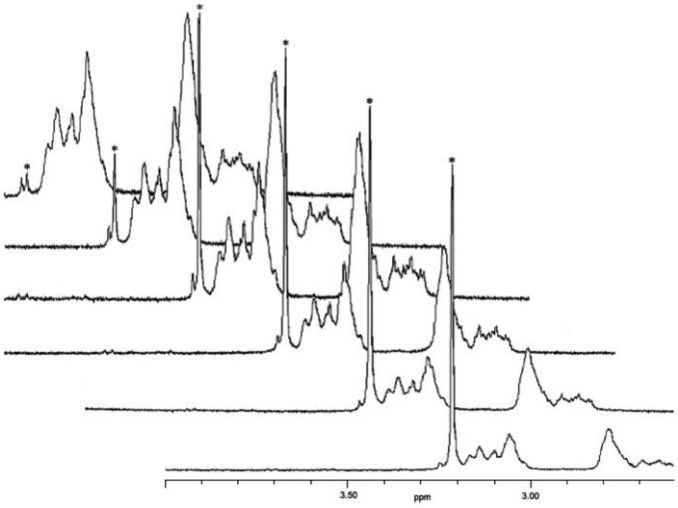

Figure 1.35 *Photo-induced release of en from $[(bpy)_2Ru(pytp)Co(en)_2]^{5+}$, as seen in aliphatic region of ^{1}H NMR spectra (pytp = 3-(pyridine-2-yl)-[1,2,4]triazino[5,5-f][1,10]phenanthroline); the peak associated with the free en molecule is marked(*). Spectra shown were taken after (from top to bottom) 0, 10, 30, 60, 120 and 180 minutes irradiation.*

The reaction scheme for the synthesis of $[Ru(bpy)_2(pytp)]^{2+}$ complex and the complexation of the cobalt(III) complex is shown in

Scheme **1.1**. One of the important facts about the synthesis of the ruthenium(II) complex is the stepwise synthesis of the bridging ligand on ruthenium(II) metal centre. The pytp: (3-pyridine-2-yl)-[1,2,4]triazino[5,6-f][1,10]phenanthroline) ligand is asymmetric in nature and the stepwise synthesis facilitates the selectivity of the bridging end for the cobalt(III) metal centre, as well as easy purification and increased yields are another important aspects of this synthesis.

$[Co(en)_2(NO_2)_2]^+$ was synthesised as a starting cobalt(III) complex and both the nitrito ligands were substituted by highly labile OTf ligands by reacting with neat trifluoromethanesulfonic acid (HOTf) to facilitate the mild reaction conditions. During the synthesis of the heterodinuclear complex, the reaction mixture should be protected from heat and light as they could lead to the decomposition of the complex, possibly due to the thermal electron transfer or the light induced electron transfer. These OTf ligands are crucial when employing extremely mild conditions during the synthesis of the heterodinuclear complex.

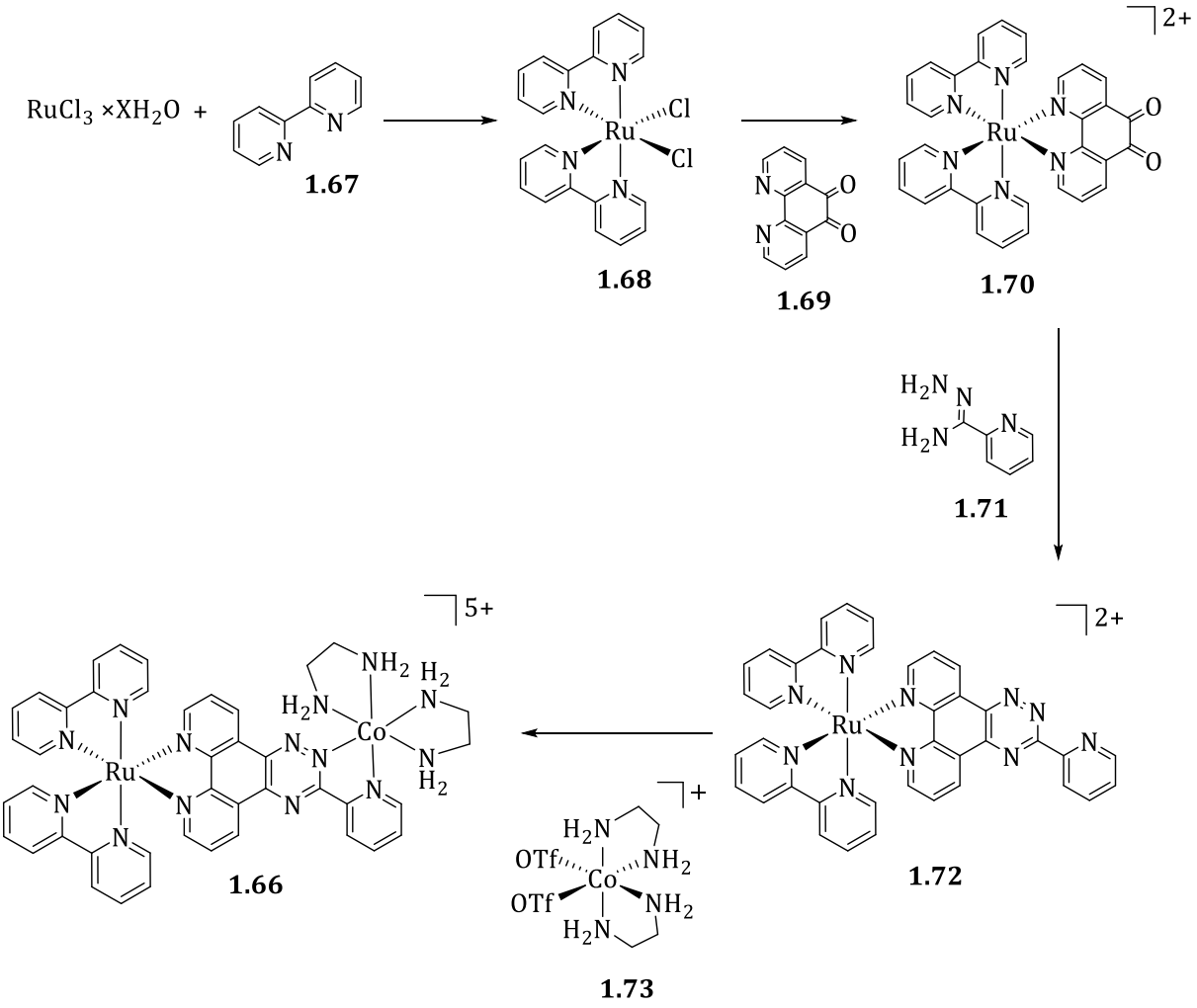

Scheme 1.1. *Reaction pathway for the synthesis of complex **1.66.***

1.7 Thesis coverage

During this research we investigated the possible modifications on both the ruthenium(II) and cobalt(III) centres. Modifications on ruthenium(II) centre to manipulate the higher total complex charge and modifications on cobalt(III) including the replacement of ethane-1,2-diamine (en) with nitrogen mustard ligands.

N-(2-chloroethyl)ethane-1,2-diamine, **L3** will replace the ethane-1,2-diamine (en) ligands shown in complex **1.66.** *N*-(2-chloroethyl)ethane-1,2-diamine (**L3**) was chosen as the cytotoxic nitrogen mustard to be synthesised on the cobalt(III) metal centre due to the easily obtained precursor $[Co(L1)_2(NO_2)_2]^+$ (L1: 2-((2-aminoethyl) amino)--ethanol) and we explore the possibility of increasing the number of chloroethyl arms on the nitrogen mustard.

Chapter 02 describes the coordination chemistry of the simplest 2-((2-amino-ethyl)amino)ethanol, **L1**, precursor ligand. **L1** ligand was of interest to us as a precursor ligand in the one step synthesis of nitrogen mustard compounds on cobalt(III) centre. The subsequent functional group chemistry required to produce mustard species was investigated and the functional group chemistry was found to both depend on and change the coordination chemistry of the cobalt(III) centre. This reaction chemistry is described in chapter 02.

Chapter 03 reports the coordination chemistry of amino alcohol ligands with cobalt(III) metal centre. Amino alcohols are an important class of ligands for the project as they act as precursors for the nitrogen mustards. The coordinated amino alcohols were converted to nitrogen mustard ligands by chlorinating the alcohol group. But these alcohol oxygen atoms can also coordinate to the cobalt(III) metal centre, which provides some synthetic challenges, but also some opportunities. We therefore report the

coordination behaviour of several different amino alcohol ligands with the cobalt(III) metal centre.

The model dinuclear complex **1.66** carried a 5+ positive charge; one of the aims of the research project is to modify the bipyridine ligands coordinated with the ruthenium metal centre in a way to lower the total complex charge. In that aspect some ligands like 4,4'-dicarboxy-2,2'-bipyridine and 4,4'-diethoxycarbonyl-2,2'-bipyridine were suggested.

Chapter 04 discusses the synthetic strategy for preparation of Ru(II)-Co(III) heterodinuclear metal complexes and describes its implementation, including the preparation of a suitable nitrogen mustard containing cobalt(III) precursor complex.

Chapter 05 summarises the current state of the project and outlines the prospects and directions of future work.

Chapter 06 provides the experimental details for synthetic work and molecular characterisation undertaken in this project.

Chapter 02

Synthesis of a nitrogen mustard ligand on a cobalt(III) metal centre and related reaction chemistry

2. Synthesis of a nitrogen mustard ligand on a cobalt(III) metal centre and related reaction chemistry

2.1 Introduction

One of the key aims of this research project is to synthesise a nitrogen mustard on an inert cobalt(III) metal centre. This synthetic route would allow us to avoid the handling of free toxic nitrogen mustard compounds during the preparation of such complexes.

The proposed methodology involves the complexation of amino alcohol compounds, such as 2-((2-aminoethyl)amino)ethanol, **L1**, 2,2'-(ethane-1,2-diylbis(azanediyl))-diethanol, **L2**, with a cobalt(III) inert metal centre, followed by the chlorination of the alcohol groups. For example, on chlorination **L1** will be converted to, **L3**, Figure 2.1.

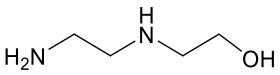

2-((2-aminoethyl)amino)ethanol (L1)

2.01

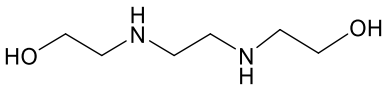

2,2'-(ethane-1,2-diylbis(azanediyl))diethanol (L2)

2.02

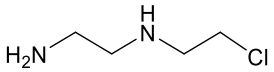

N-(2-chloroethyl)ethane-1,2-diamine (L3)

2.03

Figure 2.1. *Chemical structures of **L1**, **L2** amino alcohol ligands and **L3** nitrogen mustard.*

One of the key requirements to achieve the proposed synthetic route is the availability of a non-coordinated hydroxyethyl group. That will allow conventional functional group

chemistry to be utilised for the synthesis of a nitrogen mustard on the cobalt(III) metal centre.[115], [116]

Until now, such complexes have been prepared by the complexation of a free mustard compound onto the cobalt(III) metal centre.[66], [73], [76], [117] Detailed information on these complexes can be found in chapter 01, Section 1.4.1.2. Most of the nitrogen mustard compounds used in those studies were prepared by direct chlorination of the corresponding alcohol group of the free amino alcohol compounds.[118]

Boens *et al.*[119] recently reported a new synthetic method to synthesise eight different nitrogen mustard compounds using the reaction conditions shown in Figure 2.2. The chlorination of the alcohol group was performed under very mild conditions, utilising a thionyl chloride/pyridine system, in chloroform, at room temperature.

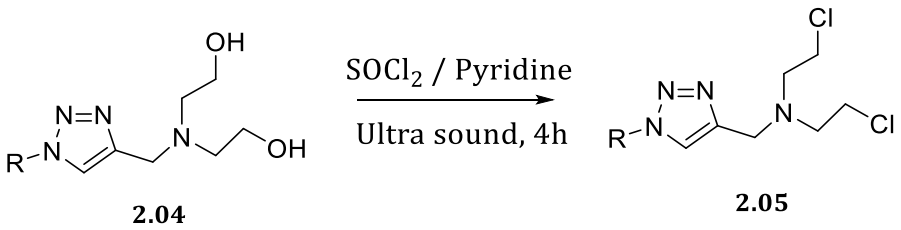

2.04 **2.05**

Figure 2.2. *Reaction scheme for the synthesis of nitrogen mustard ligands.*

Handling of these nitrogen mustard compounds is problematic due to their instability, their susceptibility to hydrolysis or solvolysis in their free base form, and their high toxicity.[73]

As a safer synthetic approach, Downward *et al.*[120] investigated the synthesis of a nitrogen mustard on the inert cobalt(III) metal centre.

2.2 Previous work

The aim of synthesising the nitrogen mustard on the cobalt(III) metal centre is to investigate a better and safer synthesis approach for these cytotoxic nitrogen mustard molecules and also later in the project these cobalt(III) nitrogen mustard complexes will take part in the Ru(II)-Co(III) pro-drug system (Refer chapter 04).

L1 was chosen as a potential ligand to synthesise a nitrogen mustard on a cobalt(III) metal centre. This synthesis was previously studied in Hartshorn group by Alan Downward.[121], [120]

After complexing **L1** ligand with the cobalt(III) metal centre according to Downward *et al.*[120] synthesis, the chlorination method reported by Truce *et al.*[116] was employed to chlorinate the pendant alcohol group. $SOCl_2$/ DMF were used to achieve chlorination, where $SOCl_2$ is a chlorinating agent and DMF acts as a catalyst for the reaction, Scheme 2.1.

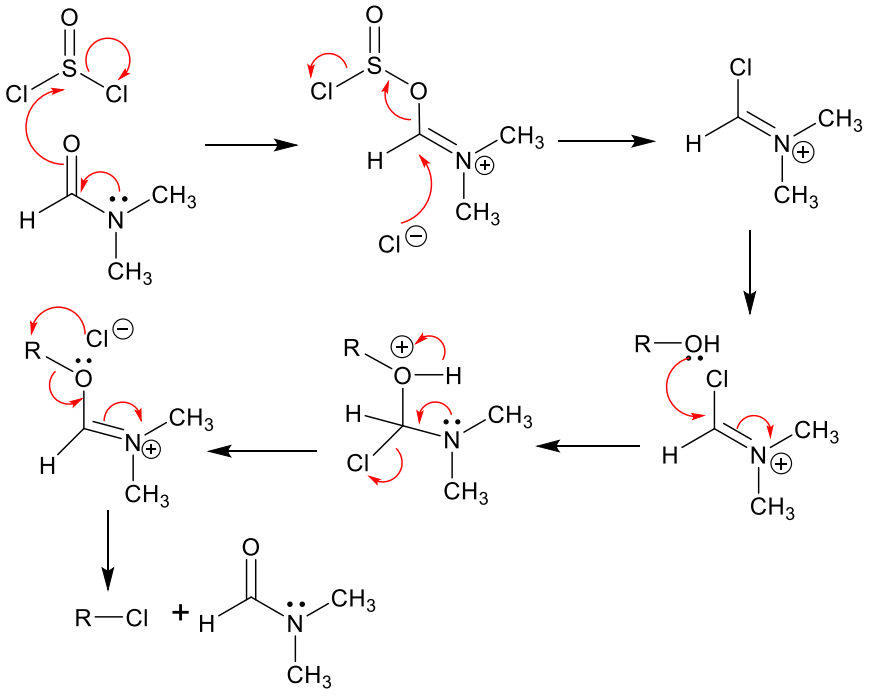

Scheme 2.1. *The reaction mechanism for chlorination of alcohol using $SOCl_2$ / DMF.*

Luca *et al.*[115] proposed a mechanism for the chlorination of alcohol groups using 2,4,6-trichloro[1,3,5]triazine (TCT) and DMF. TCT is the chlorinating agent, and DMF is a catalyst.

Downward *et al.*[120] used $SOCl_2$/DMF as a chlorinating agent for the conversion of alcohol functionality to chloro-functionality. The reaction mechanism for the chlorination of alcohol is shown in Scheme 2.1.

Downward *et al*. synthesised $[Co(L1)_2(NO_2)_2]^+$, **2.06**, and in this complex the **L1** ligand coordinated as a bidentate ligand, through the amine nitrogen atoms. The hydroxyethyl group was planned to be chlorinated using $SOCl_2$ / DMF later in the synthetic route to convert the **L1** to **L3**.

It's worth noticing at this stage, that the **L1** ligand has the potential to coordinate in a variety of ways. It can be coordinated in a bidentate binding fashion through the nitrogen atoms only, or it can coordinate as a tridentate ligand utilising both nitrogen atoms as well as the oxygen atom. The hydroxyl group of the **L1** ligand can stay protonated or be deprotonated, depending on the reaction conditions. Sarma *et al.*[122] and Drinkard *et al.*[123] previously reported tridentate coordination behaviour for the **L1** ligand. From now onward the protonated ligand will be referred to as **L1** and the deprotonated **L1** ligand, 2-(2-aminoethyl)amino]ethanoate, will be referred to as (**L1-H**),Figure 2.3**.**

L1 **L1-H**

Figure 2.3. *Protonated **L1** and the deprotonated **L1-H** ligand presenting their binding modes.*

The **L1** ligand could bind through different combinations of donor atoms as shown in Figure 2.4

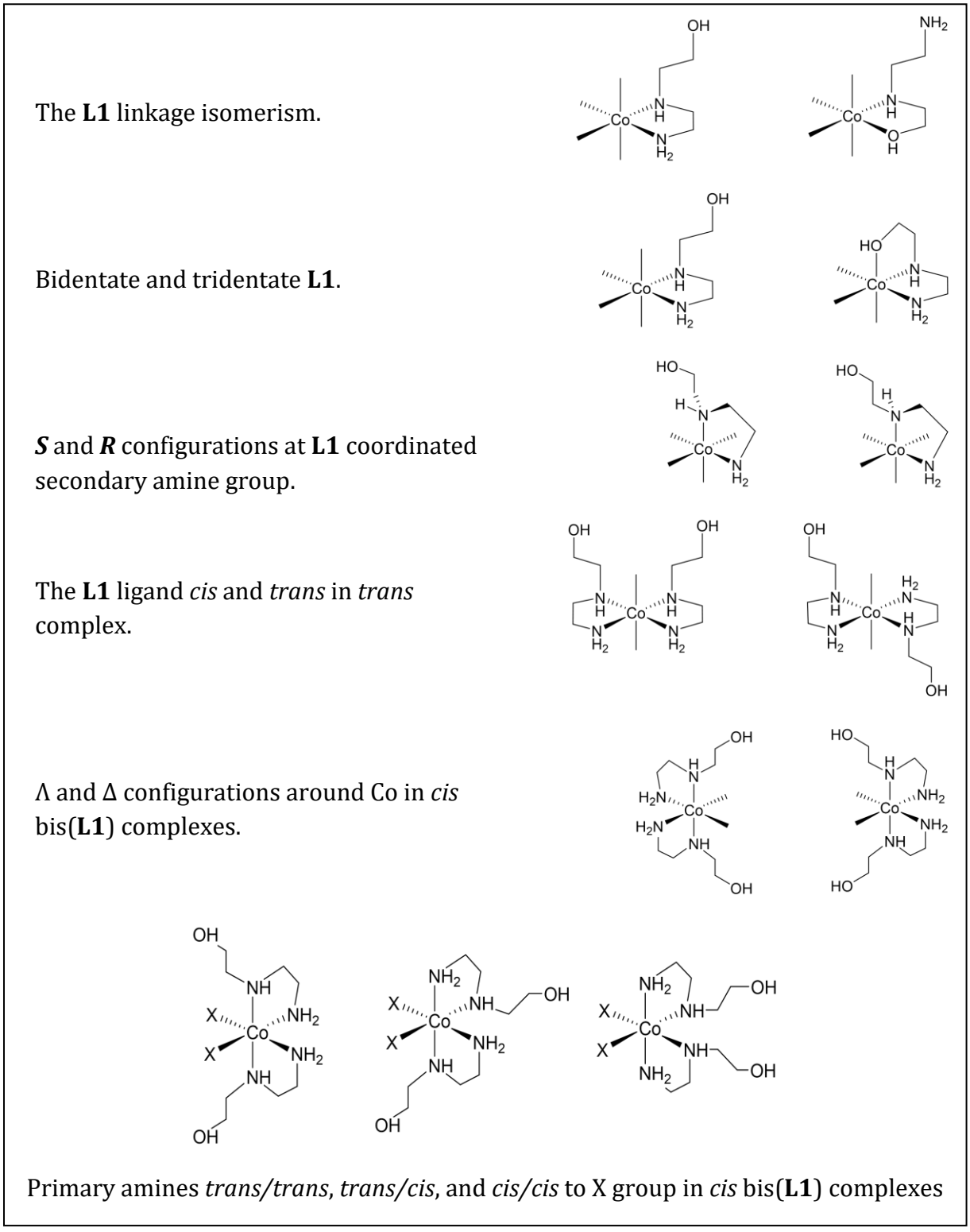

Figure 2.4. *Possible isomers of $[Co(L1)_2(X)_2]^+$ complex formed during complexation of **L1** ligand on to cobalt(III) metal centre.*

Under the reaction conditions used by Downward *et al.*[120], the **L1** ligand coordinated in bidentate fashion, leaving the hydroxyethyl arm free. Therefore, the reaction conditions shown in Figure 2.5 allowed the pendant hydroxyethyl groups to be converted to chloroethyl groups, thereby synthesising the nitrogen mustard on a cobalt(III) metal centre. Since the nitrogen lone pair is coordinated with the cobalt(III) metal centre, the nitrogen mustard is much less reactive than the free ligand. The reaction mechanism of free nitrogen mustard is discussed in the section 1.2.3.1.

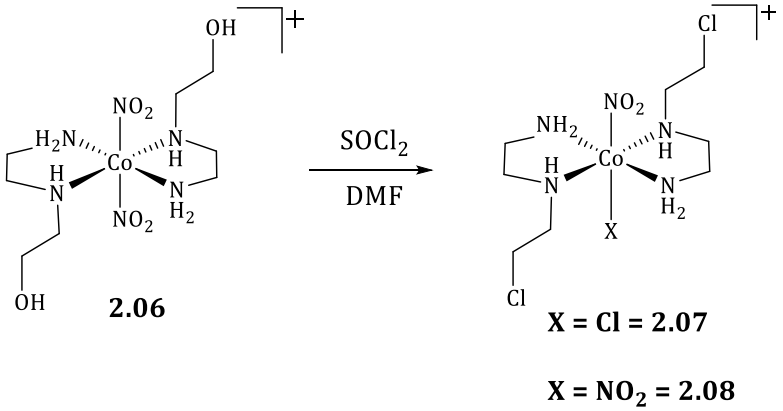

Figure 2.5. *Synthesis of a nitrogen mustard on the cobalt(III) metal centre.*

2.2.1 Synthesis of precursor complex $[Co(L1)_2(NO_2)_2]^+$, 2.06,

The synthesis of complex **2.06** was achieved under classic Wernerian conditions,[124] in which a rapid ligand exchange equilibria involving labile cobalt(II) ions led to formation of a distribution of complex ions that presumably reflects the relative stability of those complexes. This distribution is largely fixed by oxidation to inert cobalt(III) complexes.[120]

The **2.06** complex was synthesised according to the reported literature procedure by Downward *et al.*[120]

The X-ray crystal structure of complex $[Co(L1)_2(NO_2)_2]^+$ **2.06** reported in literature, Figure 2.6, revealed the presence of a single isomer in the solid phase; formation of the particular isomer of this complex may be due to its higher stability or lower solubility.

The thermodynamic stability of the complex may be due to the arrangement of hydroxyethyl arms on opposite sides of the complex, minimising steric hindrance, and making hydrogen bonding interactions between the amine hydrogen atoms and nitrite oxygen atoms.

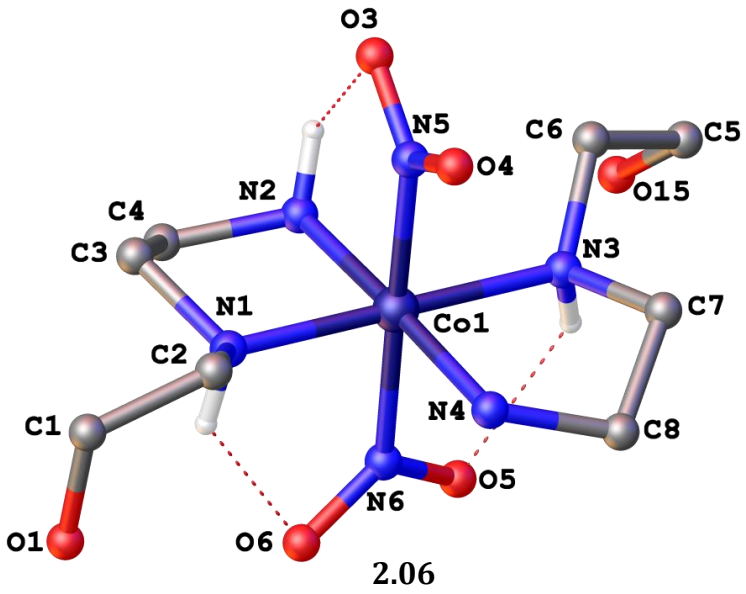

Figure 2.6. *The asymmetric unit of $[Co(L1)_2(NO_2)_2]^+$complex,* ***2.06*** *with atom-labelling. The R, R isomer is shown, but the S, S isomer is also present in the unit cell. The anion, solvent molecules and the hydrogen atoms, except amine hydrogens, have been omitted for clarity.*[120]

The X-ray crystal structure of the compound confirmed that two **L1** ligands were coordinated to the cobalt(III) centre through the amines, in a mutually *trans* bis(bidentate) manner. The other two binding sites on the octahedral metal centre, were *trans* to each other, and were occupied by *N*-bound nitrite ligands. Both the nitrite ligands were involved in hydrogen bonding interactions with amine hydrogen atoms,

which made them inequivalent as one nitrite ligand bridges the secondary amine hydrogen atoms and the other nitrite ligand bridges with the primary amine hydrogen atoms. These interactions are shown in dotted lines in Figure 2.6. The asymmetric unit in the structure shown in Figure 2.6 is chiral, due to the stereogenic secondary amine ligating group (the *R,R* isomer is shown in Figure 2.6) however the space group of the crystal structure requires the presence of the other isomer, making the crystal racemic.[120]

2.3 Results and Discussion

The precursor complex $[Co(L1)_2(NO_2)_2]^+$, **2.06** shown in Figure 2.6 was synthesised according to the procedure described by Downward *et al.*[120] The chlorination of alcohol groups using $SOCl_2$/DMF pair was carried out to synthesise the nitrogen mustard on the cobalt(III) metal centre.

2.3.1 Chlorination of alcohol groups in the complex 2.06 for the synthesis of the related nitrogen mustard

In order to use the synthetic route suggested, depending on the results reported by Downward *et al.*[113], for the preparation of ruthenium(II)cobalt(III) heterodinuclear complexes, the mustard-containing complex should have highly labile ligands to satisfy the low energy reaction conditions during the synthesis of heterodinuclear complexes.

In brief, the alcohol groups in the **2.06** complex were chlorinated aiming to synthesise the **2.08** complex shown in Figure 2.5. The *N*-bound nitrite ligands found on the complex **2.08** can be easily substituted with the highly labile trifluoromethanesulfonate ligands (OTf)[125] Another advantage of having OTf anions coordinate is to make the

cobalt(III) nitrogen mustard complex soluble in acetonitrile. This solubility was achieved through the formation of the corresponding OTf salt. This process generally involves treating either the nitrite or chloride complex with trifluoromethanesulfonic acid (HOTf) under a vacuum at a temperature between 60 and 100 °C.[125], [126]

At the initial stage of this research project various chlorinating reagents, such as HCl, PCl_3, $POCl_3$, $SOCl_2$, and SO_2Cl_2 were tested and $SOCl_2$ has been identified as the best reagent for the substitution of the hydroxyl groups with the chlorine atoms.

The precursor complex $[Co(L1)_2(NO_2)_2]^+$ **2.06** was reacted with $SOCl_2$ in the presence of catalytic amount of DMF at room temperature. After evaporating excess $SOCl_2$ under a vacuum, the resulting pink solid material was recrystallized from 1:1 ethanol/water mixture to yield pink crystals. These crystals were characterised using mass spectrometric analysis; *m/z* = 384.0166, ^{1}H NMR, ^{13}C NMR analysis, as well as X-ray crystallography, to confirm the formation of the complex $[Co(Cl)(L3)_2(NO_2)]^+$, **2.07**.

The X-ray crystal structure of complex **2.07** is shown in Figure 2.7.

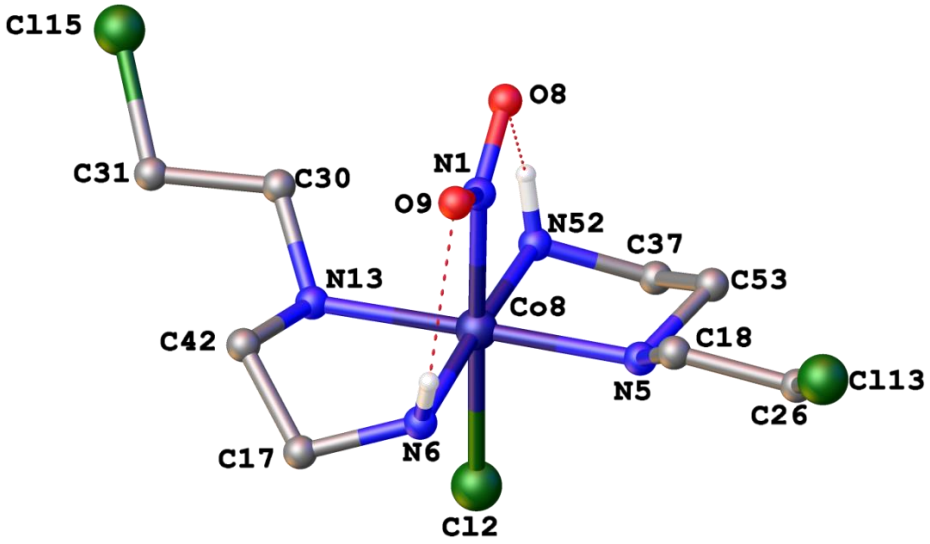

2.07

Figure 2.7. *The X-ray crystal structure of* $[Co(Cl)(L3)_2(NO_2)]^+$ ***2.07*** *with atom-labelling The hydrogen atoms, except stereogenic hydrogen atoms and anion, have been omitted for clarity. The X-ray crystal structure shows the hydrogen bonding between N-bound nitrite ligand and primary amine hydrogens atoms.*

The **2.07** complex shows distorted octahedral geometry. The amine ligands were coordinated in mutually *trans* bis(bidentate) manner. Also, one of the *N*-bound nitrite ligands seen in the precursor complex **2.06** had been replaced by a chloride ligand. The crystallographic studies revealed the replaced *N*-bound nitrite ligand was hydrogen-bonded to secondary amine hydrogens of the starting material; Figure 2.6. The remaining nitrite ligand retained the hydrogen bonding to the primary amine hydrogens as shown in Figure 2.7.

The complex **2.07** differs from the precursor complex **2.06** by having coordinated nitrogen mustard ligands and also an axial chloride ligand as shown in the Scheme 2.2.

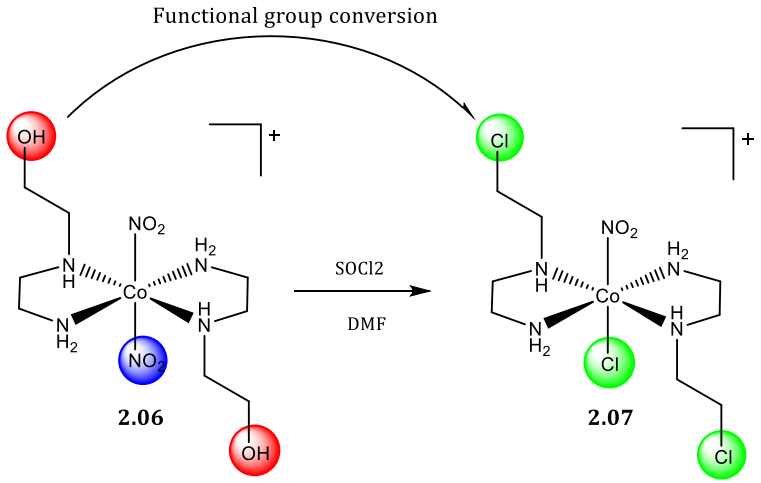

Scheme 2.2. *Synthesis of nitrogen mustard coordinated with the cobalt(III) metal centre. This reaction scheme shows the conversion of alcohol function to chloro function as well as the substitution of one of the N-bound axial nitrite ligands with chloride.*

During the chlorination of the alcohol groups, formation of the **2.07** complex was observed instead of the expected **2.08** complex, Figure 2.5.

According to the X-ray crystal structure shown in Figure 2.6, two of the *trans N*-bound nitrite ligands show differences in their hydrogen bonding with the amine hydrogen atoms. This difference may cause one of the *N*-bound nitrite ligands to be substituted by the chloride ligands.

Primary amine hydrogens are more acidic, and hence are stronger hydrogen bond donors than those on the secondary amines which led to the lower reactivity of the *N*-bound nitrite ligand.

However, the remaining Co-NO_2 bond length after chlorination seemed to be consistent with that of the Co-NO_2 bond length of the precursor complex. Accordingly, it is possible that the hydrogen-bonding interaction from the most acidic hydrogen of the primary amines stabilise the remaining *N*-bound axial nitrite ligands during the chlorination

relative to the *N*-bound nitrite ligand hydrogen bonding to secondary amine ligands, but not the *trans* influence type process. However, there was not enough evidence to confirm the chemistry behind this process.

However, this unexpected ligand exchange was challenging. Attempts to use the **2.07** for the HOTf reaction were unsuccessful and decomposition of the **2.07** complex was observed.

Therefore, a series of reactions were carried out using **2.06** as starting material, as shown in Figure 2.8, to get a better understanding about the chemistry related to ligand exchange, stability and coordination chemistry of the complex **2.06** and related complexes.

During the process of investigating the ligand exchange behaviour of the complexes presented in this chapter, we found that one product complex can act as a starting material to another complex. Using this information the reaction web diagram was developed shown in Figure 2.8. Those reaction routes will also be discussed under the different starting materials in each section respectively.

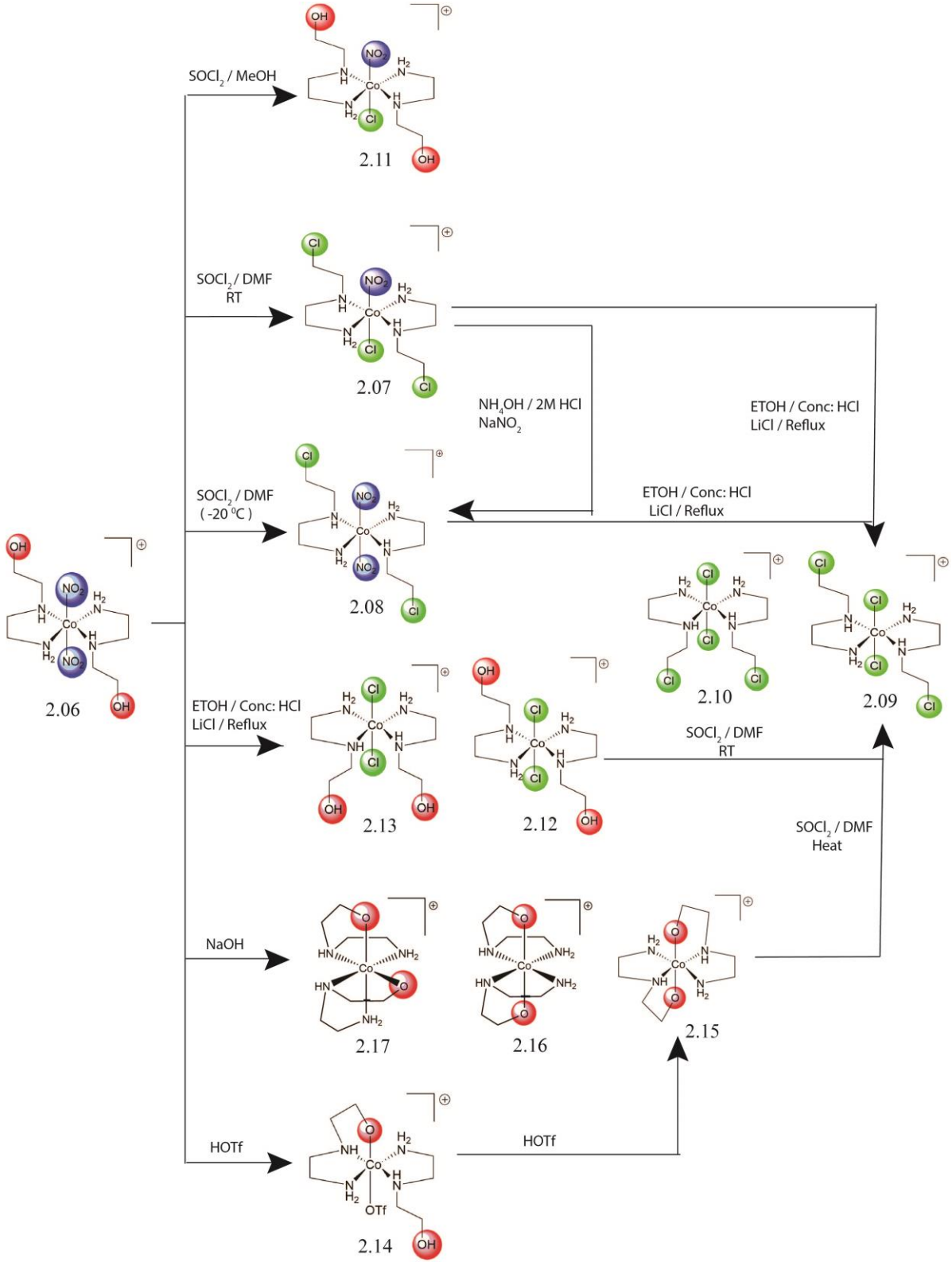

Figure 2.8. *The chemistry detailed in this chapter.*

2.3.2 Synthesis of complex $[Co(Cl)_2(L3)_2]^+$, 2.09,

After separating the crystals of **2.07** from the chlorination reaction, the remaining hot filtrate changed colour from pink to bluish-green and, after few days; the solution yielded bluish-green block shaped crystals. The obtained crystals were filtered and washed with cold ethanol and characterised by mass spectrometric analysis and X-ray crystallography.

The mass spectrometric analysis of the crystals showed the presence of both the **2.07** and **2.09** complexes confirming the non-homogeneous nature of the crystalline material. The ion appearing at m/z: 374.9897 confirmed the presence of **2.09/2.10** and the m/z relevant to 384.0167 confirmed the presence of **2.07** in the crystalline material sample.

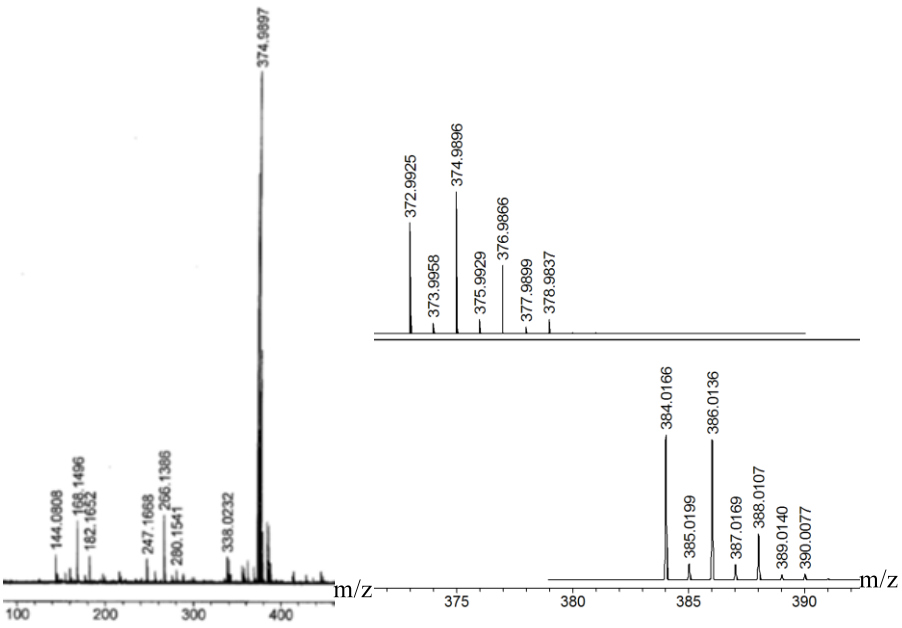

Figure 2.9. The mas*s spectrum of the crystalline material showing presence of both the complexes, $[Co(Cl)_2(L3)_2]^+$, **2.09/2.10** and $[(Co(Cl)(L3)_2(NO_2)]^+$, **2.07**. Experimental m/z signals and simulated isotope patterns are shown for both the complexes.*

The X-ray crystallographic studies of the selected crystal showed the presence of the *cis* amine *trans* chloride isomer, complex **2.10**, one of the axial chloride ligands showed mixing with nitrite ligands. This must be due to the presence of the *cis* amine isomer of **2.07** in the crystalline material and both the complexes crystallised together.

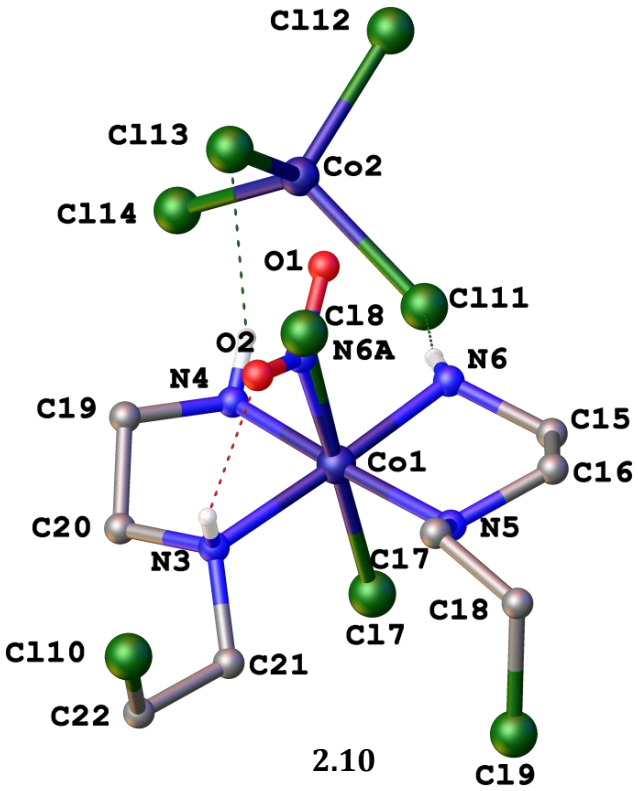

Figure 2.10 *X-ray crystal structure of* $[Co(Cl)_2(L3)_2][CoCl_4]$, ***2.10*** *with atom-labelling. A solvent molecule and the attached hydrogen atoms, except hydrogen bonding amine hydrogen atoms, were omitted for the clarity.*

The complex **2.10** shows distorted octahedral geometry having coordinated two L3 ligands and two chloride ligands around the cobalt(III) metal centre. Only one axial chloride ligand, Cl18 shows mixing / disorder with nitrite ligand. The presence of nitrite ligand in mixing with chloride is indicated by the two prominent electron densities beside the Cl8 chloride axial ligand and better refinement value was obtained after

modelling the nitrite ligand on the crystal structure. This is most likely due to the presence of both the **2.10** and the *cis* amine isomer of **2.07** in the reaction mixture and crystallising together. This finding suggests the non-homogeneous nature of the crystalline material.

The crystal structure of **2.10** shows different ligand arrangement compared to the starting material **2.06**.

The complex **2.10** shows a *cis* amine substituent configuration. But the starting material **2.06** is a *trans* amine complex. The isomerisation of the **L3** ligand could be facilitated by the generation of cobalt(II) ions in the medium. Even the small amount of cobalt(II) present in the medium could reduce more cobalt(III) species in the medium. Due to the labile nature of cobalt(II), the ligands on the cobalt(II) centre can rapidly exchange, and cobalt complexes can isomerise under these circumstances. The above crystal structure, Figure 2.10, is one of the examples of an isomerisation followed by the re-oxidation of the cobalt(II) complex. This complex does not represent the bulk sample as confirmed by the complicated ^{13}C NMR spectroscopy and the broadening of the ^{13}C NMR could also be due to the presence of a trace amount of cobalt(II) contaminant in the sample.

During the recrystallization process, ethanol acts as a solvent; the reducing nature of the ethanol may have cause the production of the cobalt(II) ions in the medium.

The findings about **2.10** guided us to develop a new synthetic route for the complex $[Co(Cl)_2(L3)_2]^+$, **2.09**.

Chlorides are much weaker ligands compared to the nitrite ligands. By having dichloride ligands coordinated with the cobalt(III) nitrogen mustard complex, there is a possibility of using it, without any modifications, to coordinate with the Ru(II) second

metal centre to synthesise the heterodinuclear complex. Therefore **2.09** could be a potential candidate during the prodrug synthesis.

There is some evidence from the previous literature about the use of dichloride complexes during the synthesis of dinuclear complexes. Liang *et al.*[127] used cis-$[Co(Cl)_2(phen)_2]Cl\cdot 3H_2O$ to coordinate to the $[(phen)_2Ru(bpibH_2)]^{2+}$ complex to synthesise the dinuclear $[(phen)_2Ru(bpibH_2)Co(phen)_2](ClO_4)_5\cdot 2H_2O$; {$bpibH_2$ = 1,4-bis([1,10]phenanthroline-[5,6-*d*]imidazole-1-yl)-benzene}.

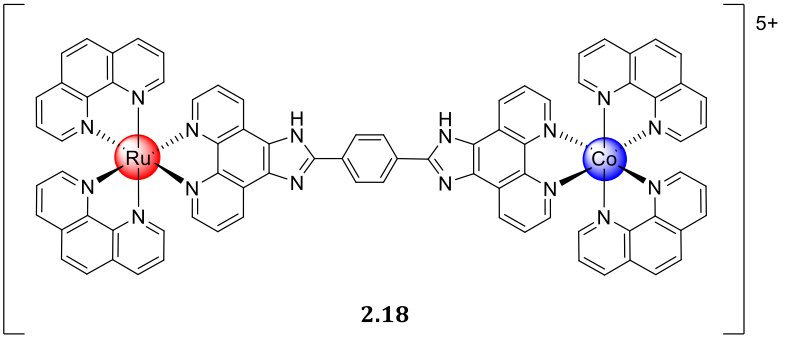

2.18

Figure 2.11. *Chemical structure of* $[(phen)_2Ru(bpibH_2)Co(phen)_2]^{5+}$, ***2.18***.

Another possibility of having dichloride ligands is to replace them with even more labile OTf ligands[72], hence employing the mild reaction conditions during the complexation. However Downward *et al.* explored the possibility of reacting $[Co(Cl)_2(en)_2]^+$ complex with $[Ru(bpy)_2(pytp)]^{2+}$ to form dinuclear complex, however the reaction failed and the synthesis of dinuclear complex was successfully completed with the $[Co(en)_2(OTf)_2]^+$ complex.

The first synthesis attempt for the complex **2.09** involved the heating of the precursor complex **2.06** at 70 °C in the presence of conc. HCl, using ethanol as a solvent and also adding LiCl to increase the chloride ion concentration in the medium. This experiment was unsuccessful as the reaction led to the decomposition of the precursor complex, the

appearance of blush-green reaction mixture confirmed the formation of cobalt(II) ions in the medium.

For the second attempt the complex **2.07** was chosen as the starting material and was heated at 70 °C with conc. HCl and EtOH in the presence of LiCl; the resulting dark green colour solution suggested the presence of *trans* dichloride ligands on the cobalt(III) metal centre.[128] After evaporating the solvent, ethanol was added to the sticky solid material to yield a light green powdered material of the complex **2.09**.

The complex **2.09** is highly sensitive to temperature; and therefore it was necessary to maintain the reaction temperature at ~70 °C. The reaction was slow and needed a longer reaction time to achieve completion. The yield of the reaction was lower due to the generation of cobalt(II) ions. The cobalt(II) propagate the reduction of cobalt(III) ions to cobalt(II) and the decomposition of the complex.

The complex was characterised using mass spectrometry (*m/z* = 374.9896), NMR spectroscopy, microanalysis and X-ray crystallography.

The ^{1}H NMR spectrum of the complex **2.09** is shown in Figure 2.12. The four different multiplets in the spectrum are relevant to eight different hydrogen atoms from each half of the complex. The three amine hydrogen (N3 and N6) peaks are placed in three different positions of the spectrum. The two primary amine hydrogens on N6 were chemically different due to the arrangement in space. The hydrogen atoms on the C1 carbon appear down field in the spectrum at around 4.0 ppm compared to other hydrogen atoms. The two multiplets observed up field in the spectrum are relevant to the chemically different H4 and H5 hydrogens.

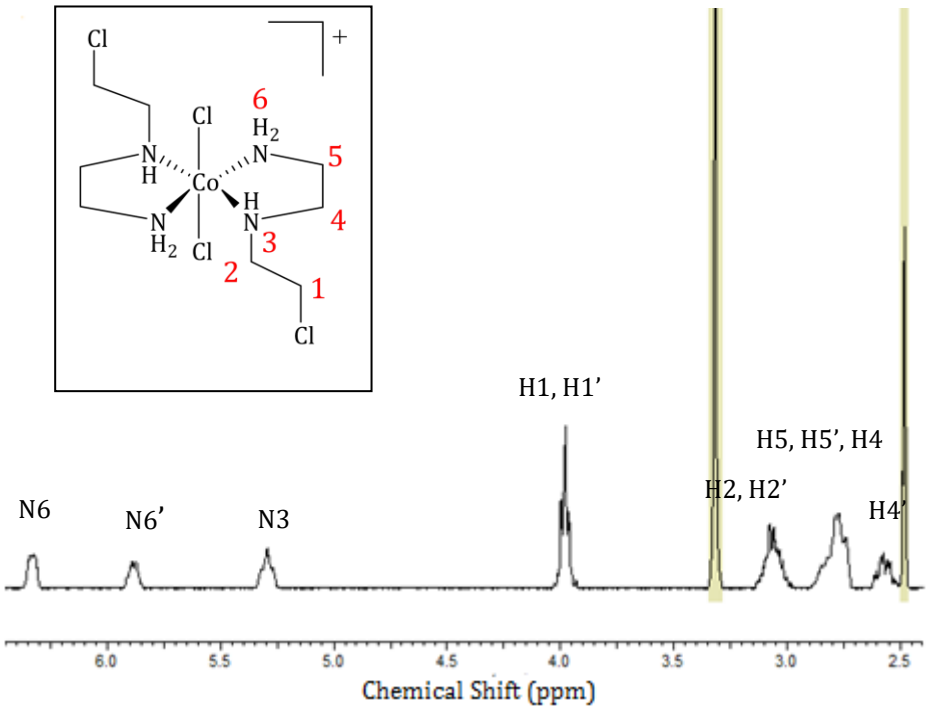

Figure 2.12. *^{1}H NMR spectrum of $[Co(Cl)_2(L3)_2]$,* ***2.09*** *in deuterated DMSO. The yellow coloured peaks are due to H_2O and DMSO respectively.*

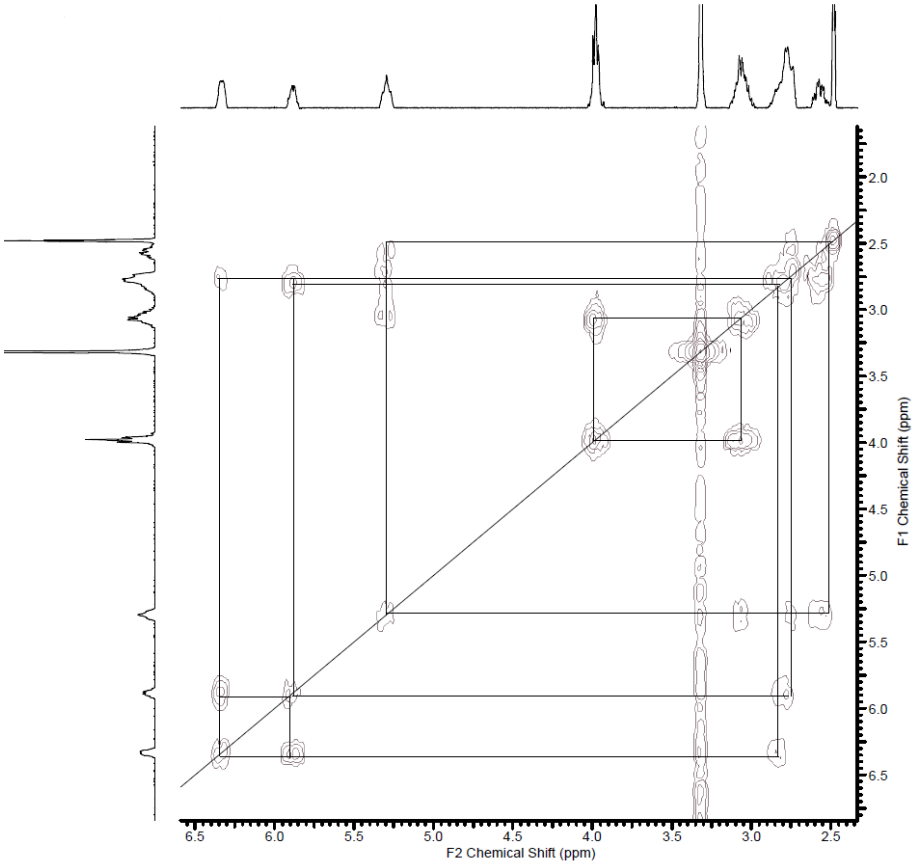

Figure 2.13. *gCOSY NMR spectra of $[Co(Cl)_2(L3)_2]^+$,* ***2.09****.*

COrrelation **S**pectroscop**Y** (gCOSY) is a 2D NMR technique that gives correlation between *J*-coupled signals by incrementing the delay between two 90° proton pulses. This can be used to identify the spins which are coupled to each other. The information obtained from this spectrum helps to find the proton-proton coupling within three bond distance and also helps to confirm the proton assignment in the ^{1}H NMR spectrum.

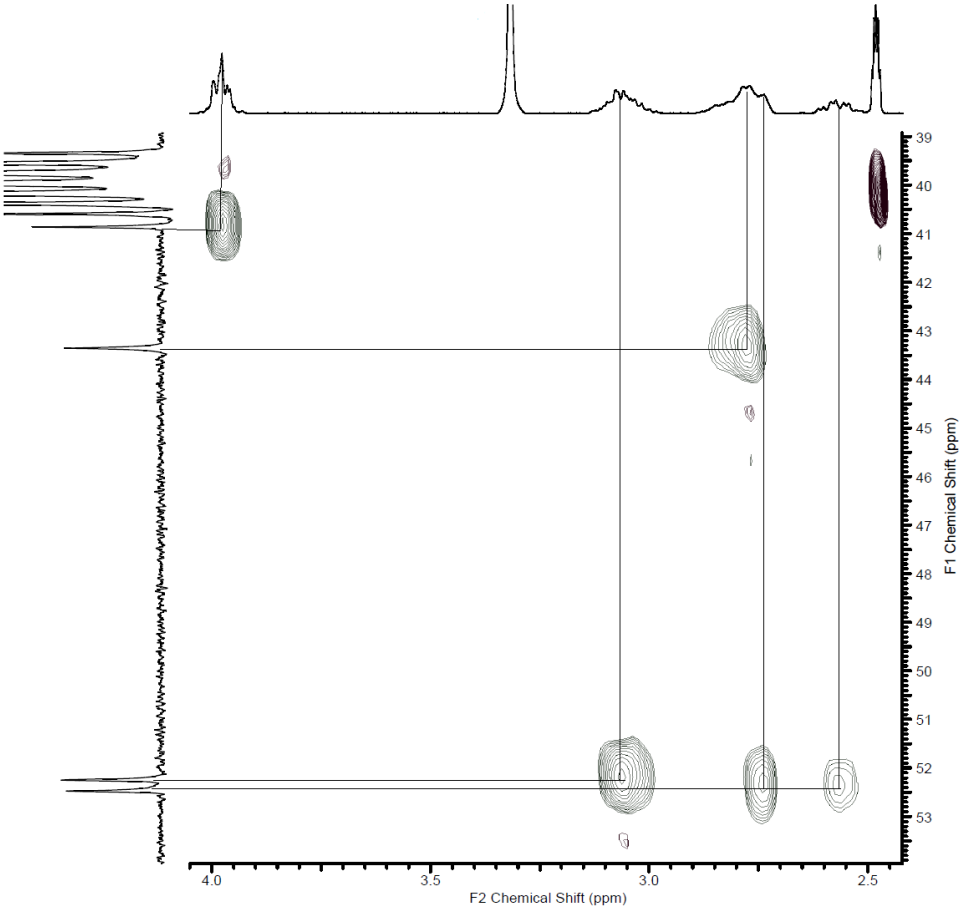

Figure 2.14. *gHSQC spectrum of* $[Co(Cl)_2(L3)_2]^+$, ***2.09***.

The gHSQC spectrum **H**eretonuclear **S**ingle **Q**uantum **C**orrelation provides chemical shift correlation between ^{1}H and ^{13}C having one-bond J-coupling of ~110 to 170Hz.

According to the above spectrum, C1 carbon appears more up field compared to the C5 and C4 which are closer to primary or secondary amine nitrogen atoms. Also it was observed that the carbon atoms directly attached onto secondary nitrogen atoms (C5)

appears more up field compared to the carbon atoms directly attached onto primary amine nitrogen atoms (C4).

The information obtained from HSQC spectra along with the ^{1}H NMR spectra supported the assigning of ^{13}C NMR peaks.

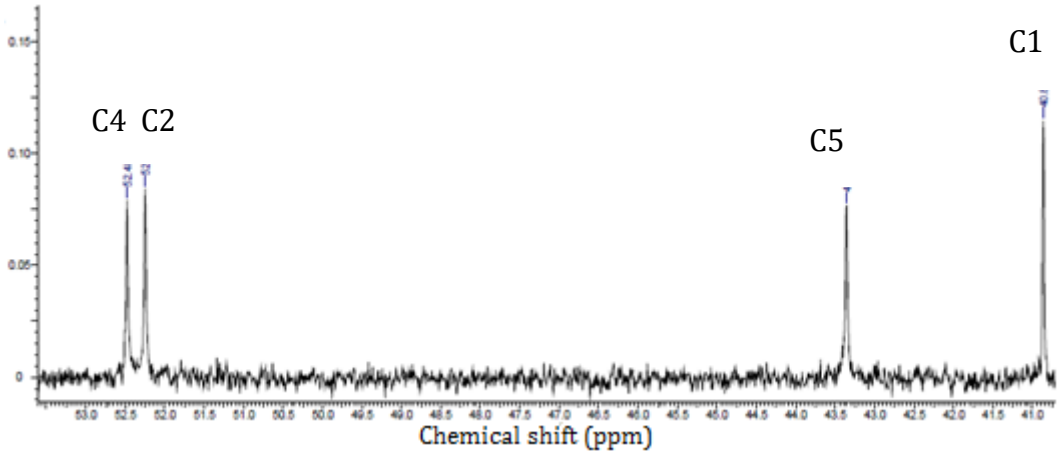

Figure 2.15. *^{13}C NMR spectra of $[Co(Cl)_2(L3)_2]^+$,* ***2.09.***

Slow evaporation of the very dilute solution of the complex in ethanol yielded green crystals suitable for X-ray crystallography studies. Mass spectrometric analysis and the NMR studies confirmed the presence of cobalt(III) complex in the crystalline material. The X ray crystal structure of the complex showed the presence of a chloride anion confirming (+1) total complex charge and cobalt(III) metal in the complex cation.

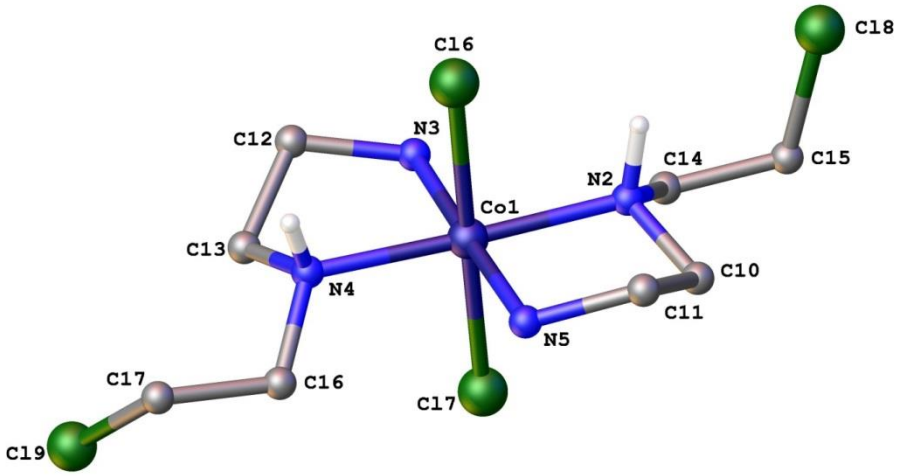

2.09

Figure 2.16. *X-ray crystal structure of $[Co(Cl)_2(L3)_2]^+$, **2.09**. Chloride anion and ethanol solvent molecules, as well as hydrogen atoms on the complex, except the hydrogen atoms on secondary amine nitrogen atoms, were omitted for the clarity.*

The asymmetric unit of the compound $[Co(Cl)_2(L3)_2]^+$;Selected bond lengths (Å) and bond angles (°); Co1-N4 1.9994(8), Co1-N3 1.9666(9), Co1-N2 1.9933(8), Co1-N5 1.9478(8), Co1-Cl6 2.2494(3), Co1-Cl7 2.2293(3), N2-C18 1.4805(1), C18-C19 1.5174(2), C19-Cl8 1.7950(1), N4-Cl4 1.4794(1), C14-C15 1.5124(2), C15-Cl9 1.7901(1), N2-Co1-N5 86.15(4), N3-Co1-N4 85.48(4), N2-Co1-N3 95.05(4), N5-Co1-N4 93.33(4), Cl6-Co1-N2 89.57(2), Cl6-Co1-N3 90.13(3), Cl6-Co1-N5 89.69(3), Cl6-Co1-N4 88.45(3), Cl6-Co1-Cl7 179.436(1), Cl7-Co1-N2 90.95(3), Cl7-Co1-N3 90.03(3), Cl7-Co1-N4 91.03(2), Cl7-Co1-N5 90.14(3).

The cobalt(III) complex, shown in

Figure **2.16**, was crystallised in the orthorhombic space group *Pbcn*. The asymmetric unit consisted of the complete cationic complex, two ethanol molecules and one chloride ion. The chloride ion was found in two different positions having half occupancies. The cobalt(III) complex possessed a distorted octahedral geometry. The two chloride ligands were *trans* to each other. The secondary amine nitrogen atoms were arranged *trans* to each other. Both the chiral nitrogen atoms, N2 and N4 have the *S* configuration. The chloride anion was hydrogen-bonded with one of the hydrogen

atoms on the stereogenic centre with the distance of 2.7553(8) Å, and the ethanol oxygen atom was hydrogen bonded with one of the primary amine hydrogen atoms with the distance of 2.3866(1) Å. Another hydrogen bonding interaction between a chloride anion and the ethanol hydroxyl hydrogen atom was observed with a distance of 2.2205(2) Å.

2.3.3 Synthesis of $[CoCl(L1)_2(NO_2)]^+$, 2.11,

The complex **2.11** is different from the precursor **2.06** by having substituted one of the nitrite ligands with chloride ligand only, as shown in Figure 2.8. The colour of the **2.11** is close to the appearance of starting material **2.06**.

The complex **2.11** was synthesised by reacting a methanolic (50 mL) solution of the precursor complex **2.06**, with 10 mL of $SOCl_2$ at room temperature and the stirring was continued overnight. The methanol solution became light pink in colour, still containing some unreacted precursor complex **2.06** suspended in the flask. The methanol solution was filtered and concentrated. Addition of ether to the solution yielded a light pink powder.

The pink powder was purified by using SP-C25 cation exchange column chromatography. The first eluted orange band was relevant to the *m/z* = 312.108 as shown in the Figure 2.17. The target complex **2.11** was eluted as a third orange colour band with 0.02M NaCl solution. The eluted band of complex **2.11** was desalted with numerous methanol extractions followed by G10 size exclusion chromatography to obtain the pure powdered material, after evaporating the solvent.

The mass spectrometric analysis of the powdered material showed the presence of **2.11** complex; m/z = 348.0839, ^{1}H NMR, and ^{13}C NMR analyses were used to characterise the **2.11** compound. The analysis results obtained suggested that **2.11** complex possessed one chloride and one nitrite ligand in the axial positions. One of the axial nitrite groups in **2.06** was replaced by a chloride ligand and the ^{1}H NMR spectrum is similar to that of the precursor complex **2.06**.

During the synthesis, the $SOCl_2$ react with methanol to form dimethoxy sulfoxide in the reaction mixture and it is an exothermic reaction. The heat produced during the reaction may have facilitated the substitution of one of the *N*-bound nitrite ligands with a chloride ligand.

The crystals suitable for X-ray crystallographic analysis were obtained by slow evaporation of concentrated methanolic solution of the compound **2.11**. The crystal structures that were obtained were highly disordered among the *N*-bound axial nitrite and a chloride ligand.

This reaction supported the findings of non-equality of axial nitrite ligands and also confirmed that one of the nitrite ligands is loosely bound to the cobalt(III) centre compared to the other nitrite ligand and under very mild reaction conditions the loosely bound nitrite ligand can be easily substituted with chloride ligands. The methanol alcohol medium contributed to stabilising the alcohol functional groups against chlorination.

If the reaction of **2.06** with $SOCl_2$ in methanol medium continued for a longer reaction time, or if there was a mild increase in temperature, the formation of $[Co(Cl)_2(L1)_2]^+$, **2.12** was observed, Figure 2.8, and also possible cobalt(III) complexes with **L1-H**

ligands were observed by mass spectrometric analysis, Figure 2.17. But the formation of nitrogen mustard complexes were not observed under any of these reaction conditions.

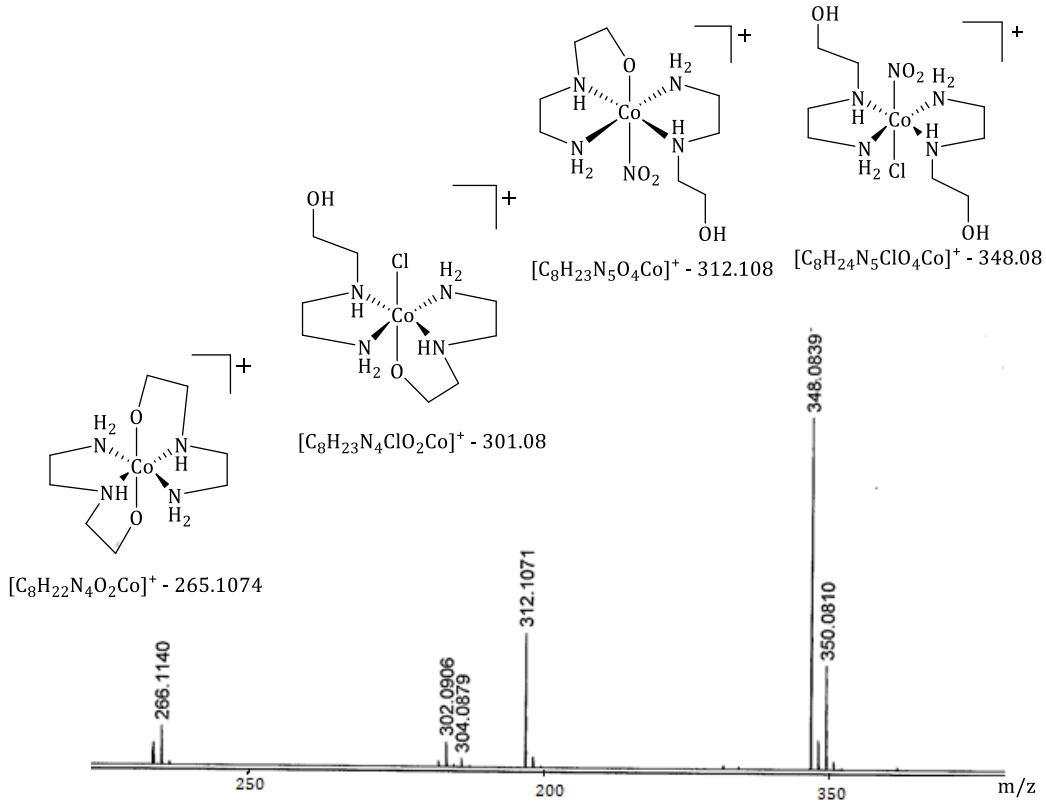

Figure 2.17. *Mass spectrum of complex **2.11**, showing other minor compounds formed during the synthesis.*

2.3.4 Synthesis of $[Co(Cl)_2(L1)_2]^+$, 2.12,

Complex **2.12** in Figure 2.8 is different from its starting material as it has two *trans* chloride ligands coordinated to the cobalt(III) centre due to the substitution of nitrite ligands on **2.06** complex.

The complex **2.12** is obtained by dissolving the precursor **2.06** in ethanol in the presence of conc. HCl, followed by continuous stirring of the mixture for 48 hours at

~70°C. After completion of the reaction the solvent was evaporated under vacuum and, the solid was dissolved into methanol. The product **2.12** was precipitated by addition of diethyl ether into the methanolic solution of the complex to yield a very sticky solid.

This residue was recrystallized from ethanol to give the complex as a bluish-green powdered material. The product was characterised by mass spectrometric analysis (*m/z* = 337.06), ^{1}H NMR, ^{13}C NMR spectroscopy, and X-ray crystallography. The bluish colour is unusual for *trans* dichloride cobalt(III) complexes, and may indicate the presence of a small amount of cobalt(II) contaminants, although not sufficient to affect the NMR analysis.

The NMR studies of the powdered material showed two fold symmetry of the complex in deuterated DMSO.

The slow evaporation of a 1:1 ethanol:water solution of **2.12** resulted the bottle green block shaped crystals (Yield: 20%) suitable for X-ray crystallographic studies.

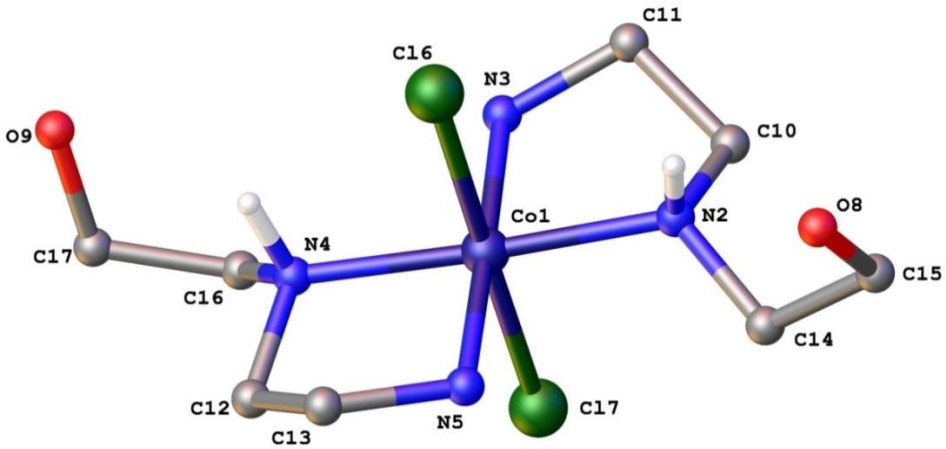

2.12

Figure 2.18. *X-ray crystal structure of $[Co(Cl)_2(L1)_2]^+$, **2.12**, with atom labelling. The diagram shows the trans **L1** ligands in trans dichloride complex. The chloride anion, ethanol solvent molecule and hydrogen atoms, except secondary amine hydrogens, were omitted for clarity.*

The asymmetric unit of the complex $[Co(Cl)_2(L1)_2]^+$; Selected bond lengths (Å) and bond angles (°); Co1-N2 1.955(3), Co1-N3 1.993(3), Co1-N4 1.998(3), Co1-N5 1.957(3), Co1-Cl6 2.2661(1), Co1-Cl7 2.2355(1), N3-C18 1.490(5), N4-C14 1.489(5), C18-C19 1.517(6), C14-C15 1.514(6), C19-O9 1.425(5), C15-O8 1.426(6), N2-Co1-N3 85.93(1), N4-Co1-N5 86.02(1), N2-Co1-N4 93.06(1), N3-Co1-N5 94.95(1), Cl6-Co1-Cl7 178.98(1), Cl6-Co1-N2 89.72(1), Cl6-Co1-N3 88.16(1), Cl6-Co1-N4 89.08(1), Cl6-Co1-N5 89.49(1).

The cobalt(III) complex crystallised in the triclinic space group Pī The asymmetric unit of the molecule contains a complete cobalt(III) cationic complex, with a chloride as an anion, and an ethanol molecule. The chloride ligands are *trans* to each other. Primary amine groups are *trans* to each other as well as the secondary amine are also arranged in a *trans* configuration.

Both the hydrogen atoms on the stereogenic nitrogen centres have S configuration.

When the bulk sample of **2.12** was dissolved in water, the solution changed from a bluish-green tint to purple. This may be due to the rapid ligand exchange of the axial chloride ligands with water molecules in the aqueous medium.

Another crystallisation experiment was set up by using the same bulk sample. The feather-like bluish crystals were obtained (yield: 5%) by slow diffusion of diethyl ether into a methanolic solution.

X-ray crystallographic analysis of these crystals confirmed the presence of **2.13**, Figure 2.8, a different isomer of the complex **2.12**.

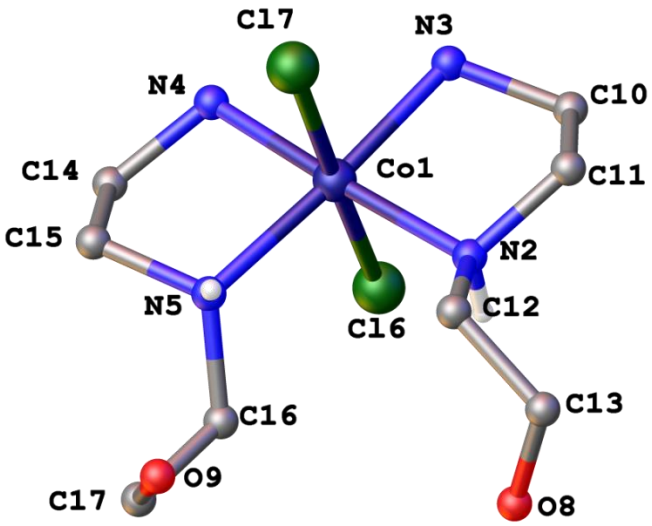

2.13

Figure 2.19. *X-ray crystal structure of $[Co(Cl)_2(L1)_2]^+$, **2.13**, with atom labelling. Chloride anion and the hydrogen atoms except the hydrogen atoms, on secondary amine hydrogens, were omitted for the clarity.*

The asymmetric unit of the complex $[Co(Cl)_2(L1)_2]^+$; Selected bond lengths (Å) and bond angles (°); Co1-N2 L16(3), Co1-N3 1.943(3), Co1-N4 1.955(4), Co1-N5 L16(3), Co1-Cl6 2.2524(1), Co1-Cl7 2.2483(1), N2-C12 1.487(5), N5-C16 1.495(5), C12-C13 1.514(6), C16-C17 1.518(5), C13-O8 1.427(5), C17-O9 1.422(5), Cl16-Co1-Cl17 178.21(4), N2-Co1-N3 86.32(1), N4-Co1-N5 86.48(1), N2-Co1-N5 97.07(1), N3-Co1-N4 90.18(1), Cl6-Co1-N2 89.57(1), Cl6-Co1-N3 88.32(1), Cl6-Co1-N4 87.95(1), Cl6-Co1-N5 92.72(1), Cl7-Co1-N2 90.99(1), Cl7-Co1-N3 90.02(1), Cl7-Co1-N4 91.31(1), Cl7-Co1-N5 88.9(1).

The X-ray crystal structure of the complex **2.13** was solved in $P2_1/n$ monoclinic space group. The asymmetric unit contains the complete cation with one chloride anion. The cobalt atom possesses a distorted octahedral geometry. Two chloride ligands were *trans* to each other. Primary amine groups are *cis* to each other leaving secondary amine nitrogen atoms *cis* to each other. Both the N5 and N2 stereogenic centres show S configuration.

The chloride anions in the coordination sphere are hydrogen bonded with the primary amine hydrogens having distances of 2.317(1) Å and 2.411(1) Å, respectively.

The comparison of calculated and experimental powder diffraction patterns were not in agreement. Many peaks observed in the calculated pattern were found in the experimental powder distribution; however, many extra peaks also appeared in the experimental powder pattern. That must be most likely due to the presence of other isomers, cobalt(II) impurities or contaminants.

Also the ^{1}H NMR and ^{13}C NMR spectra obtained for the crystalline material of complex **2.13** was highly complicated and noisy. This suggests the presence of different isomers of this complex and the broadening of the spectra suggest the presence of cobalt(II) ions in the medium.

The relative arrangement of the diamine ligands showed a different arrangement to the starting material **2.06**. This isomerisation is not surprising as we observed the presence of cobalt(II) impurity in the bulk material.

The synthesis of complex **2.13** demonstrated the suitable reaction conditions for the substitution of monodentate nitrite ligands with chloride ligands, without affecting (chlorinating) the hydroxyl groups. The stability of hydroxyl groups may be due to the solvent ethanol used during the reaction.

2.3.4.1 Synthesis of complex 2.09 using complex 2.12 as starting material

Reaction of the complex **2.12** with $SOCl_2$/DMF led to the formation of complex **2.11**. After the reaction, excess $SOCl_2$ was removed under vacuum, and the solid material was precipitated by adding ethanol. The powdered green material was characterised using

mass spectrometric analysis, ^{1}H NMR and ^{13}C NMR analysis, and the results were consistent with the compound **2.09** obtained from reaction route explained under the heading 2.3.2.

2.3.5 Tridentate binding of the L1 ligand, 2.15 to 2.17,

The uneven ligand substitution of axial nitrite ligands during the chlorination of alcohol groups in **2.06** led us to explore the possibility of changing the order of reactions to obtain **2.08**, Figure 2.8.

Therefore, the complex **2.06** was first reacted with HOTf aiming to synthesise the complex $[Co(L1)_2(OTf)_2]^+$, **2.18**. Then coordinate **2.18** with the ruthenium(II) centre to form the heterodinuclear complex. The chlorination of alcohol groups of **L1** ligands on cobalt(III) to be done later in the synthesis as shown in the Scheme 2.3.

The precursor **2.06** was reacted with neat HOTf under a nitrogen atmosphere, and the purple solid material was isolated by adding ether. The mass spectrometric analysis of the powdered material showed the presence of both **2.15** (m/z = 265.1069) and **2.14** (m/z = 415.30) complexes in the mixture, Figure 2.8. By increasing the amount of HOTf and increased reaction times, complex **2.14** can be completely converted to **2.15**.

In the presence of HOTf the nitrite ligands on **2.06** may have first been substituted by the OTf ligands. Due to the labile nature of the OTf ligand the alcohol oxygen become a strong electron donor to the central metal centre.

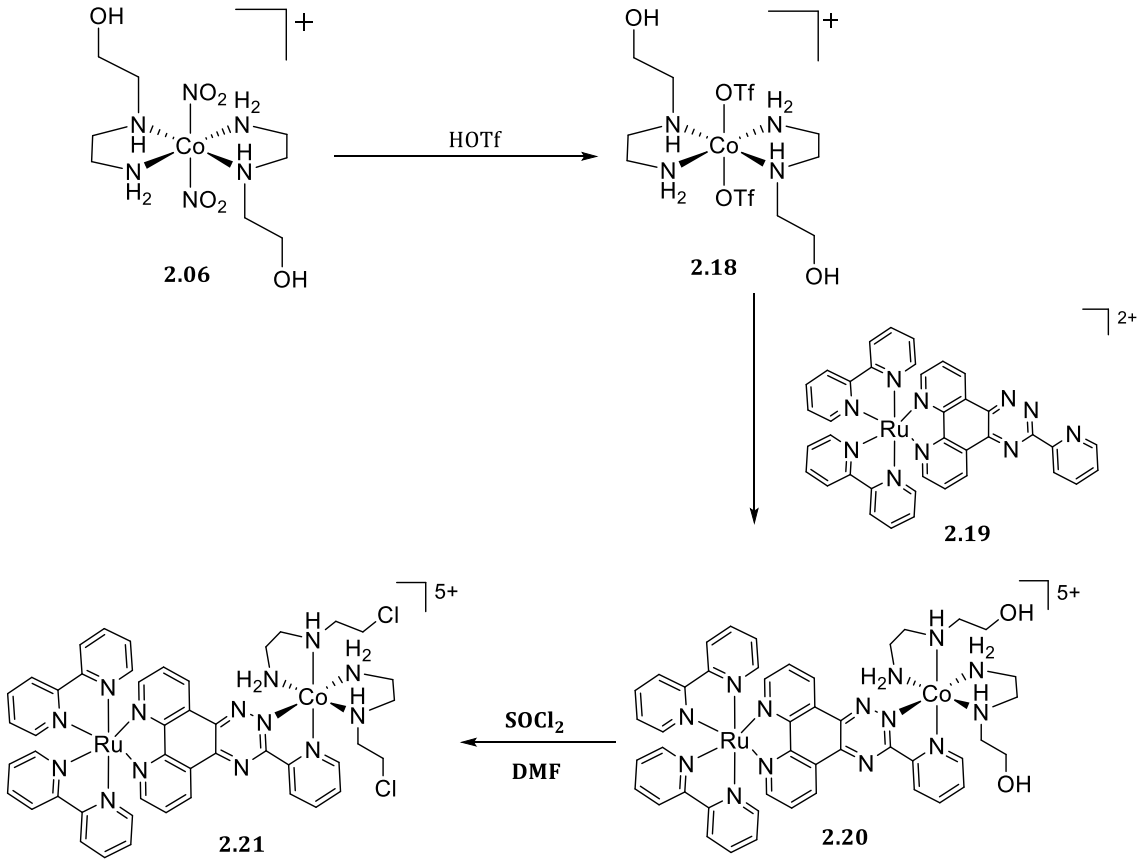

Scheme 2.3. *Proposed reaction scheme (II) for the synthesis of heterodinuclear complex.*

These complexes demonstrated the possible tridentate coordination of the **L1-H** ligand. Unfortunately, we were not able to separate **2.14** and **2.15** to characterise them separately at this stage. Similar tridentate binding behaviour of **L1-H** ligand was observed in the presence of moderately weaker chloride ligands too, Figure 2.17.

The complex **2.14** was identified from the mass spectrometric analysis, and could be an intermediate leading to the formation of complex **2.15**. Disappearance of *m/z* = 415.30 peak relevant to **2.14** in the spectrum with longer reaction times, confirmed that the complex favours tridentate binding of the ligand.

The tridentate binding of **L1-H** ligand with cobalt(III) was reported by Sarma *et al*.[129]. In their report, pH, solvent, the coordinated groups, and the relative metal to ligand

concentration were identified as the most important factors affecting the polydentate nature of the ligand.

According to Sarma *et al* the deprotonation of the acidic hydroxyl hydrogen is facilitated by the pH of the medium. Also after coordinating to the metal centre, the proton attached to hydroxyl oxygen becomes highly acidic and is easily lost under higher pH conditions.[122]

2.3.4.2 Synthesis of complex $[Co(L1\text{-}H)_2]^+$ under high pH conditions

The precursor **2.06** was stirred in an aqueous solution of NaOH (pH = 13) overnight, and the resulting brownish red material was collected after removing the solvent under reduced pressure. The residue was dissolved into a minimal amount of methanol and filtered and dried under the reduced pressure to obtain the pink powdered material. The residue was characterised by mass spectrometric analysis, (m/*z* = 265.1069), as **2.15**/ **2.16** /**2.17**. The most acidic proton on the coordinated hydroxyl group was removed under high pH conditions. According to Bailar *et al*.[124] vacating of the sites occupied by nitrite ligands must be facilitated by high pH conditions.[129] Therefore, the total system can achieve high thermodynamic stability having tridentate ligands around the central metal.

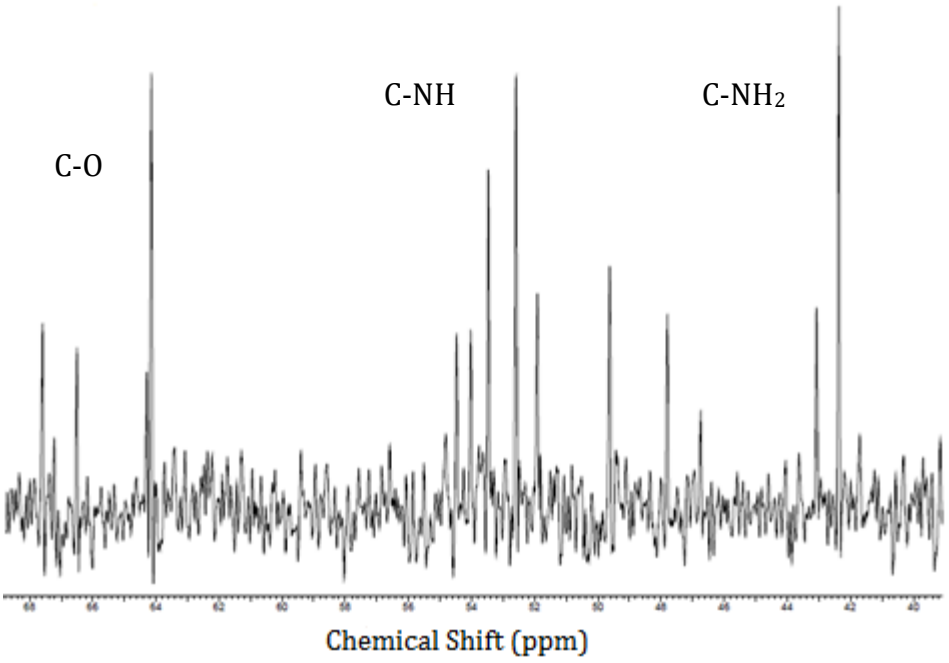

Figure 2.20. *^{13}C NMR spectrum of the bulk sample of **2.15**, **2.16**. and **2.17** recorded in D_2O.*

The ^{13}C NMR analysis of the above complex seemed complicated, as ^{13}C NMR spectrum showed fourteen different peaks. The ^{13}C NMR peaks were distributed into three different groups in the spectrum. The results were not very surprising, as there are many possible isomers as shown in the Figure 2.21.

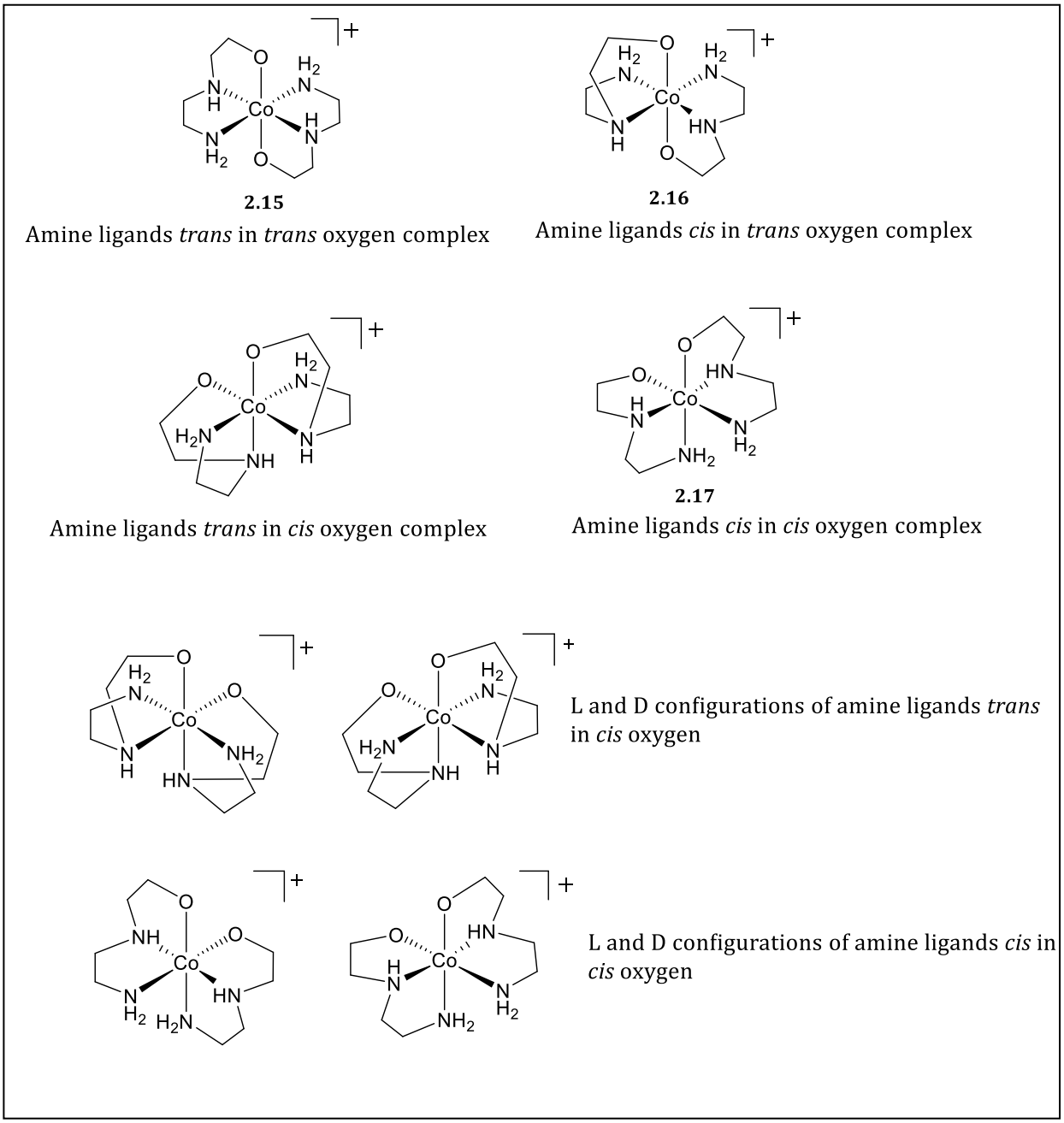

Figure 2.21. *Possible facial isomers of the complex* $[Co(L1\text{-}H)_2]^+$.

The **2.16** complex was crystallised by adding aqueous PF_6^- ions to the medium. The crystals suitable for the X-ray crystallography were grown after exchanging the chloride anion with a PF_6^- anion. Diffusion of diethylether into a methanolic solution of the complex yields bright red crystals suitable for X-ray crystallography.

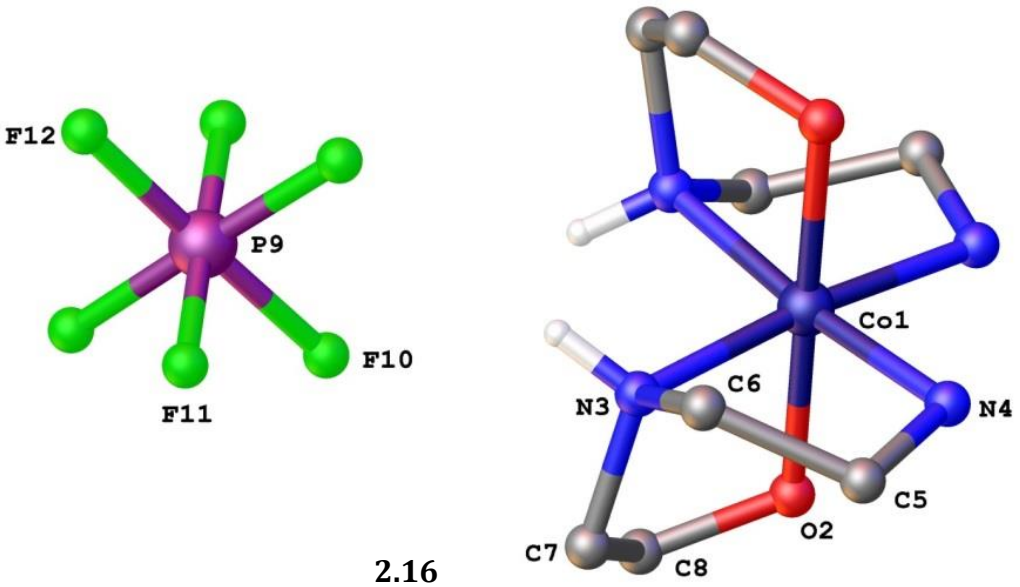

2.16

Figure 2.22. *X-ray crystal structure of* $[Co(L1\text{-}H)_2]^+$, ***2.16****, complex with atom-labelling showing cis amine trans oxygen conformation. Hydrogen atoms on the cationic complex, except chiral hydrogen atoms, were omitted for clarity.*

The molecular structure of the complex $[Co(L1\text{-}H)_2]^+$; Selected bond lengths (Å) and bond angles (°); Co1-O2 1,9082(2), Co1-N3 1.967(2), Co1-N4 1.932(2), O2-C8 1.406(3), N4-C5 1.484(4), N3-C6 1.482(3), 1.486(4), C7-C8 1.525(3), C5-C6 1.517(4); O2-Co1-N3 86.20(6), O2-Co1-N4 91.32(8), N3-Co1-N4 86.7(1)

X-ray crystal structure of the complex **2.16** was solved in orthorhombic *Pbcn* space group. The asymmetric unit of the complex consists of half of the cationic complex and half of the hexafluoridophosphate anion. The complex shows distorted octahedral geometry. The two oxygen atoms from the alcohol groups coordinate in *trans* manner. The *cis* primary amine nitrogen atoms and *cis* secondary amine nitrogen atoms completed the octahedral configuration around the metal centre. The hydroxyl groups were deprotonated. The fluoride atoms of the PF_6^- anion were hydrogen bonding with the secondary amine hydrogens, with the distance of 2.43(3) Å and also with the hydrogen atoms on C8 with the distance of 2.47(2) Å. Also another hydrogen bond was

observed between primary amine (N4) hydrogens and oxygen (O2) atoms with the distance of 2.03(2) Å.

There are a few incomplete literature reports about different alkoxide complexes [123], [130] and further studies were carried out to understand the chemistry of $[Co(L1\text{-}H)_2]^+$ under different reaction conditions.

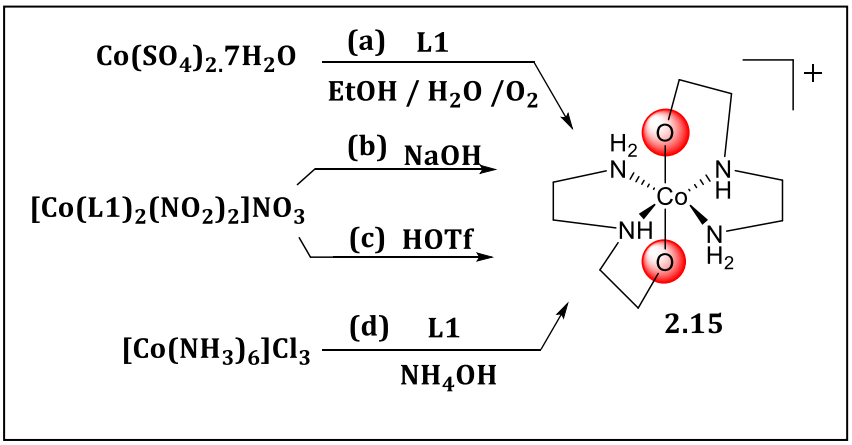

Figure 2.23. *Other possible reaction pathways for the synthesis of complex $[Co(L1\text{-}H)_2]^+$. Only one isomer of the complex $[Co(L1\text{-}H)_2]^+$ is shown in the figure.*

Reaction path (a), Figure 2.23 was described by Kotovaya *et al.*[130] during the synthesis of tris(2-aminoethanolato)cobalt (III) complexes having sulphate as an anion.

During the synthesis, **L1** was added dropwise with stirring to $CoSO_4 \cdot 7H_2O$ dissolved in 2:1, aq. ethanol mixture. The obtained red coloured solution was left for slow evaporation.

The complex $[Co(L1\text{-}H)_2]^+$ was also synthesised by reaction of the precursor complex, **2.06 ,** with either aq. NaOH or neat HOTf, as discussed in previous sections.

Reaction path (d), Figure 2.23 was discussed by Sarma *et al.*[129] in literature for the synthesis of the complex $[Co(L1\text{-}H)_2]^+$. The synthesis was done by reacting $[Co(NH_3)_6]Cl_3$ with **L1** in the presence of activated charcoal and ammonium hydroxide.

The complex **2.19** is shown in the Figure 2.24 is isolated as its iodide salt. The plate-like red crystals suitable for X-ray diffraction analysis were obtained by the slow evaporation of the aqueous solution of the complex. The total complex charge of **2.19** is (+2) due to only one of the de-protonated **L1-H** ligands.

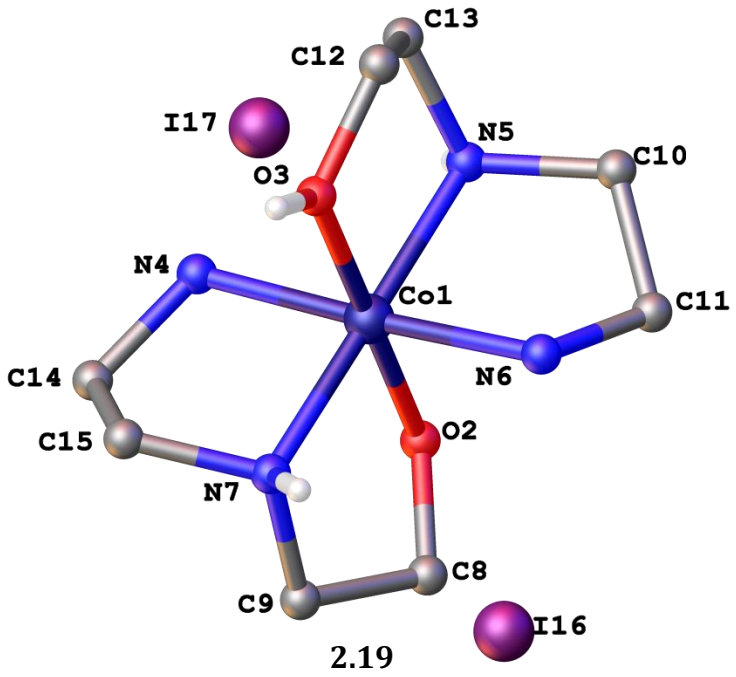

Figure 2.24. *X-ray crystal structure of $[Co((L1)L1\text{-}H)]^{2+}$, **2.19**, complex with atom labelling. The hydrogen atoms except the N7 and O3 hydrogen atoms were omitted for clarity.*

The molecular structure of $[Co(L1)(L1\text{-}H)]^{2+}$: Selected bond lengths (Å) and bond angles (°); Co1-O2 1.8921(2), Co1-O3 1.9170(2), Co1-N4 1.9513(2), Co1-N5 1.9619(2), Co1-N6 1.9482(2), Co1-N7 1.9551(2), O3-Co1-O2 179.73(7), O3-Co1-N4 87.11(8), O3-Co1-N5 85.31(7), O3-Co1-N6 90.46(7), O3-Co1-N7 94.13(7), O2-Co1-N4 92.69(8), O2-Co1-N5

94.88(7), O2-Co1-N6 89.75(7), O2-Co1-N7 85.69(7), C8-O2-Co1 108.60(1), Co1-O3-C12 113.85(1).

The crystal structure of the complex was solved in monoclinic space group $P2_1/c$. Two of the ligands were arranged in distorted octahedral geometry around the cobalt(III) metal centre showing a tridentate binding fashion for the each ligand. The two ligands were different with respect to the protonation state. This structure represents the *trans* amine, *trans* oxygen isomer of the complex. In the coordination sphere, two fully occupied iodide atoms confirms the (2+) charge of the complex cation; one of the (+) charge generated from the cobalt(III) metal centre, while the other (+) charge added from the protonated O3 oxygen atom. The prominent electron density close to O3 confirms the attached hydrogen during structure solution.

The experimental powder diffraction pattern of the bulk material of the **2.19** had extra peaks that didn't appear in the calculated powder diffraction pattern of the single crystal. This data clearly represent the presence of some contaminant or possibly a different isomer of the **2.19** present in the bulk material, and confirmed that the bulk sample is different from the single crystals.

Due to insufficient sample size, NMR spectrometry or elemental analysis were not possible. In solution state both the ligands will be chemically similar due to the fast exchange of O3 hydrogen atoms.

2.3.4.3 Complexes of $[Co(L1\text{-}H)_2]^+$ with $ZnCl_2$ or $MnCl_2$, 2.20 to 2.22,

Previously discussed ^{13}C NMR analysis of the bulk sample of $[Co(L1\text{-}H)_2]^+$.and the X-ray crystallographic studies of the **2.16** and **2.19** complexes suggested the presence of possible isomers.

The attempts to separate the different isomers of $[Co(L1\text{-}H)_2]^+$ complex using cation exchange SP-C25 column chromatography were unsuccessful. Two different isomers **2.16** and **2.19** were already presented in section 2.3.4.

During this research a new synthetic route was developed to identify different isomers of complex $[Co(L1\text{-}H)_2]^+$ by reacting them with $ZnCl_2$ /$MnCl_2$ salts.

However, apart from identifying different isomers of the complex $[Co(L1\text{-}H)_2]^+$ a new coordination chemistry of the $[Co(L1\text{-}H)_2]^+$ complex was also discovered.

These complexes showed that the oxygen atom on alkoxide complexes is capable of coordinating with metal centres like zinc(II) or manganese(II) to form heteropolynuclear complexes and here we report some of the heteropolynuclear complexes of **2.15** and **2.17** with $ZnCl_2$ or $MnCl_2$ metal salts.

The solid material obtained from the reaction path (d), Figure 2.23 was dissolved in methanol to obtained reddish purple solution and mixed with a methanolic solution of $ZnCl_2$. The mixture was heated, resulting in a pink solution. The pink reaction mixture was analysed by mass spectrometry. The mass spectrum shows the peaks that can be assigned to the following complexes:

$[C_8H_{22}N_4O_2Co_1]^+$ $[Co(L1\text{-}H)_2]^+$ = *m/z* =265.1050

$[C_8H_{22}N_4O_2Cl_2Zn_1Co_1]^+$ =*m/z*=398.9721

$[C_8H_{22}N_4O_2Cl_4Zn_2Co_1]^+$ = *m/z* =532.8406

The identified peaks relevant to above complex cations suggested the possible complexation of $ZnCl_2$ with complex $[Co(L1\text{-}H)_2]^+$

The obtained pink solution was filtered, and left for slow evaporation. The pink plate like crystals appeared in the solution were analysed by ^{13}C NMR spectroscopy and gave a highly complicated noisy spectrum.

The plate-like pink crystals that appeared in the solution (Yield: 22%) were suitable for X-ray crystallography. Randomly selected crystals from the bulk material were analysed by X-ray crystallography.

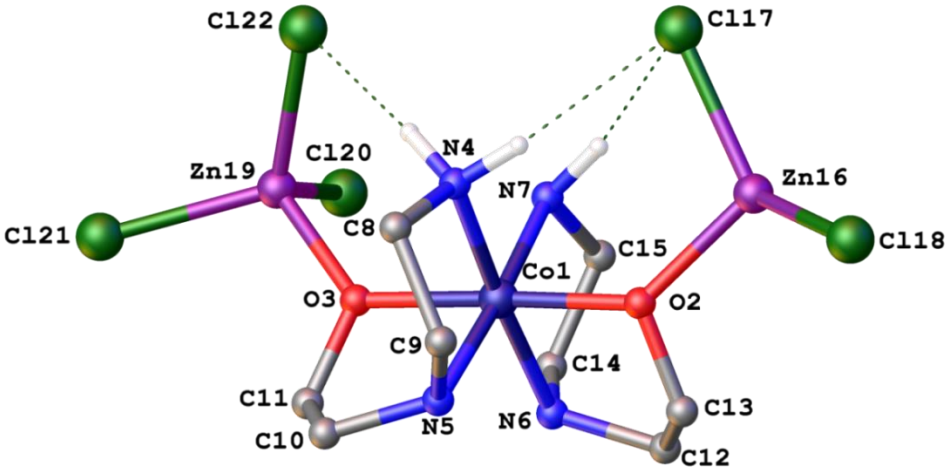

2.20

Figure 2.25. *Asymmetric unit of the complex **2.20** with atom-labelling. The picture showed the cis amine trans oxygen isomer of the complex forming trinuclear complex with $ZnCl_2$. Three of these inter connected units were present in the molecular structure.*

Molecular structure of $[Co(Cl_5)(L1\text{-}H)_2Zn_2]$; Selected bond lengths (Å) and bond angles Co1-O2 1.9177(2), Co1-O3 1.9192(2), Co1-N4 1.963(1), Co1-N5 1.9764(1), Co1-N6 1.969(4), Co1-N7 1.958(1), O2-Zn16 1.9807(1), O3-Zn19 1.9765(1), Zn19-Cl17 2.2387(2), Zn16-Cl18 2.2027(2), Zn19-Cl20 2.2640(1), Zn19-Cl21 2.2872(1), Zn19-Cl22

2.2393(2). O2-Co1-N6 85.26(4), O2-Co1-N5 1.915(1), O2-Co1-N4 90.838(6), O2-Co1-N7 91.327(6), O3-Co1-N4 1.919(1), O3-Co1-N5 84.644(6), O3-Co1-N6 93.852(6), O3-Co1-N7 90.969(6), Zn16-O2-Co1 133.894(5), Zn16-O2-C13 1.8206(1), Cl17-Zn16-Cl18 122.326(1), Cl18-Zn16-O2 109.683(5), Cl17-Zn16-O2 108.22(6), Zn19-O3-C11 120.236(5), Zn19-O3-Co1 130.43(5), Cl20-Zn19-O3 106.370(6), Cl21-Zn19-O3 110.440(5), Cl22-Zn19-O3 108.274(6).

The complex crystallises in *Pī* space group. The asymmetric unit of the complex consist of one cobalt(III) alkoxide complex with coordinated two $ZnCl_2$ molecules with *trans* oxygen atoms making a trinuclear metal complex. The positive charge of the complex is balanced by the presence of extra chloride atom on one of the zinc(II) metal centres. There is no significant change to be noticed in Co-O bond lengths between the **2.20** and **2.16** structures.

The alkoxide complex, found within the **2.20** trinuclear complex is another possible isomer of $[Co(L1\text{-}H)_2]^+$ and identified as **2.15**.

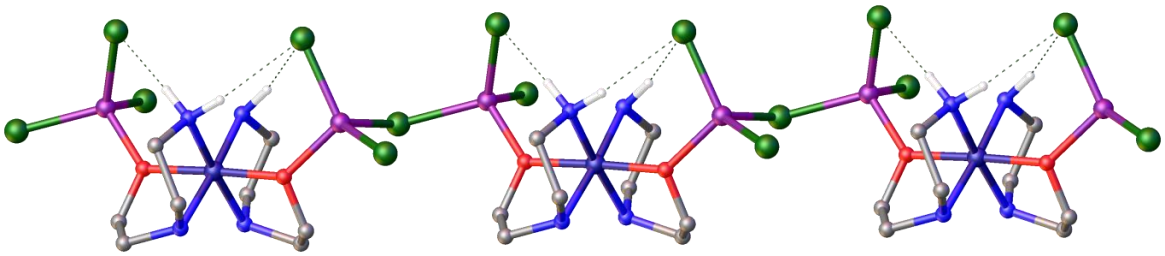

Figure 2.26. *The molecular structure of complex **2.20** showing connection of three units via chloride bridging.*

The molecular structure of the trinuclear complex shows the presence of three asymmetric units. Each of these units is bridging through chlorine atoms.

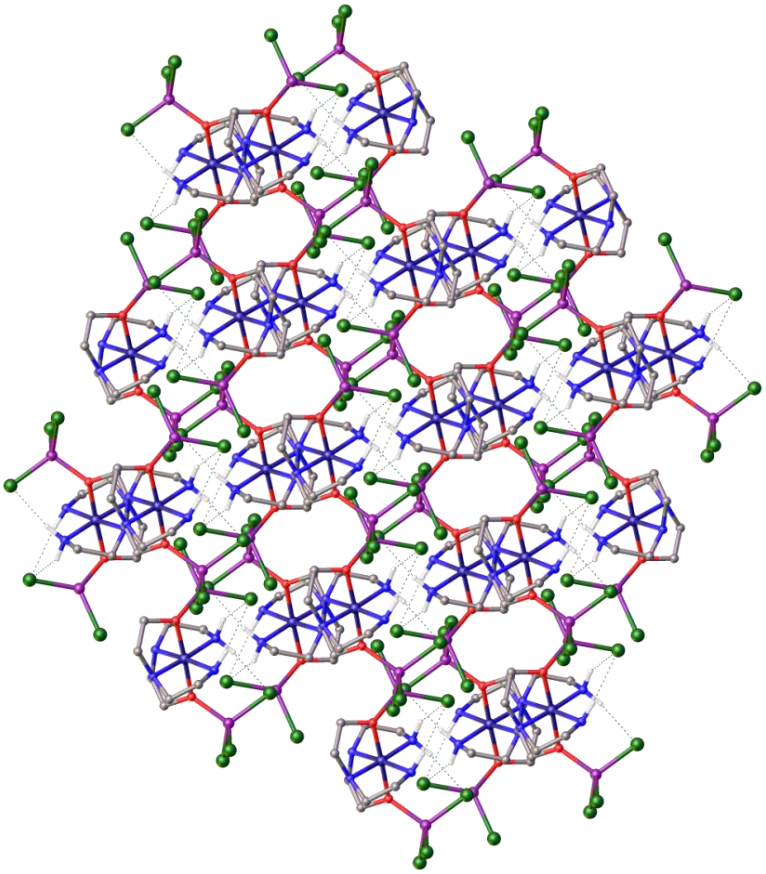

Figure 2.27. *Packing structure of the complex **2.20** through 011 planes showing the cavities present in the packing structure.*

The view of the packing structure through 011 planes shows the large empty cavities along the plane. Intermolecular hydrogen bonds are observed between primary amine hydrogen atoms and chloride atoms in the distance of 2.385Å. Intramolecular hydrogen bonds were observed between the secondary amine hydrogen atoms and the adjacent chloride atoms in the distance of 2.401 Å.

All the crystals in the bulk sample were similar in appearance. However, the X-ray crystallographic analysis of another crystal obtained from the same batch happened to be structurally different to the previously obtained crystal structure, Figure 2.28.

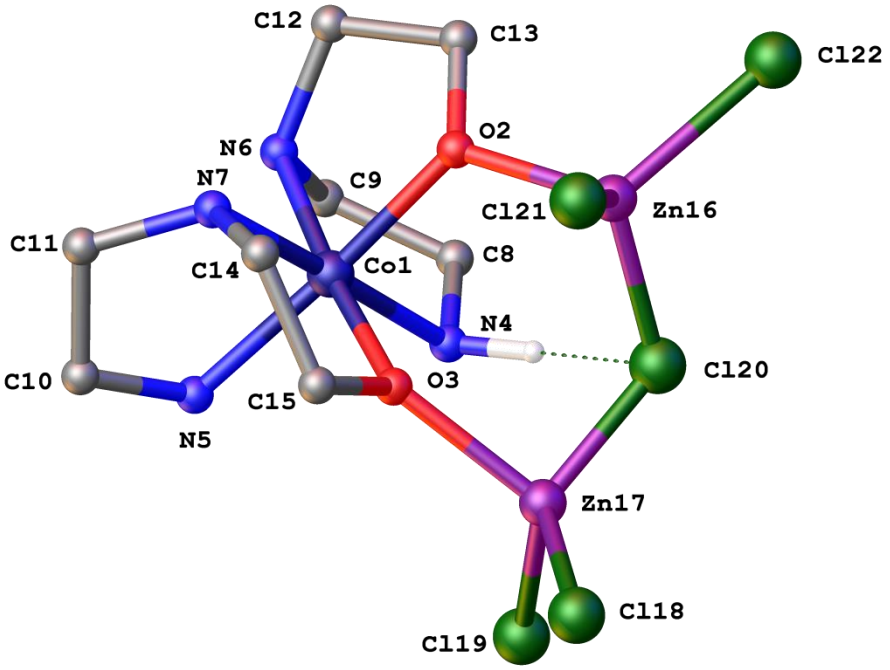

2.21

Figure 2.28. *Molecular structure of **2.21** with atom-labelling. The structure shows the presence of cis oxygen cis amine isomer complexing with $ZnCl_2$ making a trinuclear complex. The solvent water molecules and all the hydrogen atoms except the hydrogen on N4 were omitted for the clarity.*

The molecular structure of $[Co(Cl)_5(L1\text{-}H)Zn_2]$; Selected bond lengths (Å) and bond angles(°); Co1-N4 1.966(5), Co1-N5 1.955(4), Co1-N6 1.949(5), Co1-N7 1.956(5) , Co1-O2 1.957(4), Co1-O3 1.911(4), O2-Zn16 1.975(4), O3-Zn17 1.983(4), Zn16-Cl20 1.956(4), Zn17-Cl20 1.938(4), Zn16-Cl22 2.266(2), Zn16-Cl21 2.269(2), Zn17-Cl18 2.268(2), Zn17-Cl19 2.229(2). N5-Co1-O3 90.6(2), N7-Co1-N5 85.2(2), N5-Co1-O3 90.6(2), N6-Co1-N5 93.7(2), N6-Co1-O2 86.11(2), O2-Co1-O3 89.7(2), O2-Co1-N4 90.53(2), N4-Co1-N5 93.4(2), O2-Zn16-Cl20 104.26(2), O3-Zn17-Cl20 92.74(2), Zn16-Cl20-Zn17 114.92(2).

The complex **2.21** is crystallised in the *Aea 2* space group. The molecular structure of the alkoxide complex shows the *cis* amine *cis* oxygen isomer co-ordinating with $ZnCl_2$, *via* polydentate oxygen atoms forming trinuclear metal complex. Each of the *cis* oxygen atoms of the alkoxide complex is coordinated with zinc(II) metal centres. Each zinc(II)

atom shows tetrahedral geometry having three chlorine atoms and one oxygen atom coordinated. The two zinc(II) metal centres are bridged through a chlorine atom. There are three water molecules located in the sphere of the asymmetric unit of the molecule. Intramolecular hydrogen bonding is observed between one of the primary amine hydrogens and the bridging chlorine atom with the distance of 2.143 Å and intermolecular hydrogen bonding is observed between one of the primary amine hydrogens and one of the water molecules in the sphere with the distance of 2.098Å. The total complex is neutral in charge.

Reaction of the methanolic solution the complex $[Co(L1\text{-}H)_2]^+$ with the methanolic solution of $MnCl_2.4H_2O$ resulted a pink colour solution, The reaction mixture was filtered and left for slow evaporation, the small red crystals formed (yield: 13%) were analyse by mass spectrometry and X-ray crystallography. The mass spectrometric analysis of the sample shows the presence of cobalt(III) alkoxide complex. However none of the fragments represent the complexation of alkoxide complex with the $MnCl_2$.

The X-ray crystallographic analysis of the crystals represents the *cis* amine *cis* oxygen isomer complexing with $MnCl_3$ molecules to form a dinuclear complex.

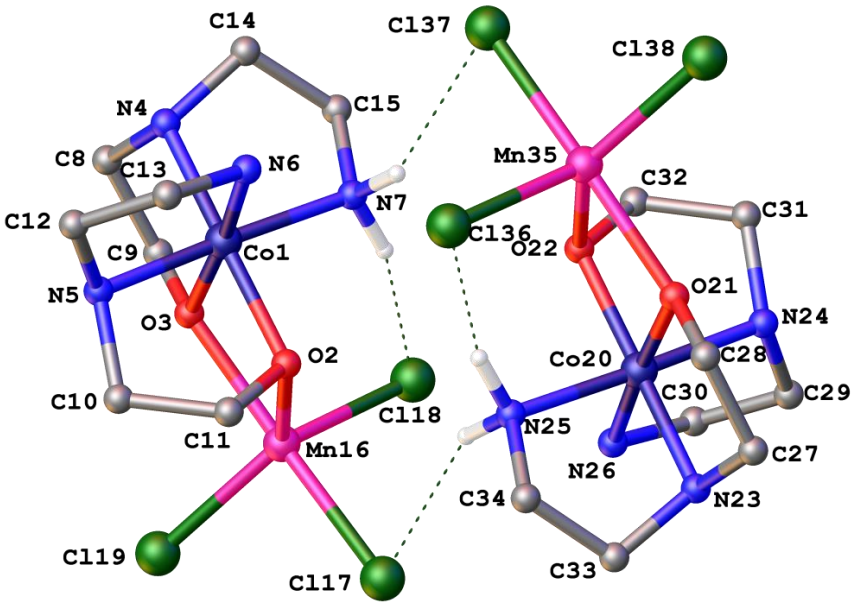

2.22

Figure 2.29. *X-ray crystal structure of **2.22** with atom-labelling. The two structures present in the asymmetric unit are related to each other from their molecular symmetry. The hydrogen atoms in the structure, except the primary amine hydrogens, were omitted for the clarity.*

Molecular structures of $[Co(Cl)_3(L1\text{-}H)_2Mn_2]$; Selected bond lengths (Å) and bond angles(°); Co1-N4 1.953(5), Co1-N5 1.9785(6), Co1-N6 1.973(5), Co1-N7 1.968(7), Co1-O2 1.906(4), Co1-O3 1.888(5), Mn16-O2 2.209(5), Mn16-O3 2.124(5), Mn16-Cl17 2.474(7), Mn16-Cl18 2.426(7), Mn16-Cl19 2.413(8), Co20-N23 1.9642(5), Co20-N24 1.96644(6), Co20-N26 1.98(5), Co20-O21 1.8825(5), Co20-O22 1.8855(4), Mn35-O21 2.1294(5), Mn35-O22 2.2008(5), Mn35-Cl36 2.4281(7), Mn35-Cl37 2.4636(7), Mn35-Cl38 2.4147(8), N4-Co1-N5 97.80(2), N5-Co1-N6 85.13(2), N5-Co1-O2 87.71(2), N5-Co1-O3 89.02(2), N7-Co1-O2 1.968(7), N7-Co1-O3 93039(2), N7-Co1-N4 1.962(6), N7-Co1-N6 1.965(7), O2-Mn16-O3 71.55(3), O2-Mn16-Cl18 110.168(2), O2-Mn16-Cl17 87.73(3), O2-Mn16-Cl19 131.857(2), O3-Mn16-Cl18 2.1147(5), O3-Mn16-Cl17 158.569(3), O3-Mn16-Cl19 94.123(2), N24-Co20-O21 88.813(4), N24-Co20-O22 87.455(2), N24-Co20-N23 97.568(2), N24-Co20-N26 86.093(2), N25-Co20-O22 90.1078(2), N21-Co20-O 21 92.253(2), N25-Co20-N23 85.168(2), N25-Co20-N26 92.116(2), O21-Mn35-O22 71.181(3), O22-Mn35-Cl36 108.044(2), O22-Mn35-Cl37

89.157(3), O22-Mn35-Cl38 135.979(1), O21-Mn35-Cl36 95.1214(2), O21-Mn35-Cl37 159.546(2), O21-Mn35-Cl38 93.937(2).

The X-ray crystal structure of the complex **2.22** was solved in $P2_1/n$ monoclinic space group. The asymmetric unit consists of two dinuclear complexes which are similar in molecular symmetry. The total complex charge is neutralised by the chlorine atoms on the manganese(II) metal centre. The two *cis* oxygen atoms of the alkoxide complex were directly coordinating to the manganese metal centre. The manganese(II) centre showed the trigonal pyramidal geometry.

There is intramolecular hydrogen bonding between one of the primary amine hydrogens and one of the chlorine atoms. Also intermolecular hydrogen bonding is observed between primary amine hydrogens with chlorine atoms on the adjacent molecule.

X-ray crystallographic analysis of the complex bulk sample confirmed the formation of three different isomers, Figure 2.30 in the reaction mixture. The fourth possible isomer with the two oxygens *cis* and the two amine groups *trans* was not observed.

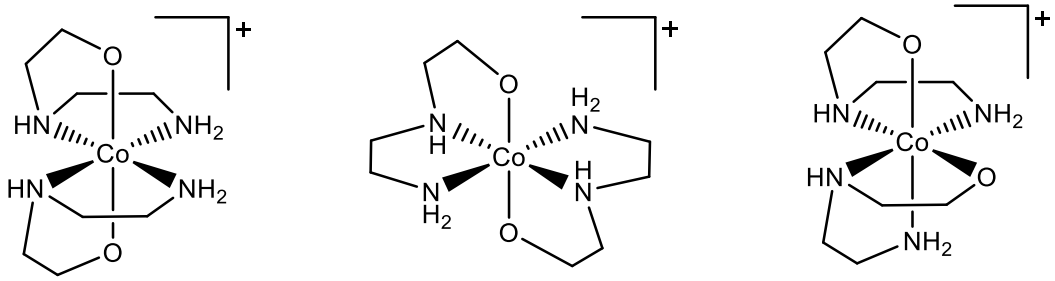

2.16 **2.15** **2.17**

Figure 2.30. *Three different isomers of the $[Co(L1\text{-}H)_2]^+$ complex.*

Each of the isomer shown in the Figure 2.30 will give rise to four signals in ^{13}C NMR spectroscopy. In combination we are expecting twelve different carbon peaks. ^{13}C NMR spectrum of the bulk sample shown in Figure 2.20 consists of fourteen different peaks and these three isomers most likely represent the twelve of those peaks.

2.3.4.4 Use of $[Co(L1\text{-}H)_2]^+$ for the synthesis of 2.09

The isomeric mixture of the bulk sample was reacted with $SOCl_2$/DMF reagent to investigate the possibility of opening the Co-O bond while introducing chloride ligands to satisfy the coordination sphere. At higher temperatures formation of **2.09** was observed. The reaction needs a longer reaction time compared to a normal alcohol chlorination reaction. The reaction was monitored by mass spectrometry to confirm the complete conversion of complex **2.15** to **2.09**. The disappearance of m/z: 265.1080 peak was monitored with the complete conversion and reaction mixture turned to a green colour. Once the reaction was completed, excess $SOCl_2$ was removed under reduced pressure. Cold ethanol was added to the obtained green coloured slurry. First ethanol washing of the complex was discarded and the green powdered material was obtained by further trituration of thick green slurry was filtered and washed with cold ethanol. The green powdered material was analysed by mass spectrometry and NMR spectroscopy.

Mass spectrometric analysis of the green powdered material shows the presence of $[Co(Cl)_2(L3)_2]^+$ complex at m/z: 374.9903. However we identified three possible isomers in the starting material, Figure 2.30. These three different isomers can result in three different isomers of the chlorinated products as shown in Figure 2.31.

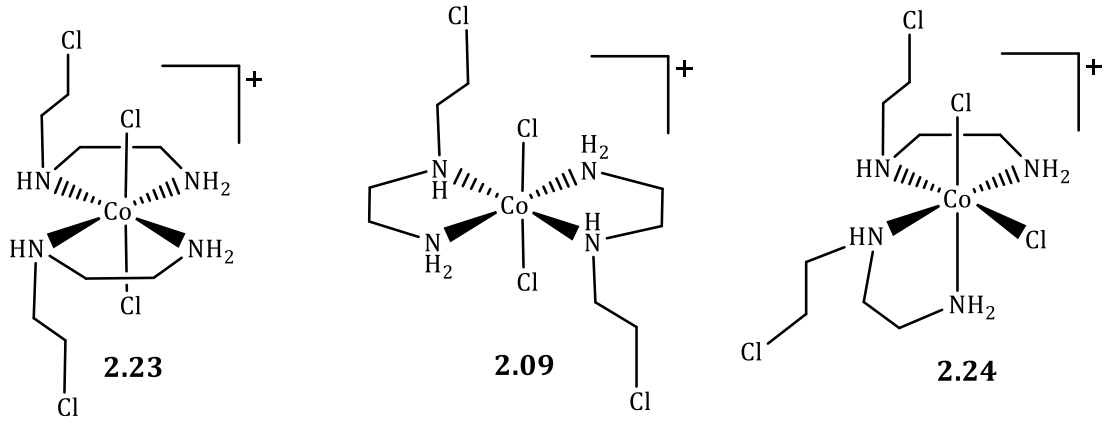

Figure 2.31. *Possible isomers of $[Co(Cl)_2(L3)_2]^+$ complex.*

However we only managed to isolate the **2.09** complex in the bulk sample and the presence of **2.09** was confirmed by NMR studies.

2.3.6 Synthesis of $[Co(L3)_2(NO_2)_2]^+$, 2.08,

The complex **2.08**, Figure 2.8, is interesting to us as it contains *trans* dinitrite ligands and two nitrogen mustard molecules coordinated with the cobalt(III) metal centre. As our final goal is to connect this nitrogen mustard cobalt(III) complex on to the $[Ru(bpy)_2(pytp)]^{2+}$ complex, the nitrite ligands can be easily converted to highly labile triflate (OTf) ligands by reacting with trifluoromethanesulfonic acid (HOTf).

When the chlorination of the alcohol was done using **2.06** at room temperature we observed the formation of complex **2.07**. The complex **2.07** showed the substitution of one of the axial nitrite ligands with chloride ligand as discussed in the section 2.3.1.

Hence we explored different reaction conditions to avoid this ligand substitution of nitrite by chloride as we were interested in having nitrite ligands in both axial positions.

A variety of modifications were introduced to the synthesis procedure, such as lowering reaction temperature. When the reaction temperature was lowered, the formation of complex **2.08** was observed along with the complex **2.07**.

The **2.08** was synthesised by reacting **2.06** with $SOCl_2$/DMF pair below 0°C. The reaction mixture was kept in the ice/salt bath throughout the reaction. The reaction was continued for eight hours to complete the reaction and the excess $SOCl_2$ was removed under vacuum. The crude product was further purified using SP-C25 cation exchange column, the yellow coloured band eluted with 0.01M NaCl was collected and desalted to obtaine (Yield:64%) the complex **2.08**. The complex was characterised using mass spectrometric analysis (m/z = 395.0407), NMR spectrometric techniques and elemental analysis.

^{1}H NMR spectrum of the complex **2.08** showed the presence of seven different multiplets relevant to eight different hydrogen atoms.

The assigning of the peaks is supported by *g*COSY and HSQCAD NMR spectroscopic techniques.

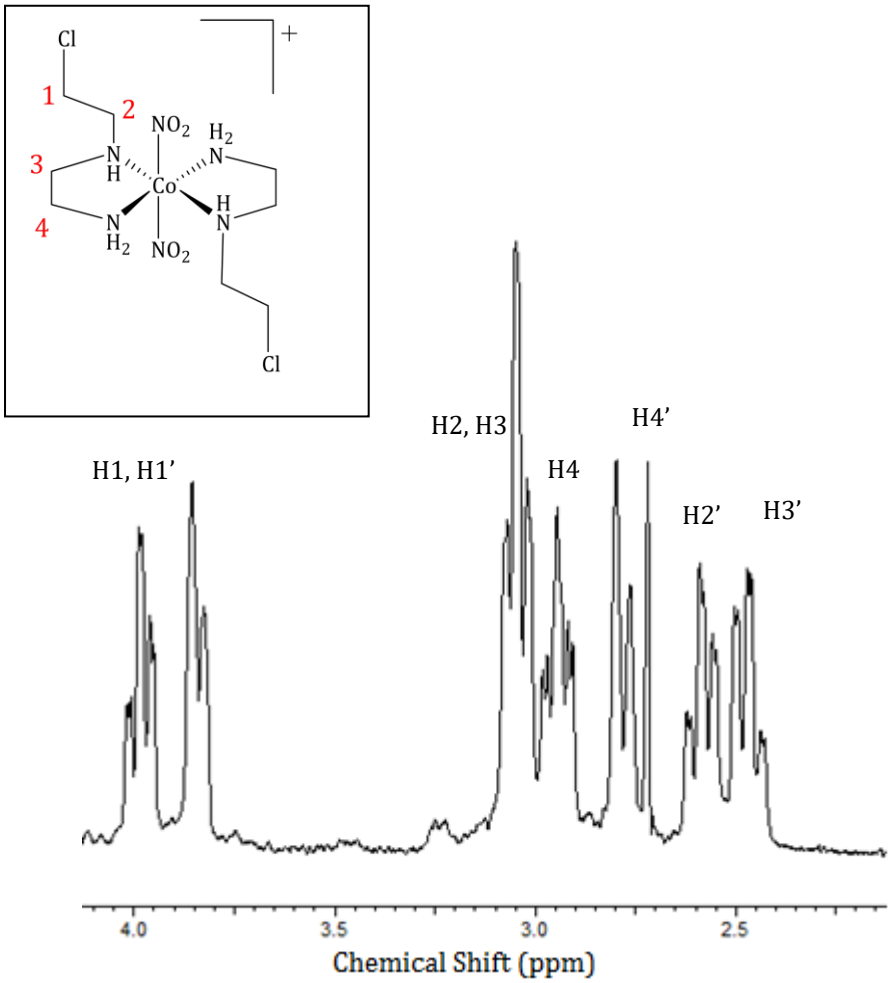

Figure 2.32. *^{1}H NMR spectrum of complex **2.08** in D_2O with reference to TMPS.*

2.3.5.1 Synthesis of 2.08 using 2.07 as a starting material

As discussed in previous section the difficult synthetic conditions for the preparation of the complex **2.08** drove us to investigate other possible synthetic procedures for the complex **2.08**. We investigated the possibility of substituting the chloride ligand on the complex **2.07** to nitrite ligand. Similar conversions were reported in literature.[131]

The complex **2.07** was reacted with $NaNO_2$ under cold conditions in the presence of ammonium hydroxide. After neutralisation, the reaction mixture was left in the fridge to

form large yellow crystals. The crystals formed were exactly similar in appearance to the crystals of the complex **2.06**.

One of the crystals formed during the very first attempt was analysed by X-ray crystallography and found to be $[Co(L3)_2(NH_3)(NO_2)]^{2+}$, **2.25**.

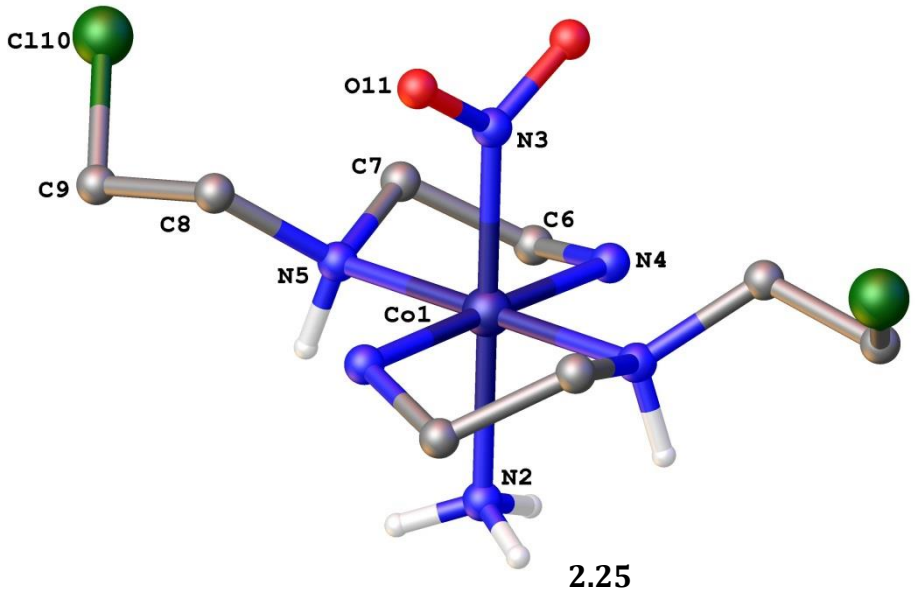

2.25

Figure 2.33. *X ray crystal structure of complex **2.25** with atom-labelling. The chloride anions, solvent water molecule and the hydrogen atoms, except N5 and N2 amine hydrogen atoms, were omitted for clarity.*

The molecular structure of $[Co(L3)_2(NH_3)(NO_2)]^{2+}$; Selected bond lengths (Å) and bond angles(°);Co1-N3 1.929(5), Co1-N2 1.987(5), Co1-N4 1.946(6), Co1-N5 1.990(6), N3-Co1-N4 90.69(2), N4-Co1-N2 1.946(6), N3-Co1-N5 90.2(3), N5-Co1-N2 89.8(3), N4-Co1-N5 85.9(3).

X-ray crystal structure of the complex **2.25** was solved in *R3c* trigonal space group. The asymmetric unit of the complex contained half the molecule, one chloride anion and a water molecule. The presence of chloride anion in the coordination sphere confirmed the (+2) total complex charge. The complex shows the distorted octahedral geometry with two **L3** ligands, nitrite ligand and an amine ligand coordinated on to the cobalt(III)

centre. In this molecule, axial chloride ligand is replaced with ammonia. The axial chloride ligand on **2.07** may have been replaced by an ammonia ligand to produce **2.25** in the reaction mixture.

The complex possesses a *C*2 symmetry axis through the axial nitrite and amine ligands. The chiral secondary nitrogen atoms show R configuration. The chloride anion in the co-ordination sphere is hydrogen bonded to the secondary amine hydrogen with the distance of 2.425(2) Å.

The analysis of the bulk sample using mass spectrometry and ^{1}H NMR spectrometry reveals the bulk material (blue) is different to the calculated powder pattern of the crystal structure **2.25** (black). The comparison of powder pattern from bulk material (blue) represents relatively similar pattern to the powder diffraction pattern calculated for **2.08** crystals.

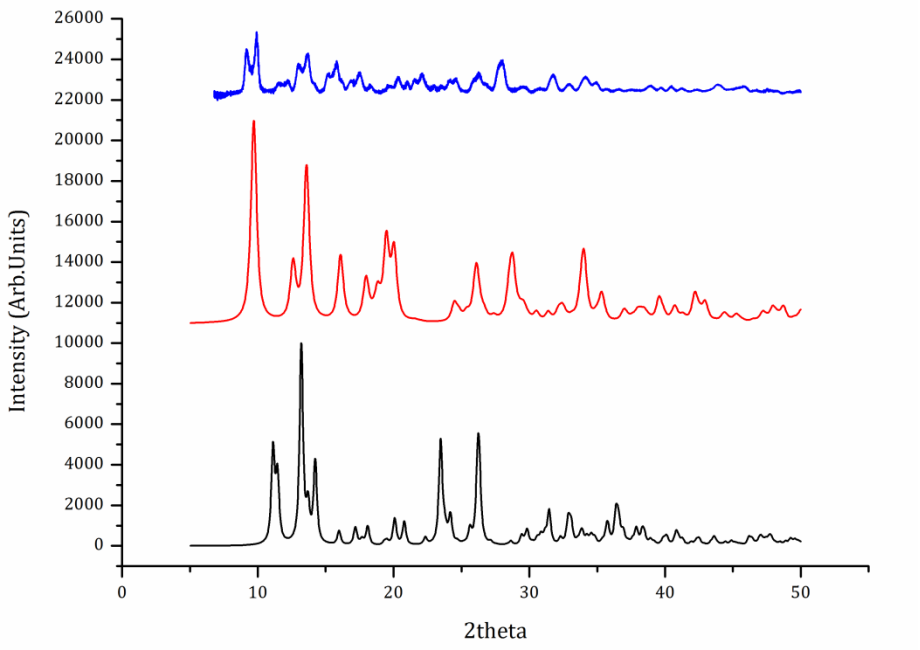

Figure 2.34. *The calculated powder patterns for the complex **2.25** (black) and **2.08** (red) in comparison with the experimental powder pattern obtained for the bulk sample of **2.25** (blue)*.

The powder diffraction analysis of the bulk sample is different to both the calculated powder pattern of complex **2.25** and **2.08** crystals. However some of the peaks in the experimental pattern follow the similar pattern to the calculated results of **2.08** crystals. This is most likely due to the mixture of **2.08** and **2.25** in the bulk sample with **2.08** in the higher percentage.

The conversion of chloride ligand to nitrite ligand reaction of **2.07** was repeated and the large block shape orange coloured crystals that appeared in the reaction mixture were analysed by mass spectrometry, NMR spectrometry and X-ray crystallography.

The yellow crystals were analysed by X-ray crystallography and solution to the structure is shown in Figure 2.35.

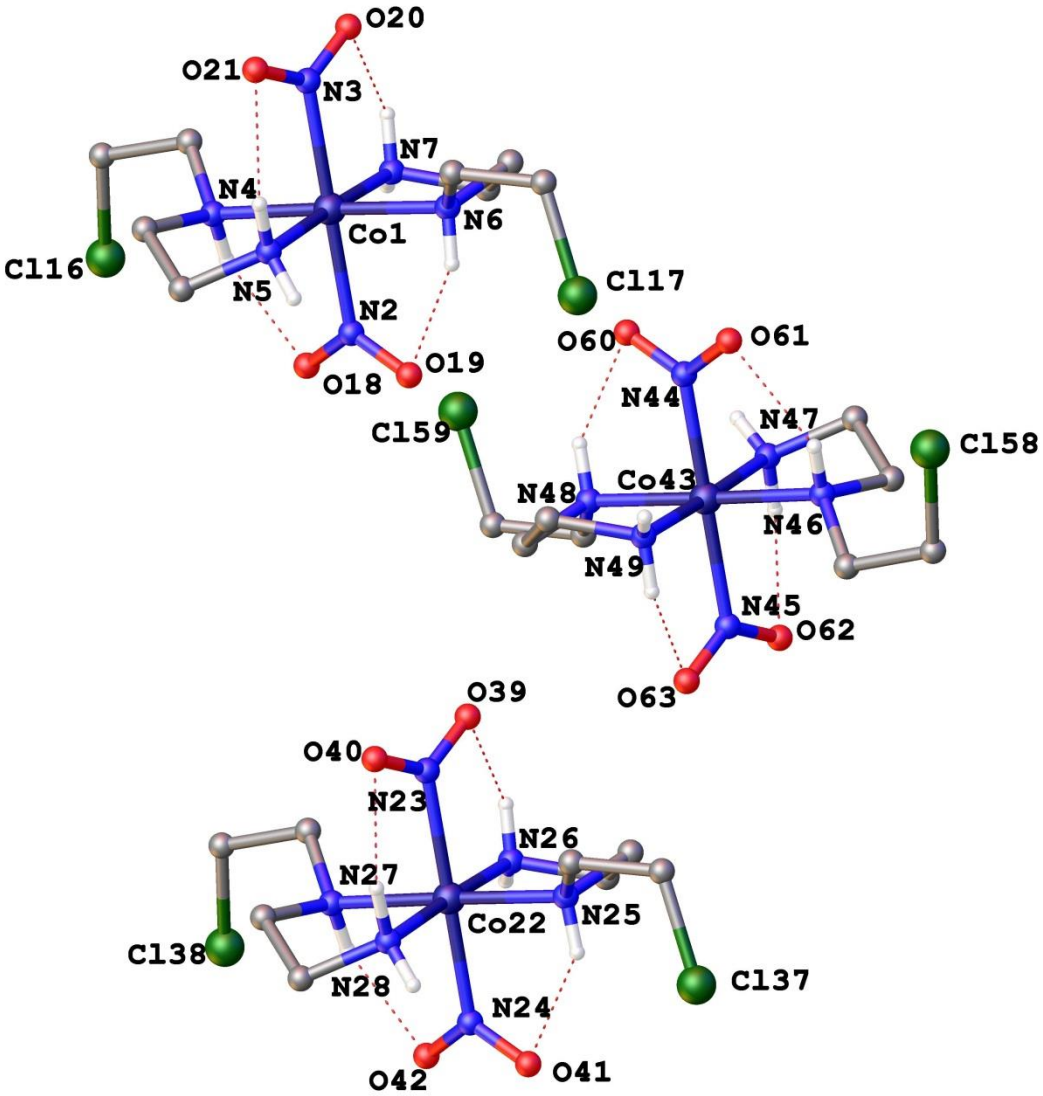

Figure 2.35. *X-ray crystal structure of $[Co(L3)_2(NO_2)_2]^+$, **2.08**, complex with atom labelling. Chloride anion and the solvent water molecules were omitted for the clarity. Hydrogen atoms, except amine hydrogen atom, have been omitted.*

Molecular structures of $[Co(L3)(NO_2)_2]^+$; Selected bond lengths (Å) and bond angles(°); Co1-N2 1790(5), Co1-N2 1,979(5), Co1-N3 2.039(5), Co1-N4 1.94(5), Co1-N5 1.948(5), Co1-N6 1.997(5), Co1-N7 1.936(5), Co22-N23 2.040(5), Co22-N24 1.979(5), Co22-N25 1.984(5), Co22-N26 1.943(5), Co22-N27 1.997(5), Co22-N28 1.949(5); N7-Co1-N3 91.1(2), N7-Co1-N4 93.6(2), N7-Co1-N5 177.6(2), N7-Co1-N6 86.0(2), N2-Co1-N3 179.9(2), N2-Co1-N4 89.4(2), N2-Co1-N6 89.0(2), N4-Co1-N3 90.7(2), N4-Co1-N6 178.3(2), N24-Co22-N23 179.7(2), N24-Co22-N25 89.5(2), N24-Co22-N23 90.5(2), N24-Co22-N27 89.4(2), N25-Co22-N27 178.8(2), N26-Co22-N23 91.5(2), N26-Co22-N23 91.5(2), N26-Co22-N24 88.8(2), N26-Co22-N25 86.5(2), N26-Co22-N28 177.6(2),

N27-Co22-N23 90.6(2), N28-Co22-N23 90.9(2), N28-Co22-N25 93.3(2), N28-Co22-N27 86.2(2).

The **2.08** complex is crystallised in Pī space group. The asymmetric unit of the complex consist of three complete molecules along with five water molecules and six half occupancy chloride anions. All three molecules are crystallised in distorted octahedral geometry. The two axial nitrite ligands are arranged perpendicular to each other. The nitrite ligands were hydrogen bonded to primary amine hydrogens and secondary amine hydrogens. Both the secondary chiral amine centres in each complex shows S configuration Figure 2.35.

The nitrite ligand, that was hydrogen bonded with secondary amine hydrogens, has a shorter bond length 1.98 (4) Å with the cobalt(III) metal compared to the nitrite ligand, that was hydrogen bonded to primary amine hydrogens and the cobalt(III) metal centre 2.041(3) Å. Both the *N*-bound nitrite oxygens have hydrogen-bonding distance with the amine hydrogens around ~2Å. There were intramolecular hydrogen bonds observed between chloride ligands and water molecules.

2.4 Electronic absorption spectroscopy

Ultraviolet-visible (UV/vis) spectroscopy is the study of the transitions involved in the rearrangements of valence electrons. In the field of inorganic chemistry, UV/vis is usually associated with d–d transitions and coloured transition metal complexes. The colour of the transition metal complexes in solution is dependent on several factors: the metal, the metal oxidation state, and the number of metal d electrons. For example;

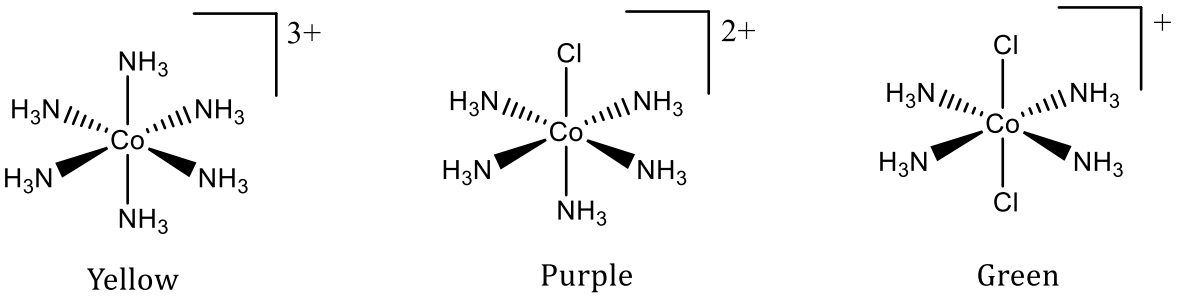

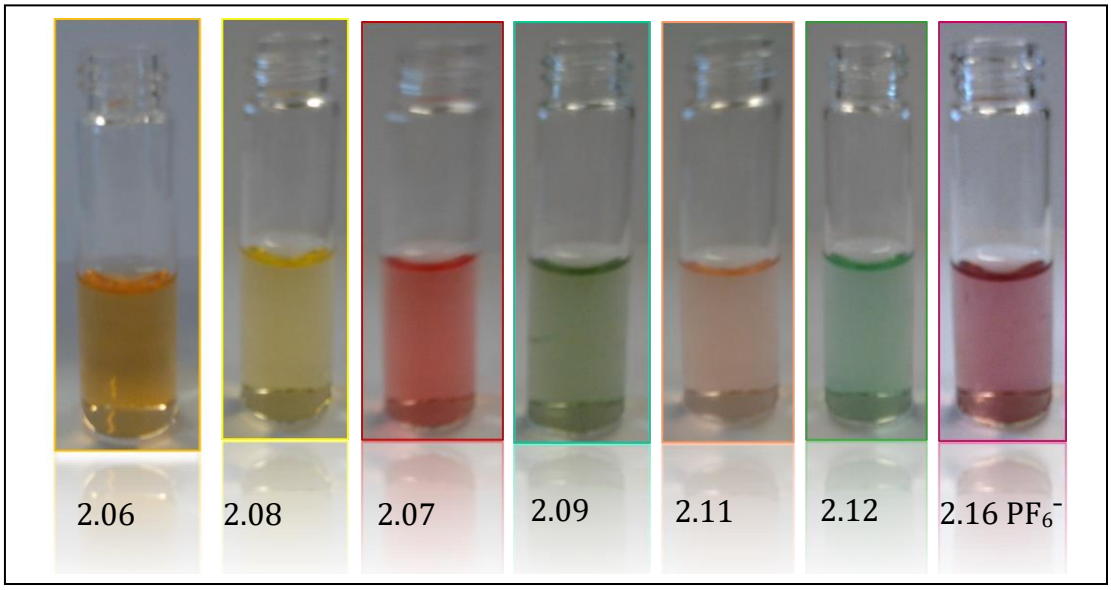

Figure 2.36. *The vibrant colours of various cobalt(III) complexes in methanolic solution.*

Similarly some of the cobalt(III) complexes discussed in this chapter showed vibrant colours with different ligands in the coordination sphere, Figure 2.36. The different colours of cobalt(III) complexes presented here are due to the different energies of d-d transitions. The different ligands coordinated to the cobalt(III) centre are responsible for changing the energy gap associated with the d-d transitions therefore, leading to different colours being observed, Figure 2.37.

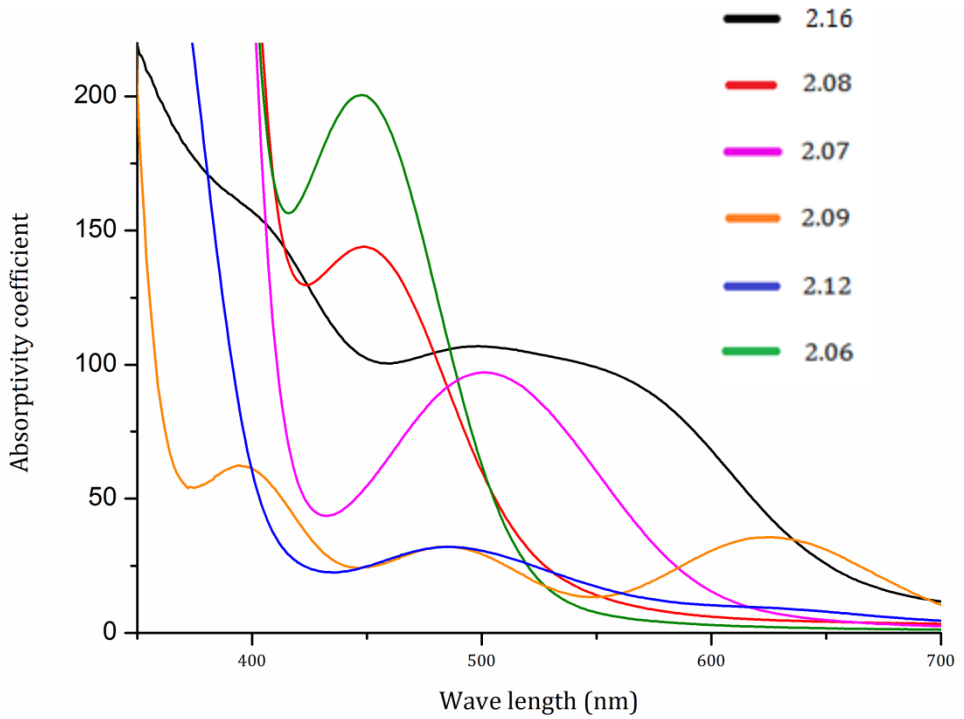

Figure 2.37. *Visible region of the spectrum showing the absorption patterns of the cobalt(III) complexes of* ***2.06***, ***2.07***, ***2.08***, ***2.09***, ***2.12*** *and* ***2.16****.*

2.5. Summary

In this chapter we reported the synthesis and characterisation of a series of cobalt(III) complexes. This study helps to understand the coordination chemistry, ligand exchange behaviour and the stability of these complexes under different reaction conditions.

Twelve different new cobalt(III) complexes, Figure 2.8, were synthesised and the sequential understanding of these complexes allowed us to successfully synthesise the desired nitrogen mustard cobalt(III) complex, **2.08**.

There is more than one new synthetic route developed for some of the complexes. All the complexes were characterised using X-ray crystallography. There are ten different new crystal structures discussed in this chapter. This chapter also included the chemistry about tridentate binding **L1** ligand and alkoxide complexes. Three different isomers of the complex $[Co(L1\text{-}H)_2]^+$ are reported in this chapter.

The oxygen atoms in alkoxide complexes can bind with other metal centres to form polynuclear complexes. Three polynuclear complexes of $[Co(L1\text{-}H)_2]^+$ with $MnCl_2$ or $ZnCl_2$ are also presented.

Chapter 03

Coordination chemistry of amino alcohols and synthesis of nitrogen mustards on a cobalt(III) metal centre

3. Coordination chemistry of amino alcohols and synthesis of nitrogen mustards on a cobalt(III) metal centre

3.1 Introduction

The work reported in this chapter describes the coordination chemistry of a series of amino alcohol ligands, **(L1-L9)**, with cobalt(III) centres. Here we report the successful synthesis of twelve different new cobalt-amino alcohol complexes and their X-ray crystallographic analysis.

A new safe synthetic route for the $[Co(bceen)_2Cl_2]^+$ (bceen = *N,N'*-bis(2-chloroethyl)ethane-1,2-diamine) complex was developed using the $[Co(L2\text{-}H)_2]^+$ (L2- 2,2'-(ethane-1,2-diylbis(azanediyl))diethanol) amino alcohol complex. A detailed description of the synthesis and characterisation is included in this chapter.

The coordination chemistry of 2-((2-aminoethyl)amino)ethanol, **L1** with the cobalt(III) metal centre was discussed in chapter 02. We were fortunate enough to obtain the single isomer of the complex $[Co(L1)_2(NO_2)_2]^+$, **2.06**, chapter 02, by reacting the **L1** ligand with $Co(NO_3)_2{\cdot}6H_2O$ under oxidising conditions.

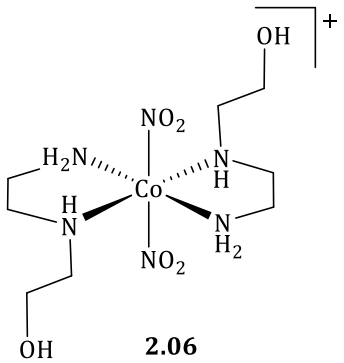

2.06

Figure 3.1. *Chemical structure of $[Co(L1)_2(NO_2)_2]^+$, **2.06**, complex.*

The potential for tridentate binding of the **L1** ligand with the cobalt(III) metal centre is also discussed in chapter 02. The reaction of complex **2.06** with aqueous sodium hydroxide exhibited the tridentate binding nature of deprotonated **L1** ligand 2-((2-aminoethyl)amino)ethanolate **(L1-H)** in the complex $[Co(L1\text{-}H)_2]^+$. Also, the reaction of **2.06** complex with trifluoromethanesulfonic acid (HOTf) leads to the tridentate binding of **L1** ligand with cobalt(III) centre. But due to the low pH conditions the protonated state of **L1** could be different.

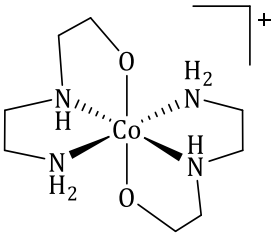

2.15

Figure 3.2. *Chemical structure of* $[Co(L1\text{-}H)_2]^+$ *complex.*

Similar tridentate coordination chemistry for the **L1** ligand and its deprotonated form was discussed earlier by Bailar *et al.*[122], [129] and Drinkard *et al.*[123] and the complex, $[Co(L1\text{-}H)(L1)]^{2+}$, was synthesised by displacement of ammonia from $[Co(NH_3)_6]Cl_3$ by **L1** ligands. According to their findings, the reaction occurs extremely slowly in an aqueous solution at steam bath temperature (~90°C), however a faster reaction could be obtained by adding activated carbon to the hot reaction mixture.[123]

Although the tridentate binding nature of **L1** ligand was suggested, there are not sufficient characterisations of those complexes to conclude the protonation state of **L1**, information about different isomers or the reactivity of these complexes.

Therefore, to obtain a better understanding about coordination behaviour of amino alcohols, different amino alcohol ligands shown in Figure 3.3, were reacted with cobalt(III) metal centres, using $[Co(NH_3)_6]Cl_3$ as the starting material, in the presence of activated carbon, in a basic solution.

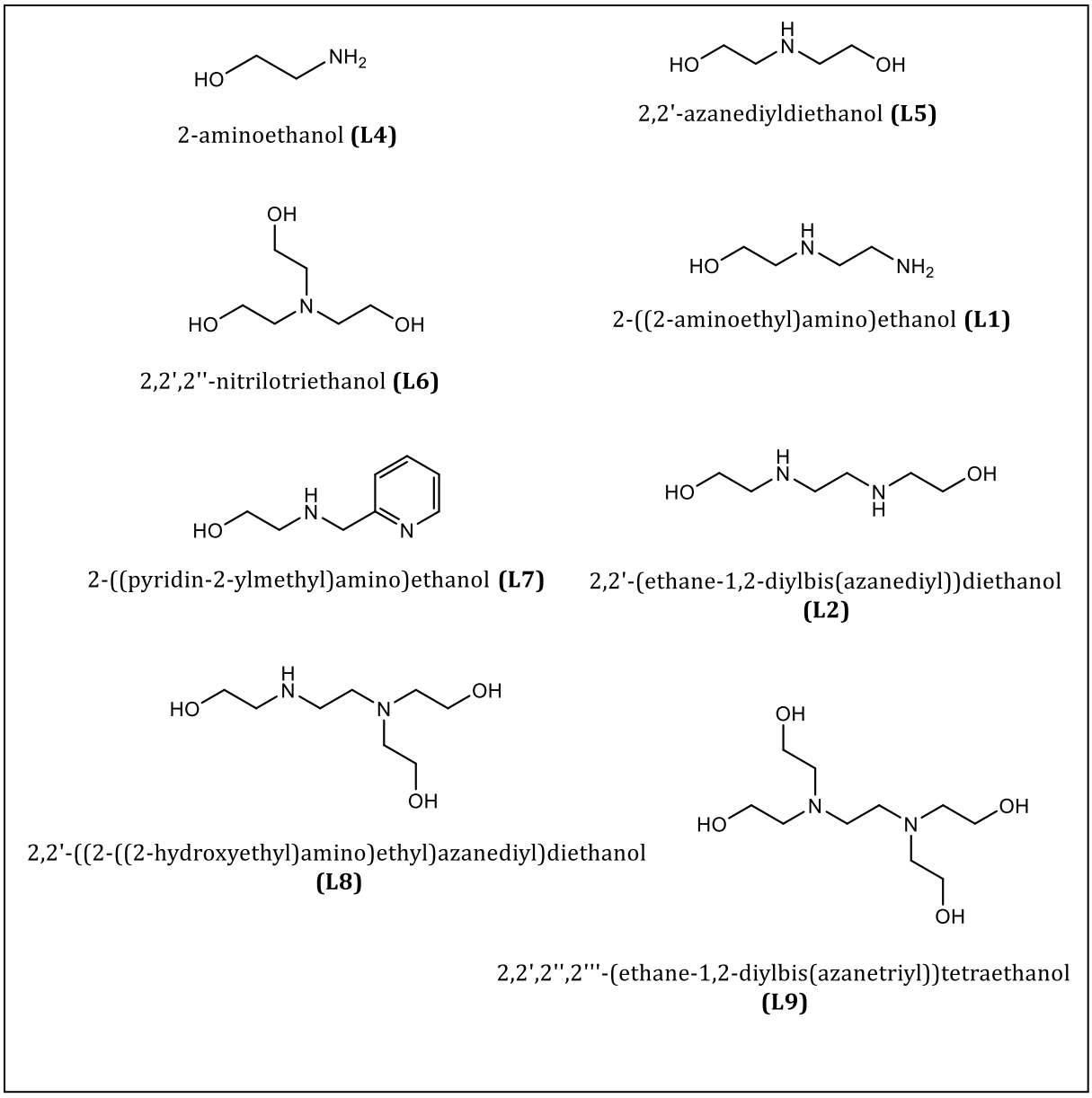

Figure 3.3. *Ligands used to synthesise range of cobalt(III) complexes*.

The complexes discussed in this chapter showed deprotonation of the alcohol groups of the ligands shown in Figure 3.3 during coordination. For example ligand **L1**, was found

to coordinate as the 2-((2-aminoethyl)amino)ethanolate anion, due to the loss of a proton, and this anionic form of the ligand will be represented as **(L1-H).** Likewise, each proton that is removed during the coordination will be denoted as (-H) having the relevant ligand number in front.

The ligands **L1, L4, L5,** and **L6** were used from commercially available sources, **L2, L7** and **L9** were synthesised according to the literature procedures, and the ligand **L8** was obtained as a by-product during the synthesis of **L2**.

Also, we investigated the possibility of using these alkoxide complexes to synthesise nitrogen mustards on a cobalt(III) metal centre by opening the bond between cobalt(III) and the ethanolate group. This is an extension of the studies reported for the **L1** derived compounds that were reported in chapter 2.

Nitrogen mustards with more than one alkylating sites are of interest because of their higher toxicity compared to mono-alkylating nitrogen mustard ligands, and their ability to form inter / intra strand crosslinks with DNA strands.[33] The synthetic attempts to prepare cobalt(III) nitrogen mustard complexes with the **L2** ligand proved unsuccessful by Alan Downward.[121] According to his results, **L2** formed a highly insoluble red powdered material reacting with $Co(NO_3)_2 \cdot 6H_2O$. In this chapter, we describe a new synthetic route for the bis alkylating nitrogen mustard cobalt(III) complexes such as $[Co(bceen)_2Cl_2]^+$ (bceen=*N,N'*-bis(2-chloroethyl)ethane-1,2-diamine) and $[Co(bceen)_2(NO_2)_2)]^+$. The synthesis involves the $[Co(L2\text{-}H)_2]^+$ type alkoxide complex as a starting material. Further information about this synthesis can be read in section 3.3.

During this research we also uncovered some interesting coordination behaviour of the alkoxide complexes with other metal salts such as $ZnCl_2$ and $MnCl_2$. The polyvalent

oxygen atoms that are already involved in Co-O bonding are also able to coordinate with other metal centres such as zinc(II) and manganese(II). Here, we report new polynuclear complexes of cobalt(III) with manganese(II) or zinc(II) metal centres and their X-ray crystallographic investigations. The complexes of $[Co(L1\text{-}H)_2]^+$ with $ZnCl_2$ and $MnCl_2$ were already reported in chapter 02.

The complexes reported in this chapter were characterised using a range of different techniques, including mass spectrometry, NMR spectroscopy, elemental analysis, UV/vis spectrometry, IR spectroscopy, and X-ray crystallography.

3.2 Results and Discussion

3.2.1 Synthesis of cobalt(III) complexes of 2-aminoethanol, L4,

2-Aminoethanol, **L4,** is an bidentate ligand, which forms $[Co(L4\text{-}H)_3]$-type chelate complexes.[132], [130] These complexes can exist as either the *fac* or *mer* isomeric forms.[132]

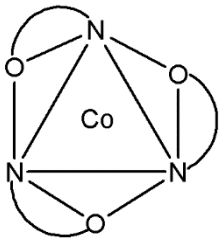

fac isomer

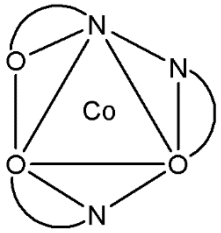

mer isomer

The first synthesis of $[Co(L4\text{-}H)_3]$ was reported by Yoneda and Kida.[133] The complex was synthesised by heating $[Co(NH_3)_5Cl]Cl_3$ or $[Co(NH_4)_4Cl_2)Cl$ with **L4**, and on the basis

of molar conductivity measurements they claimed the formation of three different compounds depending on the protonation state of the ligand such as $[Co(L4\text{-}H)_3]$, $[Co(L4)_2(L4\text{-}H)]^{2+}$ and $[Co(L4)(L4\text{-}H)_2]^{+}$.

Stepanenko *et al*.[132] synthesised the *fac* isomer of the $[Co(L4\text{-}H)_3]$ by reacting **L4** with $CoCl_2.6H_2O$ in the presence of KOH and the product was characterised by X-ray crystallography.

Extensive studies of the coordination behaviour of **L4** with cobalt(III) under different reaction conditions were reported by Kotovaya *et al.*[130]
Kotovaya analysed the pink crystals obtained by reacting **L4** with $CoSO_4 \cdot 7H_2O$ and confirmed the complex as the *fac* isomer. The X-ray crystallographic studies of the pink crystals confirmed the formation of $[Co(L4\text{-}H)_3] \cdot 3H_2O$ complex.

Further reaction of $[Co(L4\text{-}H)_3] \cdot 3H_2O$ with sulfuric acid affords three other compounds depending on the protonation state of **L4** and those compounds are $[Co(L4\text{-}H)_3]_2(SO_4)_3 \cdot 4H_2O$, $[Co(L4)_3](SO_4)(HSO_4) \cdot H_2O$ and $\{[Co(L4)_3][Co(L4\text{-}H)_3](SO_4)_3\} \cdot 7.75H_2O$.

X-ray crystallographic studies of $\{[Co(L4)_3][Co(L4\text{-}H)_3]\}(SO_4)_3 \cdot 7.75H_2O$ indicate the presence of two independent complexes, $[Co(L4)_3]^{3+}$ and $[Co(L4\text{-}H)_3]$, which are linked by O–H···O hydrogen bonding.

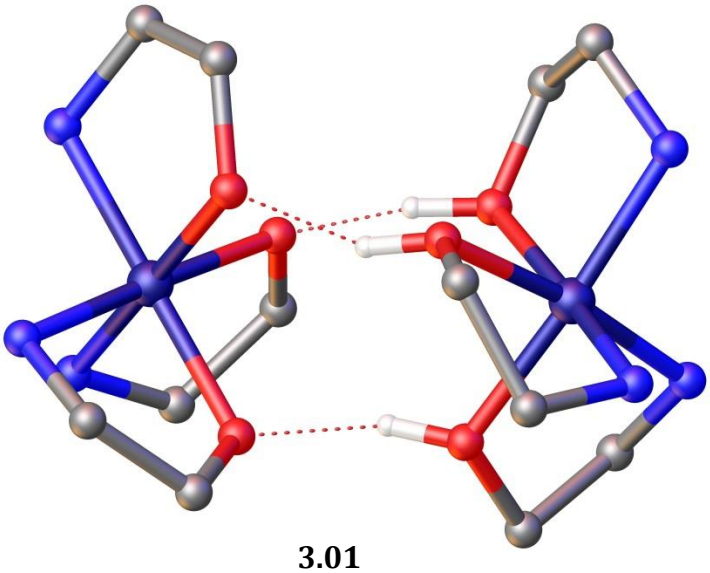

3.01

Figure 3.4. *X-ray crystal structure reported in literature of the complex {[Co(L4)$_3$][Co(L4-H)$_3$]}(SO$_4$)$_3$·7.75H$_2$O showing the binuclear structure. The SO$_4^{2-}$anions and the hydrogen atoms in the* ***3.01*** *complex, except hydroxyl hydrogen atoms, were omitted for the clarity.*

This research work began by repeating the Kotavaya *et al.*[130]procedure for the synthesis of [Co(L4-H)$_3$]·3H$_2$O. The pink rectangular shaped crystals that formed in the bulk solution were analysed using ^{1}H NMR spectroscopy and ^{13}C NMR spectroscopy, UV/vis, IR, microanalysis and X-ray crystallography and the results were consistent with the reported data in the literature.[130]

During this research we investigated the stability of the *fac* isomer under different reaction conditions. **L4** was reacted with [Co(NH$_3$)$_6$]Cl$_3$ according to the method described by Drinkard *et al.*[123], for the complexation of **L1** with cobalt(III) centres. The ^{1}H NMR spectra and ^{13}C NMR confirms the presence of two types of chemically different hydrogen atoms and chemically different carbon atoms, respectively. The two carbon shifts appeared at 60.50 ppm and 44.10 ppm confirmed the formation of highly symmetric *fac* isomer in comparison to the *mer* isomer with four chemically different peaks with two different intensities in the carbon spectrum.

Hayami *et al.*[133] also explored the reaction of **L4** with cobalt(III) metal centre. Hayami suggested two kinds of complex salt to be present, depending on elemental analysis results, in a 1:1 ratio, in the reaction mixture depending on the protonation state of the **L4**; $[Co(L4)_2(L4\text{-}H)]^{2+}$ and $[Co(L4)(L4\text{-}H)_2]^{+}$. Hayami also suggested the face-to-face bonding (Figure 3.5) of the complex. The face to face binding pattern is also in agreement with the X-ray structure reported in Figure 3.4 apart from the suggested chemical formulas are different in two individual complexes present in the dimer;$[Co(L4)_3][Co(L4\text{-}H)_3]^{3+}$, **3.01**, and $[Co(L4)_2(L4\text{-}H)][Co(L4)(L4\text{-}H)_2]^{3+}$ (Hayami).

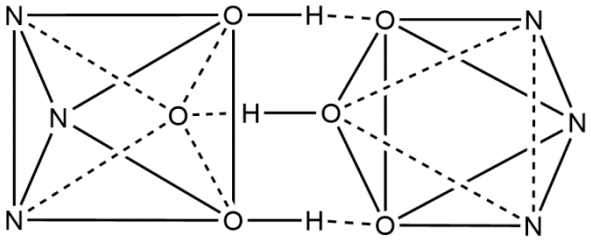

Figure 3.5. *Face-to-face bonding of $\{[Co(L4)_2(L4\text{-}H)][Co(L4)(L4\text{-}H)_2]\}^{3+}$ complex.*

3.2.2 Synthesis of cobalt(III) complexes of azanediyldiethanol, L5,

The complexes of **L5** with cobalt(III) complexes are not reported in the literature. Therefore the coordination chemistry of **L5** with cobalt(III) was studied during this research under two different reaction conditions.

Initially, the cobalt(III) complex of **L5** was synthesised according to the procedure described by Kotovaya *et al.*[130] for the synthesis of $[Co(L4\text{-}H)_3]$.

Red plate-like crystals of the iodide salt formed from a methanol solution after about a month (yield = 68%), and were analysed by mass spectrometry, NMR spectroscopy, UV/ vis and IR spectroscopy. Analysis of the bulk crystals using NMR spectrometry and mass

spectrometric results supported the two-fold symmetry of the complex, and confirmed that the bulk material is composed of a single diastereoisomer. The structure deduced by X-ray crystallography is fully supported by all the other analytical results.

A crystal suitable for X-ray crystallographic study was selected from the bulk sample and analysed, and the refined solution of the crystal structure is shown in Figure 3.6.

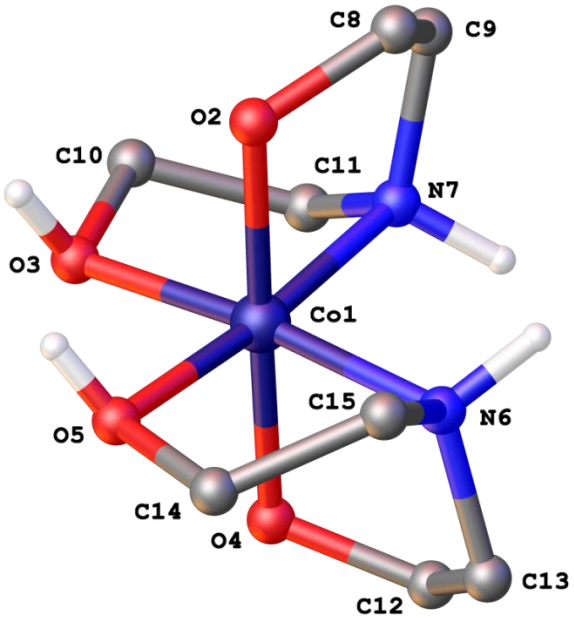

3.02

Figure 3.6. *X-ray crystal structure of $[Co(L5\text{-}H)_2]^+$, **3.02**, complex showing cis amine-trans oxygen configuration. The iodide anion and the hydrogen atoms on the complex, except the hydrogens on amine nitrogen atoms and hydroxyl oxygen atoms, were omitted for the clarity.*

The asymmetric unit of the compound $[Co(L5\text{-}H)_2]^+$; Selected bond lengths (Å) and bond angles(°) Co1-O4 1.905(8), Co1-O2 1.921(9), Co1-O3 1.938(9), Co1-O5 1.937(1), Co1-N6 1.956(1), Co1-N7 1.947(1), O2-C8 1.407(2), O4-C12 1.415(1), O3-C10 1.492(2), O5-C14 1.506(2), N6-C15 1.497(2), N6-C13 1.507(1), N7-C11 1.483(1), N7-C9 1.506(1), O4-Co1_O2 178.8(4), O4-Co1-O5 92.2(4), O2-Co1-O3 92.5(4), O5-Co1-O3 91.0(4), O4-Co1-N6 86.8(4), O4-Co1-N7 93.1(4), O4-Co1-O3 87.7(4), O2-Co1-N6 93.1(4), O2-Co1-N7 85.7(4), O2-Co1-O5 89.1(4), N7-Co1-N6 95.9(4), O3-Co1-N6 173.9(4), O3-Co1-N7 86.9(4), O5-Co1-N6 86.7(4), O5-Co1-N7 174.2(4).

The crystal structure of the complex **3.02** was solved in monoclinic space group $P2_1/c$ (R-factor of 8.07%) The asymmetric unit of the complex consists of a complete complex cation and an iodide anion. The presence of a single anion confirms the (+1) charge of the complex. The additional electron density around O3 and O5 was consistent with assignment of hydrogen atoms being bonded to these oxygen atoms, and the protonation state of the **(L5-H)** also explained the (+1) complex charge. The relatively longer bond lengths of Co1-O3 1.938(9) Å and Co1-O5 1.937(1) Å compared to Co1-O2 1.921(9) Å and Co1-O4 1.905(8) Å also supports the modelled protonation state of O3 and O5 oxygen atoms, satisfying Clarfield *et al.'s*[134] reports about the increase in Co-O bond distances with protonation.

The complex has distorted octahedral geometry. The two amine groups are arranged *cis* to each other. The amine nitrogen atoms are arranged in the *trans* configuration to the protonated oxygen atoms. The non-protonated oxygen atoms are arranged in the *trans* configuration relative to each other.

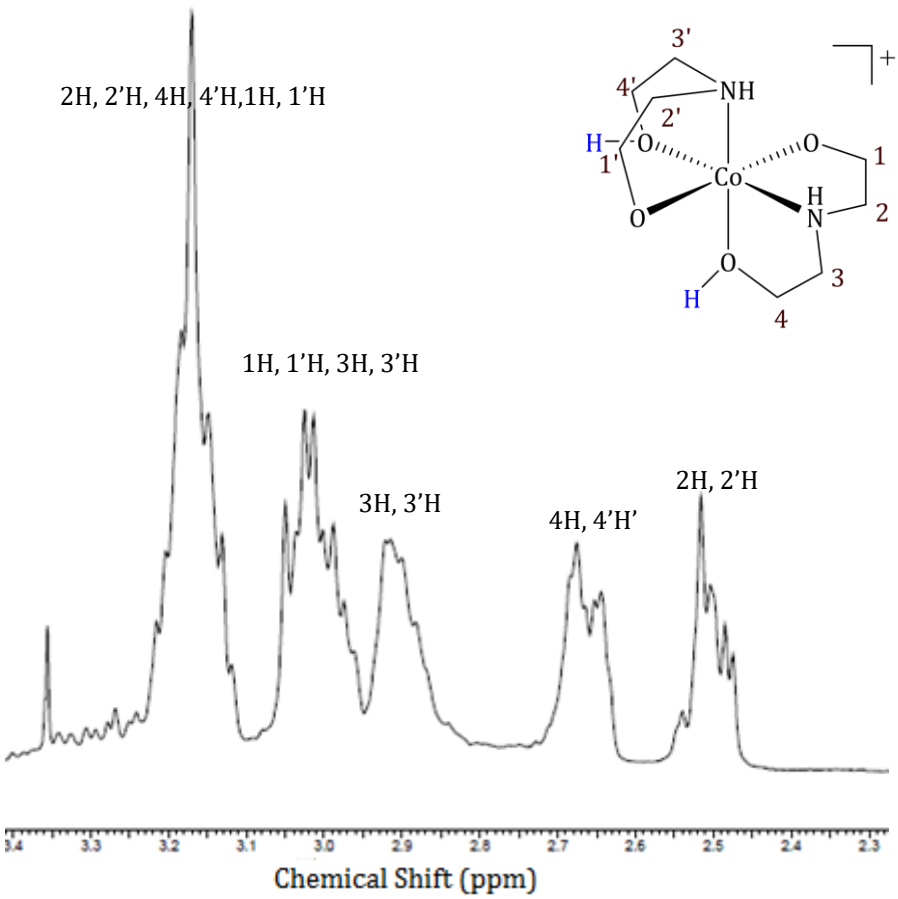

Figure 3.7. *^{1}H NMR spectrum of the $[Co(L5\text{-}H)_2]^+$,* ***3.02****, complex.*

The key portion of ^{1}H NMR spectrum of **3.02** is shown in Figure 3.7. The assignments were made by using spin-spin coupling information from gCOSY and HSQC experiments.

The HSQC spectrum shows significantly different chemical shifts for C4, C'4 carbon atoms and C1, C'1 carbon atoms 55.44 ppm and 67.10 ppm, respectively. This assignment was made as protonated oxygen atoms carry a relatively higher positive charge, causing the signals, due to the adjacent carbon atoms, to be shifted up field in the ^{13}C NMR spectrum.[135]

In a second synthetic method, **L5** was reacted with $[Co(NH_3)_6]Cl_3$ under basic conditions to investigate the influence of the reaction conditions for the complexation.

The bluish crystalline material obtained from slow evaporation of the reaction mixture was highly unstable outside the solution and not suitable for X-ray crystallographic analysis.

The mass spectrometric analysis of the crystalline material showed the presence of a prominent peak at m/z = 533.1496 and the one unit separation of the isotope peaks reveals the ion to have a (+1) charge. The mass of **3.02**, Figure 3.6 discussed in the previous synthesis, was observed in the mass spectrum at m/z = 267.07. The mass 533.1496 is nearly a double the mass of **3.02** and could be evidence for the presence of a dimeric species made up of two **3.02** type complexes. The ^{1}H NMR and ^{13}C NMR results were complicated and didn't provide sufficient information to allow a structural proposal to be made.

Numerous experimental techniques, such as changing anion, diffusion, complexing with other metal salts etc, were investigated to crystallise these alkoxide complexes in order to study their coordination chemistry throughout this work. Among them reacting with other metal salts seems to be proven as cobalt(III) alkoxide complexes tend to crystallised very easily as polynuclear complexes with manganese(II) / zinc(II), compared to the pure cobalt(III) alkoxide complexes. This is a new technique discovered during this research and there is not any precedent literature found in relation to this technique. This technique was extensively used to isolate different isomers of $[Co(L1\text{-}H)_2]^+$ complex and to perform X-ray crystallographic studies on those complexes. The detailed discussion about this technique and the coordination chemistry of $[Co(L1\text{-}H)_2]^+$ with $MnCl_2$ and $ZnCl_2$ can be read in chapter 02.

The present work reported in this chapter also used this strategy in some situations to obtain crystals suitable for X-ray crystallographic studies to explore the coordination chemistry of these complexes.

Therefore the bluish crystalline material obtained by reacting **L5** with cobalt(III) under the Drinkard reaction conditions was further reacted with $MnCl_2 \cdot 4H_2O$.

The pink crystals, suitable for X-ray crystallographic analysis, appeared in the solution were analysed by X-ray crystallography and the solution to the structure is shown in Figure 3.8.

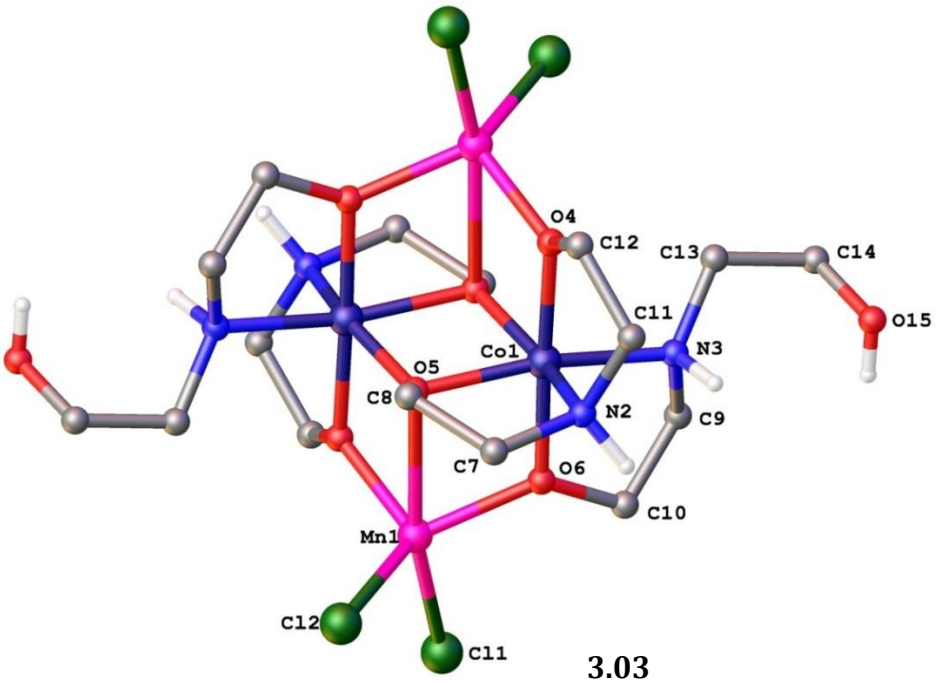

3.03

Figure 3.8. *The tetranuclear complex [{Co(L5-2H)(L5-H)}$(MnCl_2)_2$], **3.03,** with atom-labelling. The methanol solvent molecules, hydrogen atoms on the complex, except the hydrogen atoms on amine nitrogen atoms and hydroxyl oxygen atoms were omitted for the clarity.*

The molecular structure of [{Co(L5-2H)(L5-H)}$(MnCl_2)_2$]: Selected bond lengths (Å) and bond angles(°) Co-O4 1.902(3), Co1-O5 1.926(3), Co1-O6 1.887(3), Co1-N2 1.935(4),

Co1-N3 1.972(4), Mn1-O5 2.469(3), Mn1-O6 1.946(3), Mn1-Cl2 2.2956(3), Mn1-Cl1 2 2.3652(1), O15-C14 1.415(6); O4-Co1-O5 96,98(2), O4-Co1-N2 84.79, O4-Co1-N3 93.62(2), O5-Co1-N2 88.04(2), O5-Co1-N3 169.35(2), O6-Co1-O5 84.47(1), O6-Co1-N2 93.99, O6-Co1-N3 84.97(2), N2-Co1-N3 94.04(2), Cl2-Mn16-Cl1, 100.66(6), Cl2-Mn16-O5 93.00(8), Cl1-Mn16-O5 165.91(9), O6-Mn16-Cl2 127.97(1), O6-Mn16-CL48 98.68(1), Cl2-O4-Co1 115.8(3), Co1-O5-Mn16 92.2(1), C8-O5-Mn16 121.0(3), Co1-O6-Mn16 112.64(2), C10-O6-Co1 115.1(3), C10-O6-Mn16 130.9(3)

The molecular structure of **3.03** showed the tetranuclear complex composed of two manganese(II) and two cobalt(II) atoms held together by **(L5-2H)** and **(L5-H).** The distorted octahedral geometry and neutral total complex charge is consistent with the (+3) oxidation state of the cobalt centre.

Five coordinating sites of each octahedral cobalt(III) centre are satisfied by the **(L5-2H)** and **(L5-H)** ligands. The **(L5-2H)** is coordinated in tridentate binding manner, while the **(L5-H)** showed the bidentate coordination through one of the deprotonated oxygen atoms and the amine nitrogen atom. The hydroxyethyl arm of **(L5-H)** is not coordinated.

The sixth coordination site of each cobalt(III) metal centre is completed by the coordination of one oxygen donor from the **(L5-2H)** from adjacent octahedral centre.

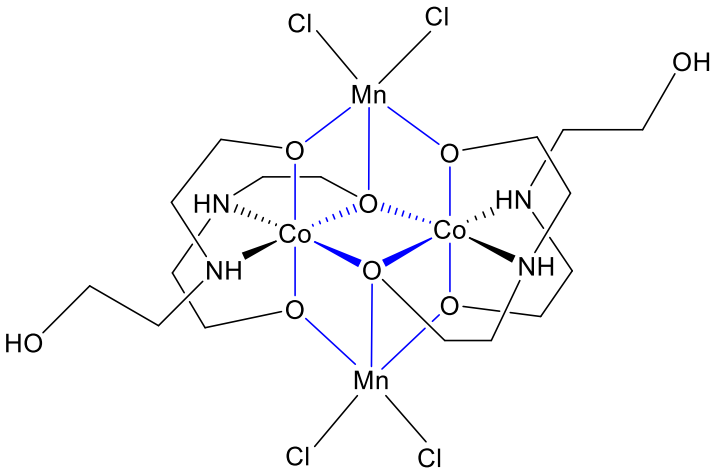

Figure 3.9. *The structural diagram of the complex **3.03**.*

The crystal structure was solved in the monoclinic space group *P*21/*c* with an R-factor of 5.82%. The ligands around the cobalt(III) metal centre were arranged in a distorted octahedral geometry, while the ligands around the manganese(II) metal centre showed trigonal bipyramidal geometry. The asymmetric unit consists of half of the molecule, and the total complex is neutral in charge, Figure 3.8. There are two disordered methanol molecules present in the asymmetric unit.

There are three different oxygen atoms from the **(L5-2H)** and **(L5-H)** coordinated to each cobalt(III) centre, two oxygens are donated from **(L5-2H)** and the third from **(L5-H)**. The two oxygens coordinated in *trans* configuration, around the cobalt(III), are from **(L5-2H)** and **(L5-H)** ligands respectively. The third oxygen atom coordinated *trans* to the amine nitrogen atoms is from **(L5-H)**, and is involved in bridging with the second metal centre as shown in Figure 3.9.

The two $MnCl_2$ molecules are coordinated to the dimer $[Co(L5\text{-}2H)(L5\text{-}H)]_2$ through oxygen bridging. Each $MnCl_2$ is bonded to two oxygen atoms, and each of the oxygen atoms is from the separate cobalt (III) centres. Likewise the two *trans* oxygens in each complex form bonds to separate $MnCl_2$ molecules. The fifth coordination of manganese(II) is satisfied by the cobalt(III)-cobalt(III) bridging oxygen; from the **(L5-2H)**.

The distance between Mn1-O5 is 2.470(3) Å. The other Mn-O bond lengths in the complex are 1.946(2)-1.955(3) Å, however, in literature reported by Kondaveeti *et al*.[136], the Mn-O bond lengths are between 2.069-2.230Å. Therefore, Mn1-O5 could be considered as a weak bonding interaction.

One of the special features of this complex is that the complex itself is composed of five tetra atomic squares Figure 3.9.

In the sphere, half of the methanol molecule is disordered over many sites, two of which are modelled. There was insufficient electron density associated with the hydrogen atoms on solvent methanol oxygen. Therefore those hydrogens were not modelled.

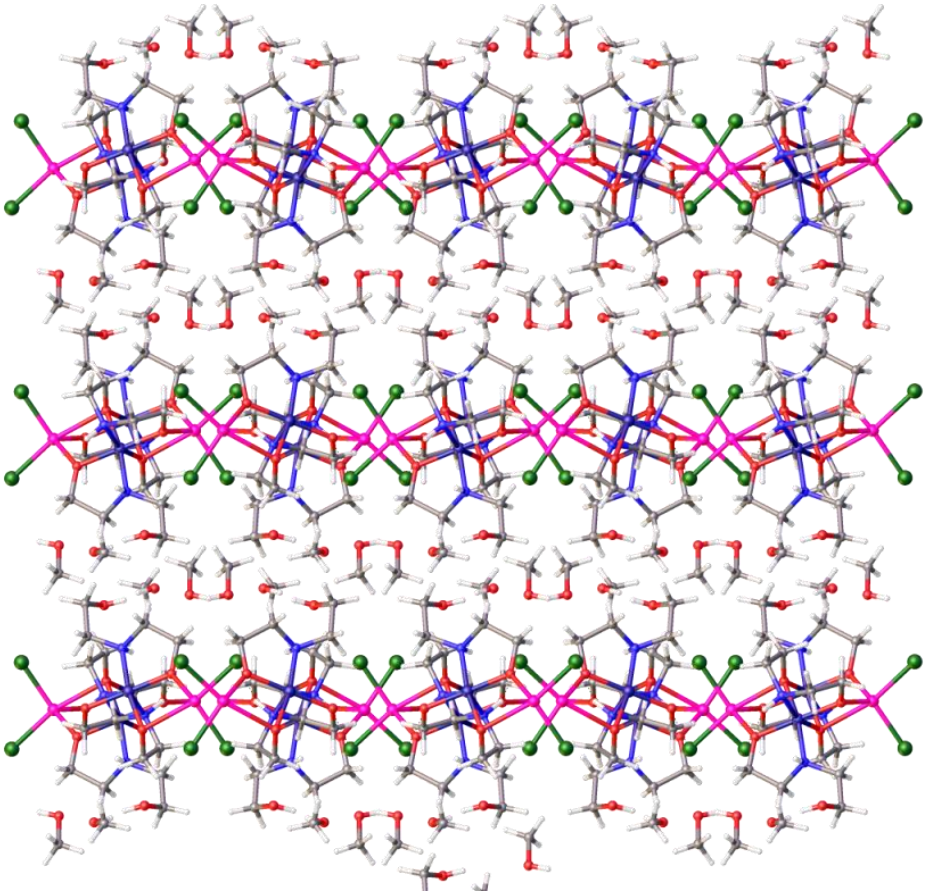

Figure 3.10. *The view through 001 plane, showing the channels filled with methanol solvent molecules, of the packed* ***3.03*** *complex.*

The packing structure, Figure 3.10, of the complex **3.03** shows that the complexes are arranged along the 001 plane. The spaces in between the complexes are filled with methanol solvent molecules. The hydrogen bonding interactions between the chlorine ligands and amine hydrogens hold the crystal packing.

The complex was also characterised in solution using mass spectrometric analysis. A molecular ion peak was observed with a matching isotopic pattern at $(M+H)^+$ = m/z = 783.0065, and fragments relevant to the complex, with matching experimental and calculated isotope patterns were also observed at $[(M-2(Cl_2))+H]^+$= m/z = 711.949, $[(M-2(Cl_2))]^{2+}$= m/z = 355.974 and $[(M-2(MnCl_2))+H]^+$=533.1427]. NMR studies of complex **3.03** could not be performed as it contains paramagnetic manganese(II) centres.

To establish whether the single crystal study is representative of the bulk sample, powder diffraction analysis was performed for the powder obtained for the complex **3.03** and compared with the calculated powder pattern obtained from the single crystal structure of **3.03.**

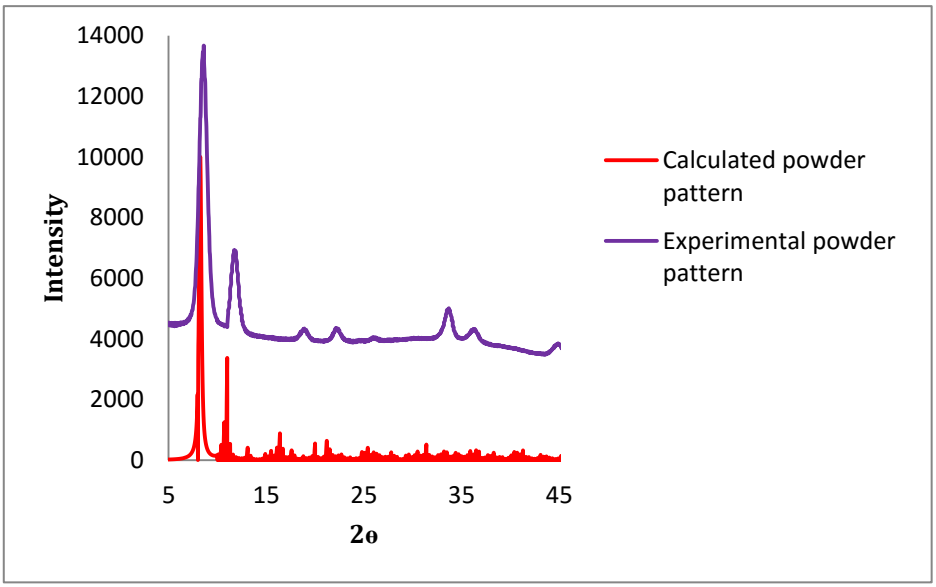

Figure 3.11. *Comparison of experimental and calculated powder diffraction patterns of the complex **3.03**.*

The powder diffraction patterns, Figure 3.11, obtained from the experimental data and calculated data from single crystal are not in agreement. The calculated powder pattern has more peaks which are absent in the experimental pattern. The few tall peaks in the

experimental pattern are similar in appearance to the calculated data, however slightly different 2ϴ value for two powder patterns were observed. This could be due to the non-crystalline nature of the powder sample.

The mass spectrometric results obtained from the reaction of ligand **L5** with $[Co(NH_3)]Cl_3$, (m/z = 533.1496) at the start of the synthesis and one of the fragments observed in the mass spectrum of the complex **3.03**, $[(M\text{-}2MnCl_2)+H^+]$ = 533.1427, represent a similar m/z ratio. Therefore in support with those mass spectrometric numbers and the X-ray crystallographic information of compound **3.03**, the chemical structure shown in Figure 3.12 is most likely to be present in the bluish powdered material obtained from the first reaction mixture.

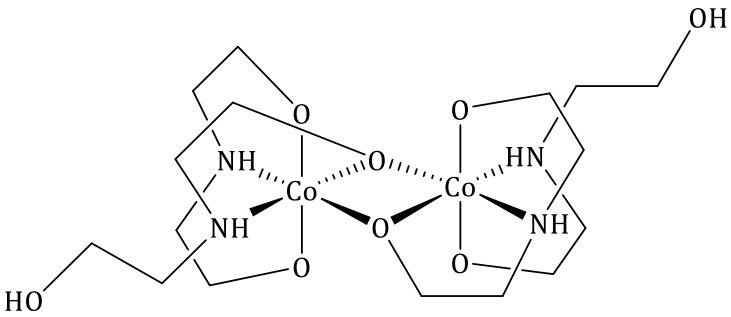

3.04

Figure 3.12. *Proposed structure of a dinuclear cobalt(III) complex, $[Co(L5\text{-}2H)(L5\text{-}H)]_2$,* ***3.04****, based on mass spectrometry data.*

Considering the bluish colour of the resulting powder and the difficulty of recording the NMR spectrum it suggests the presence of a cobalt(II) species in the mixture. This cobalt(II) species can either be present as a contaminant or can be in complexation with complex **3.04** as shown in the Figure 3.13.

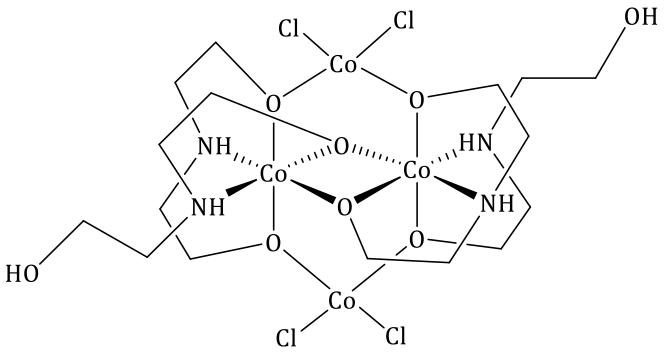

3.05

Figure 3.13*. Proposed chemical structure for the tetranuclear complex **3.05**.*

Nesterove *et al*.[137] reported metal clusters consisting of cobalt(III), copper(II) and nickel(II) metal centres coordinated through **(L5-2H)** and **(L5-H).** The synthesis method reported by Nesterov *et al.*[137] is different to the synthesis procedure we report in this work. The literature procedure involved a one-pot reaction of mixture of metal ions with the **L5**. But the tetranuclear **3.03** complex reported in this chapter was obtained by separate reaction processes which involved first, isolation of the cobalt(III) complex after reaction with **L5** ligand and then reaction of the complex with manganese chloride in methanolic solution.

3.2.3 Synthesis of cobalt(III) complexes of 2,2'-(ethane-1,2-diylbis(azanediyl))diethanol, L6,

A number of cobalt(III) complexes prepared using **L6** have been reported in literature.[138], [139], [140], [141] **L6** ligand shows different protonation states and the different coordination chemistry with cobalt(III) centres. The reported complexes are of cobalt(II), nickel(II), or copper(II).

The tetradentate binding behaviour of **L6** was reported by Reiter *et al*[138] with the en:L6 ligands in a 1:1 ratio is coordinated to the cobalt(III) metal centre.

Another cobalt(III) complex with **(L6-2H)** and glycine was also reported by Stepanenko *et al*[139] as shown in, Figure 3.14. The **(L6-2H)** shows a tridentate binding nature leaving one of the hydroxyethyl arms uncoordinated while glycinate filled two coordination sites through the amine group and one of the carboxylate oxygen atoms.

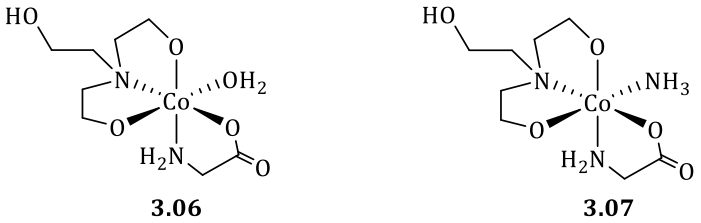

Figure 3.14. *Various coordination patterns of the ligand (L6-2H) and different ways of satisfying the octahedral geometry of cobalt(III) complexes.*

We decided to further investigate the possible coordination chemistry of **L6** with a cobalt(III) centre as part of our study of this class of ligands.

Therefore the **L6** was reacted with $[Co(NH_3)_6]Cl_3$ according to the Drinkard method. The pink aqueous solution obtained from the reaction was filtered and left for slow evaporation. Block-shaped large pink crystals appeared in the solution overnight. Attempts to characterise these crystals using mass spectrometric and NMR spectrometric analyses were unsuccessful.

The pink crystals were analysed by X-ray diffraction analysis and the solution to the crystal structure is shown below.

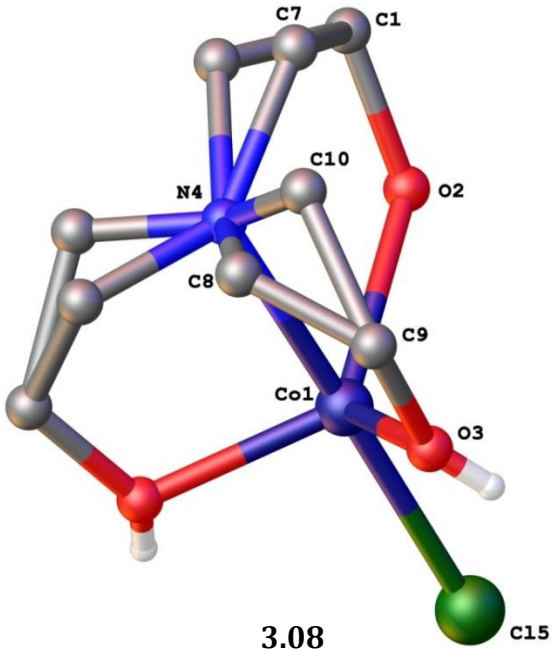

3.08

Figure 3.15. *The X-ray crystal structure of [Co(L6-H)(Cl)] , **3.08**, complex with atom labelling for the asymmetric unit. Hydrogen atoms, except the hydroxyl hydrogens were omitted for the clarity. The complex demonstrates the tetradentate binding of **(L6-H)**.*

The molecular structure of [Co(L6-H)(Cl)]; Selected bond lengths (Å) and bond angles (°); Co1-O2 2.3262(4), Co1-O3 1.9111(2), Co1-Cl5 2.335(3), Co1-N4 2.2031(5), N4-C7 1.6814(3), N4-C10 1.2870(2); C10-N4-Co1 46.39(1), Co1-N4-C7 107.316(3), N4-Co1-O2 78.845(5), O3-Co1-N4 81.305(5), O3-Co1-Cl5 97.8971(5), O2-Co1-CL45 2.2714(4).

The X-ray crystallographic analysis results of the crystals confirmed the oxidation state of the metal as cobalt(II) and further explained the impossibility of achieving NMR spectroscopy for the complex **3.08** due to the paramagnetic nature of cobalt(II) metal centre. The trigonal bipyramidal geometry of cobalt metal is unusual for cobalt(III)[142] hence further confirmed the oxidation state of the metal as (+2) and also the prominent electron density found close to two coordinated oxygen atoms were used to model the cobalt(II) cationic complex.

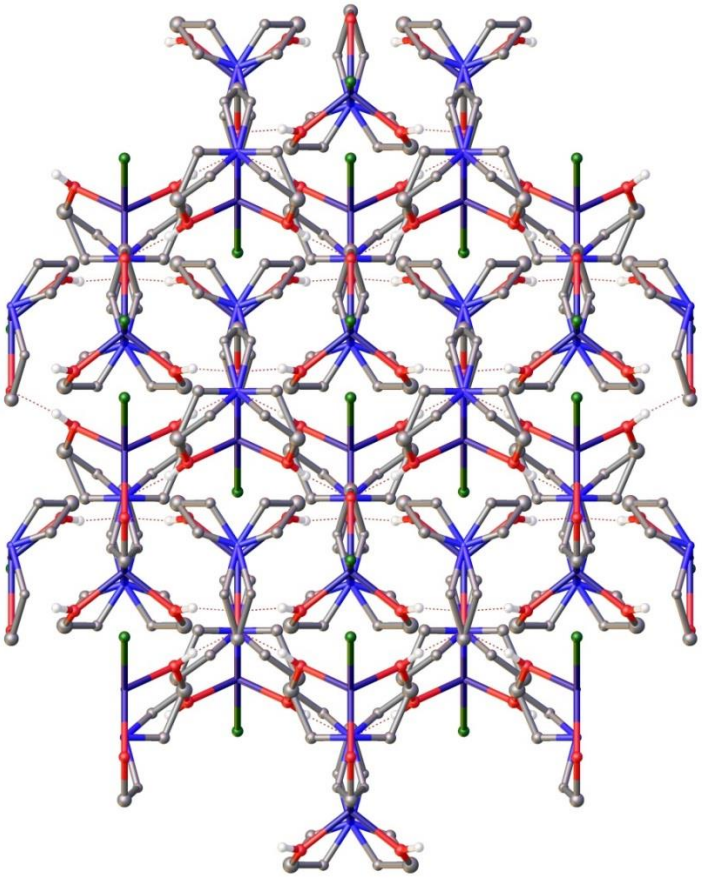

Figure 3.16. *Packing structure of [Co(L6-H)(Cl)],* ***3.08****, complex through 101 plane, showing intramolecular hydrogen bonding network stabilising the packing structure.*

The crystal structure for the complex [Co(L6-H)(Cl)] was solved in orthorhombic *Pnma* space group (R-factor of 4.39%). The asymmetric unit of the complex consisted of half of the molecule. There were no anions present in the structure. Given that cobalt(I) is a rare oxidation state, the neutral charge of the complex must result from one or more of the hydroxyl groups being deprotonated. The trigonal bipyramidal geometry of the metal centre makes the cobalt(II) oxidation state the most likely one. C8 and C10 atoms are disordered in two positions. C7 is the symmetry equivalence position. Powder diffraction pattern obtained for the bulk crystalline material is in agreement with the

calculated powder pattern of the **3.08** crystal. This result confirms that the single crystal structure obtained for the **3.08** structure represent the bulk sample.

After separating the **3.08** crystals from the solution, the liquid portion was dried under vacuum and the solid residue was dissolved back into methanol and reacted with methanolic $MnCl_2$ and $ZnCl_2$. The pink reaction mixture was filtered and left for slow evaporation.

The reaction mixture with added $MnCl_2$ did not produce any crystals, but the $ZnCl_2$ mixture yielded pink crystals suitable for X-ray crystallographic studies.

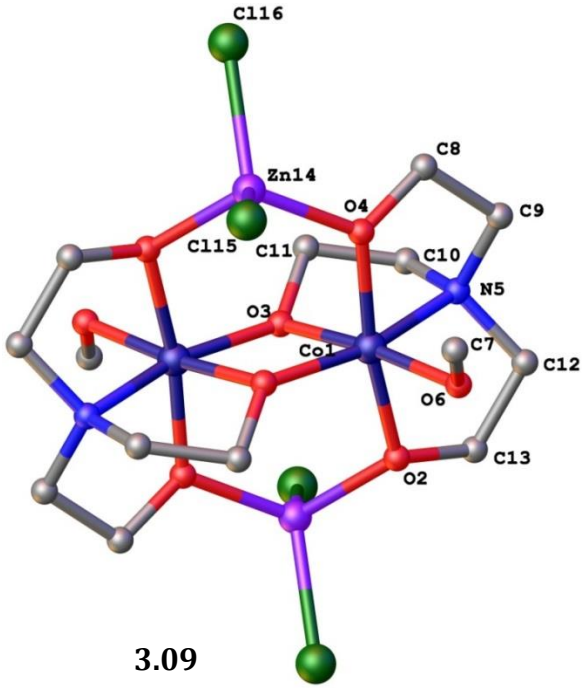

3.09

Figure 3.17. *X-ray crystal structure of **3.09** with atom-labelling for asymmetric unit showing the tetranuclear complex. Solvent molecules and hydrogen atoms were omitted for the clarity.*

The molecular structure of the complex $[Co(L6\text{-}3H)(MeOH)(ZnCl_2)]_2$; Selected bond lengths (Å) and bond angles(°); Co1-O2 1.905(4), Co1-O3 1.947(4), Co1-O6 1.951(4), Co1-N5 1.918(4), Co1 O4 1.899(4), O2-Zn14 1.987(4), Zn14-Cl15 2.244(2), Zn14-Cl16 2.249(2); O4-Co1-O6 90.23(2), O4-Co1-N5 85.14(2), O6-Co1-O2 86.7(2), O6-Co1-O3

174.11(2), O2-Co1-O3 89.29(2), O2-Co1-N5 87.06(2), O4-Zn14-Cl15 109.42(1), O4-Zn14-Cl16 110.87(1), Cl15-Zn14-Cl16 113.8(7).

The crystal structure was solved in the $C2/c$ monoclinic space group with the R factor of 5.67%, Figure 3.17. The ligand **(L6-3H)** was bound in a tetradentate binding fashion using all three oxygen atoms and a single quaternary nitrogen atom for coordination. No electron densities were found close to the coordinated oxygen atoms which confirmed the deprotonation of oxygen atoms during coordination.

The structure of the complex **3.09,** Figure 3.17, shows the formation of a tetranuclear complex with the involvement of $ZnCl_2$ molecules. There are no anions present in the crystal structure. This suggests the total complex to be neutral in charge. Each cobalt(III) centre shows distorted octahedral geometry, characteristic for the (+3) oxidation state of the metal centre.

As shown in the Figure 3.17 ligands around cobalt(III) centre were arranged in a distorted octahedral geometry The four coordinates around the cobalt(III) centre are satisfied by a ligand **(L6-3H)** and the fifth coordination is satisfied by a solvent methanol molecule. The two cobalt(III) centres of $[Co(L6{-}3H)MeOH]^{+}$ configuration associated forming a dimer, which also satisfied the sixth coordination for each the complexes through mutual single oxygen bridging.

The four oxygen atoms around each cobalt(III) centre were arranged *trans* to each other. One set of *trans* oxygens were from **(L6-3H)** ligand and the second set is from **(L6-3H)** oxygen atom and methanol oxygen coordinated with the cobalt(III) centre.

The oxygens from **(L6-3H)** that are *trans* to each other are coordinated with the zinc(II) metal centres. The two methanol molecules coordinated to cobalt(III) metal centres are arranged on opposite sides of the dimeric structure. The oxygen atoms of coordinated methanol is in the same plane with the oxygen atoms bridging the cobalt(III)centres.

The methanol solvent molecule and the water molecule in the surrounding are hydrogen bonded to the coordinated methanol hydrogen atom.

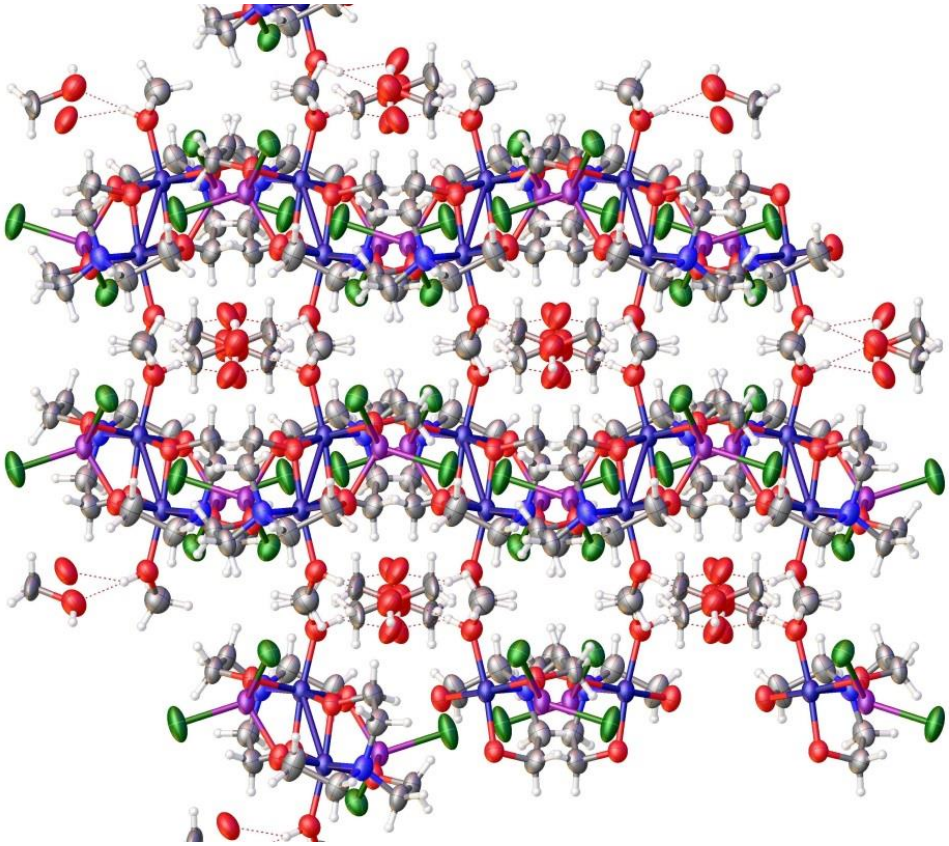

Figure 3.18. *Packing structure of the complex **3.09**. A view through a 101 plane. The channels between the crystal packing are occupied by the solvent methanol and water.*

The packing structure of the complex **3.09** through the 101 plane showed the channels between the complex molecules formed during the packing. The channels are filled with solvent waters and methanol molecules. The hydrogen bonding interactions with the

distance of 2.56(1) Å were observed between the solvent molecule oxygens and the hydroxyl hydrogen of the coordinated methanol.

Another analogue of the **3.09** obtained from a different crystallising vial was studied using X-ray crystallography. The crystal structure of the complex **3.10**, Table 3.1 is solved in $P2_1/n$ monoclinic space group, with an R factor of 2.66%.

A comparison between complexes **3.09** and **3.10** is shown in the table below.

Table 3.1. *A comparison between **3.09** and **3.10** asymmetric units.*

		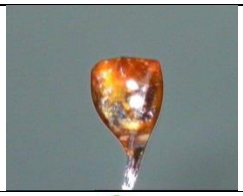
	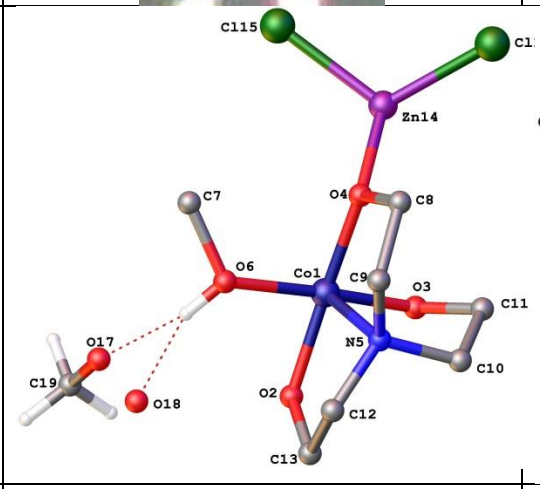	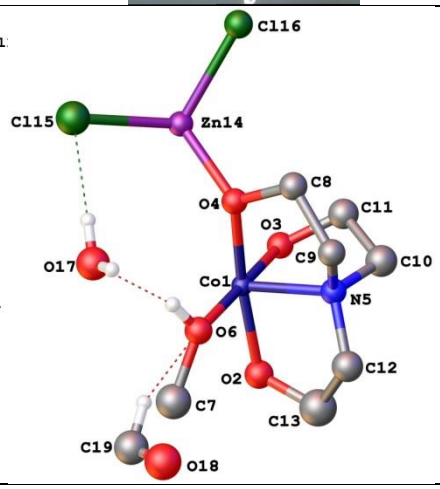
Compound number	**3.09**	**3.10**
Space group	*C*2/*c*	*P*21/*n*
R1		
Crystal dimensions	a-16.78321(15), b-10.0161(5), c-20.0251(16)	a-9.7436(14), b-10.4351(15), c-13.3043(2))
Bond lengths (Å)		
Co1-O6	1.951(4)	1.933(2)
Co1-O4	1.899(4)	1.9021(2)
Co1-O3	1.867(4)	1.8643(2)
Co1-N5	1.918(4)	1.911(2)
Bond Angles (°)		
O6-Co1-O4	90.25(2)	87.92(9)
O6-Co1-O2	86.7(2)	88.64(9)
O6-Co1-O3	174.08(2)	176.08(8)
O6-Co1-N5	95.1(2)	93.99(9)

The cationic component of complex **3.10**, is similar in coordinating pattern to the complex **3.09** shown in Figure 3.17, only the position of the water molecule has changed during crystallisation

The reason for changing the position of water molecule is unknown but the new position of water molecule facilitates some hydrogen bonding interactions. The

hydrogen bonding interactions with the water hydrogen and Cl15 chloride ligands on the zinc(II) metal centre have a distance of 2.354(1) Å, which can be considered as a weak hydrogen bonding due to the longer distance. Another hydrogen bonding interaction between the water oxygen and the coordinated methanol hydrogen with the distance of 1.844(2) Å makes this structure different from the complex **3.09**.

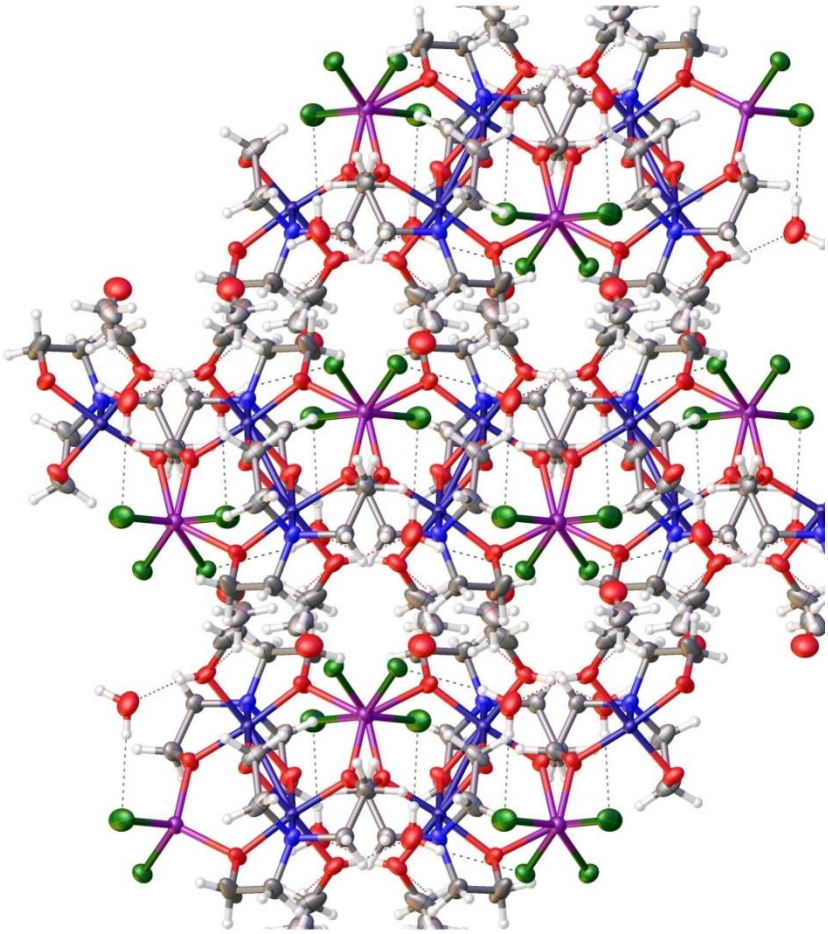

Figure 3.19. *Packing structure of complex **3.10** through 101 plane. The strong hydrogen bonding network due to the displacement of water is prominent in packing structure.*

3.2.4 Synthesis of cobalt(III) complexes of 2-((pyridine-2-ylmethyl) amino)--ethanol, L7,

The ligand **L7** was synthesised according to the procedure reported by Chmielewski *et al.*[143] Chmielewski synthesised **L7** as precursor compound to the thermo-labile protecting groups. The ligand was characterised by mass spectrometric analysis, ^{1}H NMR and ^{13}C NMR analysis, and the data obtained was found to agree the reported literature values, confirming the synthesis of the **L7**.

There is no literature reported about the coordination chemistry of this ligand. Therefore to explore the coordination behaviour of **L7**, the complex **3.11** was synthesised by reacting the **L7** with $[Co(NH_3)_6]Cl_3$ according to the Drinkard *et al.*[123] method. The resulting purple reaction mixture was filtered and concentrated under reduced pressure. Addition of few drops of concentrated aqueous ammonium hexafluoridophosphate yielded a pink powder.

The obtained powdered material was characterised using mass spectrometry m/z= (M^+) = 361.1062, ^{1}H NMR, ^{13}C NMR, gCOSY, and HSQC NMR, UV/vis, IR, elemental analysis and X-ray crystallography.

Crystals suitable for X-ray crystallographic studies were grown by slow evaporation of methanolic solution of the complex. The pink block shape crystals obtained were analysed by X-ray crystallography and solution to the structure is shown below.

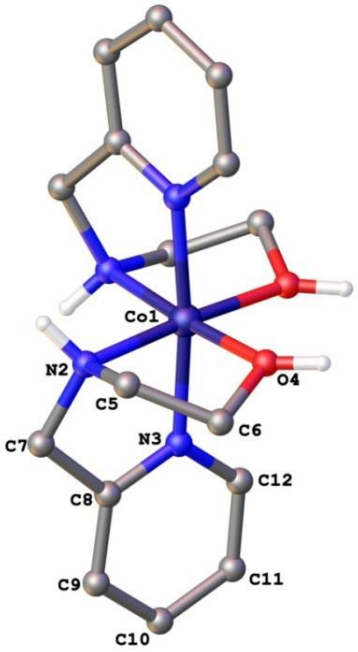

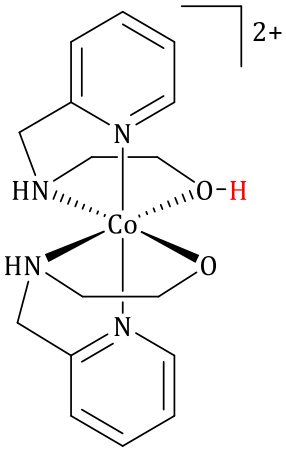

3.11

Figure 3.20. *Structure of [CoL7-H)L7]$^{2+}$, **3.11**. The solvent water molecule, two hexafluorophosphate anions and hydrogen atoms, except the amine and hydroxyl hydrogen atoms, were omitted for the clarity. The hydroxyl hydrogens are half occupancy.*

Molecular structure of [CoL7-H)L7]$^{2+}$; Selected bond lengths (Å) and bond angles(°); Co1-O4 1.920(3), Co1-N2 1.961(4), Co1-N3 1.954(5); O4-Co1-N2 85.89(2), O4-Co1-N3 90.75(2), N3-Co1-N2 83.91(2), Co1-N2-C5 106.8(3), Co1-O4-C6 111.5(3), C7-N2-Co1 109.3(3).

Compound **3.11** crystallised in the *C*2/*m* monoclinic space group. The asymmetric unit of the molecule consists of half of the complex **3.11.** The octahedral geometry and the bond lengths values around the metal centre was characteristics to cobalt(III) metal centres. The asymmetric unit consist of two halves of PF_6^- ions and one **L7** coordinated to cobalt(III).

The two PF_6 ions found in the structure confirms the (+2) charge of the complex. The prominent electron density close to the O4 atom confirms the protonated state of the

oxygen. The hydroxyl hydrogens are half occupied due to their fast exchange and confirmed the (2+) charge of the complex.

The cobalt(III) metal centre shows octahedral geometry having two of the **L7** ligands coordinated with the central metal centre, Figure 3.20, **L7** coordinated with the cobalt(III) metal centre are arranged in a *cis, trans* coordination pattern; the pyridine ligands are arranged *trans* to each other, while the secondary amine ligands are *trans* to hydroxyl oxygens. The chiral amine nitrogen atoms show S configuration.

The complete structure consists of only one cationic complex. The packing structure shows the hydrogen bonding between adjacent two cationic complexes. The hydrogen bonding interactions between hydroxyl hydrogen and the oxygen as shown in the Figure 3.22 hold the two structures together.

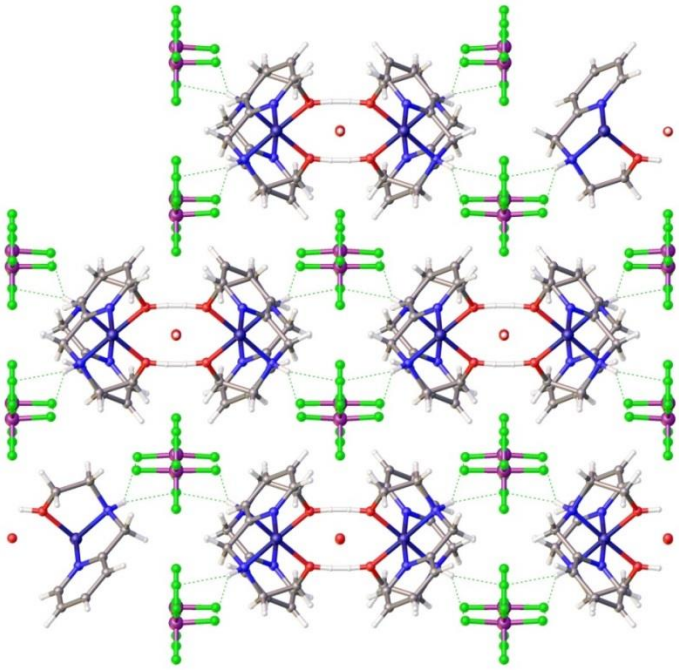

Figure 3.21. *The packing structure of complex **3.11** through 001 plane. The intramolecular hydrogen bonding interactions are prominent. The two complexes are arranged in face to face arrangement and a water molecule is found in the centre of the two complexes.*

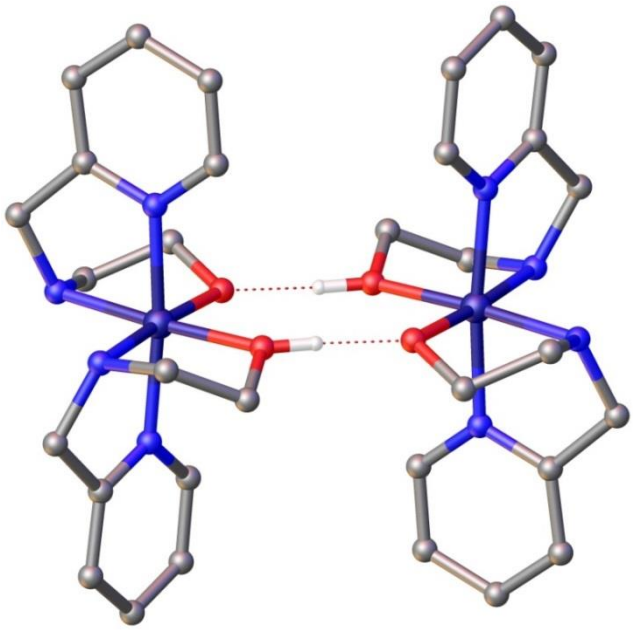

Figure 3.22. *Dimeric structure of [Co(L7-H)L7](PF$_6$)$_2$,* ***3.11****, complex*

The packing of the crystal is stabilised by the hydrogen bonding network between the chiral amine hydrogen and fluorine atoms of the hexafluoridophosphate anion. As shown Figure 3.21 two **3.11** molecules arranged facing to each other and a disordered water molecule is sitting in between the dimer. The symmetry axis runs through the water molecule which relates the two complexes by symmetry. The disordered hexafluoridophosphate anions formed hydrogen bonds with amine hydrogens while filling the spaces in the crystal packing.

^{1}H NMR studies of the complex **3.11** show nine different peaks associated with the 11 different protons. The assignment of the proton peaks was supported by gCOSY and HSQC spectral data. The data are consistent with the isomer and symmetry elements revealed by the X-ray data analysis.

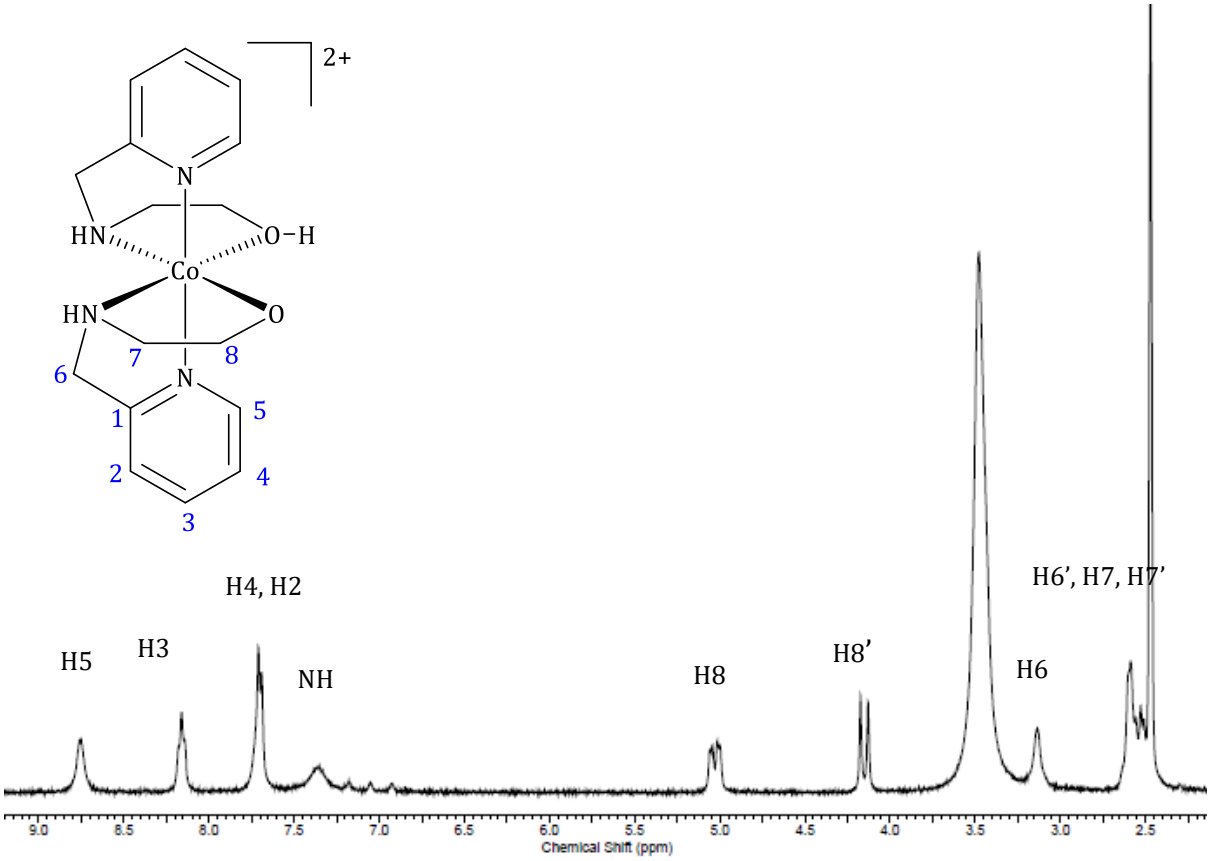

Figure 3.23. *^{1}H NMR spectrum of complex $[Co(L7\text{-}H)L7]^{2+}$,* ***3.11*** *recorded in DMSO solvent.*

The NMR studies confirmed the twofold symmetry of the complex contradicting the solid state results of coordination of two different **L7** and **(L7-H)** with the cobalt(III) centre.

The two fold symmetry of the complex is achieved by the fast proton exchange between two oxygen atoms in solution state.

The mass spectrometry data confirmed that there were two **L7** ligands coordinated to the cobalt(III) metal centre forming a (+2) charge complex with the formula of $[Co(L7\text{-}H)L7]^{2+}$.

The identical ^{1}H NMR spectra obtained for the extracted powdered material and the pink crystals were useful in confirming that the single crystal represent the bulk sample.

3.2.5 Synthesis of cobalt(III) complexes of 2,2'-(ethane-1,2-diylbis(azanediyl))diethanol, L2,

The 2,2'-(ethane-1,2-diylbis(azanediyl))diethanol **L7**, was synthesised and characterised according to the procedure described by Kira *et al.*[144] The obtained powdered material was dissolved in methanol to make a concentrated solution and, after leaving the solution for slow evaporation, transparent crystals grew into flowered shape lumps. The X-ray crystal structure of this compound is shown in Figure 3.24 below.

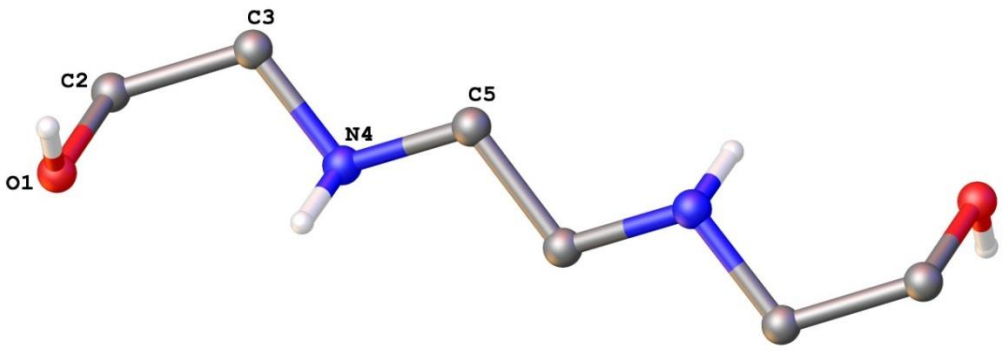

3.12

Figure 3.24. *X-ray crystal structure of ligand **L2** with atom labelling. The hydrogen atoms on carbon atoms were omitted for the clarity.*

Molecular structure of ($C_6H_{18}N_2O_2$); selected bond lengths (Å) and bond angles (°); O1-C1 1.4112(4), N4-O3 1.4676(5), 1.4670(3), N4-C3 1.4676(5); O1-C2-C3 112.5742(1), C2-C3-N4 11.0902(1), C3-N4-N5 110.503(1).

The ligand crystallised in a $P2_1/n$ monoclinic space group. The asymmetric unit contains half of the ligand. The packing structure shows that each ligand is hydrogen bonded with two adjacent molecules. The hydroxyl oxygen atom of each ligand is hydrogen bonded with the primary amine hydrogen atom of the next ligand with the distance of 2.2842(6) Å.

The X-ray crystal structure of the **L2** has been reported previously in literature as its nitrate salt.[145]

The literature reported hydrogen bonding distance of 1.869(15) Å is smaller than the hydrogen bonding distance observed in the packing structure of **3.12**. This result is not surprising as the literature compound is in its protonated state and the electro-positive nature of the ligand influence the strong interactions.

There is no literature precedent for the complexation of **L2** with cobalt(III). Therefore **L2** was reacted with a cobalt(III) metal centre according to the Drinkard *et al.* method.[123] The resulting purple reaction mixture was filtered and concentrated under the reduced pressure. A few drops of concentrated aqueous lithium iodide solution was added to the reaction mixture and left for slow evaporation.

The yellow crystals started to grow from the neck of the vial as the solution started to evaporate slowly over a period of one week.

The yellow crystals were collected and analysed by mass spectrometry, NMR spectrometric techniques, UV/vis, IR microanalysis, as well as X-ray crystallography.

Mass spectrometric analysis of the complex indicated the presence of $[Co(L2\text{-}H)_2]^+$ complex with m/z = 353.1594. There are many coordination possibilities for the **(L2-H)**

with cobalt(III), leading to many different isomers. Some of them are shown in Figure 3.25.

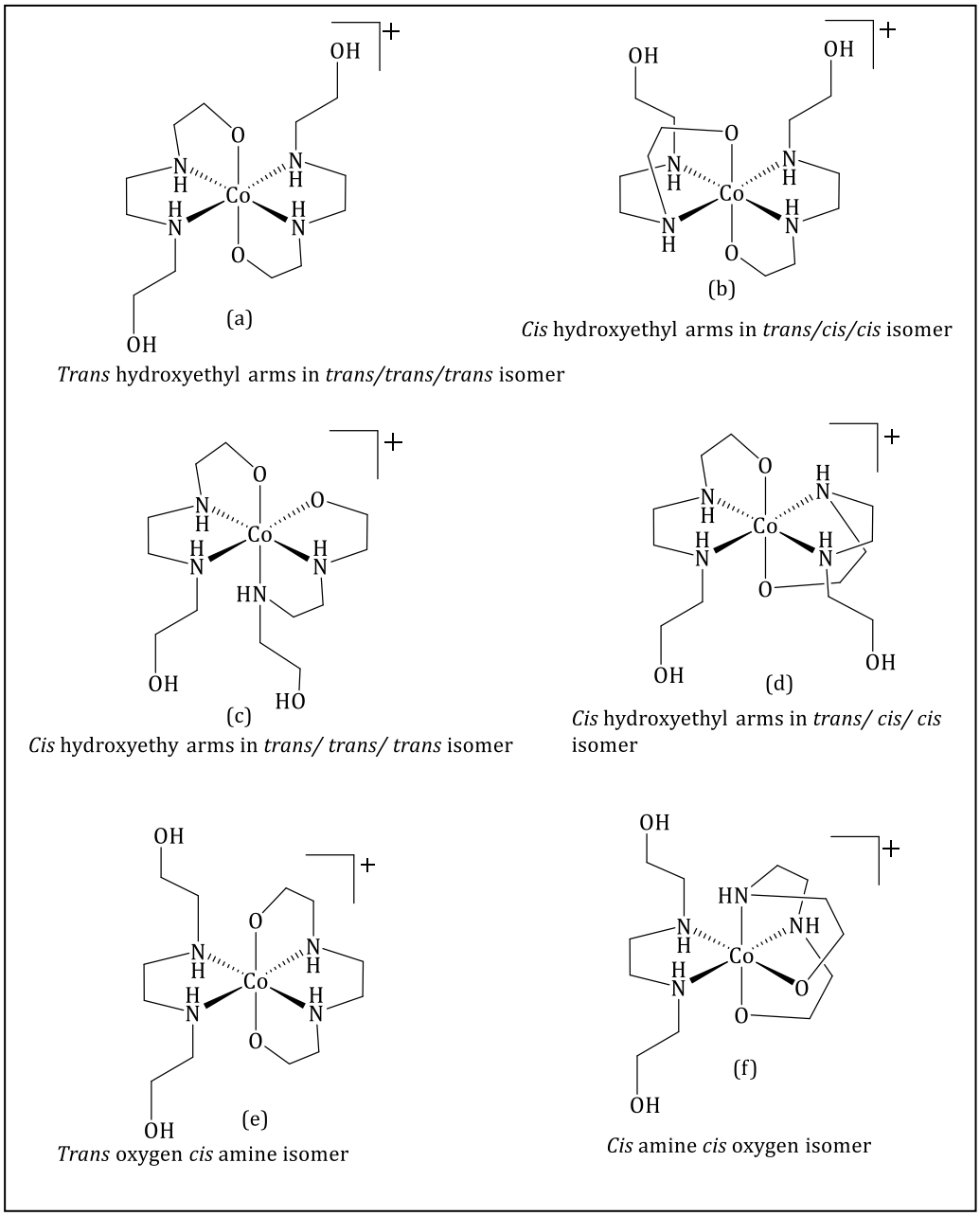

Figure 3.25. *Different possible isomers of the complex formula* $[Co(L2\text{-}H)_2]^+$.

Crystals obtained (yield 65%) by slow evaporation of an aqueous solution of the reaction mixture were suitable for X-ray crystallographic analysis.

The solution to the X-ray diffraction analysis of the crystal is shown below.

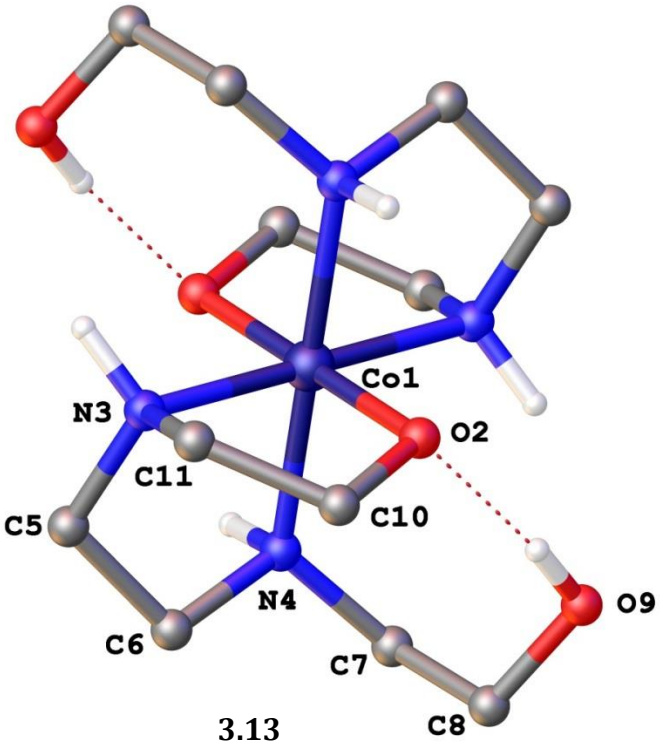

3.13

Figure 3.26. *X-ray crystal structure of $[Co(L2\text{-}H)_2]^+$, **3.13**, present as its trans/trans/trans isomer with atom-labelling. The tri iodide anion in back ground and the hydrogen atoms on the complex, except amine and hydroxyl hydrogens, are omitted for the clarity.*

Molecular structure of $[Co(L_2\text{-}H)_2]^+$; Selected bond lengths (Å) and bond angles(°); Co1-O2 1.892(2), Co1-N3 1.946(2), Co1-N4 2.00(2); O2-Co1-N3 87.63(9), N3-Co1-N4 86.71(9), O2-Co1-N4 95.03(8).

The crystal structure is solved in $P2_1/c$ monoclinic space group with the R value of 2.57. The asymmetric unit consists of half of the complex cation and half of the triiodide anion. The complex itself shows a distorted octahedral geometry. One of the hydroxyl groups from each ligand was deprotonated during coordination in *trans* manner with the cobalt(III) centre. The absence of electron density around the coordinated oxygen also supported the idea of deprotonation during coordination. The amine nitrogen atoms bonded to the coordinated oxygens are coordinated with the cobalt(III) in *trans*

manner, also the amine nitrogen atoms bonded to the free hydroxyethyl arms show *trans* coordination with the metal centre. The hydrogen atom of the hydroxyl group forms an intramolecular hydrogen bond with the deprotonated oxygen atom from the same ligand.

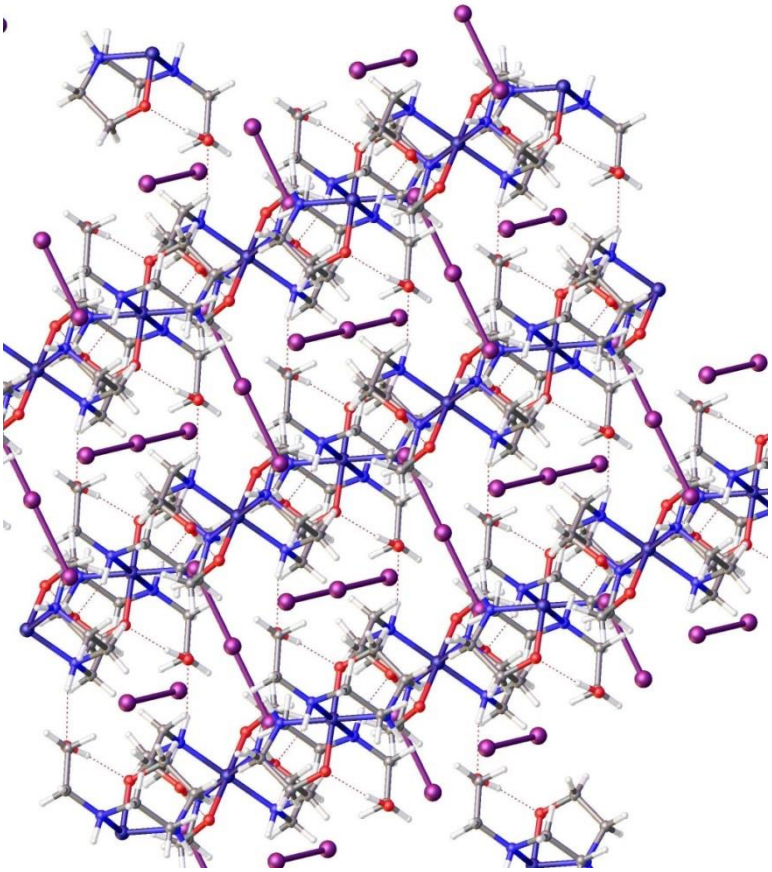

Figure 3.27. *The packing structure of complex **3.13** through 111 plane shows the arrangement of triiodide anions in space between cationic complexes.*

Intermolecular hydrogen bonding between the secondary amine hydrogen atoms and hydroxyl hydrogen from the adjacent molecule may help to stabilise the packing structure. Iodide was added as part of an exploration of whether other anions would improve the crystallisation conditions.[123] The iodide ions added need to follow the reaction process below to form rod like I_3^- anions.

$$I^- + I_2 \longrightarrow I_3^-$$

The iodide ions added to the reaction mixture need to undergo an oxidation process to produce iodine in the reaction mixture to react with iodide anion. This oxidation process could be facilitated by the reduction of cobalt(III) to cobalt(II) in the reaction mixture. The cobalt(II) contaminant observed in the product material could be produced from the above reduction process.

Also the reaction mixture was open to the atmosphere during crystallisation and the iodide anion in the reaction mixture could be oxidised by atmospheric oxygen to produce iodine molecules.

These anions arranged into two different directions and filled the spaces between crystalline complexes. These I_3^- carry the highest percentage of electron density from the electron density map generated during the X-ray crystallographic studies.

An X-ray powder diffraction analysis of the bulk crystalline material was carried out to confirm that the single crystal represents the bulk material.

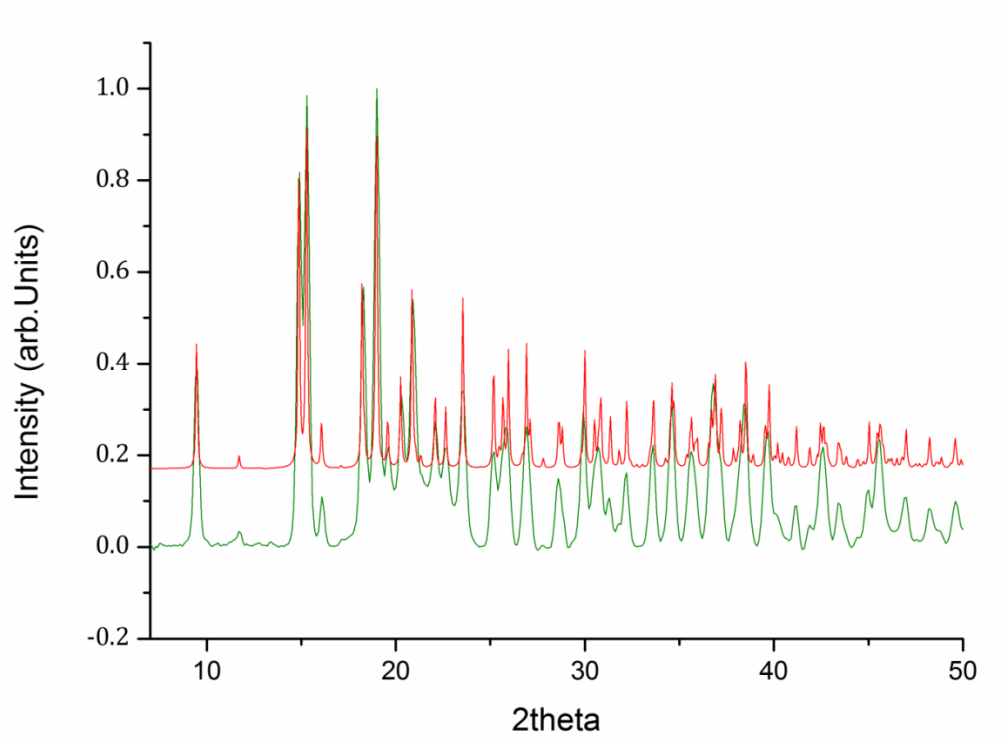

Figure 3.28. *The powder diffraction patterns of complex **3.13** showed the experimental (green) and the calculated (red) patterns are in agreement.*

The powder diffraction pattern was found to match the calculated and experimental values and unambiguously confirmed that the single crystal for **3.13** is a representative of the bulk material.

The ^{1}H NMR spectrum and ^{13}C NMR spectrum of **3.13** crystals were unexpectedly complicated as shown in Figure 3.29 and Figure 3.30.

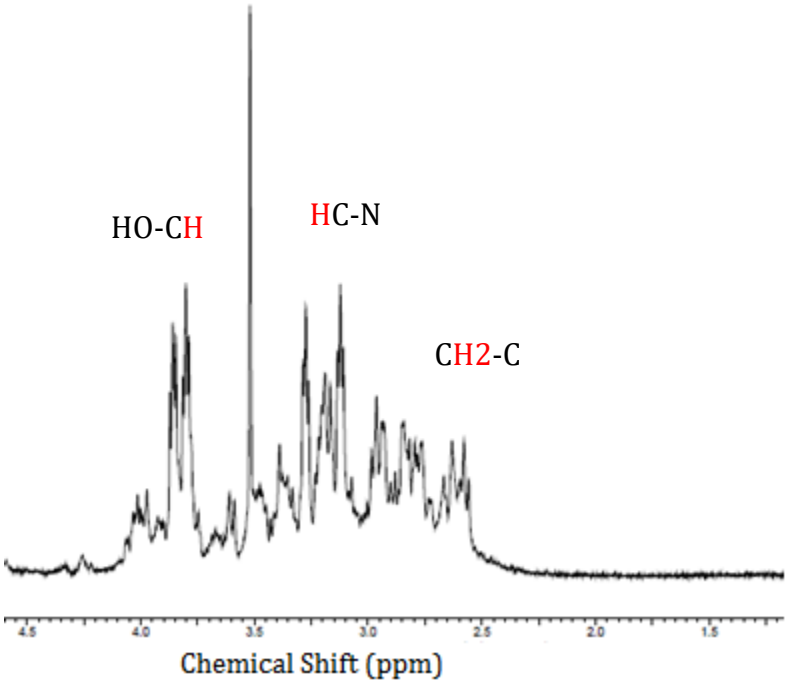

Figure 3.29. *^{1}H NMR of complex **3.13** in D_2O with reference to TMPS, showing a range of peaks due to different types of protons.*

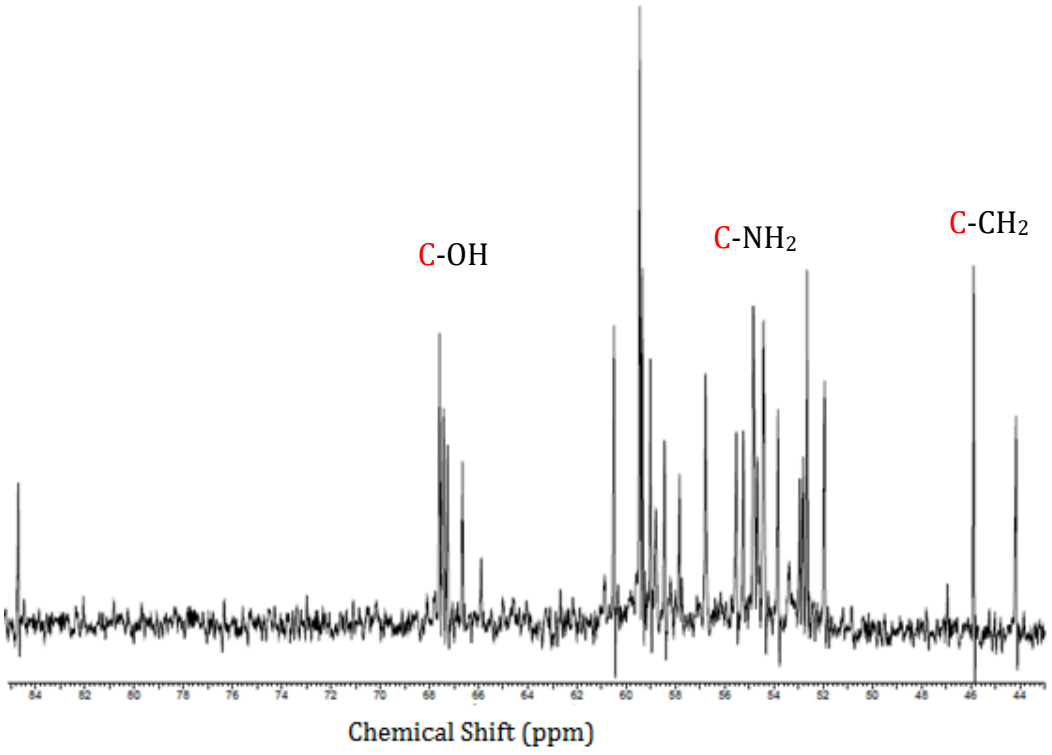

Figure 3.30. *^{13}C NMR of complex **3.13** in D_2O with reference to TMPS, showing a range of peaks due to different types of carbons.*

The NMR spectra, Figure 3.29, Figure 3.30, confirmed that the compound **3.13** has different behaviour in solution compared to the solid state. This complexity may be due to the isomerisation of the complex in solution, but the information obtained so far is not sufficient enough to draw a solid conclusion.

After extracting the crystals, the supernatant solution gave rise to a very small amount of X- ray quality crystals. The crystals were similar in appearance to the crystal of complex **3.13**. The unit cell of the new crystals had different dimensions to the crystals of **3.13** complex crystals. **3.13**: a=9.35502(1), b=(10.36870(1), c=11.02739(2); **3.14**: a=9.7243(6), b=(22.1877(7), c=(23.8537(1)).

X-ray crystallographic solution to these small crystals, **3.14** were shown in Figure 3.31

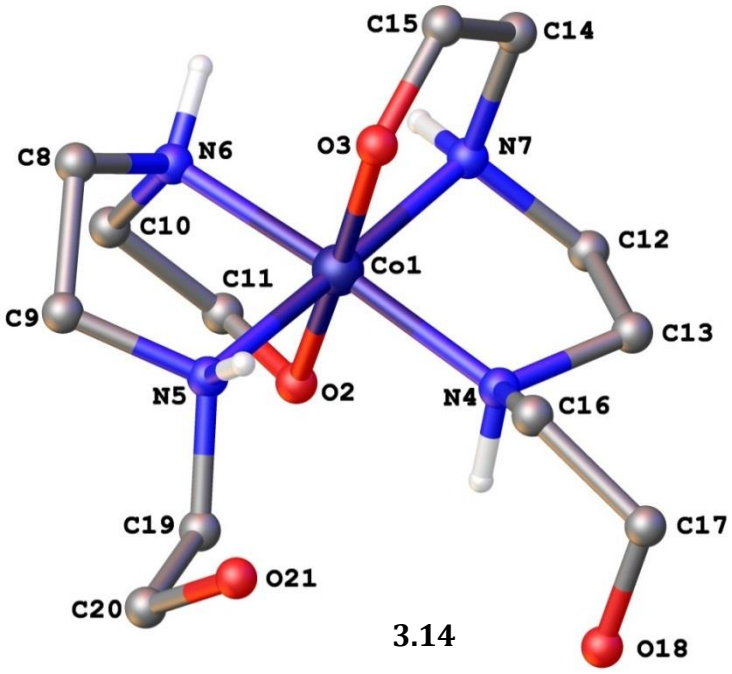

3.14

Figure 3.31. *X-ray crystal structure of isomer **3.14** of the $[Co(L2\text{-}H)_2]^{2+}$ complex. The triiodide anion, the iodine molecule and the hydrogen atoms, except the hydrogen atoms on amine groups, were omitted for the clarity.*

The molecular structure of $[Co(L2\text{-}H)_2]^+$; Selected bond lengths (Å) and bond angles(°); Co1-O2 1.876(1), Co1-O3 1.875(1), Co1-N4 1.964(2), Co1-N5 1.956(2), Co1-N6 1.958(2), Co1-N7 1.958(2); O2-Co1-O3 176.0(6), O2-Co1-N4 91.1(6), O2-Co1-N5 91(6), O2-Co1-N6 85.2(6), O2-Co1-N7 91.0(7), O3-Co1-N4 91.8(7), O3-Co1-N5 91.6(7), O3-Co1-N6 92(7), O3-Co1-N7 86.3(7), N5-Co1-N4 93.7(6), N6-Co1-N5 84.8(6), N7-Co1-N4 86.9(8), N7-Co1-N5 177.9(8), N7-Co1-N6 94.7(7).

The complex crystallised in a *Pbca* orthorhombic space group which is different to the $P2_1/c$ space group of **3.13**.The asymmetric unit consists of a complete complex cation with a triiodide anion

The **3.14** complex shows a distorted octahedral geometry with two **(L2-H)** ligands coordinated around the metal centre. The coordinated oxygen atoms are *trans* to each other and similar to the arrangement of complex **3.13** the main difference observed to the complex **3.13** is the *cis* coordination pattern of amine groups and the arrangement of hydroxyethyl arms. In the **3.13** hydroxyethyl arms arranged into the opposite side of the complex while the hydroxyethyl arms of **3.14** arranged into the same side of the complex.

In the packing structure, intermolecular hydrogen bonding interactions are observed between the hydroxyl hydrogens and coordinated oxygen atoms of the adjacent molecule. Also another hydrogen bond was found between hydroxyl group oxygen with secondary amine hydrogen atom. The complex **3.14** does not show the presence of intramolecular hydrogen bonding which is seen in the **3.13** crystal structure. This may be due to the longer distance between coordinated oxygen atom and the uncoordinated hydroxyl hydrogen atoms.

Unfortunately, other characterisation could not be performed due to the low yield of **3.14** crystals. A random selection of 10-12 crystals from this small sample were analysed by X-ray crystallography and the cell dimensions compared with the obtained cell dimensions for **3.13** and **3.14** crystal structures. While some crystal showed matching dimensions, others did not match with the **3.13** or **3.14** structure dimensions. This could be due to the formation of other isomers during the reaction in a very small yield. But the diffraction patterns of these crystals were not enough to collect data for the analysis.

3.2.6 Synthesis of cobalt(III) complexes of 2,2'-((2-((2-hydroxyethyl)amino) --ethyl)azandiyl)diethanol, L8,

The attempts to synthesise **L8** and purify the desired ligand were unsuccessful. But during the synthesis of **L2** the formation of **L8** and **L9** as by-products was observed. After crystallising **L9** from hot THF, the yellow oil obtained was mainly composed of **L8** and **L9**. The ligand mixture was reacted with $[Co(NH_3)_6Cl_3]$ under the Drinkard *et al*[123] reaction conditions.

The purple aqueous reaction mixture was filtered and few drops of concentrated LiI solution were added. The aqueous solution of the reaction mixture yielded bright red plate-like crystals (yield 40%).

These crystals were analysed by NMR techniques, mass spectrometric analysis, UV/vis, IR, microanalysis, and X-ray crystallography.

Mass spectrometric analysis of the crystals showed the presence of a possibly dimeric species giving m/z = $[M]^{2+}$ = 498.12 and half of the dimer as m/z = $[M/2]^{+}$=248.0548.

^{1}H NMR analysis of the complex and assignment of peaks is supported by ^{13}C MNR spectroscopy, HSQC and gCOSY NMR spectroscopy.

The analysis of the red crystals from above techniques confirmed the presence of the **3.15** complex Figure 3.33. The structure shows the presence of cobalt(III) complex in coordination with**(L8-2H)** ligand. The results confirmed that this reaction technique was useful to separate the cobalt(III) complex of **L8** from the **L8/L9** ligand mixture.

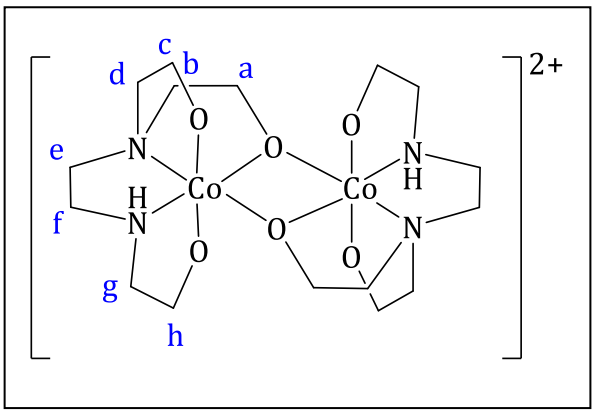

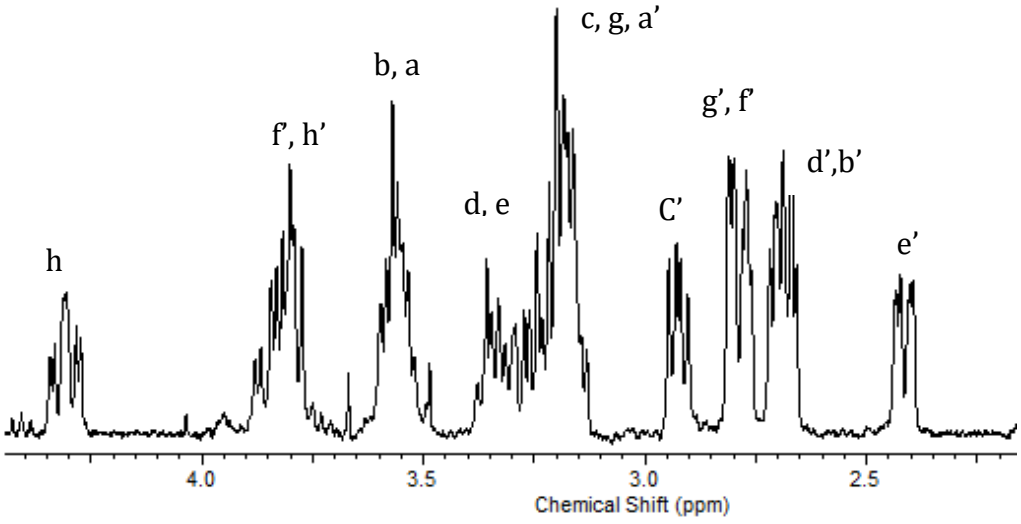

Figure 3.32. *^{1}H NMR spectrum of complex [Co(L8-2H)]$_2$]$^{2+}$, **3.15** in D_2O with reference to TMPS.*

Red crystals obtained from the reaction mixture were analysed by X-ray crystallography and solution to the crystal structure is shown below.

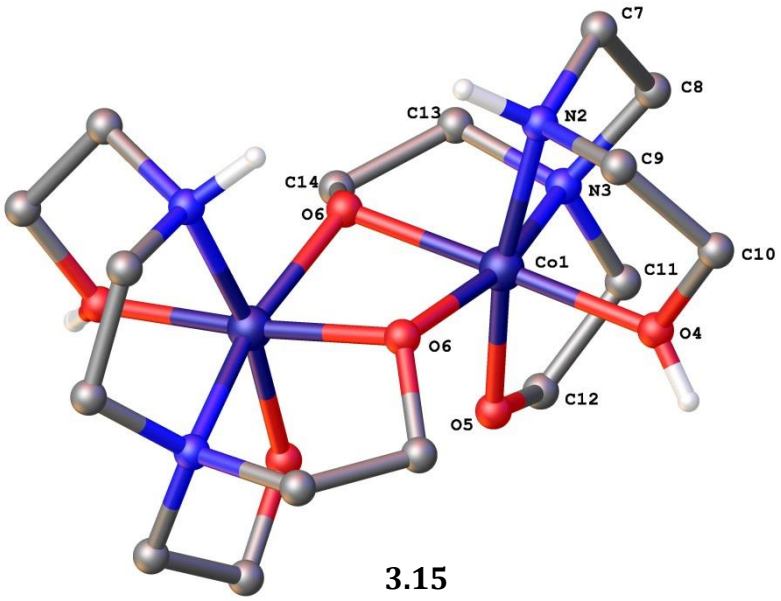

3.15

Figure 3.33. *Dimeric structure of complex **3.15.** The triiodide anion and the hydrogen atoms, except protonated amine and oxygen, were omitted for the clarity.*

The asymmetric unit of the complex $[Co_2(L8\text{-}2H)_2]^{2+;}$ Selected bond lengths (Å) and bond angles(°); Co1-O4 1.918(5), Co1-O5 1.910(5), Co1-O6 1.893(5), Co1-N2 1.933(6), Co1-N3 1.915(7), O6-Co1' 1.925(5); O4-Co1-Co1' 134.46(2), O4-Co1-N2 85.4(2), O5-Co1-O4 87.3(2), O5-Co1-N2 169.7(2), O5-Co1-N3 85.7(3), O6-Co1-O4 174.9(2), O6-Co1-O5 95.1(2), O6-Co1-N2 92.8(2), O6-Co1-N3 87.4(3), N3-Co1-N2 88.1(3).

The crystal structure of complex **3.15** was solved in the C2/*c* monoclinic space group. The asymmetric unit of the complex consists of half of the complex and a triiodide anion.

Each cobalt(III) metal centre has a distorted octahedral geometry with coordinated **(L8-2H)** filling five coordination sites. The sixth coordination site is filled by O6 oxygen atom on the ligand bound to the other cobalt(III) ion. The two cobalt(III) metal centres were found in the proximity of 2.866(2) Å.

The monomers are held together by the formation of a Co2-O2 ring across an inversion centre. The complex utilizes the hydroxylate oxygen to form two Co-O-Co bridges between the cobalt(III) centres. The Co1-O6 has a shorter bond length (1.893Å) compared to other Co-O bond lengths (1.910-1.983) Å.

Each half of the molecule present in the asymmetric unit of the complex **3.15** is associated with a triiodide anion which confirmed the (+1) charge for the each half of the molecule and (+2) charge for the complete dimer. The (+1) charge is due to one protonated oxygen atom on the **(L8-2H).** The longer bond length of Co1-O4 1.918(5) compared to Co1-O5 1.910(3) suggested the possible protonation of the O4 oxygen atom and also the lowest refinement value obtained was with an added proton on the O4 oxygen compare to the O5 confirmed the protonation of O4 atom.

The complex **3.15** is reacted with $ZnCl_2$ in a methanolic solution and the resulting pink solution was filtered and left for slow evaporation. The resulting orangish-pink plate like crystals were analysed by X-ray crystallography.

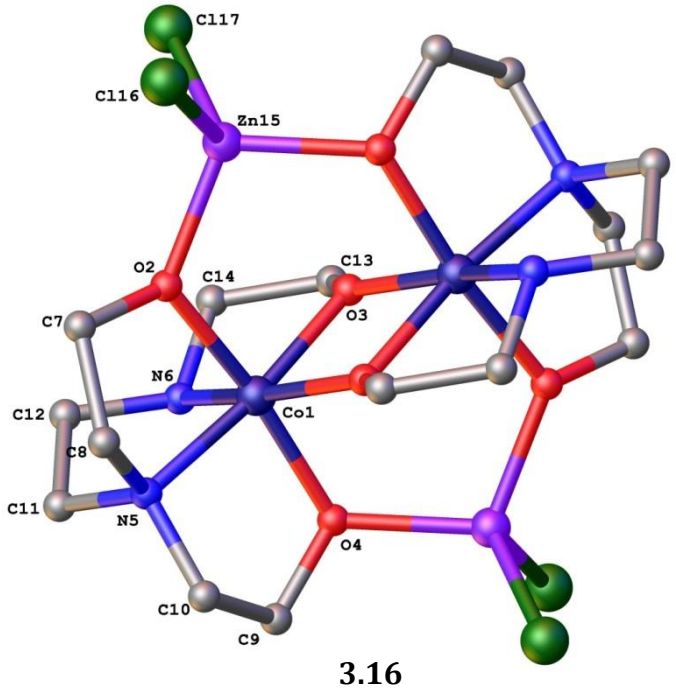

3.16

Figure 3.34. *Tetranuclear complex, **3.16** with atom-labelling for the asymmetric unit. Hydrogen atoms present on the complex were omitted for the clarity.*

The asymmetric unit of the complex $[Co(L8\text{-}3H)ZnCl_2]_2$; Selected bond lengths (Å) and bond angles(°); Zn15-Cl16 2.259(2), Zn15-Cl17 2.253(2), Zn15-O2 1.921(6), Co1-O4 1.892(5), Zn15,O4' 1.948(6), Co1-O2 1.906(6), Co1-O3 1.902(5), Co1-O3' 1.944(5), Co1-N5 1.939(6), Co1-N6 1.898(6); Cl17-Zn15-Cl16 110.36(9), O2-Zn15-Cl16 108.48(2), O2-Zn15-Cl17 111.14(2), O2-Co1-N5 84.2(2), O3-Co1-O2 91.0(2), O3-Co1-N5 172.4(2), O4-Co1-O2 171.2(2), O4-Co1-O3 97.6(2), O4-Co1-N5 87.5(2), O4-Co1-N6 88.3(3), N6-Co1-O2 93.9(3), Co1-O2-Zn15 120.4(3), Co1-O3-Co1' 100.7(2).

The tetranuclear complex **3.16** shows the complexation of a dinuclear **3.15** complex with two zinc chloride molecules. Each zinc chloride is coordinated to two of the non-bridging oxygen atoms of the **3.15** complex, respectively, from opposite directions.

The compound crystallised in the *Pbca* orthorhombic space group. The asymmetric unit of the complex consists of half of the complex and two water molecules. The two water

molecules connect with inter molecular hydrogen bonding and also hydrogen bond to the amine hydrogen of the complex.

The zinc(II) ions are bonded to oxygen atoms that are already coordinated to the cobalt(III) metal centre.

The cobalt(III) metal centre shows the distorted octahedral geometry and the zinc metal centre shows distorted tetrahedral geometry. There are no significant changes observed between the bond lengths and bond angles between **3.15** and **3.16**.The tetranuclear complex **3.16** is neutral in charge and during coordination of $ZnCl_2$ the complex **3.15** showed the deprotonation of O4 oxygens.

3.2.7 Synthesis strategy of cobalt(III) complexes of 2,2',2'',2'''-(ethane-1,2-diylbis(azanetriyl))tetraethanol, L9,

L9 was synthesised and characterised according to Herrag *et al.*[146] Attempts to isolate complexes of **L9** with cobalt(III), according to the method of Drinkard *et al*[123] were unsuccessful. The change of colour of the reaction mixture from yellow to purple indicates some complexation, presumably due to the coordination of oxygen atoms with the cobalt(III) metal centre.

The formed complex seems to be highly unstable at higher temperatures. The bluish coloured material obtained during the purification is a sign of cobalt(II), which suggests the decomposition of the complex.

The information obtained for the analysis of crude product is insufficient to understand the complexation of **L9** with cobalt(III) metal centre. Attempts made to crystallise any

possible cobalt(III) complex formed with **L9** ligand using $ZnCl_2$/$MnCl_2$ were not successful.

Oxygen atoms in the Cu_2O_2 ring have shortened bond lengths of 1.940Å and 1.959Å between oxygen and copper(II) ions in comparison to the axial protonated oxygen and copper(II) ions. This longer bond length is the characteristics of Jahn–Teller distortion observed for copper coordinated compounds.

3.3 Utilising 3.13 alkoxide complex to synthesise DNA cross-linking nitrogen mustard on cobalt(III) metal centre

Bis-alkylating nitrogen mustard compounds are highly effective as cytotoxic compounds compared to mono-alkylating counterparts.[147] While mono-alkylating nitrogen mustard compounds only alkylate a single base of a DNA molecule, bis-alkylating nitrogen mustard compounds have the capability to form inter- or intra-strand cross-links by alkylating the two nitrogen bases on the DNA molecule and this strategy was discussed in chapter 01.[148] The cross-links are strong covalent bonds highly resistant to DNA repair enzymes.[147]

L2 possesses two hydroxyethyl groups, which have the potential to be converted to chloroethyl functionalities, to give a cross-linking type of nitrogen mustard compound.

Due to the high toxicity of nitrogen mustard compounds, new synthetic procedures were investigated to append a cross-linking nitrogen mustard on cobalt(III) metal centre in its hydroxyethyl precursor form and hence avoid the free handling of toxic nitrogen mustard compounds.

Previous attempts to complex **L2** with cobalt(III), with the focus of synthesising nitrogen mustard cobalt(III) complexes, proved unsuccessful as reported by Alan Downward in his thesis.[121]

The study of the coordination chemistry of amino alcohol ligands, lead us to synthesise desired cobalt(III) precursor complexes necessary for the synthesis of cobalt(III) complexes with coordinated bis-alkylating nitrogen mustard ligands. Here we describe the chemistry required to achieve the functional group chemistry that is required to prepare the bis-alkylating nitrogen mustards.

Two different complexes of this category, $[Co(bceen)_2Cl_2]^+$, **3.17** and $[Co(bceen)_2(NO_2)_2]^+$, **3.18**, were synthesised by strictly following the safe synthesis concept during this work.

Reaction of **3.13** complex with $SOCl_2$ / DMF reaction mixture showed the formation of $[Co(bceen)_2Cl_2]Cl$, **3.17**, complex. Heating of the reaction mixture was necessary to achieve the complete conversion of **3.13** to **3.17** complex, Figure 3.36. This may be due to the strong bonding interaction between cobat(III) metal centre with coordinated hydroxyl oxygen.

Mass spectrometric analysis of the reaction mixture shows possible complex intermediates during conversion of the complex **3.13** to **3.17**. The recognised mass spectrometric cationic components are, $[C_{12}H_{30}N_4O_4Co_1]^+$ = m/z = 353.1599; $[C_{12}H_{28}N_4O_2Cl_2Co_1]^+$ = m/z = 389.0921; $[C_{12}H_{29}N_4O_2Cl_3Co_1]^+$ = m/z = 425.0688; $[C_{12}H_{30}N_4Cl_4O_2Co_1]^+$ = m/z = 463.04; $[C_{12}H_{28}N_4Cl_6Co_1]^+$ = m/z=496.978, with possible structures being shown in the Figure 3.36. This analysis helps us to develop a stepwise reaction pathway for the synthesis of complex **3.17**.

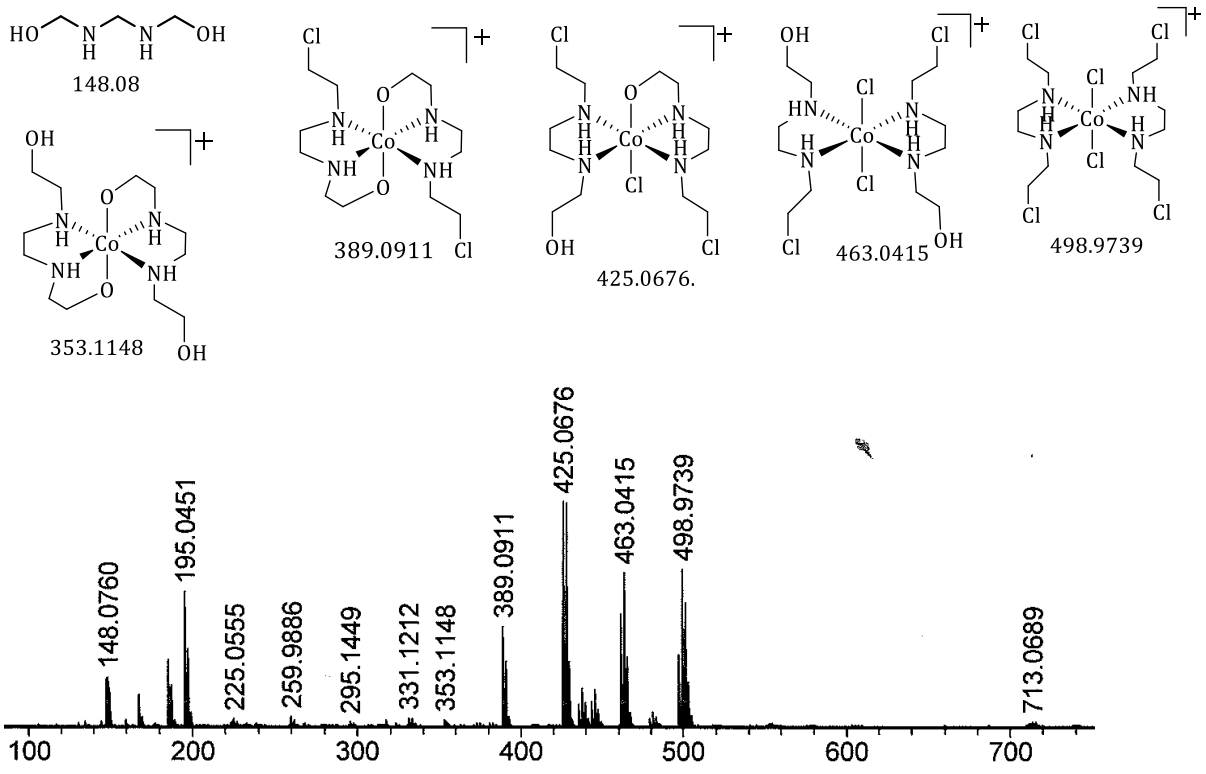

Figure 3.35. *ESI-MS(+ve mode) of reaction mixture with possible structural components.*

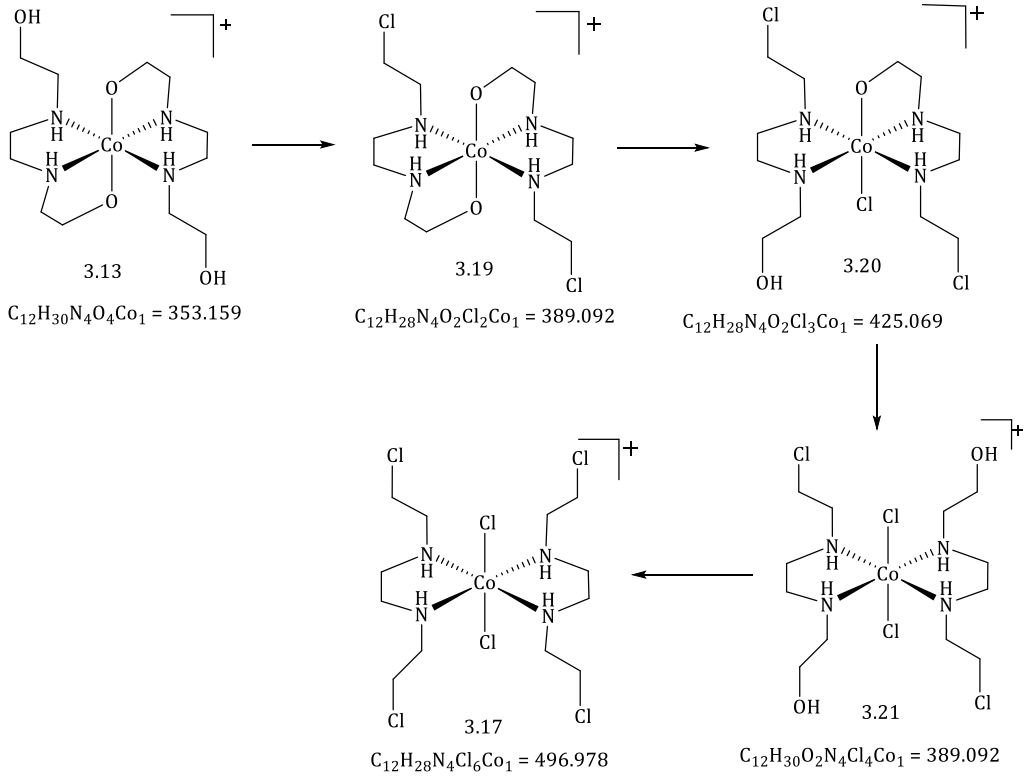

Figure 3.36. *Suggested reaction pathway for the conversion of **3.13** into **3.17** complex.*

The information obtained supported the suggested reaction route for the conversion of complex **3.13** to **3.17**, Figure 3.36. The reaction was repeated numerous times and the reaction mixtures were analysed in different intervals during the reaction. The results obtained by mass spectrometric analysis shows the presence of **3.19** throughout the reaction and suggest that the **3.19** is as a stable cationic fragment in the reaction mixture. The increased reaction temperature and the long reaction time were necessary to eliminate **3.19** from the mixture. The Co-O bond opens up as free hydroxyl ethyl groups while replacing axial coordinates with chloride ligands. The completion of the reaction, to obtain the complex **3.17**, is satisfied by the chlorination of hydroxyl groups.

Reaction mixture was heated at 70 °C overnight to obtain the complete conversion of **3.13** to **3.17.**

The green reaction mixture obtained suggested the coordination of *trans* chloride ligands with the cobalt(III) metal centre.[149] The excess thionyl chloride was removed under vacuum and the obtained green thick material was re-dissolved in ethanol.

After reacting **3.13** with $SOCl_2$ / DMF, the $SOCl_2$ was removed under the vacuum. The obtained powdered green material, after mixing the green slurry with ethanol, was filtered and washed with cold ethanol solution to obtain a pure material.

One of the disadvantages of this reaction is the formation of cobalt(II) ions in the reaction mixture. Formation of cobalt(II) ions was inferred from the bluish coloured ethanol washings. A few ethanol washings were necessary to remove cobalt(II) ions from the product material. The formation of cobalt(II) could be influenced by the heat applied during the reaction as these complexes are not very stable and also the electron

rich sulfur from DMF was most likely to facilitate the reduction of cobalt(III). The formation of cobalt(II) could lead to the reduced yield of the product.

The obtained product was analysed by mass spectrometry, ^{1}H NMR spectroscopy, ^{13}C NMR spectroscopy, gCOSY, and HSQC NMR techniques. Also UV/vis, IR and X-ray crystallographic analysis supported the structure assignment of complex **3.17**.

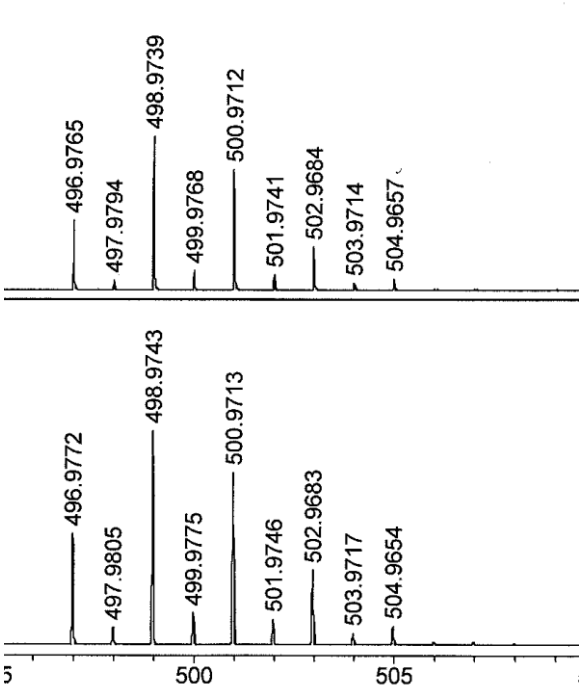

Figure 3.37. *ESI-MS analysis of complex **3.17** showing matching isotopic pattern; experimental (top) and calculated (bottom)*

The mass spectra shown in Figure 3.37 of the complex **3.17** indicate the (+1) charge of the complex. The mass spectrum of **3.17** shows a very complex isotopic pattern which clearly points to the presence of six chlorine atoms and its ^{35}Cl and ^{37}Cl isotopes in their respective natural abundances.

The ^{1}H NMR spectrum of complex **3.17** seems simple. The protons on the carbon atom directly attached to chlorine appear as two multiplets, more down field at around 4

ppm. The other twelve protons appear in four different multiplets. The assignment of the protons was supported by gCOSY and HSQC spectra.

The powdered material obtained was dissolved into a warm ethanol solution and left for slow evaporation. The plate like green crystals were analysed by X-ray crystallography.

The crystal structure for the complex **3.17** was solved in the $P2_1/c$ monoclinic space group,Figure 3.38. The asymmetric unit consist of two half complex molecules, a chloride anion and three water molecules. The two half complexes are part of two slightly different complexes that are present in the structure due to the arrangement of chloroethyl arms in space. One of the complexes show pointing of chloroethyl arms of each ligand to the same side while the other molecule shows the arrangement of chloroethyl arms of each ligand to opposite side of the molecule.

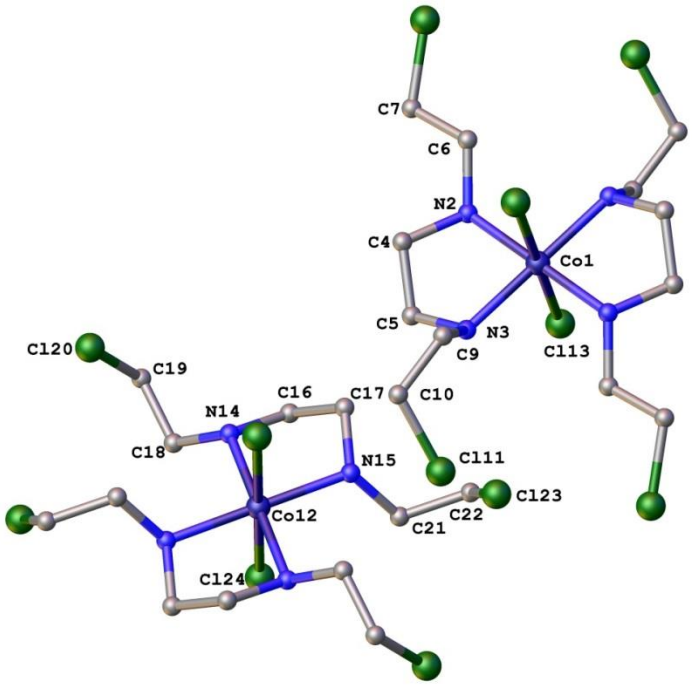

Figure 3.38. *Complete $[Co(bceen)_2Cl_2]^+$, **3.17** with atom-labelling. Complexes generated by the asymmetric units showing the different arrangement of chloroethyl arms in space. The chloride anion and hydrogen atoms were omitted for the clarity.*

Molecular structure of $[Co(bceen)_2Cl_2]^+$; Selected bond lengths (Å) and bond angles(°); Co12-Cl24 2.2398(9), Co12-N14 2.028(3), Co12-N15 2.008(3), C22-Cl23 1.798(5), Cl20-C19 1.793(5), Co1-Cl23 2.255(9), Co1-N2 2.014(3), Co1-N3 2.013(3), Cl9-C7 1.798(4), Cl11-C10 1.802(5); Cl24-Co12-Cl24' 180 N14-Co12-Cl24' 90.84(1), N14'Co12-Cl24' 89.16(1), N14'-Co12-Cl24 90.84(1), N14-Co12-N14' 180.0, N15'-Co12-Cl24 85.61(1), N15-Co12-Cl24' 94.39(1), N15-Co12-Cl24 94.39(1), N15-Co12-Cl24' 85.61(1), N15-Co12-Cl24' 85.61(1), N15-Co12-N14 85.09(1), N15'-Co12-N14 94.91(1), N15'-Co12-N15' 180.0, N2-Co1-$Cl23^2$ 90.2(9), $N2^2$-Co1-Cl13 90.2(9), $N2^2$-Co1-$Cl13^2$ 89.8(9), $N2^2$-Co1-N2 180.0, N3-Co1-Cl13 86.81(9), N3-Co1-$Cl13^2$ 93.19(9), $N3^2$-Co1-$N2^2$ 86.14(1), $N3^2$-Co1-N2 93.86 (1).

The complex crystallised in a distorted octahedral geometry. The two complexes show different arrangement of chloroethyl arms in space. Chloroethyl arms in one of the complexes were pointing to the same side of the complex and the chloroethyl arms in other complex shows the arrangement in opposite side of the complex.

Water molecules in the space form hydrogen bonds with amine hydrogens and oxygen atom of the water molecule. The second water molecule is hydrogen bonded to the chloride anion. Likewise water molecule makes an intermolecular hydrogen bonding network which stabilised the crystal packing.

The complex **3.17** also crystallised as its $[ZnCl_4]^{2-}$ salt. The block-shaped green crystals were analysed by X-ray crystallography.

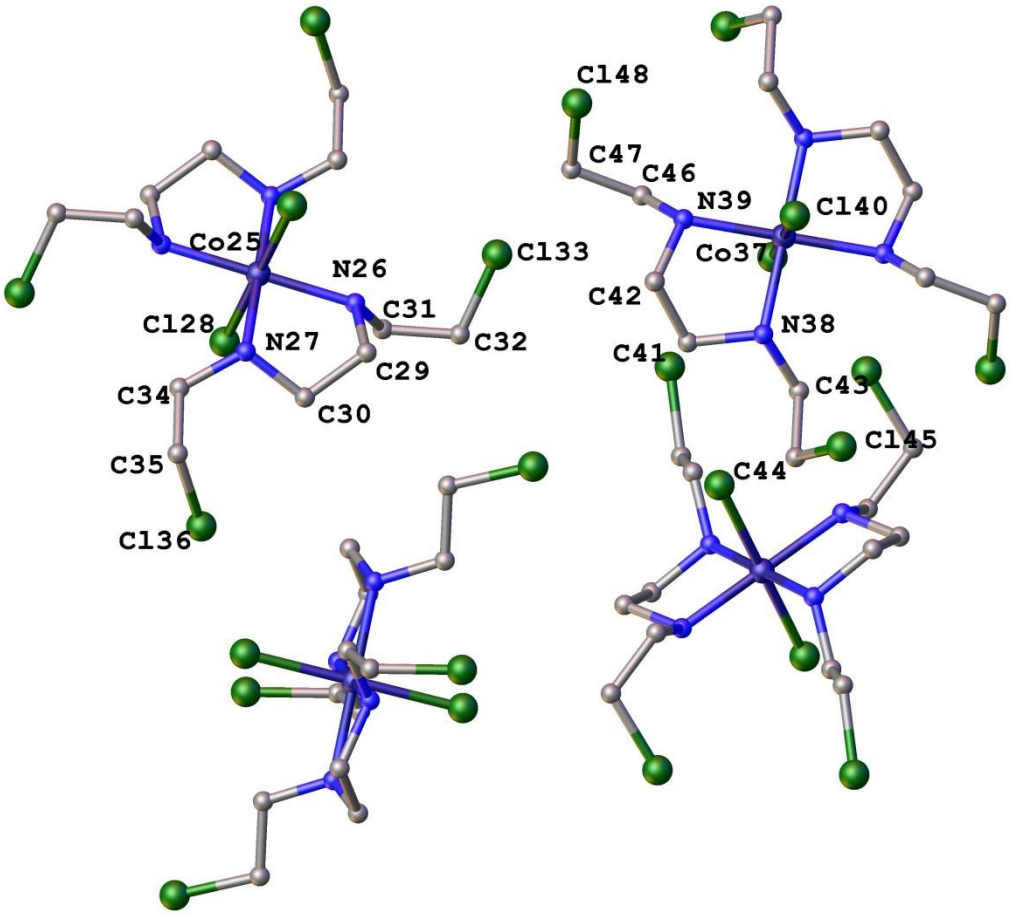

Figure 3.39. *The $[Co(bceen)_2Cl_2]_2[ZnCl_4]$, **3.22** complexes generated by different molecular segments in asymmetric unit showing their arrangement in space. The $[ZnCl_4]^{2-}$ anion is omitted for the clarity.*

The complex crystallises in *P*ī triclinic space group. The asymmetric unit consists of four half molecules and one $[ZnCl_4]^{2-}$ anion. Three of the half molecules have chloroethyl arms pointing to opposite directions and the fourth has chloroethyl arms pointing to the same direction.

A range of cobalt(III) nitrogen mustard complexes with two other labile ligands were investigated to complete the synthesis of heterodinuclear complexes. According to Downward *et al's* Findings, OTf was chosen as the suitable labile ligands. One of the ways of introducing the OTf ligands on to the cobalt(III) centre is by reacting a

cobalt(III) complex with a coordinated nitrite ligand with triflоromethanesulfonic acid. Therefore, reaction of complex **3.17** with NH_4OH and $NaNO_2$ facilitated the exchange of the chloride with the nitrite ligand. The yellow coloured reaction mixture was left in the fridge to obtain yellow powder. Mass spectrometric analysis of the yellow powder obtained under the cold conditions shows the presence of complex **3.18**.

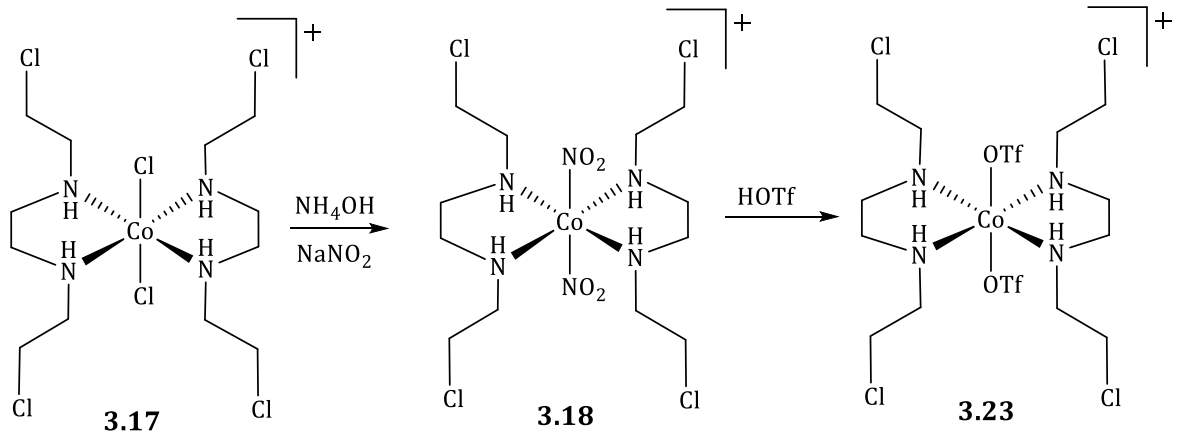

Figure 3.40. *Reaction pathway for the synthesis of complex **3.23**.*

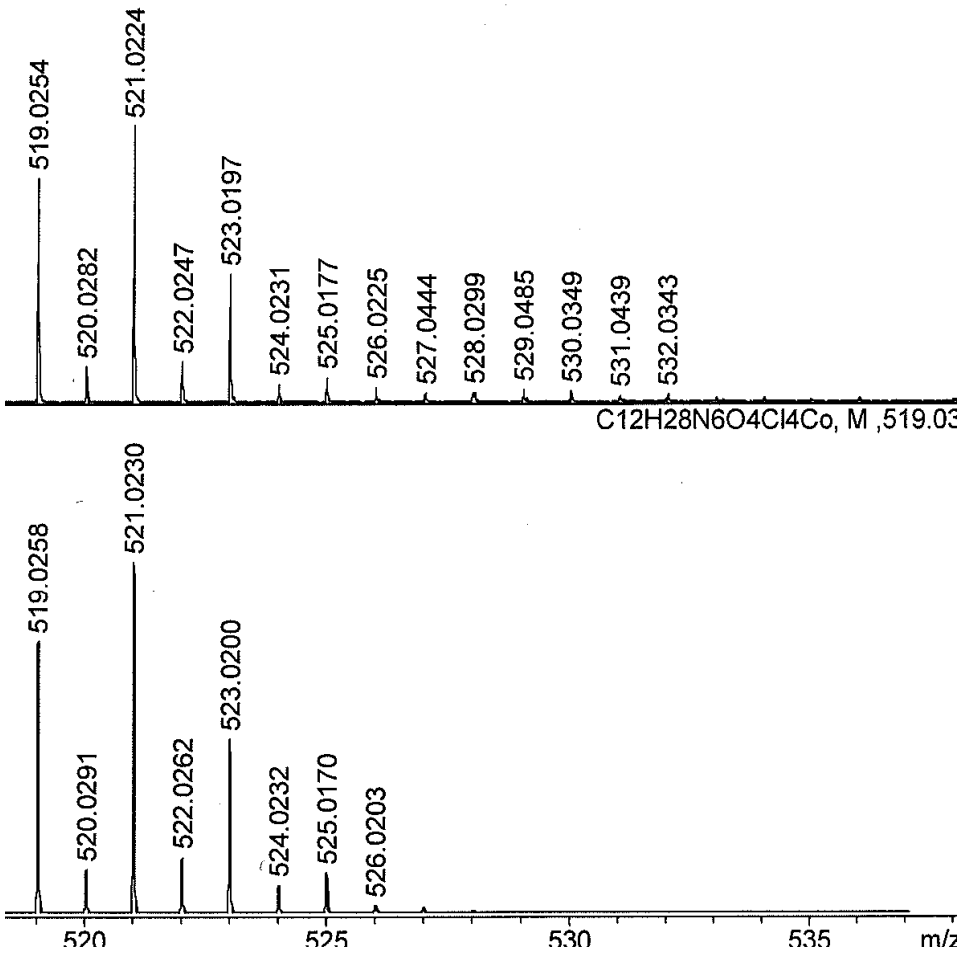

Figure 3.41. *ESI-MS analysis of the complex **3.18**.The complex isotope pattern is prominent in the spectra. Experimental (top) and calculated (below).*

The matching isotopic pattern confirms the presence of complex **3.18**. The increased complexity of the isotopic pattern is mainly due to ^{35}Cl and ^{37}Cl isotopes. As the number of chlorine atoms in the complex increases higher complexity can be expected.

3.4 Summary

This chapter describes the coordination pattern of the range of a similar class of ligands **(L1-L9)** with cobalt(III) metal centres. The focus of this project was to append a nitrogen mustard compound on a cobalt(III) metal centre, and investigating the

behaviour of hydroxyethyl groups during coordination is the main focus from these results.

This study also demonstrated the use of alkoxide complexes to synthesise bisalkylating nitrogen mustard cobalt(III) complexes.

The alkoxide complexes also exhibit interesting polynuclear coordination ability and the polunuclear complexes with zinc(II) chloride and manganese(II) chloride are reported in this chapter. This opens up wider research possibilities to investigate the coordination behaviour of these alkoxide complexes with other metal salts and also to investigate electrochemical and magnetic properties of these complexes.

Also, more complex amino alcohol ligands can be employed or changing reaction condition with **L1-L9** can be employed to synthesis metal clusters or supramolecular metal frames.

Chapter 04

Synthetic approaches to ruthenium(II) cobalt(III) heterodinuclear complexes

4. Synthetic approaches to ruthenium(II) cobalt(III) heterodinuclear complexes

4.1 Introduction

The key goal of this project is to design a ruthenium(II)-cobalt(III) heterodinuclear system as a potential prodrug system. There are dinuclear ruthenium(II)-cobalt(III) complexes reported in the literature.[107], [109], [110], [127] However, there are few reports about the use of these metal systems in medicinal applications.[110]

Models of possible photoactivated ruthenium(II)-cobat(III) systems were previously studied by Alan Downward in the Hartshorn group.[113], [114], [121] He synthesised a heterodinuclear metal system composed of a ruthenium(II) and cobalt(III) metal pair and demonstrated that the photoinduced ligand release of such systems is possible, as discussed in chapter 01.

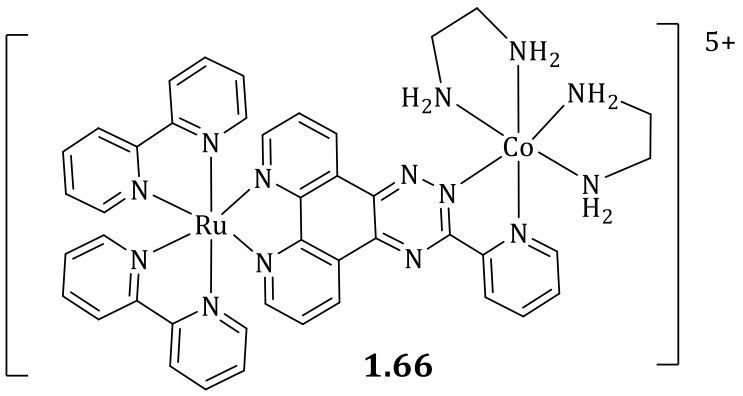

1.66

Figure 4.1. *Ruthenium(II)-cobalt(III) heterodinuclear system synthesised by Alan Downward.*

In this project, we sought to improve the system to achieve an effective prodrug in the following ways;

- 4,4'-Dicarboxylic-2,2'-bipyridine is one of the best ligands for lowering the total complex charge. Each carboxylic ligand on both the bipyridine ligands can be deprotonated over a range of pH values to lower the total complex charge down to (+1).
- Long alkyl chains on the bipyridine ligand are also another approach to introduce hydrophobicity. The hydrophobic ligands were introduced onto the fourth position of bipyridine ligands through esterification reactions.
- The cobalt(III) metal centre was modified by replacement of the ethane-1,2-diamine ligands with cytotoxic nitrogen mustard ligands.

The efficient electronic communication between the two metal centres was satisfied by the pytp (where, pytp = 3-(pyridine-2-yl)-[1,2,4]triazino[5,6f] [1,10]phenanthroline) bridging ligand. The desired heterodinuclear complexes were synthesised with the pytp bridging ligand.

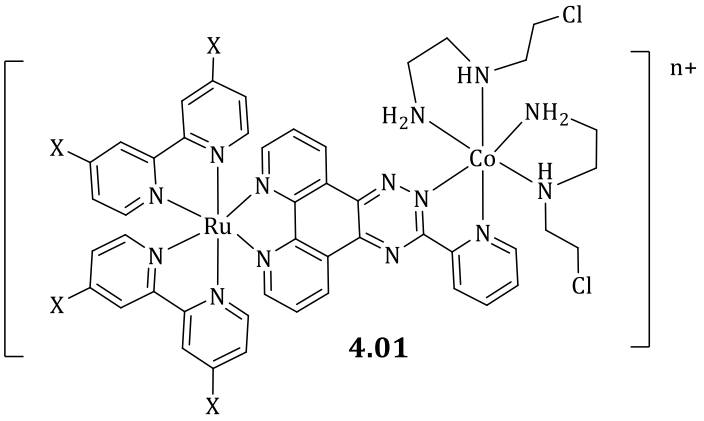

4.01

X = CH_3, -$COOC_2H_5$, -COOH

n = 1,2.....5

Figure.4.2. *Ruthenium(II) cobalt(III) heterodinuclear complex with suggested modifications. The nitrogen mustard on the cobalt(III) centre can be replaced by other mustard ligands.*

Chapter 2 and chapter 3 broadly discussed the synthetic strategy of preparing the cobalt(III) nitrogen mustard complexes without needing to handle the free mustard ligands. We have described some coordination chemistry of amino alcohol ligands with more than one hydroxyethyl arm, and the use of the resulting alkoxide complexes to synthesise possible DNA cross linking nitrogen mustards on cobalt(III) centres.

Here firstly, we investigate the possible use of $[Co(L3)_2(NO_2)_2]^+$, **2.08**, and related complexes for coordination to the ruthenium(II) metal centre through the pytp bridging ligand. The NO_2 axial ligands on the cobalt(III) metal centre need to be substituted with highly labile ligands such as trifluoromethanesulfonate (OTf) to allow the linking reaction to be carried out in very mild conditions. The synthesis and characterisation of $[Co(L3)_2(OTf)_2]^+$, **4.02**, will be discussed in this chapter.

The synthetic strategy for preparation of other ruthenium(II) cobalt(III) heterodinuclear complexes from the related ruthenium(II) complexes and $[Co(tren)(OTf)_2]^+$, **4.03** will also be included in this chapter. Proposed reaction scheme for the synthesis of **4.10(a, b, c, d)** complexes is shown in Scheme 4.1.

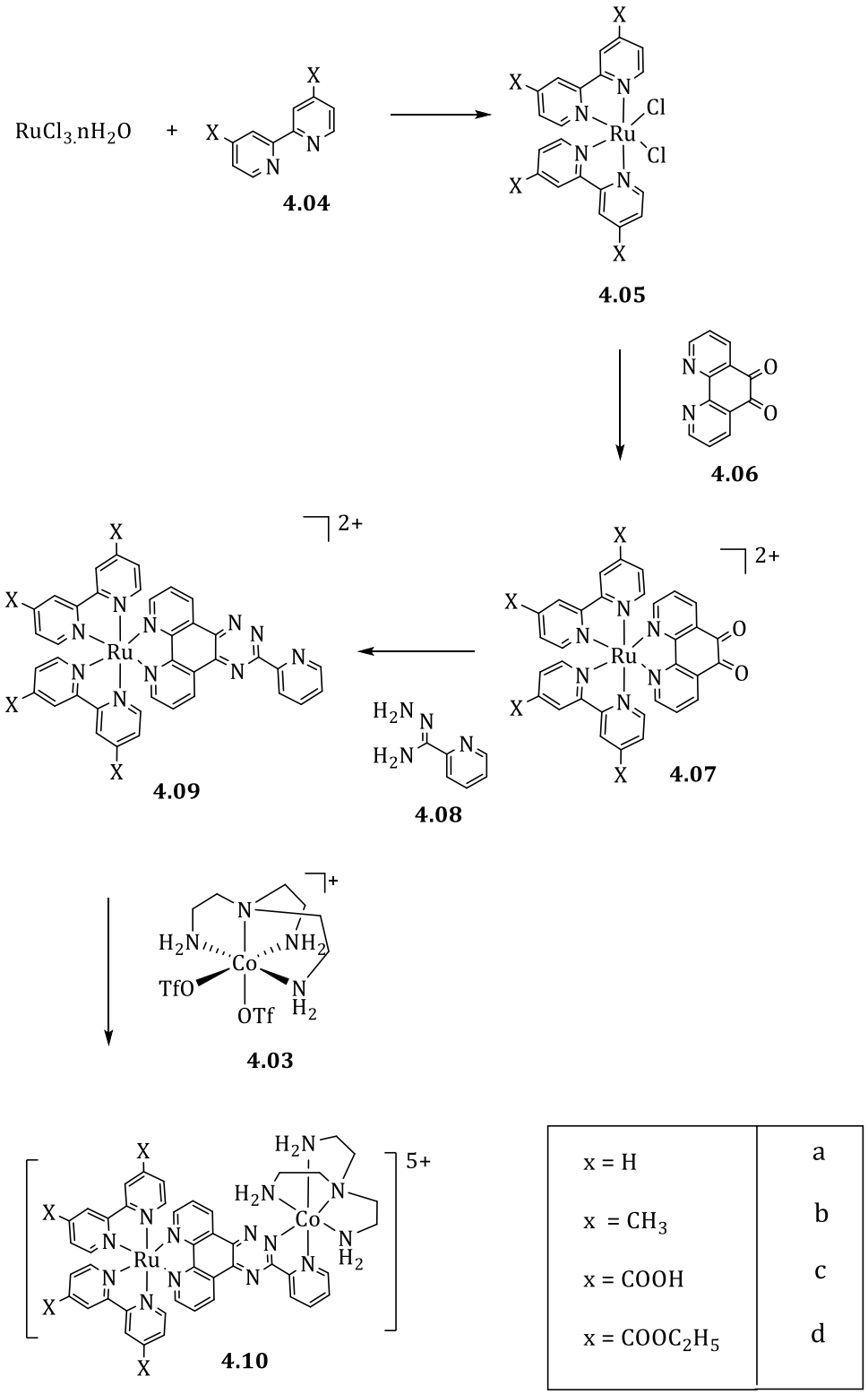

Scheme 4.1. *Synthetic route for the ruthenium(II) cobalt(III) heterodinuclear metal complexes,* ***4.10****. From now onwards, the compounds relevant to different substituents will be represented by the compound number written with relevant letter (a, b, c, or d) as shown in the table.*

Synthesis of ruthenium (II) pytp complexes **4.09a-4.09d** will be discussed in this chapter. The $[Co(tren)(NO_2)_2]^+$, **4.03**, was synthesised according to the procedure reported by Bernal *et al.*[150]

4.2 Results and Discussion

4.2.1. Synthesis of $[Ru(bpy)_2(pytp)]^{2+}$, 4.09a,

$[Ru(bpy)_2(pytp)]^{2+}$, **4.10a**, was synthesised according to the synthetic procedure developed by Downward *et al.*[113] The aromatic region of the ^1H NMR spectrum of **4.10a** in CD_3CN is shown in Figure 4.3.

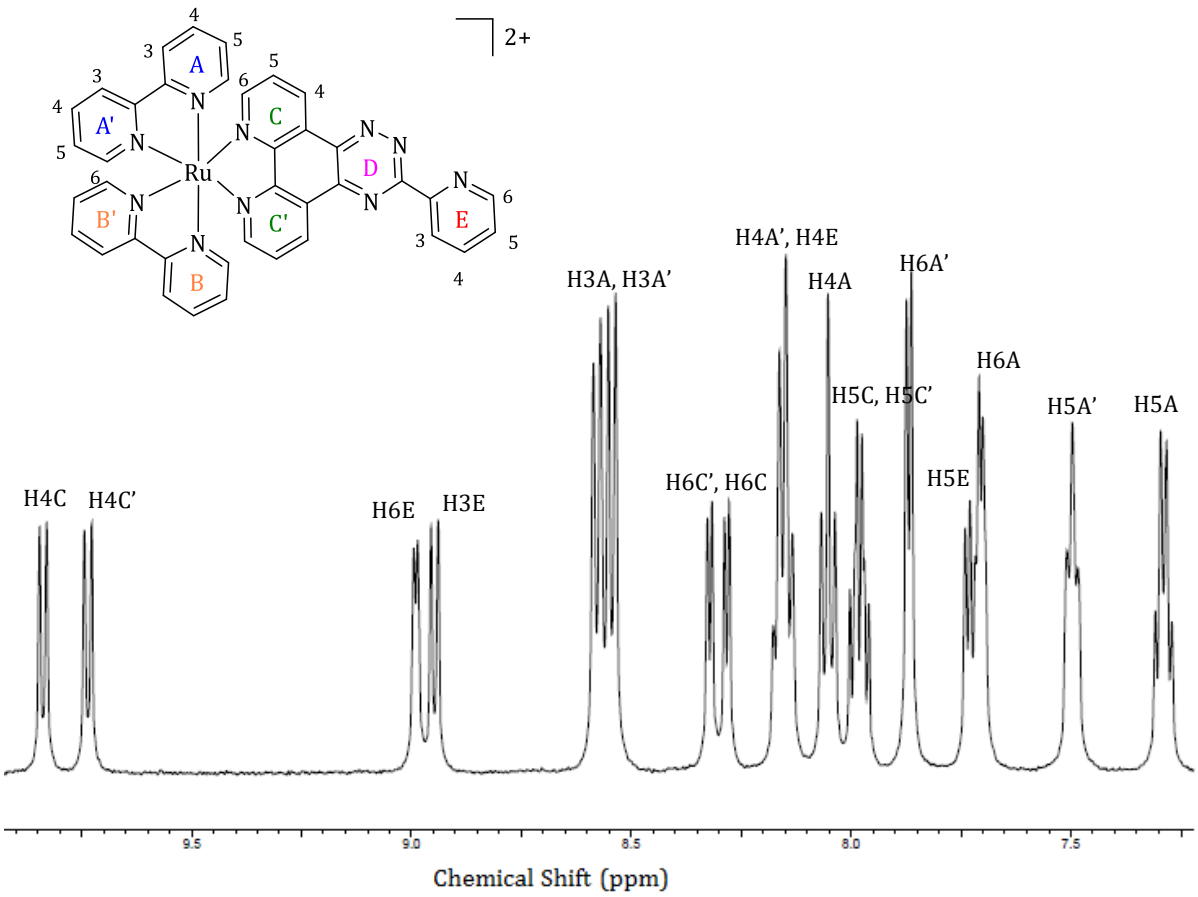

Figure 4.3. *The aromatic region of the ^1H NMR spectrum of $[Ru(bpy)_2(pytp)]^{2+}$,**4.09a**, complex in CD_3CN, showing peak assignments.*

4.2.2 Synthesis of [Ru(4,4'-dmbpy)$_2$(pytp)]$^{2+}$, 4.09b,

Commercially available 4,4'-dimethyl-2,2'- bipyridine, **4.04b**, was reacted with commercially available $RuCl_3 \cdot nH_2O$ according to the procedure described by Sullivan *et al.*[151] Formation of the complex, **4.05b** was observed by mass spectrometric analysis as a (+1) charged complex, $[M\text{-}Cl]^+ = 505.0728$.

The crude black residue of the dichloride ruthenium complex, **4.05b**, was carried onto the next step of the reaction without further purification, Figure 4.1, as is standard for these synthetic sequences.[152], [153]

1,10-Phenanthroline-5,6-dione, **4.06** was synthesised according to the reported procedure[154] and complexed with **4.05b** according to the procedure described by Reddy *et al.*[155] The complex **4.07b** was precipitated by the addition of a concentrated aqueous solution of ammonium hexafluoridophosphate, Figure 4.1.

Complex **4.07b** was then purified by silica gel column chromatography using acetonitrile as the mobile phase and dried under vacuum. The obtained red powdered material was dissolved into a minimum amount of methanol, and precipitated by addition of a concentrated aqueous solution of ammonium hexafluoridophosphate. The resulting orange powder was characterised by mass spectrometric analysis $[M]^{2+}$ = m/z = 340.07, ^{1}H NMR, and gCOSY spectroscopy.

4.09b was synthesised by the procedure described by Downward *et al.*[113] Condensation reaction between the complex **4.07b** with pyridine-2-carbohydrazonamide, **4.08**, was carried out in ethanol. The resulting complex was purified by column chromatography (silica gel, acetonitrile/saturated aqueous KNO_3, 7:1), and the product, **4.09b**, was isolated as its hexafluoridophosphate salt.

The product was then characterised by mass spectrometric analysis, NMR spectroscopic techniques as well as UV/vis, IR, and fluorescence techniques. A key signal from the mass spectrum of complex **4.09b,** with a matching calculated isotope pattern, is shown in Figure 4.4.

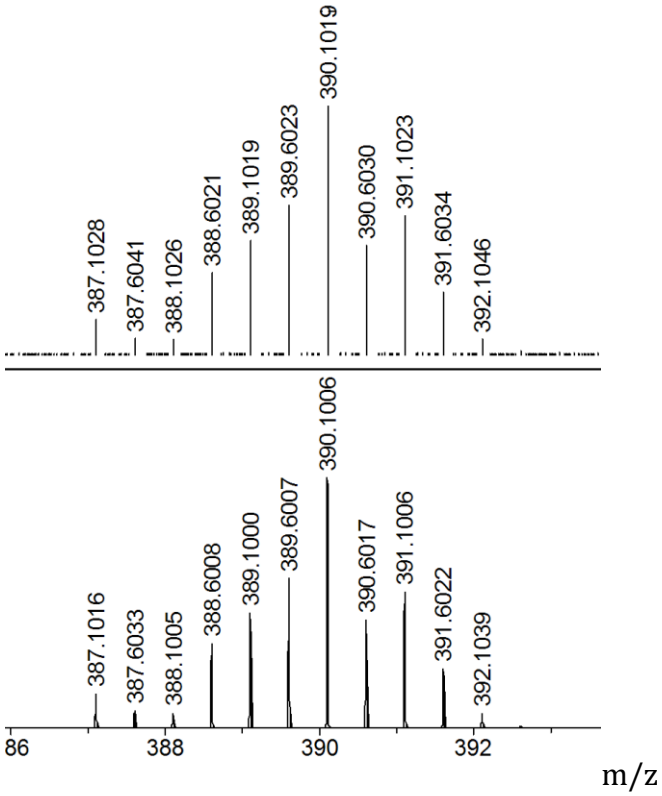

Figure 4.4. *A key signal from the mass spectrum of $[Ru(4,4'\text{-dmbpy})_2(pytp)]^{2+}$,* ***4.09b****, (top), and a matching calculated isotope pattern (bottom).*

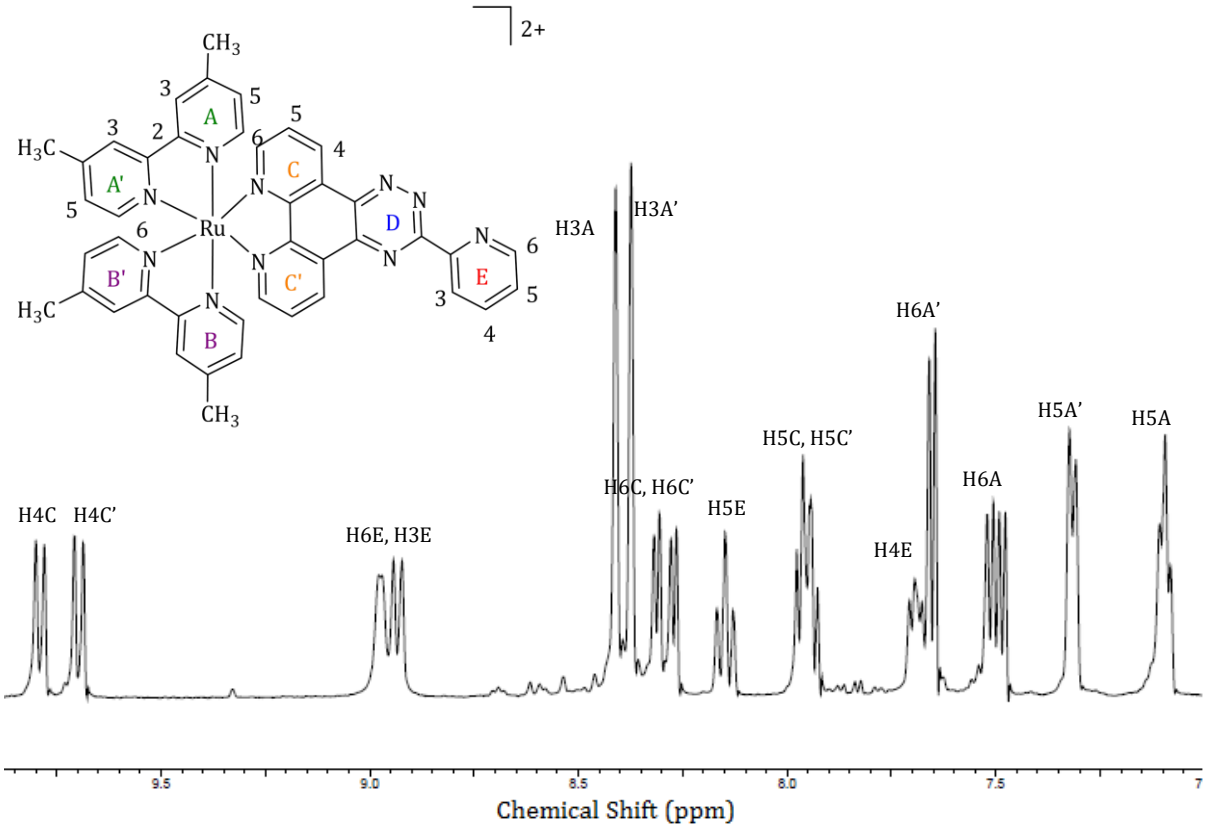

Figure 4.5. *The aromatic region of ^1H NMR spectrum of the complex $Ru(dmbpy)_2(pytp)]^{2+}$,* ***4.09b****, in CD_3CN.*

The ^1H NMR spectrum of complex **4.09b** shows fifteen non-equivalent proton signals. Some of them are overlapping, as shown in Figure 4.5. Six different pyridine systems exist within the complex. The complex becomes unsymmetrical after the addition of **4.08** to complete pytp bridging. The peaks assigned to the C4 and C4' protons appear further downfield on the spectrum compared to the E3 and E6 protons, due to the anisotropic ring current effect. Assigning of the peaks in the spectrum was substantially supported by the gCOSY NMR spectroscopy. The H3A, H3B from the bipyridine ligands (8.40 ppm) were highly deshielded from ring currents of the C aromatic rings.

H5A and H5A' were highly shielded due the ring current arising from the C aromatic rings and the peaks relevant to H5A and H5A' appeared upfield, with chemical shifts of 7.09 ppm and 7.32 ppm, respectively.

The twelve methyl protons appeared in two different sets in the alkyl region, each representing the integration of six protons.

The two different ^{1}H NMR spectra obtained for complexes **4.09a** and **4.09b** represent a similar distribution pattern for the ^{1}H NMR peaks except the multiplets relevant to H4A, H4A', H4B and H4B' in **4.09a** spectrum.

The assignment of the sole singlet in the spectrum (8.41 ppm, H3A) of **4.09b** was straightforward. It is also worth noticing the remarkable deshielding of H3 protons upon complexation with the ruthenium(II) centre. In the gCOSY spectrum, correlation among *ortho, meta*, and *para* protons are normally observable. Also the differences between *J*-coupling has greatly aided assignments, especially of H3 and H6 aromatic protons.

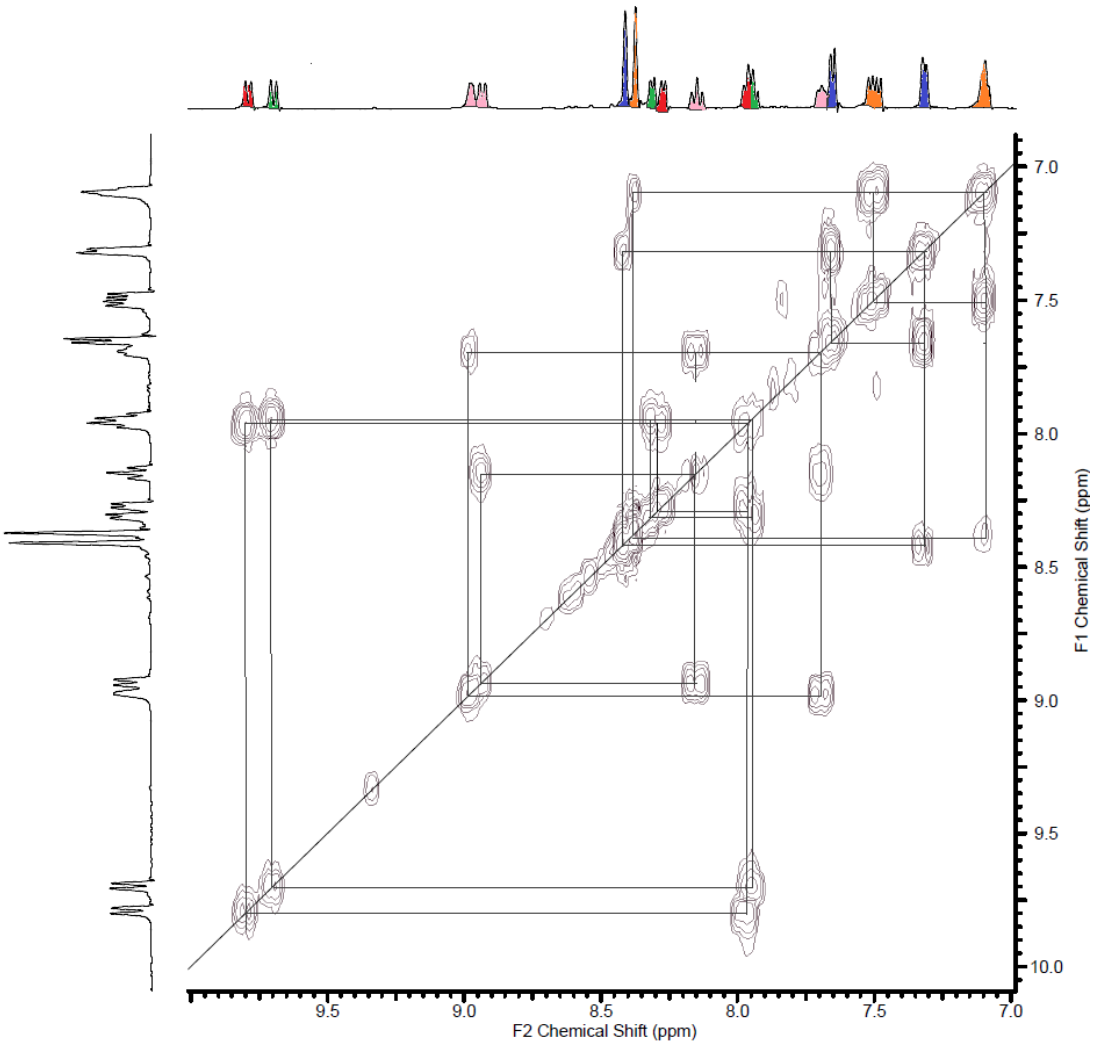

Figure 4.6. *The aromatic region of gCOSY NMR spectrum of* $[Ru(dmbpy)_2(pytp)]^{2+}$, ***4.09b*** *complex. The spectra shows coupling between adjacent protons. Each colour represents a different ring system in the* ***4.09b*** *complex.*

The gCOSY NMR spectrum shown in Figure 4.6 is consistent with the assignment of peaks in the ^{1}H NMR spin system.

4.2.3 Synthesis of [Ru(decbpy)$_2$(pytp)]$^{2+}$, 4.09d,

(decbpy =4,4'-diethoxycarbonyl-2,2'-bipyridine), **4.04d**,

The ligand, decbpy, **4.05d**, was synthesised according to the following reaction, Scheme 4.2.

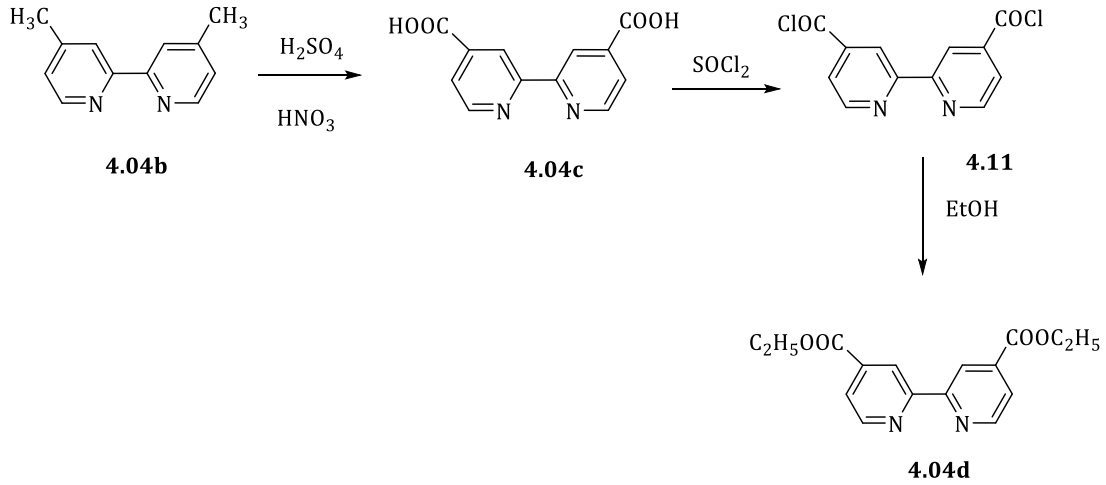

Scheme 4.2. *Reaction scheme for the synthesis of **4.04d.***

The compound **4.04c** was synthesised by oxidising commercially available **4.04b** according to the procedure described by Zhou *et al.*[156] After characterisation, **4.04c** was used for the esterification reaction.

4.04d was obtained by esterifying **4.04c** according to the procedure described by Garelli *et al*.[157]. Similar analysis results with the reported literature values confirmed the formation of the product.[158]

The complex **4.07d** was synthesised according to the procedure described by Schmidt *et al*.[159]

Complex **4.07d** was reacted with **4.08** by condensation to complete the pytp bridging ligand, Scheme 4.1. The condensation reaction was performed to produce **4.09d** by refluxing complex **4.07d** and **4.08** in a 1:1 molar ratio in ethanol. The completion of reaction was confirmed by TLC analysis. The product was precipitated as its hexafluoridophosphate salt by the addition of a concentrated aqueous solution of ammonium hexafluorophosphate into a concentrated reaction mixture.

The resulting residue was chromatographed on a silica gel column using an ethanol:$NaOH_{(aq)}$ (1:1) solvent system. The orange second band was dried under vacuum and the solid material was dissolved into a minimum amount of water. The product was separated from NaCl by a few dichloromethane (DCM) extractions. The complex affinity for the dichloromethane layer was influenced by adding a few millilitres of concentrated aqueous solution of ammonium hexafluoridophosphate. After complete extraction, the DCM layer was dried with anhydrous magnesium sulfate and then the solvent was evaporated under vacuum to obtain the desired complex.

The obtained product was characterised by mass spectrometric analysis, UV/vis, IR, NMR techniques.

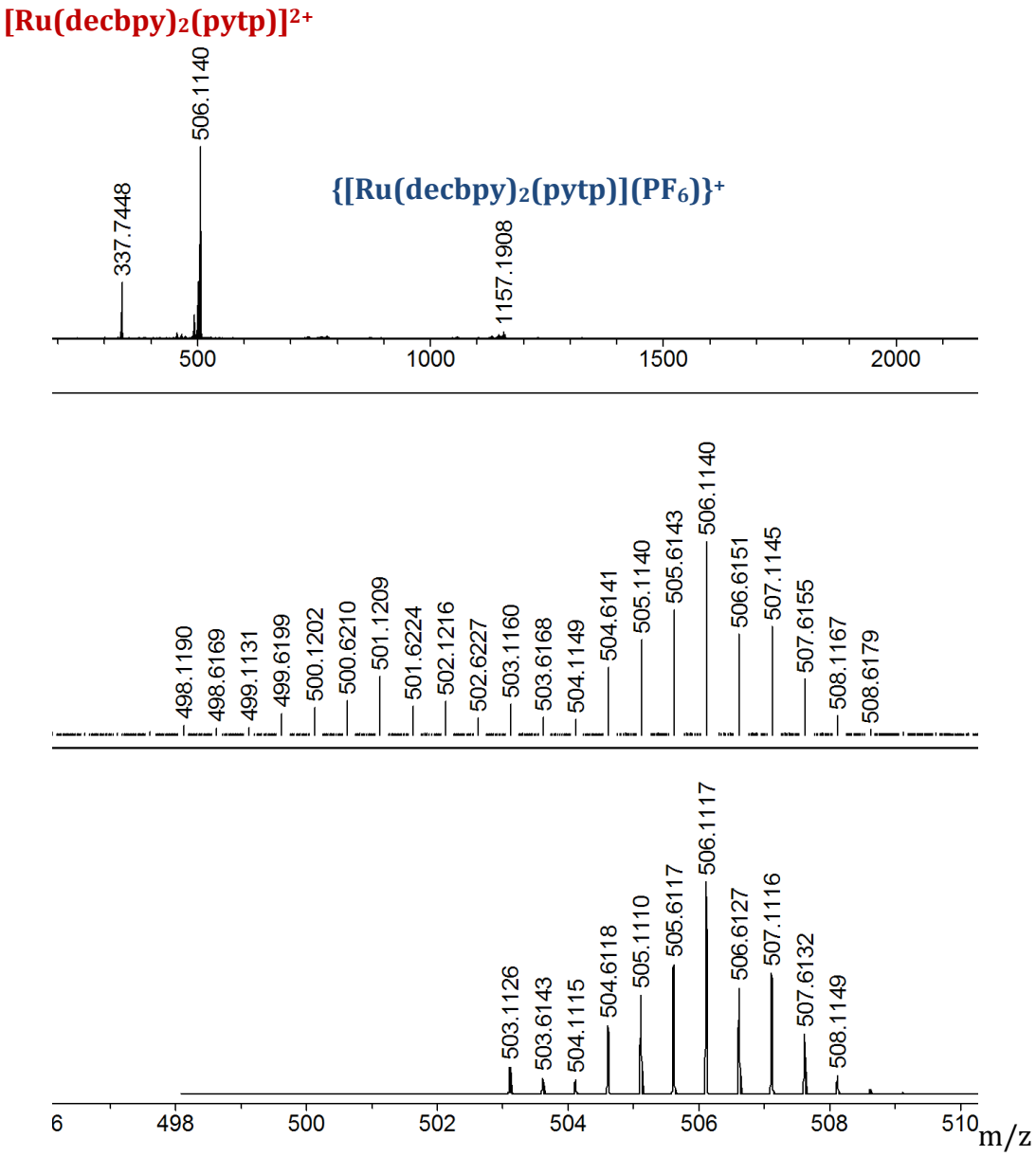

Figure 4.7. *The key signal of the mass spectrum of **4.09d** (top), experimental isotopic pattern (middle), simulated isotopic pattern (bottom).*

The mass spectrum shown in Figure 4.7, confirmed the formation of the complex **4.09d**. After condensation of **4.07d** with **4.08**, the complex becomes asymmetric. Each of the peaks corresponding to the methyl and ethyl groups at 1.52 and 4.15 ppm were separated into two different groups.

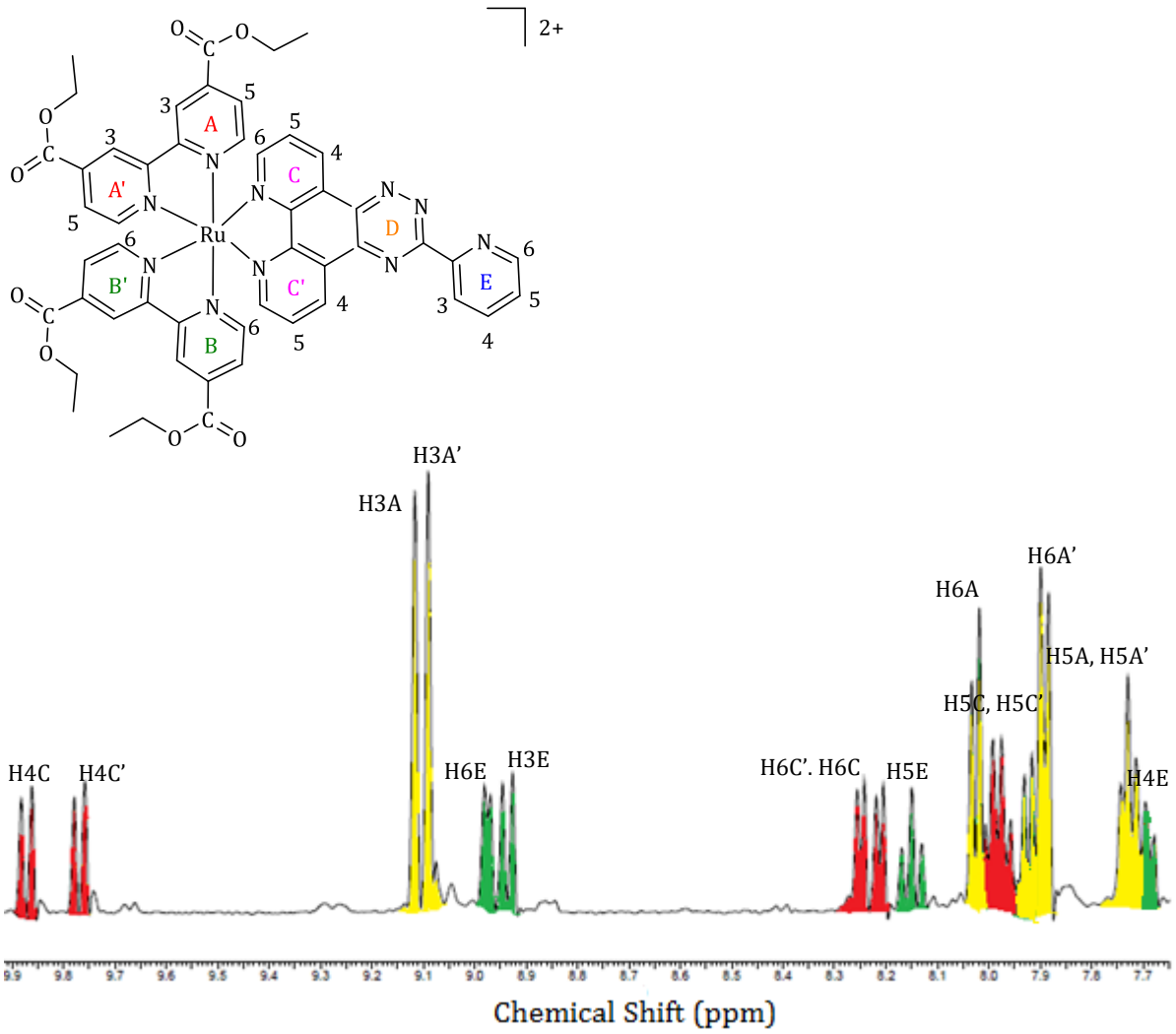

Figure. 4.8. *The aromatic region of the ^{1}H NMR of the complex [Ru(decbpy)$_2$(pytp)]$^{2+}$* ***4.09d****. The ^{1}H NMR signals belonging to each ring system has the similar colour. For example all the ^{1}H NMR peaks from E pyridine ring were coloured in green.*

The ^{1}H NMR spectrum of the complex showed eighteen different peaks in relation to forty two different protons.

The assigning of the peaks in ^{1}H NMR spectrum was achieved using gCOSY NMR and 1D TOCSY experiments.

The 8.02 ppm region of the gCOSY spectrum is complicated due to the overlap of peaks from different ring systems, e.g. HC, HC', HE. 1D TOCSY spectrum is useful to confirm the

accuracy of the assigned peaks from the gCOSY experiment and was mainly used for the assigning of proton peaks from the E ring system.

The splitting pattern observed in the spectrum, Figure. 4.8 had similar features to the splitting pattern of the complex **4.09b**.

One of the differences observed in this spectrum compared to the spectrum shown in Figure 4.3 is the shifting of H3A and H3A' proton signals to the down field in the spectrum.

4.2.4 Synthesis of $[Ru(dcbpy)_2(pytp)]^{2+}$, 4.09c,

4,4'-Dicarboxy-2,2'-bipyridine was selected as a potential ancillary ligand on the ruthenium(II) metal centre to manipulate the higher total complex charge of the Ru(II)-Co(III) heterodinuclear complex.

During this research we wanted to explore the hydrophobic and hydrophilic properties and a range of different charges of the ruthenium(II) complex , and the influence on the properties of the dinuclear complex due to the different charges of the ruthenium(II) centres.

The carboxylic moieties on ancillary ligands can be deprotonated by varying the pH of the medium. The four carboxylic groups on the bipyridine ligands can be deprotonated to create four carboxylate groups lowering the net charge of the metal complex to (+1).

The complex, **4.05c** was synthesised by coordinating 2,2'-bipyridine-4,4'-dicarboxy acid, **4.04c** with $RuCl_3.nH_2O$, Scheme 4.1, according the procedure reported by Nazeeruddine *et al*.[152] The formation of **4.05c** was confirmed by UV/vis

spectrophotometric analysis, as well as mass spectrometric analysis $[M\text{-}Cl]^{+}$= m/z = 624.9698. The product was used for the next step of the synthesis without further purification. The condensation of **4.05c** with 1,10-phenanthroline-5,6-dione, **4.06** was carried out under vigorous microwave reaction conditions. This procedure was adopted from reports by Freys *et al.*[160] and the reaction mixture turned yellow indicating the complexation of **4.06**. The reaction was monitored by TLC. Formation of the product, **4.07c** was observed by mass spectrometric analysis $[M]^{2+}$ = m/z = 400.022. Attempts to purify the product using silica gel column chromatography, as described in the literature procedure were unsuccessful.

The complex **4.07c** was used in the next step without further purification. As shown in Figure 4.9, the pytp bridging ligand was synthesised by reacting **4.07c** with **4.08** in methanol. The progress of the reaction was monitored by TLC throughout the reaction to minimise time spent at reflux.

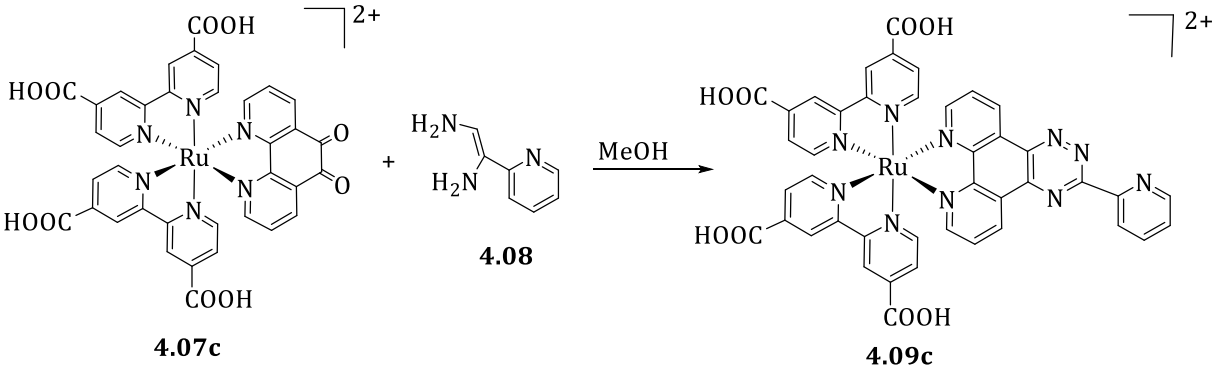

Figure 4.9. *Reaction path for the condensation between **4.07c** with **4.08** for the stepwise synthesis of pytp bridging ligand to produce **4.09c**.*

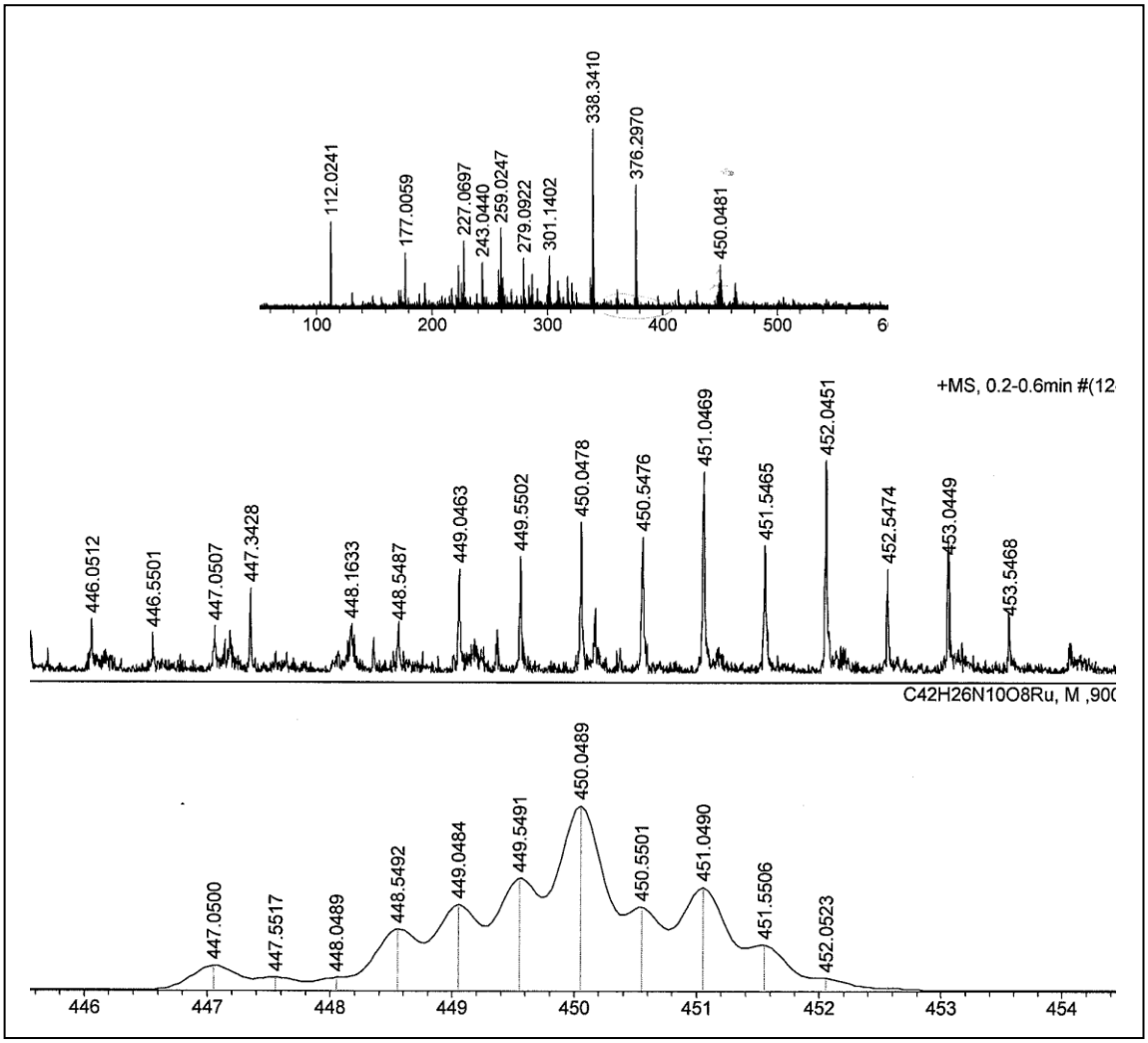

Figure 4.10. *The mass spectrum of **4.09c** complex (top), including experimental (middle) and simulated (bottom) patterns.*

Attempts made to purify the complex using various numbers of chromatographic techniques were unsuccessful. The **4.09c** complex behaves completely differently in solubility to **4.09a** and **4.09b** complexes. The hexafluoridophosphate salt of the **4.09c** is insoluble in acetonitrile.

One of the possible strategies to investigate the solubility of the complex **4.09C** is deprotonation of the carboxylic acid moieties by changing the pH of the medium.

4.2.5 Fluorescence studies of 4.09a, 4.09b and 4.09d,

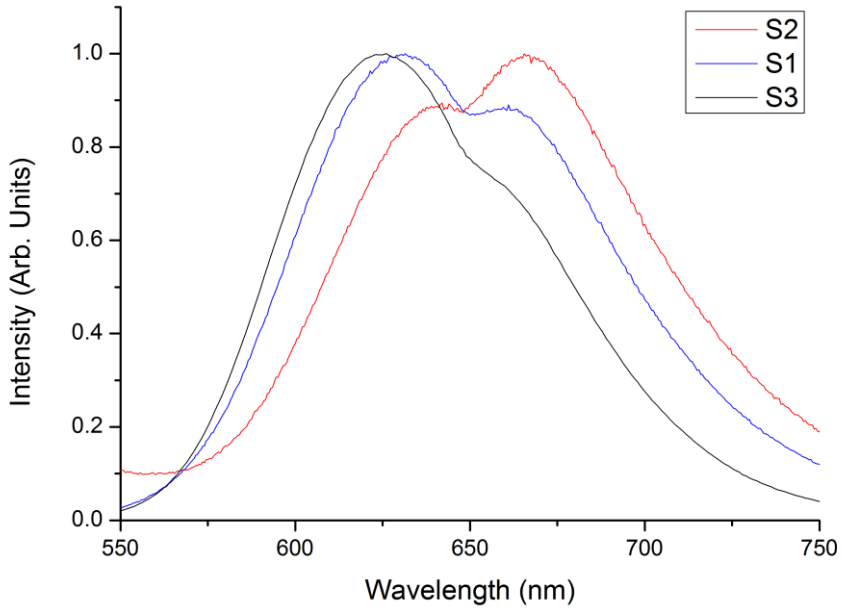

Figure 4.11. *Florescence spectrum for the complexes* ***4.09a (S1), 4.09b (S2)*** *and* ***4.09c(S3)*** *reported in methanol as a solvent.*

The photochemistry of ruthenium polypyridyl complex was previously discussed in the chapter 01. The fluorescence spectrum is observed due to the electron transfer from an excited triplet state to singlet ground state. Due to the slight differences on the ligand substituents differences in the florescence spectrum is observed.

4.2.6. Synthesis of ruthenium(II)-cobalt(III) heterodinuclear metal complex, 4.10b and 4.10d,

The main purpose of synthesising complexes **4.09b**, **4.09c** and **4.09d** was to incorporate them as part of a ruthenium(II)-cobalt(III) heterodinuclear metal complex.

Therefore, to investigate the possibility of utilising these complexes NMR scale reactions were carried out between **4.09b** or **4.09d** with **4.03**, as shown in the Scheme 4.1.

^{1}HNMR experiments were used to monitor this reaction between ruthenium(II) pytp complex , **4.09b / 4.09d**, with the complex **4.03**.

The dinitrite ligands on $[Co(tren)(NO_2)_2]^+$, **4.12** are strong coordination ligands. It is important to replace these nitrite ligands with labile ligands to facilitate the formation of the heterodinuclear complex under very mild reaction conditions. Therefore, the nitrite ligands were replaced with the highly labile OTf ligands by reacting **4.12** with trifluoromethanesulfonic acid (HOTf), under the conditions reported by Chang *et al*.[71]

The^{1}H NMR experiment was carried out in 5mm NMR tube by mixing complexes **4.09b** with **4.03** and **4.09d** with **4.03** in separate 5mm NMR tubes in acetonitrile in a 1:1 molar ratio. The NMR reaction mixture was kept in the dark throughout the reaction and only exposed to light during submitting the sample for analysis. The spectra were recorded in different time intervals and upon complexation, **4.09b** with **4.03** or **4.09d** with **4.03** showed the changing chemical shifts in the aromatic region of the ruthenium(II) complex shown in Figure 4.12 and Figure 4.13. The completion of the reaction was monitored by complete disappearance of some of the peaks in the ^{1}H NMR spectrum of ruthenium(II)pytp complex, **4.09b** and **4.09d** and complete appearance of new peaks in the spectrum. The reaction took about twenty four hours to achieve the completion.

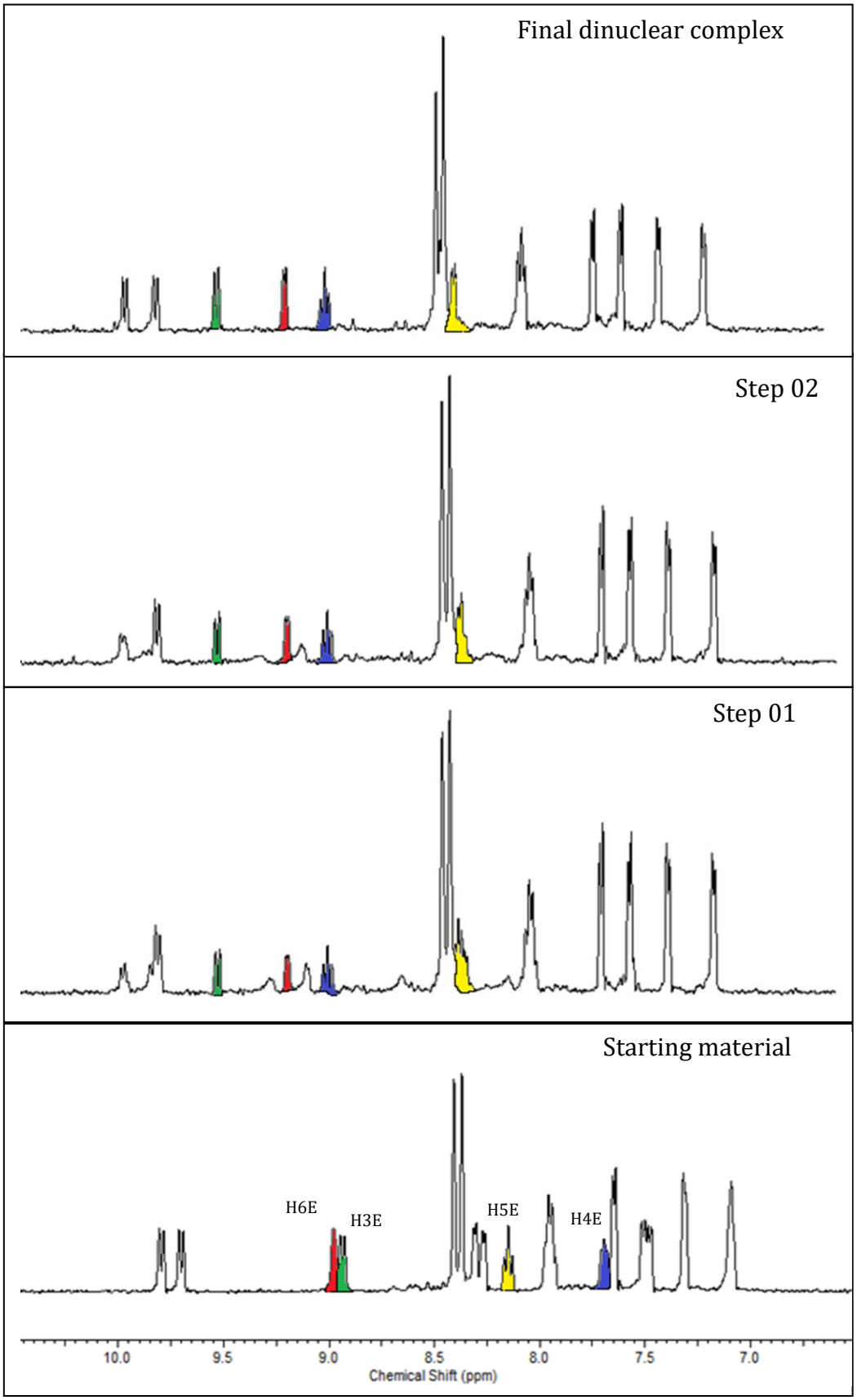

Figure 4.12. *The aromatic region of the ^{1}H NMR spectrum of* ***4.09b*** *showing changing chemical shifts of proton peak on complexation with $[Co(tren)(OTf)_2]^+$* ***4.03***. *Each peak in E pyridine ring Figure 4.5 is coloured to track the changes.*

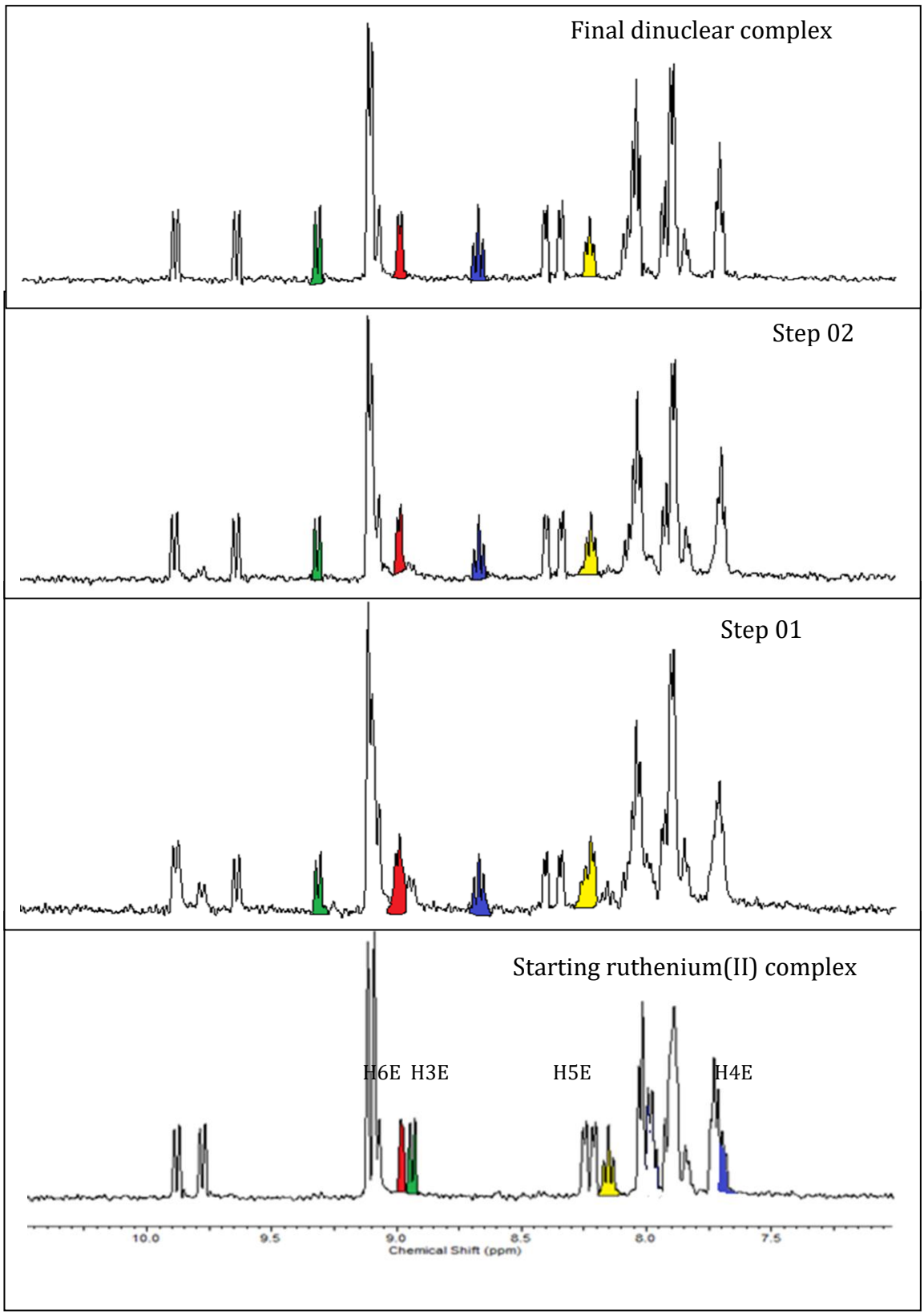

Figure 4.13 *The aromatic region of the ^{1}H NMR spectrum of* ***4.09d*** *showing changing chemical shifts of proton peak on complexation with $[Co(tren)(OTf)_2]^+$,* ***4.03*** *complex. Each peak in E pyridine ring Figure. 4.8 is coloured to track the changes.*

4.2.7 Preparation of $[Co(L3)_2(NO_2)_2]^+$, 2.08, to be complexed with 4.09b or 4.09d

$[Co(L3)_2(OTf)_2]^+$, **4.02** complex was interesting to us because of highly labile trifluoromathanesulfonate (OTf) ligands. The highly labile OTf leaves easily during the coordination with the ruthenium(II)pytp complex, **4.09b** or **4.09d**. The synthesis of $[Co(L3)_2(OTf)_2]^+$, **4.02** using **2.08** is as follows.

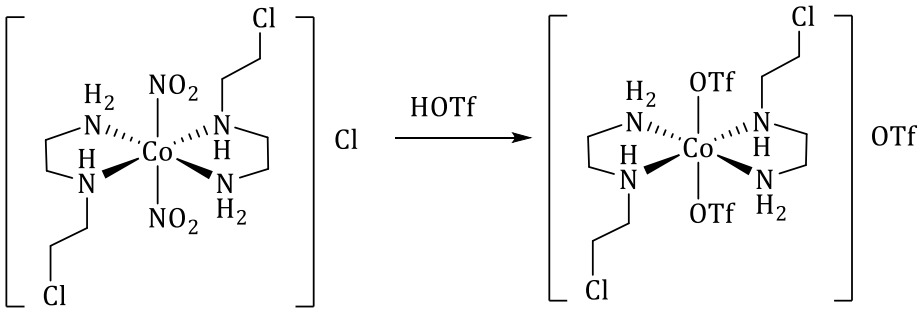

2.08 **4.02**

Scheme 4.3. *Reaction scheme for the preparation of **4.02**.*

For the synthesis of the complex **4.02**, initially complex **2.08** was reacted with neat HOTf under the nitrogen atmosphere. The gaseous nitrogen was passed through the reaction mixture to avoid moisture getting into the system. In the presence of moisture OTf ligands can get substituted by water.

The reaction mixture was kept in the ice–salt bath (below 0 °C). After completion of the reaction, cold ether was added to precipitate the product from the reaction mixture. Analysis of the product shows it to be the protonated **L3** ligand, presumably from the decomposition of the complex. The above results confirmed the requirements of employing mild reaction conditions. The complex **2.08** was kept under gaseous nitrogen; nitrogen was bubbled through the reaction mixture. The reaction flask was

kept in an acetone-dry ice bath while adding neat HOTf. The HOTf solidified on addition (mp: -40°C) but the slow increase of the temperature resulted in a melting of the HOTf which facilitated the mild reaction conditions for the complex. Later, the reaction mixture was transferred to an ice-salt bath, and reaction was continued for eight hours to achieve completion. The product was separated from the reaction mixture by the addition of cold ether to the reaction mixture. The resulting purple sticky material was analysed by mass spectrometry.

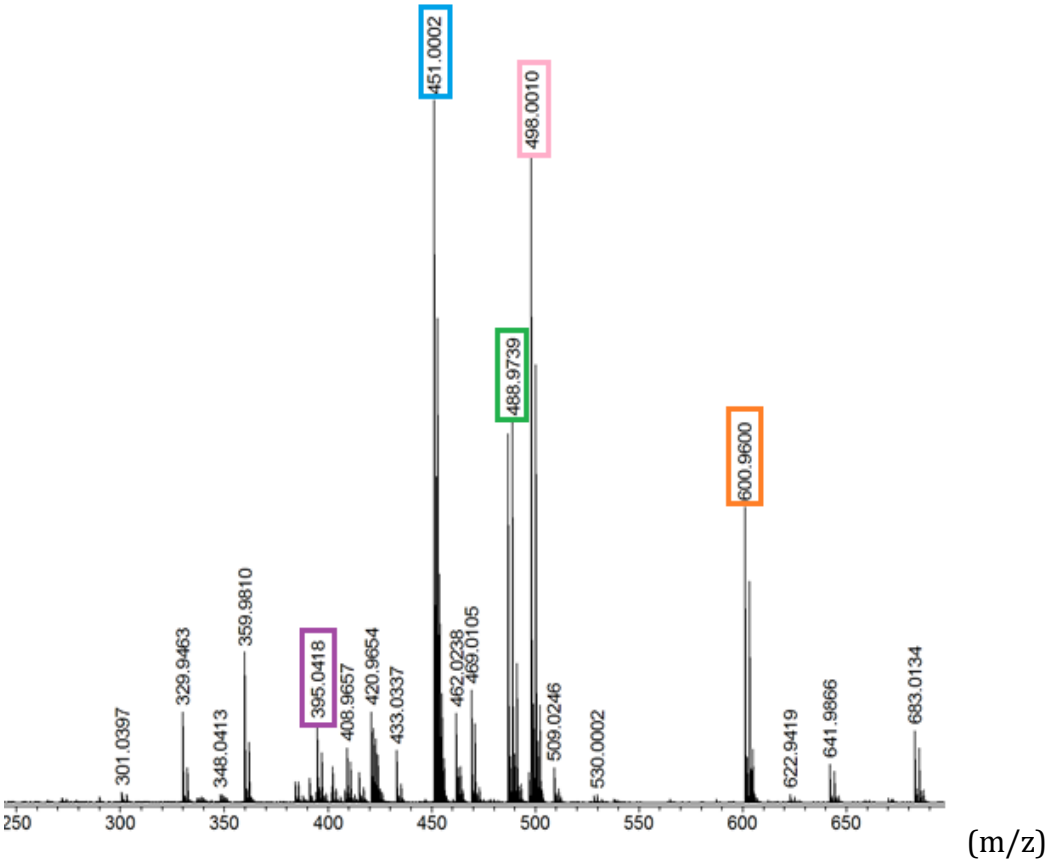

Figure 4.14. *Mass spectrometric analysis of the complex* ***4.02****.*

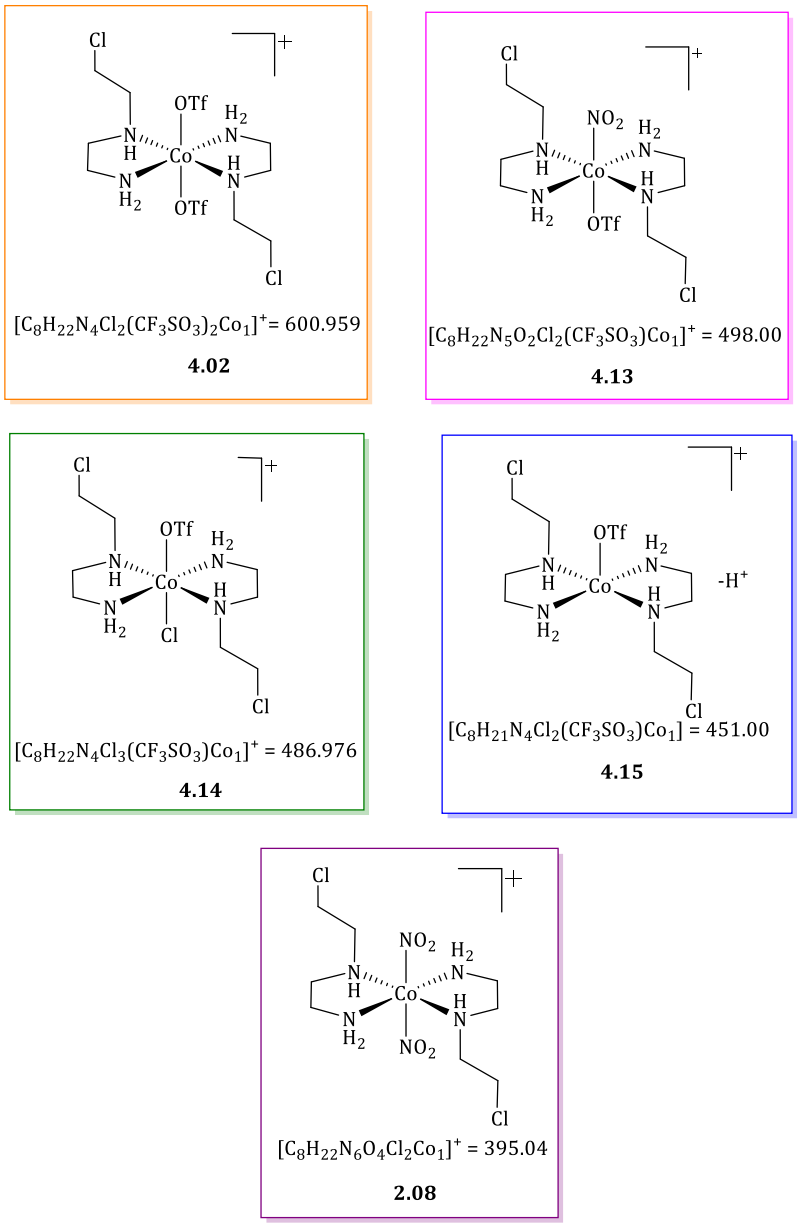

Figure 4.15. *Possible cationic components identified in the mass spectrum shown in Figure 4.14. Relevant peak in the mass spectrum and the chemical structure are colour coded for easy identification.*

Mass spectrometric analysis of the extracted product material revealed the formation of the desired complex **4.02** and several other fragments produced from molecular ion.

The m/z=395.04 peak present in the mass spectrum shows the presence of unreacted starting material, **2.08** in the reaction mixture. Also the presence of **4.13** cationic

complex appearing at m/z= 498.00 is due to the substitution of only one nitrite ligand with OTf ligand. The formation of the **4.13** cation is most likely due to the different chemical nature of two nitrite ligands in the starting material, **2.08**. This different chemical nature of nitrite ligands in the precursor complex is previously discussed in the section 2.3.1.

The complex **4.14** was also an interesting find, showing the replacement of an axial ligand (OTf or NO_2) with a chloride ligand. The source of chloride ions could be the anionic chloride associated with the starting material or the hydrochloric acid generated during the HOTf acid reaction. Therefore bubbling nitrogen into the reaction mixture is important to efficiently remove HCl from the reaction mixture. As we know from the work in chapter 02, the affinity of the chloride ion for these axial positions is high; therefore the cationic **4.14** fragment is not surprising in the presence of even a trace amount of chloride ions in the medium.

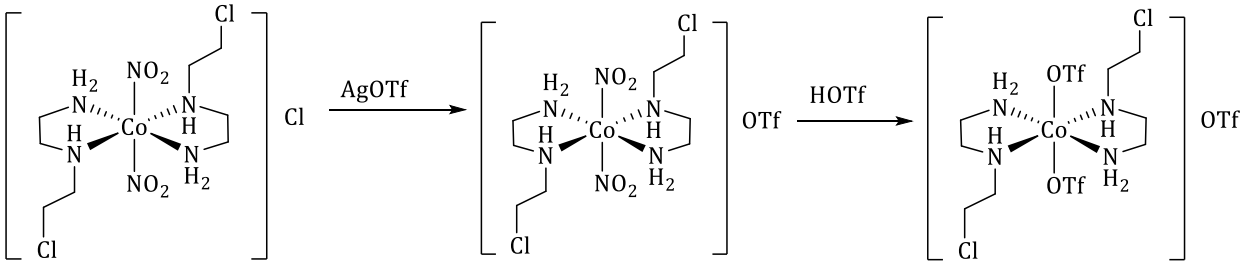

Scheme 4.4. *Reaction scheme for the synthesis of $[Co(L3)_2(OTf)_2]^+$, **4.02**, complex.*

Therefore, to remove any chloride ions in the medium, an alternate approach was used. The starting material was reacted with equimolar amount of silver trifluoromethanesulfonate (AgOTf) in a methanolic medium to replace any sort of ionic chlorides in the medium with OTf ions. After stirring the AgOTf and the complex **2.08** in the methanolic solution for five hours, the white silver chloride precipitate was filtered.

The filtrate was dried under vacuum to obtain a yellow powdered material, and was then used for the reaction with the neat HOTf acid under nitrogen bubbling.

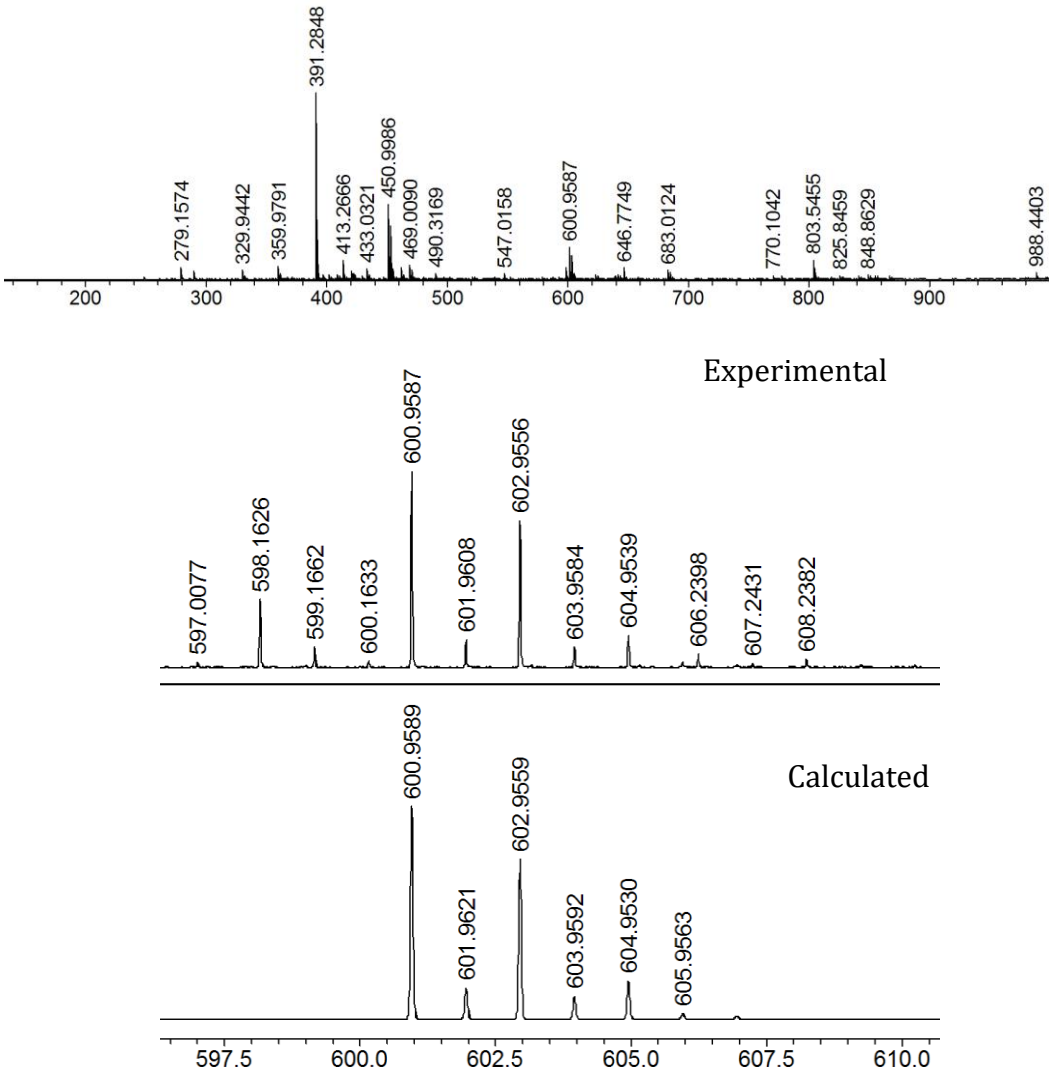

Figure 4.16. *Mass spectra obtained under new reaction conditions shown in Scheme 4.4 and the experimental (top) and calculated (below) isotope pattern for the complex* $[Co(L3)_2(OTf)_2]^+$, ***4.02.***

After removing the chloride counter ions from the complex **2.08** using AgOTf, followed by the reaction with HOTf, the mass spectrum of the isolated light pink powdered material showed the disappearance of **4.13** and **4.14** from the mass spectrum, Figure 4.14, with m/z relevant to 498.00 and 486.976, respectively.

The results obtained also proved that the chlorine substituent on **4.14** is mainly due to the associated chloride anion, or the HCl produced due to the reaction of anionic chloride with HOTf rather than the HCl acid generated during the neat HOTf acid reaction.

The inability to record the ^{1}H NMR spectrum of the extracted material suggested the possible contamination with cobalt(II) ions. It could be due to the generation of cobalt(II) due to the decomposition of some material in the reaction mixture. Therefore the purity of the obtained product was insufficient to proceed to the next level of the synthesis.

4.3 Summary

The complexes $[Ru(bpy)_2(pytp)]^{2+}$, **4.09a**, $[Ru(dmbpy)_2(pytp)]^{2+}$, **4.09b**, and $[Ru(decbpy)_{2(}pytp)]^{2+}$, **4.09d**, were successfully synthesised and characterised by NMR, UV/vis, IR, ESI-MS and fluorescence spectroscopic techniques. $[Ru(dcbpy)_2(pytp)]^{2+}$, **4.09c**, was synthesised and characterised by ESI-MS but purification of the product was unsuccessful due to the lower solubility of the complex.

$[Co(L3)_2(OTf)_2]OTf$, **4.02**, is an important complex to synthesis ruthenium(II)-cobalt(III) heterodinucler complex. The highly labile OTf ligands on the **4.02** were important for employing mild reaction conditions during the synthesis of heterodinuclear complex. The proposed synthetic route for the synthesis of $[Co(L3)_2(OTf)_2]OTf$, **4.02**, using $[Co(L3)_2(NO_2)]^{+}$, **2.08** as starting material was also discussed in this chapter.

As an approach for the synthesis of Ru(II)-Co(III) heterodinuclear complex, the results obtained from the NMR studies, by complexation of $Ru(dmbpy)_2(pytp)]^{2+}$, **4.08b**, with $[Co(tren)(OTf)_2]^+$, **4.03**, and $[Ru(decbpy)_2(pytp)]^{2+}$, **4.09d**, with $[Co(tren)(OTf)_2]^+$, **4.03**, are also discussed in this chapter. ^1H NMR studies presented in this chapter supported the formation of ruthenium(II)-cobalt(III) heterodinuclear complex.

Chapter 05

Conclusions & Future Prospects

5. Conclusions and Future Prospects

5.1 Conclusions

The work reported in this thesis has focused on the synthesis of a photoactivated prodrug system consisting of heterodinuclear metal centres; in particular Ru(II) and Co(III) centres.

A key outcome of this research project is the safer synthetic approach to complexes of toxic nitrogen mustard compounds. The synthetic procedure focused on first the coordination of amino alcohol ligands onto the cobalt(III) inert metal centre, followed by the conversion of hydroxyethyl groups to chloroethyl groups. A detailed discussion of this chemistry is outlined in chapter 02.

However, due to the proven complexity of coordination chemistry of amino alcohol ligands with cobalt(III) centres and lack of information about these complexes, a thorough investigation was included with regards to the cobalt(III) alkoxide complexes in chapter 02 and chapter 03.

In chapter 02, the synthesis and crystallographic studies of twelve different cobalt(III) complexes derived from the precursor $[Co(L1)_2(NO_2)_2]NO_3$, **2.06**, under different reaction conditions is reported. These complexes were discussed extensively in chapter 02, in relation to their stability, coordination chemistry, reactivity, ligand exchange reactions, and isomerisation. Many of these complexes were synthesised multiple times *via* different synthetic routes. The results are presented in a reaction web that was developed and is shown in Figure 2.8, chapter 02.

More importantly, an understanding of the reaction web allowed for the synthesis and full characterisation of the complex, $[Co(L3)_2(NO_2)_2]Cl$, **2.08**, which was considered as one of the important complexes to reach the research goals and was unable to be synthesised by previous members of the Hartshorn group.

The $[Co(L1\text{-}H)_2]^+$ alkoxide complex is one of those twelve complexes. The synthesis and isomerisation of this complex was discussed in chapter 02, and also reported the new technique by which these alkoxide complexes could be isolated in their neutral form by complexing them with $ZnCl_2$ or $MnCl_2$ metal salts. Using this technique three different isomers of complex $[Co(L1\text{-}H)_2]^+$ were isolated and X-ray crystallographic analysis of these were reported in chapter 02.

The $[Co(L1\text{-}H)_2]^+$ complex could act as a starting material for the synthesis of a nitrogen mustard ligand on a cobalt(III) centre. This synthetic procedure is safer than established techniques that involve the handling of the free nitrogen mustard.

Chapter 03 presents ten new cobalt(III) alkoxide complexes that were synthesised using seven different amino alcohol ligands. Many of the complexes were characterised by X-ray crystallographic techniques.

The new coordination chemistry of cobalt(II) alkoxide complexes demonstrated the dimerization of two cobalt(III) alkoxide complexes *via* hydrogen bonded oxygen bridging to form dinuclear complexes (**3.03, 3.09, 3.10, 3.15, 3.16**) and these complexes had not been reported in the literature.

Four tetranuclear complexes (**3.03, 3.09, 3.10, 3.16**) with Co(III)/Zn(II) and Co(III)/Mn(II) were synthesised and reported in chapter 03. One of the special features of these tetranuclear complexes are they are uncharged and easily crystallised out from

a methanolic solution; hence we were able to investigate and report on the coordination chemistry of them.

One of the reasons the coordination chemistry of amino alcohol ligands with cobalt(III) centres was investigated was to establish the potential use of such species in the synthesis of cobalt(III) nitrogen mustard complexes. In particular, amino alcohol ligands, with more than one alcohol group, are of interest as they are possible precursor ligands for the synthesis of poly-alkylating nitrogen mustard coordinated cobalt(III) complexes.

The successful synthesis and characterisation of polyalkylating nitrogen mustard cobalt(III) complex **3.17** using a cobalt(III) alkoxide complex, **3.13** was discussed in chapter 03.

Chapter 04 focuses on the synthesis of heterodinuclear complexes. Two different ruthenium(II)pytp complexes were successfully synthesised. The results obtained from ^{1}H NMR studies for the complexation of, $[Ru(dmbpy)_2(pytp)]^{2+}$, **4.09b** and $[Ru(decbpy)_2(pytp)]^{2+}$, **4.09d** with $[Co(tren)(OTf)_2]^{+}$, **4.03**, are consistent with the formation of dinuclear Ru(II)-Co(III) heterodinuclear complexes.

Unfortunately, due to the time restrictions, the isolation of these complexes from a large scale reaction could not be completed. The synthesis and isolation of $[Co(L3)_2(OTf)_2]^{+}$,**4.02**, complex and Ru(II)-Co(III) heterodinuclear complex with a cytotoxic nitrogen mustard cobalt(III) complex appears challenging and so far we have been unsuccessful. The modifications suggested for the synthesis of such complexes will be discussed in future prospects section.

5.2 Future Prospects

At the conclusion of our study, there were a number of avenues for future experiments which could still be pursued; here we outline some of these possibilities. In some cases, we have already done some preliminary experiments towards these studies and details will be given where appropriate.

The following synthetic approach is suggested as an improvement to some of the work discussed in this thesis.

5.2.1 Suitable precursor ligands for the synthesis of cobalt(III) nitrogen mustard complexes.

In general, $[Co(L3)_2(NO_2)_2]^+$, **2.08** and its derivatives were found to be unstable at high temperatures. The robust polydentate ligands stabilise the cobalt(III) complexes under the vigorous reaction conditions. For example, $[Co(tren)Cl_2]^+$ is stable compared to $[Co(en)_2Cl_2]^+$. Therefore, the ligands shown in Figure 5.1 are proposed as potential precursor ligands to investigate the synthesis of nitrogen mustard on a cobalt(III) centre. The interconnected nitrogen atoms of these ligands will be able to form a robust coordination sphere on coordination with the cobalt(III) centre. The hydroxyethyl groups on the ligand can also be coordinated to the central metal or may stay un-coordinated and later can be easily converted to the chloroethyl functionality to synthesise nitrogen mustard cobalt(III) complexes.

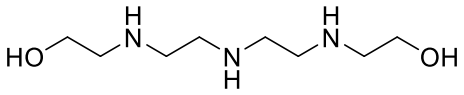

5.01

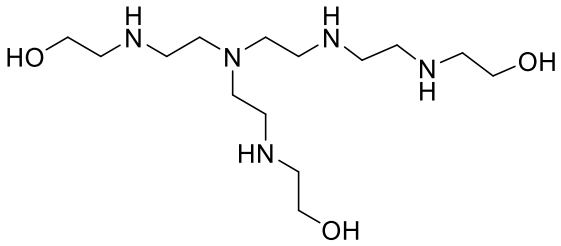

5.02

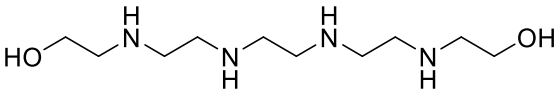

5.03

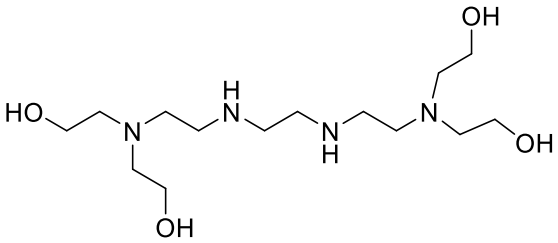

5.04

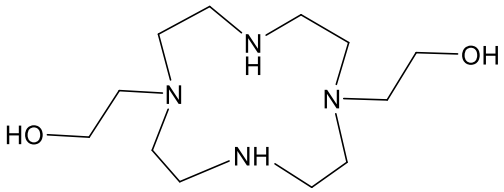

5.05

Figure 5.1. *Precursor ligands suggested for the complexation with cobalt(III) centres.*

The procedure published by Drinkard *et al.*[123] can be employed to synthesise cobalt(III)alkoxide complexes. The increased number of coordinating atoms present in the ligands, Figure 5.1, compared to the ligands discussed in chapter 03, may lead to the

formation of cobalt(III) clusters. This would be an interesting investigation to study the coordination chemistry of these ligands with cobalt(III) centres.

5.2.2 Synthesis of [Ru(4,4'-dcbpy)$_2$(pytp)]$^{2+}$,4.09c,

Method 01;

A possible synthetic route for the preparation of [Ru(4,4'-dcbpy)$_2$(pytp)]$^{2+}$, **4.09c**, was described in chapter 04. Due to the insolubility of **4.09c**, obtaining purified material was unsuccessful.

Changing the pH of the medium to deprotonate the carboxylic acid groups of **4.09c** would improve the solubility of this complex. The complex needs to be examined over a range of pH values to understand the deprotonation stages of the four carboxylic acid ligands.

Method 02;

The hydrolysis of the (Ru(decbpy)$_2$(pytp)]$^{2+}$ complex can also be attempted.

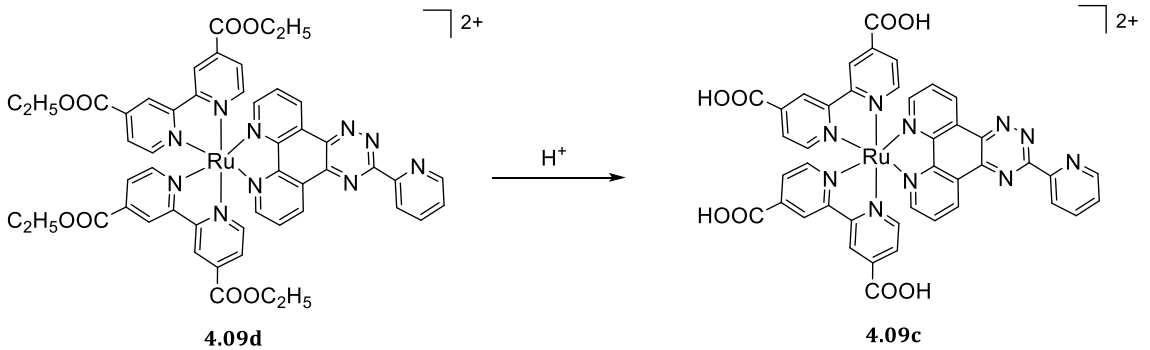

4.09d **4.09c**

Scheme 5.1*. Reaction scheme for the conversion of* ***4.09d*** *to* ***4.09c*** *via hydrolysis reaction.*

5.2.3 Changing the bridging ligand

During the course of this research program, pytp (pytp = 3-(pyridine-2-yl)-[1,2,4]triazino[5,6-f][1,10]phenanthroline) was the only ligand we were interested in, as it has been proved successful by Alan Downward.[114] However, use of a symmetric bridging moiety would be of interest as the ligand can be synthesised separately and then complexed with the ruthenium(II) centres.

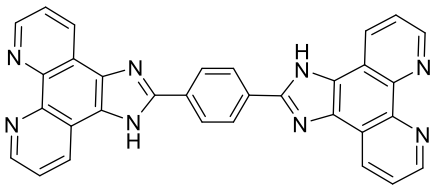

5.06

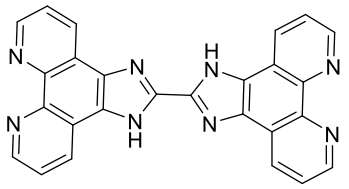

5.07

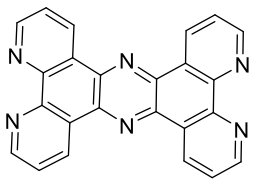

5.08

Figure 5.2. *Proposed symmetric bridging ligands for the synthesis of heterodinuclear complexes*.

One of the disadvantages of synthesising the bridging ligand separately is that after complexation, the resulting mixture consists of mononuclear and dinuclear complexes. However, the two complexes will be significantly different in total complex charge, hence easily separable using cation exchange column (Sephadex SP C-25) chromatography.

Liang *et al.* reported the synthesis of **5.06** ligand,[127] and **5.07** and **5.08** were reported by Gholamkhass *et al.*[161]

5.2.4 Synthesis of metal clusters and polynuclear complexes

The dinuclear and polynuclear metal assemblies reported in chapter 03 opened up avenues for a number of research possibilities. The poly-coordinating ability of oxygen atoms in amino alcohol ligands and the heteropolynuclear complexes, Co(III)-Zn(II), Co(III)-Mn(II), showed interesting coordination chemistry.

Instead of zinc(II) and manganese(II) it would be interesting to study the coordination chemistry of other metal salts such as Ni(II), Fe(II), Fe(III), Cu(II), Ag(I), *etc* with the alkoxide complexes. Some of the metal salts have already been tested (e.g. $FeCl_3$, $AgNO_3$, $CuCl_2$, $NiCl_2$), however we were unable to grow crystals from those compounds. There are large numbers of experimental techniques that remain untested, such as changing the crystallising solvent system, or use of different crystallisation techniques to obtain the desired material. Also, column chromatography would be helpful to separate these neutral compounds from charged by-products formed during the complexation.

Amino alcohol ligands with a number of hydroxyl ethyl side arms, for example **5.03** and **5.04** presented in Figure 5.1, could be reacted with desired metal salts to synthesise metal clusters or supramolecular assemblies.

Especially by synthesising metal clusters using manganese(II) and cobalt(II) paramagnetic metal centres, we would be able to perform magnetic measurements on those complexes. There are some publications in the literature about the synthesis and

characterisation of metal clusters. Most of the ion clusters reported in the literature are about iron(III) metal centres[162], [163] and investigations about magnetic properties.

Chapter 06

Experimental procedures

6. Experimental procedures

6.1 General Information

Unless otherwise stated, reagents were obtained from commercial sources and used as received. Water was purified by reverse osmosis *in–house*. HPLC–grade solvents were used for reactions and in case of moisture–sensitive reactions; solvents were dried by literature procedures, solvents stored under N_2 in the solvent system and freshly distilled as required. Melting points were recorded on an Electrothermal melting point apparatus. Elemental analysis was done by the Campbell Microanalytical Laboratory, University of Otago.

Nuclear Magnetic Resonance

^{1}H and ^{13}C NMR spectra were recorded on Varian Unity 300, Agilent 400–MR, or Varian 500 INOVA instruments operating for ^{1}H NMR at 400 and 500 MHz, respectively and at 75, 100 and 125 MHz, respectively, for ^{13}C NMR. All the ^{1}H NMR spectra recorded in deuterated solvents were referenced to the solvent peak or TMPS: $CDCl_3$, 7.26 ppm; CD_3CN, 2.0 ppm; CD_3OD, 3.3 ppm; DMSO, 2.6 ppm. ^{13}C NMR were all referenced to their solvent peaks: chloroform, 77.0 ppm; acetonitrile, 36.8 ppm; methanol, 49.3 ppm; DMSO, 39.6 ppm. When required, gCOSY, 1–D TOCSY, HSQC and HMBC experiments were performed using standard pulse sequences. The assignments for the compounds are denoted with primes to indicate the symmetry equivalence ligands and with letters to distinguish the pyridine rings.

Mass Spectrometry

Mass spectra were recorded by Dr. Marie Squire, Dr. Meike Holzenkaempfer, Dr. Alexandra Goroncy or Dr. Amelia Albrett on either a DIONEX Ultimate 3000 or Bruker MaXis 4G spectrometer, operated in high resolution positive ion electrospray mode. Samples were prepared by dissolving in an appropriate solvent at the required concentration.

Infrared Spectroscopy

Infrared spectra were recorded on a Perkin–Elmer Spectrum One FTIR instrument operating in diffuse reflectance mode with samples prepared as KBr pellets (KBr) or on Bruker FTIR spectrometer with Alpha's Platinum ATR single reflection diamond where the neat samples were recorded. The following abbreviations are used: vs: very strong, s: strong, m: medium, w: weak, sh: sharp, br: broad.

UV/Visible Spectroscopy

UV / visible spectra were recorded on a Varian CARY Probe 50 UV / visible spectrometer (range 200 – 800 nm) at room temperature. Quartz cuvettes of 1cm path length and approximately 3 mL volume were used.

X-Ray Crystallography

X-Ray data were collected on an Oxford-Agilent Supernova instrument with a focused microsource Mo Kα [λ = 0.71073 Å] or Cu Kα [λ = 1.5405 Å] radiation and an ATLAS CCD area detector. CrysAlisPro 171.37.31 was used for the data collection and data processing. Multi-scan absorption corrections were applied using SCALE3 ABSPACK. The crystals were mounted on a nylon loop using a perfluorinated polyethylene glycol. Each crystal was kept at 120.00(10) K during data collection. All structures were solved using direct methods with SHELXS-358 and refined on *wF*2 using all data by full matrix least square procedures with SHELXL-14 using OLEX-2.359 for visualisation. Hydrogen atoms were included in calculated positions for carbon atoms and manually located from residual electron density for heteroatoms, with isotropic displacement parameters 1.2 or 1.5 times the isotropic equivalent of their carrier atoms. Heteroatom hydrogen atoms were fixed at distances, O-H 0.84 Å and N-H 0.90 Å. Graphical presentation of crystallographic data was prepared using OLEX-2.359.

Powder X-ray Diffraction

X-ray powder diffraction data were collected using an Oxfort-Agilent SuperNova instrument using Cu Kα (λ = 1.5418Å) radiation and an ATLAS CCD area detector. Samples were dried at 60°C overnight and stored under vacuum prior to analysis. Approximately 5 mg of sample were prepared for analysis by grinding. The powder was filled in a 1cm long CG column and mounted on to the goniometer head. The sample was centred directly in the X-ray beam path and the diffraction data were recorded using averaged 360° scan in ϕ with 150 second exposure time per rotation frame. The

diffraction data were integrated radially and a background correction was manually applied to approximate the absorbance due to the fibre.

Fluorescence studies

Fluorescence data was collected using HORIBA JOBINXVOW, Fluorolog FL3-22 fluorimeter.

6.2 Synthesis of precursors and ligands

The following compounds were prepared according to the literature procedures. $[Ru(bpy)_2Cl_2]$[151], $[Ru(bpy)_2(phendione)]^{2+}$[159], $[Ru(dmbpy)_2(phen)]^{2+}$[164], $\{Ru(dmbpy)_2Cl_2]$[165], $[Ru(dmbpy)_2(phendione)]^{2+}$[164], $[Ru(bpy)_2(pytp)]^{2+}$[113], $[Ru(dcbpy)_2Cl_2]^{2+}$[166, 152] $[Ru(dcbpy)_2(phendione)]^{2+}$[160], $[Co(tren)(NO_2)_2]^{+}$[150], $[Co(tren)(OTf)_2]^{+}$[125], $[Ru(decbpy)_2Cl_2]$, $[Ru(decbpy)_2(phendione)]^{2+}$[167], $[Co(NH_3)_6]Cl_3$ was obtained from (CHEM 111) undergraduate chemistry laboratories.

4,4'-dicarboxy-2,2'-bipyridine[156], pyridine-2-carbohydrazonamide, 4,4'-diethoxy--carbonyl-2,2'-bipyridine[168, 169], 2,2'-(ethane-1,2-diylbis(azanediyl)diethanol[144] 2-((pyridine-2-ylmethyl)amino)ethanol[143], 2,2',2'',2'''-(ethane-1,2-diylbis(azanetriyl))--tetraethanol[146], *N*-(2-pyridylmethanimidamido)pyridine-2-carboximidamide[170], 1,10-phenanthroline-5,6-dione.[171]

6.3 Synthesis of chapter 02 compounds

$[Co(L1)_2(NO_2)_2]NO_3$, 2.06,

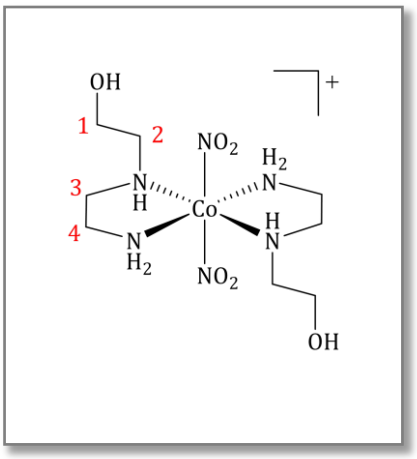

$Co(NO_3)_2 \cdot 6H_2O$, (11.64 g, 0.04 mol) and $NaNO_2$,(6 g, 0.09 mol)) were dissolved in H_2O (20 mL) and placed in a bubbler. In a separate beaker **L1**, (8.30 g, 0.08 mol) was dissolved in distilled water (10 mL) and conc. HNO_3 (3 mL) was added dropwise. The two solutions were mixed and air was vigorously bubbled through the solution for 1 hr. The reaction mixture was left at 4 °C overnight. The yellow crystalline powder that deposited overnight was separated by filtration through a sintered crucible. The solid material was washed with diethyl ether (2×20 mL) and dried under vacuum. Yields: 11.52 g (79%), M. p: 140-142°C.

^{1}H NMR (400 MHz; D_2O): δ 3.95 (1H, m, H1), 3.74 (1H, m, H1), 3.01 (4H, m, H3, H4), 2.81 (2H, m, H2), 2.59 (2H, m, H3) 2.46 (4H, m, H2, H4). **^{13}C NMR** (100 MHz, D_2O): δ 59.54 (C1), 56.39 (C2), 54.32 (C3), 46.13 (C4). **ESI-MS**: Calc. for $[C_8H_{24}N_6O_6Co]^+$: 359.1084, Found: 359.1084. **IR** υ_{max} 3357(br), 3229(br), 3157(br), 906(s), 823(s), 751(s), 692(m), 558(m), 525(s), 521(s) cm^{-1}. **UV/vis** (CH_3OH) 357, 260 nm **Analysis** Calc for $C_8H_{24}N_7O_9Co_1.H_2O$ (439.27): C, 21.87; H, 5.97; N, 22.32%. Found: C, 21.85; H, 6.01; N, 21.99 %.

[CoCl(L3)$_2$(NO$_2$)]Cl, 2.07,

$[Co(L1)_2(NO_2)_2]NO_3$, **2.06**, (2.0 g, 4.75 mmol) was dissolved in DMF (0.5 mL) and $SOCl_2$ (10.0 mL) was added drop-wise. The reaction mixture was stirred at room temperature for 5 hrs and excess $SOCl_2$ was removed under reduced pressure. The obtained pink solid material was recrystallized from ethanol /water mixture. Yield: 1.7 g (79.5%). M.p: 155 °C.

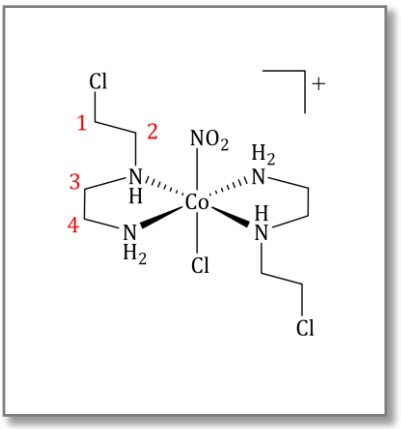

^{1}H NMR: (400MHz; DMSO-d_6) δ 3.84 (2H, m, H1), 2.90 (4H, m, H2. H4, H3), 2.50 (1H, m, H3), 2.29 (1H, m, H2). **^{13}C NMR** (100MHz; DMSO-d6) δ 52.99 (C2), 51.93 (C4), 43.16 (C3), 40.53 (C1). **ESI-MS:** Calc for $[C_8H_{22}N_5O_2Cl_3Co_1]^+$:384.0168, Found:384.0166. **IR:** υ_{max} 3214(br), 3139(br), 1584(sh), 1409(sh), 1321(s), 1178(s), 1002(sh), 749(m). cm^{-1}**. UV/vis**(CH_3OH): 350, 256 nm**. Analysis:** Calc for ($C_8H_{22}N_5O_2Cl_4Co_1$): C, 22.82; H, 5.27; N, 16.63%. Found: C, 22.83; H, 5.27; N, 16.65%.

[Co(L3)$_2$(NO$_2$)$_2$]Cl, 2.08,

<u>Method 01</u>

All the reagents and reaction vessels were cold below 0°C, before start of the reaction.

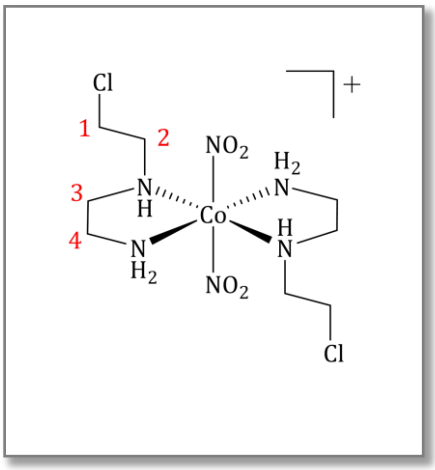

$[Co(L1)_2(NO_2)_2]NO_3$, **2.06**, (2.0 g, 4.75 mmol) was stirred in $SOCl_2$ (5.0 mL) in an ice-salt bath and DMF (0.5 mL) was added dropwise to the above solution and stirred for 5 hrs, while bubbling N_2 gas in to the reaction mixture. Excess $SOCl_2$ was removed under vacuum, while keeping the reaction mixture in ice salt-

bath. The resulting yellow solid was dissolved in a minimum amount of cold methanol while keeping the reaction vessel in dry ice / acetone bath, and dropwise addition of the methanolic solution of the complex into the ice-cold ether solution yielded a yellow coloured powdered material.

The solid material was solved with water (300 mL) and the mixture separated using a Sephadex SP-C25 cation exchange column (60×3.5 cm). The yellow band first eluted with 0.02 M NaCl was collected and evaporated to dryness and the characterisation was done after removing the salt, by a few methanolic extractions followed by G-10 size exclusion column chromatography and the compound was collected as the first yellow band eluted from the column. Yield: 1.40 g (63.6%)

Method 02

$[CoCl(L3)_2(NO_2)]Cl$, **2.07** (5.0 g, 0.01 mol) was completely dissolved in a minimum amount of warm water and filtered. $NaNO_2$ (5.0 g) was added to the reaction mixture while stirring. The stirring was continued for 8 hrs. The obtained yellow solution was filtered and kept in the fridge to obtain yellow crystals over a week. Yield: (3.54 g, 69%). M.p**:** 139 °C

^{1}H NMR: (400 MHz, D_2O) δ 4.01 (1H, m, H1), 3.95 (1H, m, H1), 3.06 (2H, m, H2, H3), 2.97 (1H, m, H4), 2.76 (1H, m, H4), 2.61 (1H, m, H2), 2.49 (1H, m, H3). **^{13}C NMR:** (25 MHz, D_2O) δ 55.90 (C2), 54.02 (C3), 46.44 (C4), 43.48 (C1). **ESI-MS:** Calc for $[C_8H_{22}N_6O_4Cl_2Co]^+$: 395.0406, Found: 395.0414. **IR:** υ_{max} 3253 (br), 1582 (s), 1397 (m), 1313 (sh), 1189 (s), 1015 (m), 825 (m) cm^{-1}. **UV/vis**(CH_3OH): 353, 256 nm. **Analysis** Calc for ($C_8H_{22}N_6O_4Cl_5Co_1$): C, 22.26; H, 5.14; N, 19.47%. Found: C, 22.24; H, 5.17; N, 19.49%.

[CoCl$_2$(L3)$_2$]Cl, 2.09,

Method 01

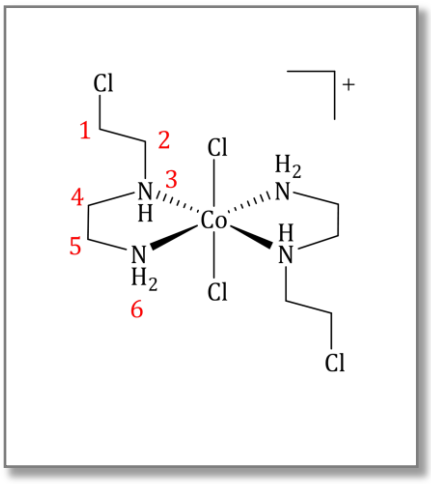

[CoCl(L3)$_2$(NO$_2$)]Cl, **2.07**, (2.0 g, 5.51 mmol) was suspended in 25 mL ethanol and conc HCl (20 mL) was added. The reaction mixture was heated for 48 hrs at 70 °C in the presence of 0.3 g of LiCl. The resulting dark green reaction mixture was filtered and dried under the reduced pressure.

The resulting green coloured solid material was washed few times with cold ethanol and the remaining solid was recrystallized from warm ethanol. The crystals were filtered and washed with cold ethanol followed by diethyl ether to obtain the pure product. Yield: 0.63 g (30%).

Method 02

[Co(L1-H)$_2$]+, **2.15**, (3.0 g, 7.31 mmol) was suspended in DMF (1.0 mL) and stirred in room temperature. SOCl$_2$ (10 mL) was added dropwise to the stirring solution and the reaction mixture was left stirring at room temperature for about three hours. Then the reaction mixture temperature was increased to 70 °C and left stirring overnight. The green thick slurry obtained was dried under vacuum to remove excess SOCl$_2$. The obtained green paste was washed with cold ethanol and remaining solid was dissolved into a minimum amount of ethanol to obtained a light green powdered material. The powder was extracted by filtering and dried under the vacuum to obtain the pure product. Yield: (1.69 g, 48%).

Method 03

$[CoCl_2(L1)_2]Cl$, **2.12** (2.0 g, 5.53 mmol) was suspended in DMF (1.0 mL) and stirred at room temperature. $SOCl_2$ (5.0 mL) was added dropwise to the stirring reaction mixture. The reaction was continued for 5 hrs and the excess $SOCl_2$ was removed under vacuum. The obtained green slurry was washed a few times with cold ethanol to remove bluish washings. The remaining green solid was slowly dispersed in ethanol to yield a green powdered material. Yield: 0.98 g (38%)

Method 04

$[Co(L3)_2(NO_2)_2]Cl$, **2.08** (1.50 g 3.48 mmol) was suspended in ethanol (25 mL) and LiCl 0.30 g was added while stirring. Conc. HCl, (10 ml) was added dropwise to the reaction mixture while stirring at room temperature. The reaction mixture was heated to 70 °C and stirring was continued overnight. The reaction was monitored by mass spectrometry to confirm the completion of the reaction. The obtained green coloured reaction mixture was dried under vacuum to remove excess HCl and ethanol. (Bubbling nitrogen in to the reaction mixture to remove excess HCl is also suggested as the compound tends to decompose under high acidic conditions in vacuum).

The obtained solid material was dissolved into cold ethanol to obtain the compound as a green powdered material. Yield: 0.81 g (48%). M.p: 205°C.

^{1}H NMR: (400MHz; DMSO-d6) δ 6.32(1H, m, N6), 5.91(1H, m, N6), 5.30(1H, m, N3), 3.98(2H, t, H1), 3.04(2H, m, H2), 2.79(3H, m, H5, H4), 2,61(1H, m, H4).**^{13}C NMR:** (25 MHz, DMSO-d6): δ 52.48 (C4), 52.25 (C2), 43.36 (C5), 40.87 (C1). **ESI-MS**: Calc for $[C_8H_{22}N_4Cl_4Co]^+$: 374.9896, Found: 374.9896 **IR:** υ_{max} 1535(w), 1387(br), 932(w), 896(w), 722(m), 681(m), 530(sh) cm^{-1}. **UV/vis** (CH_3OH) 625.00, 484.00 and 396.00 nm: **Analysis** Calc for $C_8H_{22}N_4Cl_5Co$ (410.40): C, 23.44; H, 5.46; N, 13.52%. Found: C, 23.41; H, 5.40; N, 13.65%.

[CoCl$_2$(L3)]Cl, 2.10,

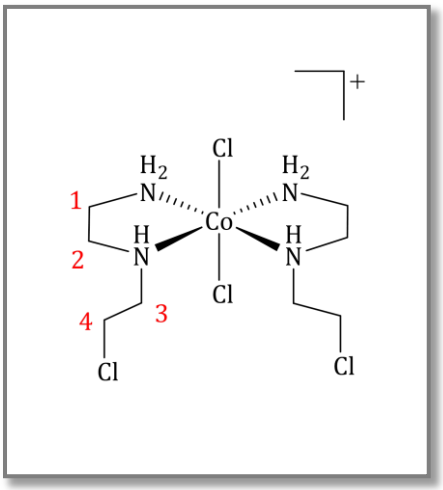

The complex [CoCl(L3)(NO$_2$)]Cl, **2.07** was synthesised according the procedure reported above and crystals of **2.07** was obtained by recrystallizing the pink crude product using 1:1, EtOH:H$_2$O mixture. After separating the pink crystals of the complex the **2.07**, the warmed filtrate was left for slow evaporation, which yielded bluish green crystals. These crystals were filtered and washed with cold ethanol solution. Yield: 0.093 mg (0.05%). **ESI-MS**: Calc for $[C_8H_{24}N_4Cl_4Co_1]^+$ 374.9798, found: 374.9897. Mp: 204.5°C. The crystals were analysed by X-ray crystallography.

[CoCl(L1)$_2$(NO$_2$)]Cl, 2.11,

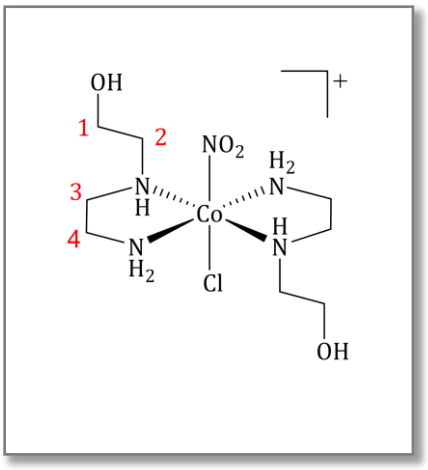

A suspension of [Co(L1)$_2$(NO$_2$)$_2$]NO$_2$, **2.06**, (0.50 g, 1.19 mmol) in MeOH (20 mL), was added to dil. HCl (10 mL) and stirred at room temperature for about 10 hours. The resulting orange solution was filtered and concentrated. The concentrated solution was added dropwise into cold diethyl ether solution to yield a fine orange powdered material. The obtained powder material was separated on a Sephadex SP-C25 cation exchange column (60×3.0 cm) using 0.02 M NaCl as an eluent. The third yellow band was collected, desalted and passed through the G-10 size exclusion column to obtain the yellow aqueous solution. The sample was dried under vacuum to obtain the yellow powdered material. Yield**:** 0.36 g (80%). M.p: 240 °C**.**

^{1}H NMR (400 MHz; D_2O): δ 3.96 (1H, m, H1), 3.75 (1H, m, H1), 3.01 (4H, m, H3, H4), 2.811 (2H, m, H2), 2.58 (2H, m, H3) 2.44 (4H, m, H2, H4). **^{13}C NMR** (100 MHz, D_2O): δ 59.56 (C1), 56.40 (C2), 54.30 (C3), 46.14 (C4); **ESI-MS:** Calc for $[C_8H_{24}N_5O_4ClCo]^+$ 348.0839, Found: 384.0843. **IR**:υ_{max} 3214(br), 3139(br), 1584(m), 1441(sh), 1409(sh), 1321(s), 1271(s), 1178(s), 1078(m), 1045(m), 1002(s), 984(s), 939(m), 881(m), 825(m), 749(m) cm^{-1}. **UV/vis** (CH_3OH): 350, 256 nm.

[Co(Cl)$_2$(L1)$_2$](Cl), 2.12,

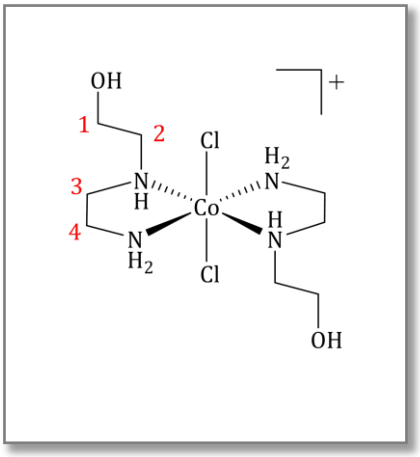

A solution of $[Co(L1)_2(NO_2)_2]NO_2$, **2.06**, (2.0 g, 4.75 mmol) in EtOH (50.0 mL) was mixed with conc. HCl (25.0 mL) and LiCl (0.3 g) and refluxed overnight. The reaction was monitored by mass spectrometry for the complete disappearance of the starting material, to confirm the completion of the reaction. Once the reaction was complete, the reaction mixture was cooled to room temperature and filtered. The solution was evaporated under vacuum. The collected solid material was stored under ethanol to collect the green powdered material. Yield: 0.86 g (45%). M.p:204-206 °C

^{1}H NMR: (400 MHz; DMSO-d6) δ 6.31 (1H, s, NH), 5.89 (1H, s, NH), 5.28 (1H, s, NH), 3.97 (2H, m, H1), 3.24 (1H, m, H1), 3.07 (2H, m, H2), 2.76 (3H, m. H3, H4), 2.56 (1H,m, H3). **^{13}C NMR**: (100MHz, DMSO-d6) δ 52.74 (C4), 52.33 (C1), 49.11(C2), 43.60 (C3). **ESI-MS:** Calc for$[C_8H_{24}N_4O_2Cl_2Co]^+$ 337.0603. Found: 337.0607. **IR:** υ_{max} 3216 (m), 3140 (m), 1548 (sh), 1440 (m), 1362 (m), 1289 (m), 1176 (m), 1158 (m), 1081 (m), 1048 (m), 998 (m), 939 (m), 880 (w) cm^{-1} **UV/vis**(CH_3OH):498, 358, 348 nm

[Co(Cl$_2$)(L1)$_2$]$^+$, 2.13,

The green powdered material obtained for the complex **2.12** (0.5g, 0.013 mol) was dissolved into methanol (5.0 mL) to make a concentrated solution and filtered. The filtered solution was separated into two different glass vials and set for slow diffusion crystallisation. After about a months' time feather like bluish crystals appeared in the vials and were collected and washed with diethyl ether. Yield: 1.5 mg (0.03%)

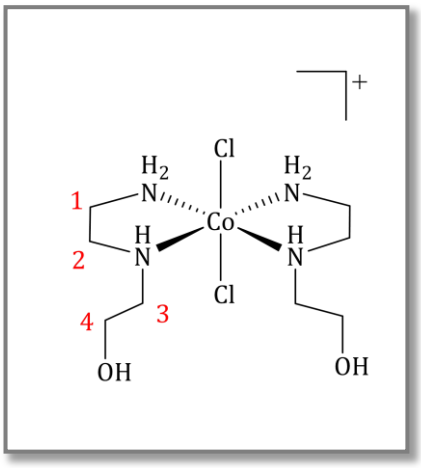

ESI-MS: Calc for[$C_8H_{24}N_4O_2Cl_2Co$]$^+$ 337.0603. Found 337.0607. **UV/vis**(CH_3OH):498, 358, 348 nm

The bluish feather like crystals were analysed by X-ray crystallography.

[Co(L1-H)$_2$]PF$_6$, 2.16,

The crystalline material of the complex [Co(L1-H)$_2$]$^+$, **2.15**, (0.5 g, 0.0962 mmol) was dissolved in methanol (15 mL) while stirring. To the methanolic solution of the complex, a few drops of a concentrated solution of methanolic ammonium hexafluoridophosphate were added dropwise while stirring. The reaction mixture was warmed up for about 30 minutes and filtered hot.

The methanolic solution of the complex was separated into few glass vials and set for the diffusion crystallisation with diethyl ether. After about a month time a few red crystals appeared and were separated from the solution. Yield: 0.02 g (5%)

ESI-MS: Calc for [$C_8H_{22}N_4O_2Co$]$^+$ 265.1073, Found 265.1072, The X ray crystallographic analysis of the **2.16** is reported in chapter 02.

[Co(L1)(L1-H)$_2$]2I, 2.19,

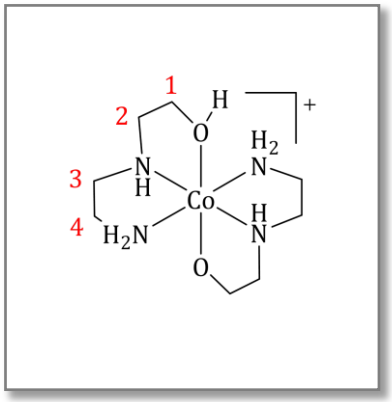

Finely powdered $[Co(NH_3)_6]Cl_3$ (5.3 g, 0.02 mol) was mixed with activated charcoal (1 g), and concentrated ammonium hydroxide (5.0 mL) and **L1** (4.28g 0.04 mol) was added to the solid mixture. The reaction mixture was heated on the steam bath until the odour of ammonia could no longer be detected. The precipitate which forms was separated from the carbon by heating the mixture with 40 mL of hot water and filtering. The solution was concentrated to ~15 mL under vacuum and a concentrated aqueous solution of LiI (5 mL) was added and left for slow evaporation. The precipitated crystalline solid material was collected by filtration and washed with water. Yield: 2.67 g (20.7 %). M.P: stable over 240°C

ESI-MS: Calc for $[C_8H_{22}N_4O_2Co]^+$ 265.1073, Found 265.1072, **IR:** υ_{max} 3211 (br), 3135(br), 1583 (sh), 1440 (w), 1282 (w), 1170 (w), 1041 (vs) cm^{-1} **UV/vis** (CH_3OH): 511, 252 nm. **Analysis** Calc for ($C_8H_{23}N_4O_2Co_1I_2{\cdot}2H_2O$): C, 17.86; H, 4.68; N, 10.41 %. Found: C, 17.83; H, 4.65; N, 10.43 %.

[Co(Cl)$_5$(L1-H)$_2$Zn$_2$], 2.20 and 2.21,

The crystalline powder of **2.19** (0.5 g, 0.77 mmol,) was dissolved in warm methanol (20 mL) while stirring. Methanolic solution of $ZnCl_2$ (0.5 g, 3.7 mmol) was added dropwise to the reaction mixture while stirring. The reaction was continued for 20 minutes and filtered hot and left for slow evaporation to yield pink crystals. Yield: 0.90 g, (22%), Mp: > 250 °C

ESI-MS: Calc for $[C_8H_{22}N_4O_2Co_1]^+$ $[Co(L1\text{-}H)_2]^+$, 265.1074, found: 265.1050; Calc for $[C_8H_{22}N_4O_2Cl_2Zn_1Co_1]^+$, 398.9873, found: 398.9721, Calc for $[C_8H_{22}N_4O_2Cl_4Zn_2Co_1]^+$, 532.8411, found: 532.8406, **IR:** υ_{max} 1583 (sh), 1445 (w), 1283 (s), 1170 (w) cm^{-1} **UV/vis** (CH_3OH): 511, 252.

The complex was characterised X-ray crystallography.

[Co(Cl)$_3$(L1-H)$_2$Mn$_2$], 2.22,

The crystalline powder of **2.19** (0.5 g, 0.77 mmol,) was dissolved in warm methanol (20 mL) while stirring. Methanolic solution of $MnCl_2 \cdot 4H_2O$ (0.5g, 2.5 mmol) was added dropwise to the reaction mixture while stirring. The reaction was continued for 20 minutes and filtered hot and left for slow evaporation to yield pink crystals. Yield: 0.05 g, (15%), Mp: > 250 °C

The complex was characterised X-ray crystallography.

[Co(L3)$_2$(NH$_3$)(NO$_2$)]Cl, 2.25,

$[CoCl(L3)(NO_2)]^+$, **2.07** (1.5g, 5.30 mmol) was dissolved in warm water (15 mL) and filtered. The aqueous solution of **2.07** was brought to 0°C in an ice bath and 35% NH_4OH (10 mL) and $NaNO_2$ (0.5 g, 7.24 mmol) were added. The mixture was stirred for complete dissolution and kept at 4 °C to obtain large yellow crystals over a period of three days. Yield: 0.8 ng (56%)

The crystals were suitable for the X-ray crystallographic analysis. The crystal structure of the complex **2.25** is discussed in chapter 02.

6.4 Synthesis of chapter 03 compounds

[Co(L4-H)$_3$], 3.01,

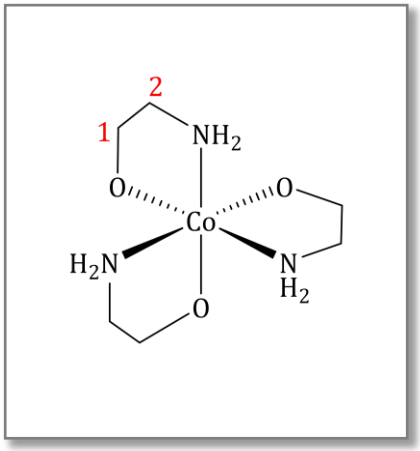

$[Co(NH_3)_6]Cl_3$, (5.0 g, 0.019 mol) was dissolved in concentrated ammonium hydroxide (20 mL) solution and activated charcoal (1.0 g) and **L4** (4.00 g, 0.07 mol) was added to the reaction mixture. The reaction mixture was placed on the steam bath for 5 hrs. The obtained red reaction mixture was filtered while the solution is warm to remove the activated charcoal. The filtrate was dried under vacuum and redissolved in methanol (10 mL). The red coloured methanolic solution is filtered and left for slow evaporation to obtain red coloured plate like crystals. Yield: 2.184 g, (65%). M.p:>240 °C.

^{1}H NMR: (400MHz; D_2O) δ 3.83 (2H, t, H1), 3.15 (2H, t, H2). **^{13}C NMR** (100MHz;D_2O) δ 60.50(C1), 44.10(C2). **UV/vis**(CH_3OH): 531 nm. **IR**:υ_{max} 2912.78(br), 1587(w), 1433(w), 1050(vs) cm^{-1} **Analysis** Calc for ($C_6H_{18}N_3O_3Co_1H_2O{\cdot}CH_3OH$) C, 29.07; H, 8.36; N, 16.34%. Found C, 30.01; H, 8.34; N, 16.33%.

[Co(L5-H)$_2$]I, 3.02,

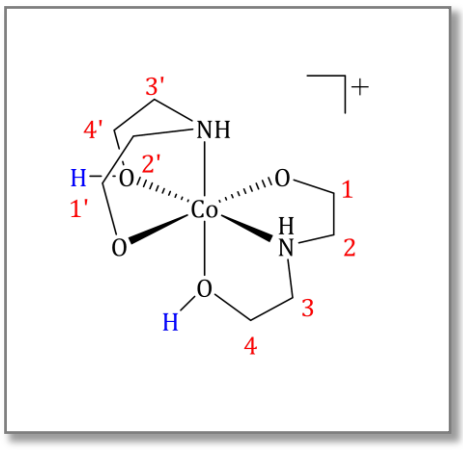

L5 (4.49 g, 0.043 mol) was added dropwise to a stirred solution of $CoSO_4{\cdot}7H_2O$ (4.0 g, 0.014 mol) in an aqueous-ethanol mixture (20 mL of ethanol and 10 mL of water). The ethanol solution was completely evaporated under vacuum and obtained red sticky solid material was dissolved in to a warm methanol solution containing LiI. The warm methanolic

solution was filtered and left for slow evaporation. After a few days the solution yielded plate like red crystals. The precipitated red plate like crystals of compound $[Co(L5\text{-}H)_2]^+$ were filtered off and washed with ethanol and ether. Yield: 2.58 g, (68%). M.p: > 240°C.

^{1}H NMR: (400MHz; D_2O) δ 3.17 (3H, m, H1, H2, H4), 3.02 (2H, m, H1,H3), 2.91 (1H, m, H3), 2.66 (1H, m, H4), 2.51 (1H,m, H2). **^{13}C NMR** (100MHz;D_2O) δ 67.104 (C1), 57,25 (C2), 55.44 (C4), 44.83 (C3) . **ESI-MS:** Calc for $[C_8H_{20}N_2O_4]^+$ 267.0755, Found: 267.0725. **IR:** 3306(w), 3158(w), 2912(m, sh), 2838(m, sh), 2787(m, sh), 1615(m), 1460(m), 1432(m), 1090(w), 1030(s), 811(s), 590(s), 524(s), 499(s), 456(s) cm^{-1}**. UV/Vis:** 556, 402 nm **Analysis** Calc for: $C_8H_{18}N_2O_4I_3Co_{1.}H_2O$: C, 23.32; H, 5.38; N, 6.80%. Found: C, 23.31; H, 5.35; N, 6.82 %.

[{Co(L5-2H)(L5-H)}($MnCl_2$)$_2$], 3.03,

$[Co(NH_3)_6]Cl_3$ (3.0 g, 0.01 mol) was added to concentrated ammonium hydroxide (20 mL) and activated charcoal (1.0 g). To the reaction mixture **L5** (3.0g, 0.03 mol) was added and placed on the steam bath for about 5 hrs. The reaction mixture was filtered and left for low evaporation to yield a bluish green powder. The powder was separated, washed and dried. Then the bluish powder was dissolved in MeOH (10 mL) and warmed up while stirring. $MnCl_2.4H_2O$ (4.0 g, 0.02 mol) was added and stirring was continued for another 10 min. The solution was filtered and left for slow evaporation to obtained X-ray quality pink crystals. The yields of these crystals were insufficient to carry out other analysis. The crystal structure of the complex is reported in chapter 03.

[Co(L6-H)Cl], 3.08,

Commercially available **L6** (3.346 g, 0.02 mol) was dissolved in concentrated ammonium hydroxide (20 mL). $[Co(NH_3)_6]Cl_3$ (3.0 g, 0.01 mol) and activated charcoal (1.0 g) were added to the ammonium hydroxide solution. The reaction mixture was placed on the steam bath for about four hours. The reaction mixture was filtered and

the filtrate left for slow evaporation. Blue coloured crystals appeared overnight. Yield: 0.57 g (21%). Mp:> 250 °C.

IR: 2836(w), 1453(m), 1369(m), 1269(m), 1073(sh), 887(sh), 608(m), 557(m) cm^{-1}. **Analysis:** Calc for: ($C_6H_{14}NO_3CoCl$) C, 29.71; H, 5.82; N, 5.77 %. Found: C, 29.69; H, 5.92 ; N, 5.77%.

[{Co(L6-3H)(CH_3OH)$ZnCl_2$}$_2$], 3.09,

Commercially available **L6** (3.35 g, 0.02 mol) was dissolved in concentrated ammonium hydroxide (20 mL). $[Co(NH_3)_6]Cl_3$ (3.0 g, 0.011 mol) and activated charcoal (1.0 g) were added to the reaction mixture. The reaction mixture was placed on the steam bath for about four hours for the completion of the reaction. The reaction mixture was filtered and dried under vacuum. The solid residue obtained was dissolved in warm methanol (10 mL) while stirring. A methanolic solution of $ZnCl_2$ was added to the warm reaction mixture while stirring. The reaction was continued for about 30 min and filtered. The purple reaction mixture was left for slow evaporation to give purple coloured crystals. Yield: 1.26 g (18%). M.p: 140-143 °C.

IR: υ_{max} 2876.09(br), 1621.09(s), 1052.15(sh), 906.08(s), 660.91(s) cm^{-1}. **UV/vis**(H_2O): 558 nm. **Analysis**: Calc for ($C_{14}H_{32}N_2O_8Cl_4Zn_2Co_2 \cdot 2CH_3OH \cdot 2H_2O$) C, 22.69; H, 5.24; N, 3.31%. Found: C, 22.67; H, 5.23; N, 3.30%.

[Co(L7-H)L7](PF$_6$)$_2$, 3.11,

$[Co(NH_3)_6]Cl_3$ (0.956 g, 3.574 mmol) was reacted with **L7,** synthesised according to the literature procedure, (1.089 g, 7.14796 mol) in the presence of concentrated ammonium hydroxide (20 mL) and activated charcoal (0.8 g). The reaction mixture was heated on a steam bath for ~5 hrs and the obtained pink coloured solution was filtered hot. The pink solution was concentrated and a few drops of concentrated ammonium hexafluoridophosphate were added. The pink powder that resulted was filtered and washed with cold acetonitrile followed by cold ethanol. Yield: 1.03 g (80%). M.p:>200 °C.

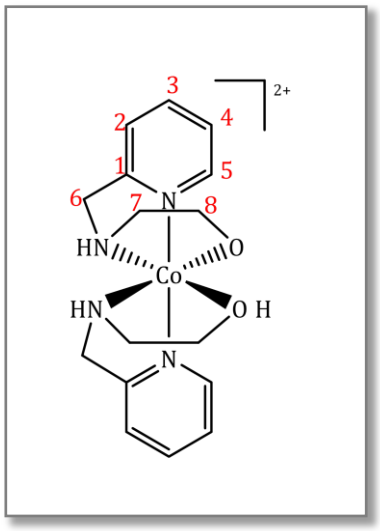

^{1}H NMR:(400 MHz, DMSO-d6) δ 8.76 (1H, d, H1), 8.14 (1H, t, H3), 7.69 (1H, t, H5), 7.31 (1H, d, H2), 5.03 (2H, dd, H8), 4.16 (2H, d, H6), 2.58 (2H, d, H7)**^{13}C NMR**:(100MHz, DMSO) δ).150.13 (C5), 158.01 (C4), 133.98 (C3), 137.14 (C1). **ESI-MS:** Calc for $[C_{16}H_{22}N_4O_2Co_1]^+$ 361.1069. Found 361.1062. **IR:** υ_{max} 3306(w), 820(s, sh), 555(sh), 464.87(w) cm^{-1}. **UV/vis**(CH_3OH):513, 257, 218 nm. **Analysis:** Calc for: ($C_{16}H_{23}N_4O_2(PF_6)_2Co_1{\cdot}CH_3CN$) C, 31.18; H, 3.78; N, 10.10%. Found: C, 31.20; H, 3.79; N, 10.06.

[Co(L2-H)$_2$]I$_3$, 3.13,

To finely powdered $[Co(NH_3)_6]Cl_3$,(1.80 g, 6.7 mmol) was added activated charcoal (0.5 g), followed concentrated ammonium hydroxide (10.0 mL) and **L2**(1.82 g, 0.04 mol). The mixture was heated in the steam bath until the odour of the ammonia could no longer be detected. The formed precipitate was separated from the carbon by heating the mixture with hot water (40 mL) and filtering. The solution was concentrated to ~15 mL under vacuum

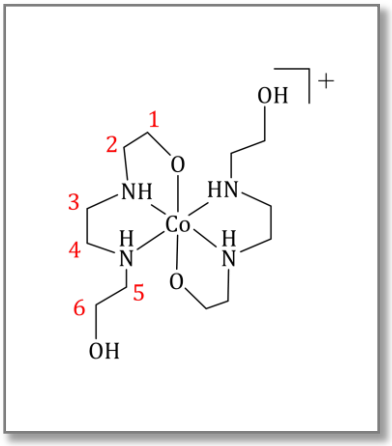

and a concentrated solution (~2 $molL^{-1}$) of LiI (3 mL) was added and left for slow evaporation. The yellow crystalline material formed over the time was collected by filtration and washed with water. Yield**:** 3.47 g (70%). M.p**:** 170°C.

ESI-MS: Calc for $[C_{12}H_{30}N_4O_4Co_1]^+$ 353.1594, Found: 353.1608**. IR:** 3136(br), 1588(w, br), 1433(w), 1014(vs) cm^{-1}**. UV/vis:** 360, 288 nm **Analysis Calc for**: $C_{12}H_{30}N_4O_4I_3Co_1$: C, 21.35; H, 4.48; N, 8.30%. Found: C, 21.31; H, 4.48; N, 8.32%.

[(Co(L8-2H))$_2$](I$_3$)$_2$, 3.15,

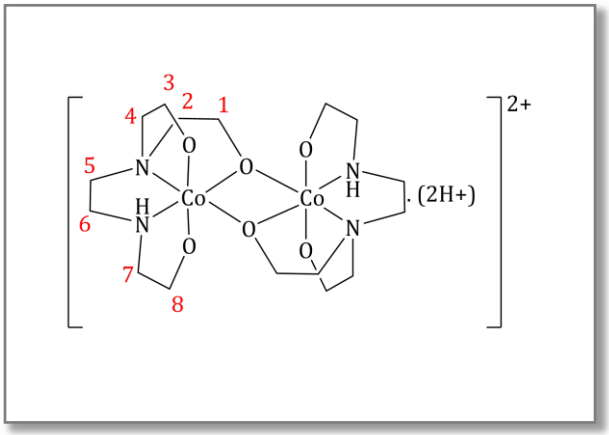

2-(2-aminoethylamino)ethanol, **L1**, (20.8 g, 0.2 mol) was added to 2-chloroethanol (16 g, 0.2 mol). Powdered Na_2CO_3 (16.96g, 0.2 mol) was added and the mixture was stirred at 135 °C for 25 hrs. After cooling the reaction mixture to room temperature MeOH (300 mL) was added and the mixture was filtered. The methanolic solution was evaporated under vacuum to obtain the crude product. The yellow oil was recrystallized twice from THF to obtain the **L2** as a product from the yellow reaction mixture. After recrystallization of the **L2** ligand, the remaining crude oil, which was composed of **L8** and **L9,** was directly used for the next step of the reaction.

$[Co(NH_3)_6]Cl_3$ (4.169 g, 0.016 mol) was mixed with the crude oil (3.0 g). Ammonium hydroxide (20 mL) and activated charcoal (1.0 g) was added to the mixture. The reaction mixture was heated on the steam bath for five hours and filtered hot. The collected solution was reduced in volume under vacuum to ~15 mL and an aqueous solution of LiI (1 mL) was added. The aqueous solution was left for slow evaporation. The precipitated red crystalline solid was collected and washed with cold water and dried under vacuum. Yield: 5.62 g (40%). M.p: 210°C**.**

^{1}H NMR:(400MHz, D_2O) δ 4.20 (1H, m, H1), 3.69 (2H, m, H1, H7), 3.46 (2H, m, H5, H8), 3,24 (2H, m, H2, H6), 3.09 (3H, m, H4, H3, H5), 2.82 (1H, dd, H3), 2.67 (2H, m, H7, H4), 2.59(2H, m, H2, H7), 2.29 (1H, m, H6). **^{13}C NMR**:(100MHz, D2O) δ 68.41(C8), 67.91(C3), 66.88(C1), 65.11(C7), 64.90 (C6), 64.10(C4), 58.59(C2), 56.77(C5). **ESI-MS:** Calc $[C_8H_{18}N_2O_3Co_1]^+$ 250.0722, Found:250.0704. **IR:** υ_{max} 3220(br), 1459(w), 1383(w), 1034(m), 1003(m), 825(s), 555(sh), 492(w) cm^{-1} **UV/vis**(CH_3OH):569, 258, 226 nm**. Analysis:** Calc for:$C_{16}H_{36}N_4O_6I_6Co_2{\cdot}H_2O$ C, 15.06; H, 2.84; N, 4.39%. Found: C, 15.00; H, 2.84; N,.4.38%.

[Co(L8-3H)($ZnCl_2$)]$_2$, 3.16,

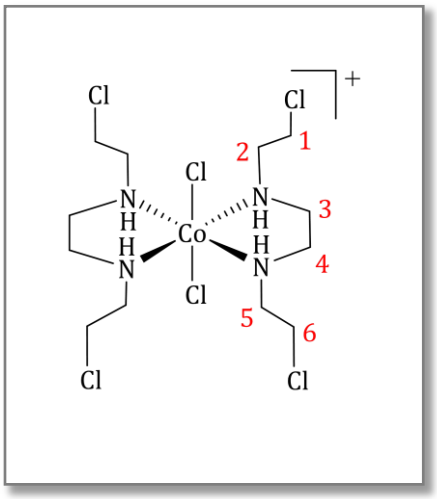

3.17(2.0 g, 1.6 mmol) was dissolved in MeOH (10 mL) and $ZnCl_2$ (0.3 g, 2.2 mmol) was added to the methanolic solution. The reaction mixture was warmed and stirred for about 10 minutes. The reaction mixture was filtered and left for slow evaporation to yield pink crystals. Yield: 1.10 g, (80%), M.p: 215-220°C.

IR: υ_{max} 1550(sh), 1200(s), 987(w), (850(s) cm^{-1} **UV/vis**(CH_3OH): 568, 255 nm. **Analysis**: Calc for: $C_{16}H_{34}Cl_4N_4O_6Co_2Zn_2{\cdot}CH_3OH$ C, 25.49; H, 4.78, N 6.99%. Found: C, 25.48, 4.81, 6.95%.

The complex was characterised by X-ray crystallography.

[Co(bceen)$_2$Cl$_2$]Cl, 3.17,

[Co(L2-H)$_2$](I_3), **3.15**, (0.98 g, 2.52 mmol) was dissolved in $SOCl_2$ (10.00 mL) and DMF (0.5 mL) was added while stirring. Stirring was continued at room temperature for about 5 hrs. The temperature of the reaction mixture was slowly brought up to 70 °C. The stirring was continued overnight and reaction was monitored by mass spectrometry for the complete disappearance of starting material to confirm the completion of the reaction. The obtained green slurry was dried under vacuum to

remove excess thionyl chloride. The obtained thick green solid was dissolved in ethanol and first few bluish coloured washing were discarded. The green coloured powdered material left was filtered and washed with cold ethanol to obtain the pure material. Yield: 0.54 g, (40%). M.p: 165-170 °C.

^{1}H NMR: (400MHz, CD_3OD) δ 4.059 (2H, m, H1), 3.02 (4H, m, H6), 3.50 (1H, m, H2), 3.40 (1H, m, H5), 3.10 (2H, m, H3, H4), 2.90 (2H, m, H2, H5), 2.76 (2H, m, H3, H4. **^{13}C NMR** (100MHz, CD_3OD) δ 39.39(C1), 39.44(C6), 52.43(C2), 52.40(C5), 49.55 C3), 49.08(C4) . **ESI-MS:** Calc for $[C_{12}H_{28}N_4Cl_6Co_1]^+$ 498.9743, Found 498.9760. **IR:** 3176(br), 1584(m), 1434.04(m), 1042(vs) cm^{-1}**. UV/vis** (H_2O):645, 413 nm. **Analysis:** Calc for $C_{12}H_{28}N_4Cl_8Zn_1Co_1$: C, 26.92; H, 5.27; N, 10.46. Found: C, 25.95; H, 5.56; N, 10.45%.

$[Co(bceen)_2Cl_2]_2[ZnCl_4]$, 3.22,

(O.5 g, 1.2 mmol) of **3.17** was dissolved in to a warm EtOH (10 mL) while stirring and (0.2g, 1.5 mmol) of $ZnCl_2$ was added to the ethanoic solution of the compound. The solution was warmed and stirred for about 5 min, filtered and left for slow evaporation to yield long green coloured crystals. The crystals were sepearted and washed with cold ethanol. Yield 0.21g (30%)

The crystals were analysed by X-ray crystallography.

6.5 Synthesis of chapter 04 compounds

[(dmbpy)$_2$Ru(pytp)](PF$_6$)$_2$, 4.09b,

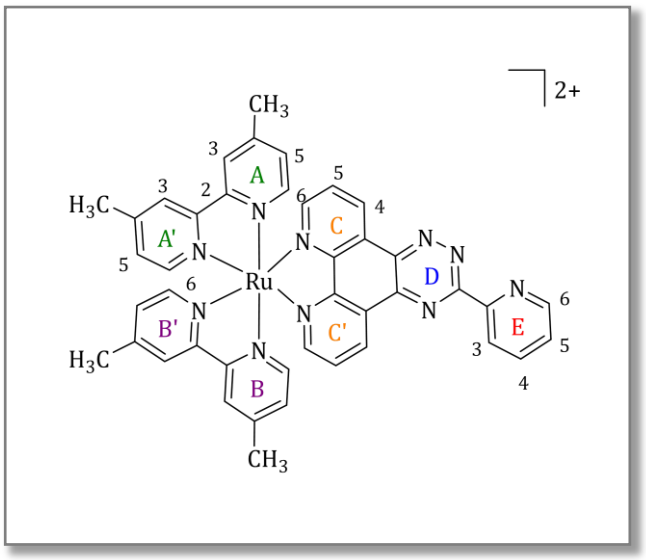

[(dmbpy)$_2$Ru(phendione)](PF$_6$)$_2$ (1.0 g, 1.031 mmol) was dissolved into 15 mL of methanol. Pyridine-2-carbohydrazonamide (0.14 g, 1.03 mmol) was dissolved in ethanol (5 mL). The solutions were mixed together. The reaction mixture was then heated at reflux for 1hr and the reaction mixture was dried under vacuum. The crude material obtained was dissolved in the minimum amount of methanol and the product was precipitated as its hexafluoridophosphate salt by adding aqueous ammonium hexafluoridophosphate. The red powdered precipitate was chromatographed on a silica column to obtain the pure product. The acetonitrile fraction was collected and dried under vacuum and dissolved in the minimum amount of methanol and precipitated as a hexafluoridophosphate salt by adding aqueous solution of ammonium hexafluoridophasphate. Yield: 0.53 g (48%). M.p: decomposed at 260-265 °C

^{1}H NMR:(400MHz, CD_3CN) δ 2.492(6H,s), 2.587(6H,s), 7.092(2H, m, H5AB), 7.319(2H, d, H5A'B'), 7.485(2H, m, H6A), 7.654(2H, d, H6A'B'), 7.693(1H, m, H4E), 7.960(2H, m, H5CC'), 8.150(1H, t, H5E), 8.314(2H, dd, H6CC'), 8.369(2H, s, H3AB), 8.406(2H, s, H3A'B'), 8.927(1H, d, H3E), 8.979(2H, s, H6E), 9.710(1H, d, H4C'), 9.785(1H, d, H4C) **ESI-MS:** Calc for $[C_{38}H_{26}N_{10}Ru_1]^{2+}$ 362.0692, Found: 362.0690 **IR:** υ max 407.20(sh), 833.46(s),1368.32(w), 1618.11(w) cm^{-1} **UV/vis**: 444, 283 nm. **Analysis**: Calc for $C_{42}H_{34}N_{10}P_2F_{12}Ru_1 \cdot H_2O \cdot CH_3CN$: C, 46.81; H, 4.48; N, 13.65, Found: C, 46.79; H, 4.47; N, 13.59.

[(decbpy)$_2$Ru(pytp)](PF$_6$)$_2$, 4.09d,

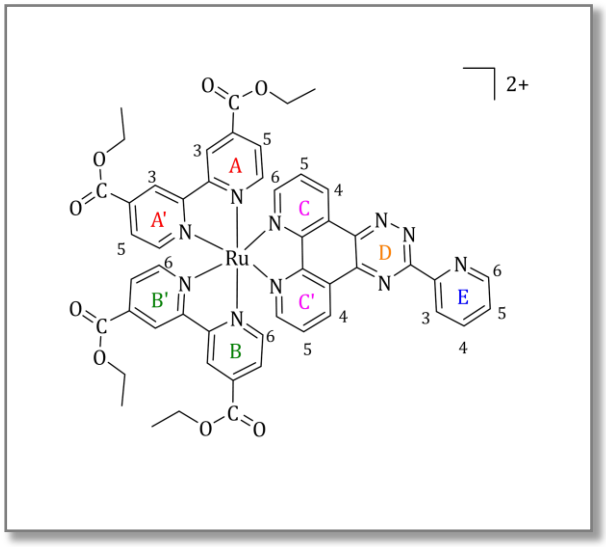

[(decbpy)$_2$Ru(phendione)](PF$_6$)$_2$ (1.0 g, 0.83 mmol) was dissolved in methanol (15 mL). Pyridine-2-carbohydrazonamide (0.14 g, 1.03 mmol) was dissolved in ethanol (5 mL). The two solutions were mixed together. The reaction mixture was then heated at reflux for 1 hr and dried under vacuum. The crude material obtained was dissolved in a minimum amount of methanol and the product was precipitated as its hexafluoridophosphate salt by adding aqueous ammonium hexafluoridophosphate. The red powdered precipitate was chromatographed on a silica gel column using (1:1, ethanol:10% NaCl) as an eluent. The second red band was collected, dried under vacuum and dissolved in the minimum amount of water. The product was extracted into dichloromethane while adding concentrated aqueous ammonium hexafluoridophosphate (5-10 mL) into the separatory funnel. The collected extracts were dried under vacuum to obtain the pure product as a hexafluoridophosphate salt.

Yeild: 0.325g (30%). M.p:>240°C

^{1}H NMR:(400MHz, CD_3CN) δ 1.41 (15H, m), 4.46 (8H, m), 7.69 (1H, dd, H5E), 7.73 (2H, m, H5A), 7.89 (2H, d, H5'A), 7.91 (2H, d, H5'A), 7.97 (m, 2H, H'5C), 8.03 (2H, d, H5'A), 8.15 (m, 1H, H5E), 8.24 (2H, dd, H6C, H6C'), 8.94 (1H, d, H3E), 8,98 (1H, d, H6E), 9.77 (1H, dd, H4C'), 9.88 (1H, dd, H4C). **ESI-MS:** Calc for $[C_{50}H_{42}N_{10}O_8Ru_1]^{2+}$ 506.1170, Found: 506.1140. **IR:** υ_{max} 556(sh)**,** 765(sh)**,** 833(w)**,** 1015(s), 1127(sh), 1251(m), 1320(s), 1369(m), 1432(s), 1722(sh). **UV/vis**: 466, 305 nm. **Analysis**: Calc for, $C_{50}H_{42}N_{10}O_8P_2F_{12}Ru_1 \cdot PF_6 \cdot H_2O$ C, 40.99; H, 3.03; N, 9.56. Found: C, 40.87, H, 2.98, N, 9.53.

[Ru(dmbpy)$_2$(phen)](PF$_6$)$_2$

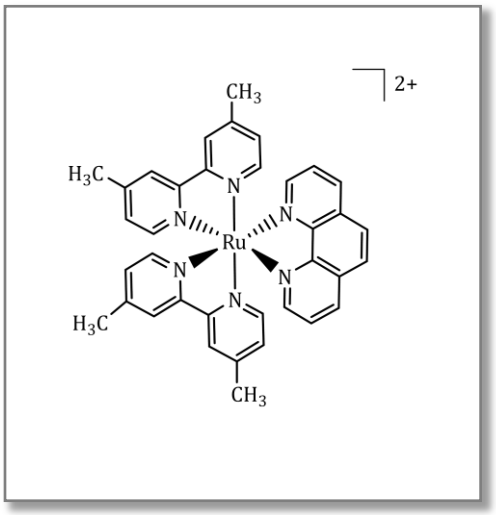

$[RuCl_2(dmbpy)_2]\cdot 2H_2O$ (0.33 g, 1.85 mmol) and 1,10-phenanthroline were heated at 70°C in ethanol (50 mL). The solution was concentrated to ≈20 ml and then water (50 mL) was added. The product was precipitated by addition of a saturated methanolic solution of NH_4PF_6 (1.0 mL). The precipitate was collected by vacuum filtration and washed with cold (0˚C) ethanol. The product was further purified using a silica gel column (2.5 cm diameter and 1.5 m length) packed using ethyl acetate. The mixture was loaded on to the column bed after adsorbing it on to a small amount of silicagel. Acetonitrile was used as the eluent. The middle red band was collected and precipitated using methanolic ammonium hexafluoridophosphate. The resulting orange-red solid was filtered off, washed with cold water and diethyl ether and then dried under vacuum. Yield 1.22 g, (70%). M.p:142-143 °C

1H NMR: (400 MHz, CD_3CN):δ 8.60 (2H,d), 8.39 (2H, s), 8.34 (2H, s), 8.24 (2H, s), 8.10 (2H, d), 7.75 (2H, dd,) 7.67 (2H, d), 7.34 (2H, d), 7.29 (2H, d), 7.04 (2H, d) 2.58 (6H, s, CH_3), 2.48 (6H, s, CH_3). **ESI-MS**:Calc for $[C_{36}H_{32}N_6Ru]^{2+}$795.13, Found (M/z)325.08. **IR**:υ_{max} 3639(w), 1619(m), 1479(m), 1431(m), 821(sh), 721(m), 555(s), 526(m) cm^{-1}. **UV/vis**(CH_3CN): 455nm. **Analysis**: Calc for ($C_{36}H_{32}N_6RuP_2F_{12}$) C, 46.01; H, 3.4; N, 8.14%. Found: C, 46.35; H, 3.77; N 8.55%.

Appendix

Crystallographic Tables

Appendix – Crystallography

Table A–H list the crystal data and X–ray experimental details for the twenty three crystal structures discussed in this thesis. Selected bond lengths and bond distances are listed in the discussion of the structures, while the remaining distances and angles, as well as the atomic coordinates, anisotropic displacement parameters and hydrogen atom coordinates are available on request from the Department of Chemistry, University of Canterbury.

All the X–ray crystallographic data was collected on either a Bruker APEX–II instrument with graphite–monochromatised Mo Kα (λ = 0.71073 Å) radiation or on an Oxford–Agilent SuperNova instrument with focussed microsource Mo Kα (λ = 0.71073 Å) and Cu Kα radiation (λ = 1.5418 Å) and ATLAS CCD area detector. The structures were solved using direct methods with SHELXT[172] and refined on F2 using all data by full–matrix least square procedures with SHELXL.[173] Multiscan absorption corrections were done using SADABS or SCALE3 ABSPACK. The non–hydrogen atoms were refined with anisotropic displacement parameters. All the hydrogen atoms were included in calculated positions with isotropic displacement parameters 1.2 or 1.5 times the isotropic equivalent of their carbon atoms

Table B. *Crystal data and X–ray experimental data for complexes 2.09, 2.12 and 2.13*

Identification code	**2.09 (KJK 48a)**	**2.13 (KJK35ab)**	**2.12 (KJK46a)**
Empirical formula	$C_{12}H_{34}Cl_5CoN_4O_2$	$C_8H_{24}Cl_3CoN_4O_2$	$C_8H_{26}Cl_3CoN_4O_3$
Formula weight	502.61	373.59	391.61
Temperature/K	120.01(10)	120.01(10)	120.01(10)
Crystal system	orthorhombic	monoclinic	triclinic
Space group	*Pbcn*	*P*21/*n*	*P*-1
a/Å	19.2961(3)	11.5210(7)	9.7046(5)
b/Å	8.06940(10)	10.6094(6)	10.3901(5)
c/Å	27.6193(5)	12.7807(8)	10.4141(6)
α/°	90	90	62.180(5)
β/°	90	98.647(6)	63.266(5)
γ/°	90	90	88.467(4)
Volume/Å3	4300.54(12)	1544.44(16)	806.81(9)
Z	8	4	2
ρcalcg/cm3	1.553	1.607	1.612
μ/mm 1	1.433	13.508	13.004
F(000)	2096.0	776.0	408.0
Crystal size/mm3	0.3873 × 0.1887 × 0.173	0.1147 × 0.0697 × 0.0572	0.1379 × 0.1054 × 0.1017
Radiation	MoKα (λ = 0.71073)	CuKα (λ = 1.54184)	CuKα (λ = 1.54184)
2Θ range for data collection/°	5.472 to 74.996	9.642 to 153.088	9.896 to 153.714
Reflections collected	244186	11823	15569
Independent reflections	11307 [Rint = 0.0523, Rsigma = 0.0149]	3154 [Rint = 0.0610, Rsigma = 0.0510]	3374 [Rint = 0.0474, Rsigma = 0.0329]
Data/restraints/parameters	11307/8/253	3154/9/172	3374/10/194
Goodness-of-fit on F2	1.173	1.015	1.103
Final R indexes [I>=2σ (I)]	R1 = 0.0319, wR2 = 0.0724	R1 = 0.0452, wR2 = 0.1037	R1 = 0.0411, wR2 = 0.1214
Final R indexes [all data]	R1 = 0.0397, wR2 = 0.0785	R1 = 0.0640, wR2 = 0.1151	R1 = 0.0444, wR2 = 0.1243
Largest diff. peak/hole / e Å-3	0.76/-0.93	0.71/-0.41	0.90/-0.54

Table C. *Crystal data and X–ray experimental data for complexes 2.16, 2.19 and 2.20.*

Identification code	**2.16 (KJK33ab)**	**2.19 (EXP 72a)**	**2.20 (exp 76 a)**
Empirical formula	$C_8H_{22}CoF_6N_4O_2P$	$C_8H_{23}CoI_2N_4O_2$	$C_8H_{22}Cl_5CoN_4O_2Zn_2$
Formula weight	410.19	520.03	573.21
Temperature/K	120.01(10)	120.01(10)	202(110)
Crystal system	orthorhombic	monoclinic	triclinic
Space group	*Pbcn*	*P*21/c	*P*-1
a/Å	10.0855(6)	14.*0248*(3)	8.0188(6)
b/Å	18.6517(10)	9.5014(2)	9.4646(6)
c/Å	7.9440(4)	11.3201(2)	13.1434(8)
α/°	90	90	76.033(5)
β/°	90	102.667(2)	79.660(5)
γ/°	90	90	74.106(6)
Volume/Å3	1494.36(14)	1471.75(5)	924.12(11)
Z	4	4	2
ρcalcg/cm3	1.823	2.347	2.060
μ/mm 1	10.788	5.360	16.711
F(000)	840.0	992.0	572.0
Crystal size/mm3	0.2612 × 0.2139 × 0.1609	0.1988 × 0.082 × 0.0342	0.1529 × 0.1025 × 0.0697
Radiation	CuKα (λ = 1.54184)	MoKα (λ = 0.71073)	CuKα (λ = 1.54184)
2Θ range for data collection/°	9.484 to 152.63	5.22 to 61.01	6.982 to 153.59
Reflections collected	6979	37497	17370
Independent reflections	1564 [Rint = 0.0379, Rsigma = 0.0278]	4277 [Rint = 0.0462, Rsigma = 0.0231]	3851 [Rint = 0.0629, Rsigma = 0.0374]
Data/restraints/parameters	1564/5/121	4277/9/174	3851/4/199
Goodness-of-fit on F2	1.041	1.097	1.149
Final R indexes [I>=2σ (I)]	R1 = 0.0379, wR2 = 0.1054	R1 = 0.0207, wR2 = 0.0448	R1 = 0.0822, wR2 = 0.2970
Final R indexes [all data]	R1 = 0.0432, wR2 = 0.1102	R1 = 0.0273, wR2 = 0.0489	R1 = 0.0845, wR2 = 0.2979
Largest diff. peak/hole / e Å-3	0.37/-0.68	0.64/-1.01	2.11/-1.32

Table D. *Crystal data and X–ray experimental data for complexes 2.21, 2.22 and 2.25.*

Identification code	**2.21 (exp_84)**	**2.22 (exp 85 a)**	**2.25 (exp92a)**
Empirical formula	$C_8H_{27.11}Cl_{4.5}CoN_4O_3.15Zn_2$	$C_8H_{19.5}Cl_3CoMnN_4O_2$	$C_8H_{25}Cl_4CoN_6O_{2.67}$
Formula weight	579.13	423.99	448.74
Temperature/K	120.00(10)	119.98(14)	284.94(10)
Crystal system	orthorhombic	monoclinic	trigonal
Space group	*Aea*2	*P*21/*n*	*R*-3*c*
a/Å	25.8579(7)	11.9261(5)	15.9005(8)
b/Å	11.1659(3)	17.6711(5)	15.9005(8)
c/Å	13.2095(3)	15.8350(5)	37.310(2)
α/°	90	90	90
β/°	90	100.318(3)	90
γ/°	90	90	120
Volume/Å3	3813.94(17)	3283.2(2)	8169.2(10)
Z	8	8	18
ρcalcg/cm3	2.017	1.716	1.642
μ/mm 1	15.616	18.702	12.988
F(000)	2335.0	1716.0	4164.0
Crystal size/mm3	3.2731 × 0.757 × 0.2278	0.2204 × 0.0855 × 0.0572	0.1868 × 0.1463 × 0.0709
Radiation	CuKα (λ = 1.54184)	CuKα (λ = 1.54184)	CuKα (λ = 1.54184)
2Θ range for data collection/°	6.836 to 134.976	7.566 to 134.998	7.98 to 134.92
Reflections collected	34884	30764	14770
Independent reflections	3453 [Rint = 0.0651, Rsigma = 0.0272]	5915 [Rint = 0.1169, Rsigma = 0.0628]	1651 [Rint = 0.1015, Rsigma = 0.0356]
Data/restraints/parameters	3453/1/237	5915/2/343	1651/0/101
Goodness-of-fit on F2	1.077	1.138	1.058
Final R indexes [I>=2σ (I)]	R1 = 0.0272, wR2 = 0.0688	R1 = 0.1145, wR2 = 0.2768	R1 = 0.0836, wR2 = 0.2146
Final R indexes [all data]	R1 = 0.0275, wR2 = 0.0690	R1 = 0.1479, wR2 = 0.3132	R1 = 0.0938, wR2 = 0.2271
Largest diff. peak/hole / e Å-3	0.76/-0.39	5.38/-0.67	1.43/-0.86
Flack parameter	0.040(3)		

Table E. *Crystal data and X–ray experimental data for complexes 2.08, 3.02 and 3.03.*

Identification code	**2.08 (exp 98a)**	**3.02 (kjk106a)**	**3.03 (kjk103b)**
Empirical formula	$C_8H_{26}Cl_3CoN_6O_6$	$C_8H_{20}CoIN_2O_4$	$C_{17.5}H_{43.5}Cl_4Co_2Mn_2N_4O_9$
Formula weight	467.63	394.09	823.60
Temperature/K	120.01(10)	120.00(10)	285.22(10)
Crystal system	triclinic	monoclinic	monoclinic
Space group	*P*-1	*P*21/*c*	*P*21/*c*
a/Å	13.5798(13)	8.0740(8)	11.9266(6)
b/Å	14.7189(12)	9.2453(10)	13.4376(4)
c/Å	15.3910(13)	17.4637(19)	11.8605(6)
α/°	77.760(7)	90	90
β/°	78.576(7)	91.580(8)	115.955(6)
γ/°	83.603(7)	90	90
Volume/Å3	2939.1(5)	1303.1(2)	1709.11(16)
Z	6	4	2
ρcalcg/cm3	1.585	2.009	1.600
μ/mm 1	10.966	28.975	16.616
F(000)	1452.0	776.0	841.0
Crystal size/mm3	0.4345 × 0.2133 × 0.1539	0.0998 × 0.0863 × 0.0254	0.235 × 0.1392 × 0.0404
Radiation	CuKα (λ = 1.54184)	CuKα (λ = 1.54184)	CuKα (λ = 1.54184)
2Θ range for data collection/°	6.658 to 153.986	10.134 to 153.542	8.246 to 134.14
Reflections collected	42586	5819	16466
Independent reflections	12257 [Rint = 0.0826, Rsigma = 0.0586]	2656 [Rint = 0.0604, Rsigma = 0.0659]	3023 [Rint = 0.0534, Rsigma = 0.0328]
Data/restraints/parameters	12257/14/770	2656/4/161	3023/0/204
Goodness-of-fit on F2	0.908	1.058	1.095
Final R indexes [I>=2σ (I)]	R1 = 0.0834, wR2 = 0.2624	R1 = 0.0927, wR2 = 0.2507	R1 = 0.0581, wR2 = 0.1839
Final R indexes [all data]	R1 = 0.1278, wR2 = 0.3294	R1 = 0.1033, wR2 = 0.2649	R1 = 0.0677, wR2 = 0.1933
Largest diff. peak/hole / e Å-3	1.95/-1.69	4.94/-2.29	1.26/-0.77

Table F. *Crystal data and X–ray experimental data for complexes 3.08, 3.09 and 3.10.*

Identification code	**3.08 (kjk111a)**	**3.09 (exp 107a)**	**3.10 (kjk105a)**
Empirical formula	$C_6H_{16}ClCoNO_3$	$C_{15}H_{35}Cl_4Co_2N_2O_{10}Zn_2$	$C_{13\cdot5}H_{34.5}Cl_4Co_2N_2O_{11}Zn_2$
Formula weight	244.58	793.85	791.33
Temperature/K	120.01(10)	120.01(10)	120.00(10)
Crystal system	orthorhombic	monoclinic	monoclinic
Space group	*Pnma*	*C*2/*c*	*P*21/*n*
a/Å	16.8974(2)	16.7832(15)	9.71438(14)
b/Å	6.75045(10)	10.0161(5)	10.43951(15)
c/Å	7.89318(13)	20.0251(16)	13.3043(2)
α/°	90	90	90
β/°	90	121.448(12)	96.6759(14)
γ/°	90	90	90
Volume/Å3	900.34(2)	2871.8(5)	1340.08(3)
Z	4	4	2
ρcalcg/cm3	1.804	1.836	1.961
μ/mm 1	17.449	14.639	15.710
F(000)	508.0	1604.0	799.0
Crystal size/mm3	0.2236 × 0.1859 × 0.0542	0.0991 × 0.0786 × 0.0591	0.1193 × 0.0696 × 0.046
Radiation	CuKα (λ = 1.54184)	CuKα (λ = 1.54184)	CuKα (λ = 1.54184)
2Θ range for data collection/°	10.47 to 172.446	10.356 to 148.926	10.706 to 134.16
Reflections collected	15674	6472	24622
Independent reflections	850 [Rint = 0.0615, Rsigma = 0.0182]	2916 [Rint = 0.0368, Rsigma = 0.0503]	2397 [Rint = 0.0442, Rsigma = 0.0181]
Data/restraints/parameters	850/0/86	2916/3/177	2397/2/181
Goodness-of-fit on F2	1.129	1.069	1.041
Final R indexes [I>=2σ (I)]	R1 = 0.0428, wR2 = 0.1157	R1 = 0.0567, wR2 = 0.1557	R1 = 0.0266, wR2 = 0.0698
Final R indexes [all data]	R1 = 0.0437, wR2 = 0.1167	R1 = 0.0684, wR2 = 0.1674	R1 = 0.0273, wR2 = 0.0705
Largest diff. peak/hole / e Å-3	1.03/-1.01	1.01/-0.46	0.55/-0.31

Table G. *Crystal data and X–ray experimental data for complexes 3.11, 3.12 and 3.13.*

Identification code	**3.11 (kjk109a)**	**3.12 (exp 65a)**	**3.13 (74a)**
Empirical formula	$C_{16}H_{25}CoF_{12}N_4O_{2.25}P_2$	$C_6H_{18}N_2O_2$	$C_{12}H_{30}CoI_3N_4O_4$
Formula weight	658.27	150.22	367.01
Temperature/K	120.01(10)	120.02(10)	120.01(10)
Crystal system	monoclinic	monoclinic	monoclinic
Space group	*C*2/*m*	*P*21/*n*	*P*21/*c*
a/Å	18.5973(10)	4.62754(10)	9.35502(12)
b/Å	13.2022(4)	5.52326(14)	10.36870(14)
c/Å	11.3282(6)	15.7209(5)	11.02739(15)
α/°	90	90	90
β/°	117.982(7)	95.608(3)	92.3146(12)
γ/°	90	90	90
Volume/Å3	2456.2(2)	399.889(18)	1068.78(2)
Z	4	2	2
ρcalcg/cm3	1.780	1.248	2.281
μ/mm 1	7.812	0.753	5.158
F(000)	1328.0	168.0	696.0
Crystal size/mm3	0.0762 × 0.0653 × 0.0446	0.5721 × 0.3144 × 0.2727	0.1639 × 0.0747 × 0.0353
Radiation	CuKα (λ = 1.54184)	CuKα (λ = 1.54184)	MoKα (λ = 0.71073)
2Θ range for data collection/°	8.594 to 148.992	11.312 to 133.87	5.868 to 60.802
Reflections collected	19771	6972	27187
Independent reflections	2422 [Rint = 0.0857, Rsigma = 0.0420]	716 [Rint = 0.0299, Rsigma = 0.0091]	3126 [Rint = 0.0441, Rsigma = 0.0255]
Data/restraints/parameters	2422/5/199	716/0/47	3126/0/113
Goodness-of-fit on F2	1.084	1.151	1.083
Final R indexes [I>=2σ (I)]	R1 = 0.0735, wR2 = 0.2076	R1 = 0.0469, wR2 = 0.1250	R1 = 0.0257, wR2 = 0.0488
Final R indexes [all data]	R1 = 0.0813, wR2 = 0.2166	R1 = 0.0476, wR2 = 0.1256	R1 = 0.0367, wR2 = 0.0526
Largest diff. peak/hole / e Å	1.01/-0.94	0.20/-0.72	1.34/-0.69

Table H. *Crystal data and X–ray experimental data for complexes 3.14, 3.17 and 3.22.*

Identification code	**3.14 (exp 86 a)**	**3.17 (exp 87a)**	**3.22 (exp 94a)**
Empirical formula	$C_{12}H_{24}CoI_5N_4O_4$	$C_{12}H_{33}Cl_7CoN_4O_3$	$C_{12}H_{28}Cl_8CoN_4Zn_{0.5}$
Formula weight	981.78	582.85	457.14
Temperature/K	120.00(11)	120.00(11)	284.94(10)
Crystal system	orthorhombic	monoclinic	triclinic
Space group	*Pbca*	*P*21/*c*	*P*-1
a/Å	9.7243(6)	15.7392(3)	8.4851(2)
b/Å	22.1877(7)	19.4645(4)	14.7967(5)
c/Å	23.8537(10)	7.44147(14)	18.5333(6)
α/°	90	90	85.403(3)
β/°	90	93.7731(19)	86.993(2)
γ/°	90	90	86.890(3)
Volume/Å3	5146.7(4)	2274.80(7)	2313.26(13)
Z	8	4	4
ρcalcg/cm3	2.534	1.7017	1.6406
μ/mm 1	52.524	13.661	14.884
F(000)	3584.0	1203.0	1104.9
Crystal size/mm3	0.1296 × 0.0647 × 0.0249	0.4698 × 0.0793 × 0.0656	0.2861 × 0.2077 × 0.1463
Radiation	CuKα (λ = 1.54184)	Cu Kα (λ = 1.54184)	Cu Kα (λ = 1.54184)
2Θ range for data collection/°	7.412 to 134.15	5.62 to 124.94	7.38 to 134.16
Reflections collected	10982	18949	19642
Independent reflections	4198 [Rint = 0.0864, Rsigma = 0.0803]	3631 [Rint = 0.0445, Rsigma = 0.0305]	8225 [Rint = 0.0449, Rsigma = 0.0438]
Data/restraints/parameters	4198/0/237	3631/4/282	8225/0/200
Goodness-of-fit on F2	1.084	1.041	2.463
Final R indexes [I>=2σ (I)]	R1 = 0.0869, wR2 = 0.2384	R1 = 0.0453, wR2 = 0.1268	R1 = 0.1016, wR2 = 0.3016
Final R indexes [all data]	R1 = 0.1185, wR2 = 0.2852	R1 = 0.0493, wR2 = 0.1309	R1 = 0.1048, wR2 = 0.3072
Largest diff. peak/hole / e Å	2.57/-2.61	1.20/-0.91	3.23/-3.43

Table I. *Crystal data and X–ray experimental data for complexes 3.15 and 3.16.*

Identification code	**3.15 (exp36a)**	**3.16 (EXP102a)**
Empirical formula	$C_{16}H_{36}Co_2I_6N_4O_6$	$C_{16.5}H_{32}Cl_4Co_2N_4O_{7.5}Zn_2$
Formula weight	1259.75	796.86
Temperature/K	120.01(10)	120.01(10)
Crystal system	monoclinic	orthorhombic
Space group	*C*2/*c*	*Pbca*
a/Å	26.6352(18)	15.1651(8)
b/Å	10.7268(3)	9.7152(5)
c/Å	14.3346(9)	19.6368(12)
α/°	90	90
β/°	129.336(11)	90
γ/°	90	90
Volume/Å3	3167.7(5)	2893.1(3)
Z	4	4
ρcalcg/cm3	2.642	1.829
μ/mm 1	54.422	14.492
F(000)	2320.0	1604.0
Crystal size/mm3	0.1656 × 0.0339 × 0.0264	0.1894 × 0.1324 × 0.1049
Radiation	CuKα (λ = 1.54184)	CuKα (λ = 1.54184)
2Θ range for data collection/°	8.584 to 134.132	9.006 to 134.142
Reflections collected	7341	7823
Independent reflections	2821 [Rint = 0.0425, Rsigma = 0.0441]	2583 [Rint = 0.0410, Rsigma = 0.0356]
Data/restraints/parameters	2821/5/161	2583/0/181
Goodness-of-fit on F2	1.050	1.068
Final R indexes [I>=2σ (I)]	R1 = 0.0442, wR2 = 0.1187	R1 = 0.0658, wR2 = 0.1905
Final R indexes [all data]	R1 = 0.0500, wR2 = 0.1249	R1 = 0.0738, wR2 = 0.2001
Largest diff. peak/hole / e Å-3	2.14/-1.41	1.42/-0.59

Experimental

A suitable crystal were selected and mounted on a SuperNova, Dual, Cu/Mo at zero, Atlas diffractometer. The crystal was kept at 120.01(10) K during data collection. Using Olex2 [174], the structure was solved with the ShelXT [172] structure solution program using Direct Methods and refined with the ShelXL [173] refinement package using Least Squares minimisation.

References

References

[1] F. Bray, B. Moller. Predicting the future burden of cancer. Nat Rev Cancer. **2006**, *6*, 63.
[2] T. Finkel, M. Serrano, M. A. Blasco. The common biology of cancer and aging. Nature **2007**, *448*, 767.
[3] A. Jemal, F. Bray, M. M. Center, J. Ferlay, E. Ward, D. Forman. Global cancer statistics. Cancer J Clin. **2011**, *61*, 69.
[4] N. Ministry of Health. **2015,** (Ministry of Health, NZ: New Zealand).
[5] R. J. Duchovic, J. A. Vilensky. Mustard gas: its pre-World War I history. J Chem Educ. **2007**, *84*, 944.
[6] S. Ciavarella, A. Milano, F. Dammacco, F. Silvestris. Targeted therapies in cancer. BioDrugs. **2010**, *24*, 77.
[7] V. T. DeVita, Jr., E. Chu. A History of Cancer Chemotherapy. Cancer Res. **2008**, *68*, 8643.
[8] O. Rixe, T. Fojo. Is Cell Death a Critical End Point for Anticancer Therapies or Is Cytostasis Sufficient. Clin Cancer Reas. **2007**, *13*, 7280.
[9] R. Martinez, L. Chacon-Garcia. The search of DNA-intercalators as antitumoral drugs: What it worked and what did not work. Curr Med Chem. **2005**, *12*, 127.
[10] L. S. Lerman. Structural considerations in the interaction of deoxyribonucleic acid and acridines. J Mol Biol. **1961**, *3*, 18.
[11] M. J. Waring, C. Bailly. DNA recognition by intercalators and hybrid molecules. J Mol Recognit. **1994**, *7*, 109.
[12] C. Rehn, U. Pindur. Molecular modeling of intercalation complexes of antitumor active 9-aminoacridine and a [d,e]-anellated isoquinoline derivatives with base paired deoxytetranucleotides. Monatsh Chem. **1996**, *127*, 645.
[13] C. Rehn, U. Pindur. Model building and molecular mechanics calculations of mitoxantrone-deoxytetranucleotide complexes. Molecular foundations of DNA intercalation as cytostatic active principle. Monatsh Chem. **1996**, *127*, 631.
[14] M. Baginski, F. Fogolari, J. M. Briggs. Electrostatic and non-electrostatic contributions to the binding free energies of anthracycline antibiotics to DNA. J Mol Biol. **1997**, *274*, 253.
[15] X. Shui, M. E. Peek, L. A. Lipscomb, Q. Gao, C. Ogata, B. P. Roques, et al. Effects of cationic charge on three-dimensional structures of intercalative complexes: structure of a bis-intercalated DNA complex solved by MAD phasing. Curr Med Chem. **2000**, *7*, 59.
[16] H.-K. Liu, P. J. Sadler. Metal Complexes as DNA Intercalators. Acc Chem Res. **2011**, *44*, 349.
[17] J. Minford, Y. Pommier, J. Filipski, K. W. Kohn, D. Kerrigan, M. Mattern, et al. Isolation of intercalator-dependent protein-linked DNA strand cleavage activity from cell nuclei and identification as topoisomerase II. Biochemistry. **1986**, *25*, 9.
[18] L. F. Liu. DNA topoisomerase poisons as antitumor drugs. Annu Rev Biochem. **1989**, *58*, 351.
[19] K. W. Kohn, M. J. Waring, D. Glaubiger, C. A. Friedman. Intercalative binding of ellipticine to DNA. Cancer Res. **1975**, *35*, 71.
[20] D. R. Boer, A. Canals, M. Coll. DNA-binding drugs caught in action: the latest 3D pictures of drug-DNA complexes. Dalton Trans. **2009**, 399.

[21] M. Stiborova, J. Poljakova, E. Martinkova, L. Booek-Dohalska, T. Eckschlager, R. Kizek, et al. Ellipticine cytotoxicity to cancer cell lines a comparative study. Interdiscip Toxicol. **2011**, *4*, 98.
[22] L. D. Willimas, M. Egli, Q. Gao, A. Rich. **1992,** pp. 107-25 (Adenine Press).
[23] H. Song, J. T. Kaiser, J. K. Barton. Crystal structure of Δ-$[Ru(bpy)_2dppz]^{2+}$ bound to mismatched DNA reveals side-by-side metalloinsertion and intercalation. Nat Chem. **2012**, *4*, 615.
[24] I. M. Williams, H. L. Hancock, S. C. Haefner. **2015,** pp. 863 (J. Am Chem. Soc).
[25] B. A. D. Neto, A. A. M. Lapis. Recent developments in the chemistry of Deoxyribonucleic Acid (DNA) intercalators: principles, design, synthesis, applications and trends. Molecules. **2009**, *14*, 1725.
[26] H. Ihmels, K. Faulhaber, D. Vedaldi, F. Dall'Acqua, G. Viola. Intercalation of organic dye molecules into double-stranded DNA. Part 2: The annelated quinolizinium ion as a structural motif in DNA intercalators. Photochem Photobiol. **2005**, *81*, 1107.
[27] B. M. Zeglis, V. C. Pierre, J. K. Barton. Metallo-intercalators and metallo-insertors. Chem Commun (Cambridge, U K). **2007**, 4565.
[28] P. G. Baraldi, A. Bovero, F. Fruttarolo, D. Preti, M. A. Tabrizi, M. G. Pavani, et al. DNA minor groove binders as potential antitumor and antimicrobial agents. Med Res Rev. **2004**, *24*, 475.
[29] G. S. Khan, A. Shah, R. Zia ur, D. Barker. Chemistry of DNA minor groove binding agents. Journal of Photochemistry and Photobiology B: Biology. **2012**, *115*, 105.
[30] S. K. Kim, B. Nordén. Methyl green: A DNA major-groove binding drug. FEBS Lett. **1993**, *315*, 61.
[31] S. M. Nelson, L. R. Ferguson, W. A. Denny. Non-covalent ligand/DNA interactions: Minor groove binding agents. Mutat Res. **2007**, *623*, 24.
[32] S. Agarwal, D. K. Jangir, R. Mehrotra, N. Lohani, M. R. Rajeswari. A structural insight into major groove directed binding of nitrosourea derivative nimustine with DNA: a spectroscopic study. PLoS One. **2014**, *9*, 3.
[33] S. Puyo, D. Montaudon, P. Pourquier. From old alkylating agents to new minor groove binders. Cr, Rev Oncol Hemat. **2014**, *89*, 43.
[34] M. Esteller, J. Garcia-Foncillas, E. Andion, S. N. Goodman, O. F. Hidalgo, V. Vanaclocha, et al. Inactivation of the DNA-Repair Gene MGMT and the Clinical Response of Gliomas to Alkylating Agents. N Engl J Med. **2000**, *343*, 1350.
[35] T. Bando, H. Sugiyama. Synthesis and Biological Properties of Sequence-Specific DNA-Alkylating Pyrrole−Imidazole Polyamides. Acc Chem Res. **2006**, *39*, 935.
[36] E. A. Hillard, F. C. de Abreu, D. C. M. Ferreira, G. Jaouen, M. O. F. Goulart, C. Amatore. Electrochemical parameters and techniques in drug development, with an emphasis on quinones and related compounds. Chem Commun (Cambridge, U K). **2008**, 2612.
[37] S. R. Rajski, R. M. Williams. DNA Crosslinking Agents as Antitumor Drugs. Chem Rev (Washington, D C). **1998**, *98*, 2723.
[38] D. T. Beranek. Distribution of methyl and ethyl adducts following alkylation with monofunctional alkylating agents. Mutat Res, Fundam Mol Mech Mutagen. **1990**, *231*, 11.
[39] F. Drabløs, E. Feyzi, P. A. Aas, C. B. Vaagbø, B. Kavli, M. S. Bratlie, et al. Alkylation damage in DNA and RNA—repair mechanisms and medical significance. DNA Repair. **2004**, *3*, 1389.
[40] N. Shrivastav, D. Li, J. M. Essigmann. Chemical biology of mutagenesis and DNA repair: cellular responses to DNA alkylation. Carcinogenesis. **2010**, *31*, 59.

[41] K. V. Shooter, R. Howse, S. A. Shah, P. D. Lawley. Molecular basis for biological inactivation of nucleic acids. Action of methylating agents on the ribonucleic acid-containing bacteriophage R17. Biochem J. **1974**, *137*, 303.
[42] A. Pullman, B. Pullman. Molecular electrostatic potential of the nucleic acids. Q Rev Biophys. **1981**, *14*, 289.
[43] Y. Mishina, E. M. Duguid, C. He. Direct reversal of DNA alkylation damage. Chem Rev (Washington, DC, U S). **2006**, *106*, 215.
[44] K. S. Gates. An overview of chemical processes that damage cellular DNA: Spontaneous hydrolysis, alkylation, and reactions with radicals. Chem Res Toxicol. **2009**, *22*, 1747.
[45] G. Fronza, B. Gold. The biological effects of N3-methyladenine. J Cell Biochem. **2004**, *91*, 250.
[46] Y. Shao, X. Lu, K. Li, Z. Zhao, X. Shi, D. Jin, et al. Theoretical insight into photo-induced intramolecular electron transfer in heterodinuclear Ru(II)–Co(III) complexes. Mater Chem Phys.
[47] K. W. Kohn, A. Orr, P. M. O'Connor, L. J. Guziec, F. S. Guziec, Jr. Synthesis and DNA-sequence selectivity of a series of mono- and difunctional 9-aminoacridine nitrogen mustards. J Med Chem. **1994**, *37*, 67.
[48] L. F. Povirk, D. E. Shuker. DNA damage and mutagenesis induced by nitrogen mustards. Mutat Res Rev Mutat. **1994**, *318*, 205.
[49] J. Folkman, P. Hahnfeldt, L. Hlatky. Opinion: cancer: looking outside the genome. Nat Rev Mol Cell Biol. **2000**, *1*, 76.
[50] P. Vaupel. Tumor microenvironmental physiology and its implications for radiation oncology. Semin Radiat Oncol. **2004**, *14*, 198.
[51] J. M. Brown. Exploiting the hypoxic cancer cell: mechanisms and therapeutic strategies. Molecular Medicine Today. **2000**, *6*, 157.
[52] K. L. Bennewith, S. Dedhar. Targeting hypoxic tumour cells to overcome metastasis. BMC Cancer. **2011**, *11*, 504.
[53] T. W. Hambley. Physiological Targeting to Improve Anticancer Drug Selectivity. Aust J Chem. **2008**, *61*, 647.
[54] M. C. Brahimi-Horn, J. Chiche, J. Pouyssegur. Hypoxia and cancer. J Mol Med (Berl). **2007**, *85*, 1301.
[55] M. Höckel, P. Vaupel. Tumor Hypoxia: Definitions and Current Clinical, Biological, and Molecular Aspects. J Natl Cancer Inst. **2001**, *93*, 266.
[56] G. M. Anlezark, R. G. Melton, R. F. Sherwood, W. R. Wilson, W. A. Denny, B. D. Palmer, et al. Bioactivation of dinitrobenzamide mustards by an E. coli B nitroreductase. Biochem Pharmacol. **1995**, *50*, 609.
[57] H. H. Lee, B. D. Palmer, W. R. Wilson, W. A. Denny. Synthesis and hypoxia-selective cytotoxicity of a 2-nitroimidazole mustard. Bioorg Med Chem Lett. **1998**, *8*, 1741.
[58] J. Wang, K. A. Biedermann, J. M. Brown. Repair of DNA and chromosome breaks in cells exposed to SR 4233 under hypoxia or to ionizing radiation. Cancer Res. **1992**, *52*, 4473.
[59] J. M. Brown. The hypoxic cell: a target for selective cancer therapy-eighteenth Bruce F. Cain memorial award lecture. Cancer Res. **1999**, *59*, 5863.
[60] J. M. Brown, W. R. Wilson. Exploiting tumour hypoxia in cancer treatment. Nat Rev Cancer. **2004**, *4*, 437.
[61] J.-T. Hwang, M. M. Greenberg, T. Fuchs, K. S. Gates. Reaction of the Hypoxia-Selective Antitumor Agent Tirapazamine with a C1‘-Radical in Single-Stranded and

Double-Stranded DNA: The Drug and Its Metabolites Can Serve as Surrogates for Molecular Oxygen in Radical-Mediated DNA Damage Reactions. Biochemistry. **1999**, *38*, 14248.
[62] L. H. Patterson, S. R. McKeown. AQ4N: a new approach to hypoxia-activated cancer chemotherapy. Br J Cancer. **2000**, *83*, 1589.
[63] S. R. McKeown, M. V. Hejmadi, I. A. McIntyre, J. J. A. McAleer, L. H. Patterson. AQ4N: An alkylaminoanthraquinone N-oxide showing bioreductive potential and positive interaction with radiation in vivo. Br J Cancer. **1995**, *72*, 76.
[64] I. Tranoy-Opalinski, A. Fernandes, M. Thomas, J. P. Gesson, S. Papot. Design of self-immolative linkers for tumour-activated prodrug therapy. Anticancer Agents Med Chem. **2008**, *8*, 618.
[65] I. Ott, R. Gust. Non platinum metal complexes as anti-cancer drugs. Arch Pharm (Weinheim, Ger). **2007**, *340*, 117.
[66] D. C. Ware, B. D. Palmer, W. R. Wilson, W. A. Denny. Hypoxia-selective antitumor agents. 7. Metal complexes of aliphatic mustards as a new class of hypoxia-selective cytotoxins. Synthesis and evaluation of cobalt(III) complexes of bidentate mustards. J Med Chem. **1993**, *36*, 1839.
[67] M. C. Heffern, N. Yamamoto, R. J. Holbrook, A. L. Eckermann, T. J. Meade. Cobalt derivatives as promising therapeutic agents. Curr Opin Chem Biol. **2013**, *17*, 189.
[68] G. O. Ahn, K. J. Botting, A. V. Patterson, D. C. Ware, M. Tercel, W. R. Wilson. Radiolytic and cellular reduction of a novel hypoxia-activated cobalt(III) prodrug of a chloromethylbenzindoline DNA minor groove alkylator. Biochem Pharmacol. **2006**, *71*, 1683.
[69] C. Karnthaler-Benbakka, D. Groza, K. Kryeziu, V. Pichler, A. Roller, W. Berger, et al. Tumor-Targeting of EGFR Inhibitors by Hypoxia-Mediated Activation. Angew Chem, Int Ed. **2014**, *53*, 12930.
[70] G.-L. Lu, R. J. Stevenson, J. Y.-C. Chang, P. J. Brothers, D. C. Ware, W. R. Wilson, et al. N-alkylated cyclen cobalt(III) complexes of 1-(chloromethyl)-3-(5,6,7-trimethoxyindol-2-ylcarbonyl)-2,3-dihydro-1H-pyrrolo[3,2-f]quinolin-5-ol DNA alkylating agent as hypoxia-activated prodrugs. Bioorg Med Chem. **2011**, *19*, 4861.
[71] J. Y.-C. Chang, R. J. Stevenson, G.-L. Lu, P. J. Brothers, G. R. Clark, W. A. Denny, et al. Syntheses of 8-quinolinolatocobalt(III) complexes containing cyclen based auxiliary ligands as models for hypoxia-activated prodrugs. Dalton Trans. **2010**, *39*, 11535.
[72] J. Y.-C. Chang, G.-L. Lu, R. J. Stevenson, P. J. Brothers, G. R. Clark, K. J. Botting, et al. Cross-Bridged Cyclen or Cyclam Co(III) Complexes Containing Cytotoxic Ligands as Hypoxia-Activated Prodrugs. Inorg Chem. **2013**, *52*, 7688.
[73] D. C. Ware, P. J. Brothers, G. R. Clark, W. A. Denny, B. D. Palmer, W. R. Wilson. Synthesis, structures and hypoxia-selective cytotoxicity of cobalt(III) complexes containing tridentate amine and nitrogen mustard ligands. Dalton Trans. **2000**, 925.
[74] D. C. Ware, W. R. Wilson, W. A. Denny, C. E. F. Rickard. Design and synthesis of cobalt(III) nitrogen mustard complexes as hypoxia selective cytotoxins. The X-ray crystal structure of bis(3-chloropentane-2,4-dionato)(RS-N,N[prime or minute]-bis(2-chloroethyl)ethylenediamine)cobalt(III) perchlorate, $[Co(Clacac)_2(bce)]ClO_4$. J Chem Soc, Chem Commun. **1991**, 1171.
[75] W. R. Wilson. Tumor hypoxia: Challenges for cancer chemotherapy. **1992**, 87.
[76] D. C. Ware, H. R. Palmer, P. J. Brothers, C. E. F. Rickard, W. R. Wilson, W. A. Denny. Bis-tropolonato derivatives of cobalt(III) complexes of bidentate aliphatic nitrogen mustards as potential hypoxia-selective cytotoxins. J Inorg Biochem. **1997**, *68*, 215.
[77] W. A. Denny, B. D. Palmer, D. C. Ware, W. P. Wilson, *US5348977A* **1994**.

[78] D. C. Ware, H. R. Palmer, F. B. Pruijn, R. F. Anderson, P. J. Brothers, W. A. Denny, et al. Bis(dialkyl)dithiocarbamato cobalt(III) complexes of bidentate nitrogen mustards: synthesis, reduction chemistry and biological evaluation as hypoxia-selective cytotoxins. Anticancer Drug Des. **1998**, *13*, 81.
[79] A. M. Bond, R. L. Martin. Electrochemistry and redox behavior of transition metal dithiocarbamates. Coord Chem Rev. **1984**, *54*, 23.
[80] A. M. Bond, A. R. Hendrickson, R. L. Martin, J. E. Moir, D. R. Page. Electrochemical reduction and oxidation of cobalt(III) dithiocarbamates. Inorg Chem. **1983**, *22*, 3440.
[81] P. R. Craig, P. J. Brothers, G. R. Clark, W. R. Wilson, W. A. Denny, D. C. Ware. Anionic carbonato and oxalato cobalt(III) nitrogen mustard complexes. Dalton Trans. **2004**, 611.
[82] W. A. Denny. Prodrug strategies in cancer therapy. Eur J Med Chem. **2001**, *36*, 577.
[83] N. J. Farrer, L. Salassa, P. J. Sadler. Photoactivated chemotherapy (PACT): the potential of excited-state d-block metals in medicine. Dalton Trans. **2009**, 10690.
[84] M. Goeldner, R. Givens, Editors. *Dynamic Studies in Biology: Phototriggers, Photoswitches and Caged Biomolecules* **2005** (Wiley-VCH Verlag GmbH & Co. KGaA).
[85] E. C. Glazer. Light-Activated Metal Complexes that Covalently Modify DNA. Isr J Chem. **2013**, *53*, 391.
[86] K. Szacilowski, W. Macyk, A. Drzewiecka-Matuszek, M. Brindell, G. Stochel. Bioinorganic Photochemistry: Frontiers and Mechanisms. Chem Rev (Washington, DC, U S). **2005**, *105*, 2647.
[87] T. J. Dougherty, C. J. Gomer, B. W. Henderson, G. Jori, D. Kessel, M. Korbelik, et al. Photodynamic Therapy. J Natl Cancer Inst. **1998**, *90*, 889.
[88] V. Vanaclocha, N. S. Sapena, M. Sureda, I. Azinovic, J. Rebollo, R. Canon, et al. Photodynamic therapy in the treatment of brain tumours. A feasibility study. Photodiagnosis Photodyn Ther. **2015**.
[89] O. J. Stacey, S. J. A. Pope. New avenues in the design and potential application of metal complexes for photodynamic therapy. RSC Adv. **2013**, *3*, 25550.
[90] S. A. Mackowiak, A. Schmidt, V. Weiss, C. Argyo, C. von Schirnding, T. Bein, et al. Targeted Drug Delivery in Cancer Cells with Red-Light Photoactivated Mesoporous Silica Nanoparticles. Nano Lett. **2013**, *13*, 2576.
[91] J. Kasparkova, F. S. Mackay, V. Brabec, P. J. Sadler. Formation of platinated GG cross-links on DNA by photoactivation of a platinum(IV) azide complex. JBIC, J Biol Inorg Chem. **2003**, *8*, 741.
[92] F. S. Mackay, J. A. Woods, P. Heringova, J. Kasparkova, A. M. Pizarro, S. A. Moggach, et al. A potent cytotoxic photoactivated platinum complex. Proc Natl Acad Sci U S A. **2007**, *104*, 20743.
[93] N. A. Kratochwil, M. Zabel, K.-J. Range, P. J. Bednarski. Synthesis and X-ray Crystal Structure of *trans,cis*-[$Pt(OAc)_2I_2$(en)]: A Novel Type of Cisplatin Analog That Can Be Photolyzed by Visible Light to DNA-Binding and Cytotoxic Species in Vitro. J Med Chem. **1996**, *39*, 2499.
[94] F. R. Hartley. *The Chemistry of Platinum and Palladium with Particular Reference to Complexes of the Elements* **1973** (Halsted).
[95] D. Loganathan, H. Morrison. 'Photocisplatin' reagents. Curr Opin Drug Discovery Dev. **2005**, *8*, 478.
[96] N. A. Kratochwil, P. J. Bednarski, H. Mrozek, A. Vogler, J. K. Nagle. Photolysis of an iodoplatinum(IV) diamine complex to cytotoxic species by visible light. Anti-Cancer Drug Des. **1996**, *11*, 155.

[97] A. W. Adamson. Recent advances in the photochemistry of coordination compounds. Pure Appl Chem. **1970**, *24*, 451.
[98] V. Balzani, V. Carassiti. *Photochemistry of Coordination Compounds* **1970** (Academic).
[99] V. Balzani. New aspects of photochemistry of coordination compounds. Chim Ind (Milan). **1973**, *55*, 711.
[100] A. Gandioso, E. Shaili, A. Massaguer, G. Artigas, A. Gonzalez-Canto, J. A. Woods, et al. An integrin-targeted photoactivatable Pt(IV) complex as a selective anticancer pro-drug: synthesis and photoactivation studies. Chem Commun (Cambridge, U K). **2015**, *51*, 9169.
[101] J. L. Van der Veer, A. R. Peters, J. Reedijk. Reaction products from platinum(IV) amine compounds and 5'-GMP are mainly bis(5'-GMP)platinum(II) amine adducts. J Inorg Biochem. **1986**, *26*, 137.
[102] M. D. Hall, H. R. Mellor, R. Callaghan, T. W. Hambley. Basis for Design and Development of Platinum(IV) Anticancer Complexes. J Med Chem. **2007**, *50*, 3403.
[103] D. G. Whitten, P. P. Zarnegar. Photochemistry of ruthenium complexes. Ligand isomerization via orbitally different excited states. J Am Chem Soc. **1971**, *93*, 3776.
[104] L. De Cola, F. Barigelletti, M. J. Cook. Photophysical properties and photochemical behavior of ruthenium(II) complexes containing the 2,2'-bipyridine and 4,4'-diphenyl-2,2'-bipyridine ligands. Helv Chim Acta. **1988**, *71*, 733.
[105] E. Tfouni, F. Gorzoni Doro, A. J. Gomes, R. Santana da Silva, G. Metzker, P. Graca Zanichelli Benini, et al. Immobilized ruthenium complexes and aspects of their reactivity. Coord Chem Rev. **2010**, *254*, 355.
[106] E. Tfouni, F. G. Doro, L. E. Figueiredo, J. C. M. Pereira, G. Metzker, D. W. Franco. Tailoring NO donors metallopharmaceuticals: ruthenium nitrosyl ammines and aliphatic tetraazamacrocycles. Curr Med Chem. **2010**, *17*, 3643.
[107] N. Komatsuzaki, Y. Himeda, T. Hirose, H. Sugihara, K. Kasuga. Synthesis and Photochemical Properties of Ruthenium-Cobalt and Ruthenium-Nickel Dinuclear Complexes. Bull Chem Soc Jpn. **1999**, *72*, 725.
[108] W. R. Browne, N. M. O'Boyle, J. J. McGarvey, J. G. Vos. Elucidating excited state electronic structure and intercomponent interactions in multicomponent and supramolecular systems. Chem Soc Rev. **2005**, *34*, 641.
[109] X. Song, Y. Lei, S. Van Wallendal, M. W. Perkovic, D. C. Jackman, J. F. Endicott, et al. Photoinduced electron-transfer processes involving covalently linked ruthenium and cobalt polypyridyl complexes: comparison of electronic coupling in bridged and nonbridged ruthenium and cobalt complexes. J Phys Chem. **1993**, *97*, 3225.
[110] R. J. Holbrook, D. J. Weinberg, M. D. Peterson, E. A. Weiss, T. J. Meade. Light-Activated Protein Inhibition through Photoinduced Electron Transfer of a Ruthenium(II)-Cobalt(III) Bimetallic Complex. J Am Chem Soc. **2015**, *137*, 3379.
[111] S. K. S. Zawacky, H. Taube. Intramolecular electron-transfer reactions in bridged binuclear ruthenium(II)-cobalt(III) molecules. J Am Chem Soc. **1981**, *103*, 3379.
[112] A. Yoshimura, K. Nozaki, N. Ikeda, T. Ohno. Temperature-Dependent Rates of Electron Transfers and Intersystem Crossing on the Laser Excitation of Ligand-Bridged Ru(II) and Co(III) Compounds. J Phys Chem. **1996**, *100*, 1630.
[113] A. M. Downward, R. T. Jane, M. I. J. Polson, E. G. Moore, R. M. Hartshorn. Heterodinuclear ruthenium(II)-cobalt(III) complexes as models for a new approach to selective cancer treatment. Dalton Trans. **2012**, *41*, 14425.

[114] A. M. Downward, E. G. Moore, R. M. Hartshorn. Photoinduced ligand release in a ruthenium(II)-cobalt(III) heterodinuclear system. Chem Commun (Cambridge, U K). **2011**, *47*, 7692.
[115] L. De Luca, G. Giacomelli, A. Porcheddu. An Efficient Route to Alkyl Chlorides from Alcohols Using the Complex TCT/DMF. Org Lett. **2002**, *4*, 553.
[116] W. E. Truce, G. H. Birum, E. T. McBee. Chlorination of Dimethyl Sulfide and Some of Its Derivatives with Sulfuryl Chloride and Thionyl Chloride1. J Am Chem Soc. **1952**, *74*, 3594.
[117] W. R. Wilson, J. W. Moselen, S. Cliffe, W. A. Denny, D. C. Ware. Exploiting tumor hypoxia through bioreductive release of diffusible cytotoxins: the cobalt(III)-nitrogen mustard complex SN 24771. Int J Radiat Oncol, Biol, Phys. **1994**, *29*, 323.
[118] B. D. Palmer, W. R. Wilson, S. M. Pullen, W. A. Denny. Hypoxia-selective antitumor agents. 3. Relationships between structure and cytotoxicity against cultured tumor cells for substituted N,N-bis(2-chloroethyl)anilines. J Med Chem. **1990**, *33*, 112.
[119] B. Boens, T.-S. Ouk, Y. Champavier, R. Zerrouki. Synthesis and Biological Evaluations of Click-Generated Nitrogen Mustards. Nucleosides, Nucleotides Nucleic Acids. **2015**, *34*, 500.
[120] A. M. Downward, M. I. J. Polson, W. R. Kerr, J. Kariyawasam, R. M. Hartshorn. Synthesis of a nitrogen mustard ligand on a cobalt(III) metal centre. Polyhedron. **2013**, *52*, 617.
[121] A. M. Downward. PhD **2010**, (University of Canterbury).
[122] B. Das Sarma, J. C. Bailar, Jr. Chemistry of metal complexes with polydentate ligands. Complexes of N-hydroxyethylethylenediamine. J Am Chem Soc. **1969**, *91*, 5958.
[123] W. C. Drinkard, H. F. Bauer, J. C. Bailar Jr. Reactivity of Organic Hydroxy Groups β to the Coördination Site in Cobalt (III) Complexes1. J Am Chem Soc. **1960**, *82*, 2992.
[124] J. C. Bailar, Jr., R. W. Auten. Stereochemistry of complex inorganic compounds. I. The Walden inversion as exhibited by diethylenediaminocobaltic compounds. J Am Chem Soc. **1934**, *56*, 774.
[125] N. E. Dixon, W. G. Jackson, M. J. Lancaster, G. A. Lawrance, A. M. Sargeson. Labile (trifluoromethanesulfonato)cobalt(III) amine complexes. Inorg Chem. **1981**, *20*, 470.
[126] P. Comba, N. J. Curtis, W. G. Jackson, A. M. Sargeson. Synthesis and substitution stereochemistry of trans-chlorobis(ethylenediamine)(trifluoromethanesulfonato)cobalt(III) trifluoromethanesulfonate. Aust J Chem. **1986**, *39*, 1297.
[127] X. Liang, X. Zou, L. Tan, W. Zhu. Study on nucleic acid (CT-DNA and yeast tRNA) binding behaviors and cytotoxic properties of a heterodinuclear Ru(II)-Co(III) polypyridyl complex. J Inorg Biochem. **2010**, *104*, 1259.
[128] S. Kawaguchi, H. Fujioka. Photoinduced isomerization of cis-dichlorobis(ethylenediamine)cobalt(III) chloride in methanol. Bull Chem Soc Jpn. **1967**, *40*, 802.
[129] B. Das Sarma, G. J. Tennenhouse, J. C. Bailar, Jr. Complexes of N-(hydroxyethyl)ethylenediamine. J Am Chem Soc. **1968**, *90*, 1362.
[130] A. S. Kotovaya, S. G. Shova, Y. A. Simonov, A. P. Gulya. New complexes of tris(2-aminoethanolato-O,N)cobalt(III) sulfates: synthesis and structure. Russ J Coord Chem. **2009**, *35*, 226.
[131] B. Bosnich, C. K. Poon, M. L. Tobe. Complexes of cobalt(III) with a cyclic tetradentate secondary amine. Inorg Chem. **1965**, *4*, 1102.
[132] O. N. Stepanenko, V. V. Trachevskii, O. P. Kachorovskaya. Spectroscopic study of Cobalt(III) β-aminoethylate complexes. Russ J Coord Chem. **2001**, *27*, 175.

[133] H. Yoneda, S. Kida. Preparation and properties of trisethanolaminecobalt(III) complexes. J Am Chem Soc. **1960**, *82*, 2139.
[134] A. Clearfield, P. Rudolf, J. G. Wardeska. Cobalt(III) complexes of amino alcohols. Structural consequences of protonation. Inorg Chem. **1983**, *22*, 2713.
[135] T. W. G. Solomons. *Organic Chemistry, 11th Edition* **2013** (Wiley).
[136] S. K. Kondaveeti, S. Vaddypally, C. Lam, D. Hirai, N. Ni, R. J. Cava, et al. Synthesis, Structure, and Magnetic Studies of Manganese–Oxygen Clusters of Reduced Coordination Number, Featuring an Unchelated, 5-Coordinate Octanuclear Manganese Cluster with Water-Derived Oxo Ligands. Inorg Chem. **2012**, *51*, 10095.
[137] D. S. Nesterov, V. G. Makhankova, O. Y. Vassilyeva, V. N. Kokozay, L. A. Kovbasyuk, B. W. Skelton, et al. Assembling Novel Heterotrimetallic Cu/Co/Ni and Cu/Co/Cd Cores Supported by Diethanolamine Ligand in One-Pot Reactions of Zerovalent Copper with Metal Salts. Inorg Chem. **2004**, *43*, 7868.
[138] L. G. Reiter, Y. I. Pavlenko, O. A. Tarasenko. Polynuclear M(II)-Co(III) complexes with bridging oxygen atoms of deprotonated triethanolamine. Ukr Khim Zh (Russ Ed). **1997**, *63*, 106.
[139] O. N. Stepanenko, V. A. Potaskalov, V. V. Trachevskii. Heteroligand cobalt(III) complexes with triethanolamine and aminoacetic acid. Russ J Coord Chem. **2001**, *27*, 51.
[140] Y. Topcu, O. Andac, V. T. Yilmaz, W. T. A. Harrison. Synthesis, characterization and spectral studies of triethanolamine complexes of metal saccharinates. Crystal structures of $[Co(TEA)_2](SAC)_2$ and $[Cu_2(\mu\text{-}TEA)_2(SAC)_2]\cdot 2(CH_3OH)$. J Coord Chem. **2002**, *55*, 805.
[141] S. N. Adamovich, G. A. Kuznetsova, T. V. Kashik, E. V. Zykova, N. N. Chipanina, T. N. Aksamentova, et al. Complexes of triethanolamine with aroxyacetic acids and their metal salts as a new class of biologically active compounds. Russ J Gen Chem. **2008**, *78*, 1754.
[142] L. J. Boucher. Advanced Inorganic Chemistry, Fifth Edition (Cotton, Albert F.; Wilkinson, Geoffrey). J Chem Educ. **1989**, *66*, A104.
[143] M. K. Chmielewski, E. Tykarska, W. T. Markiewicz, W. Rypniewski. Engineering N-(2-pyridyl)aminoethyl alcohols as potential precursors of thermolabile protecting groups. New J Chem. **2012**, *36*, 603.
[144] J. Kira, P. Niedzialkowski, T. Ossowski. Potentiometric and AM1d studies of the equilibria between silver(I) and diaza-15-crown and diaza-18-crown ethers with nitrogen in different positions in various solvents. J Coord Chem. **2013**, *66*, 180.
[145] A. S. de Sousa, S. A. Reisinger, M. A. Fernandes, C. B. Perry, P. R. Varadwaj, H. M. Marques. The structure of N,N[prime or minute]-bis(2-hydroxyethyl)ethane-1,2-diamine and its complexes with Zn(ii) and Cd(ii). Dalton Trans. **2009**, 10208.
[146] L. Herrag, B. Hammouti, S. Elkadiri, A. Aouniti, C. Jama, H. Vezin, et al. Adsorption properties and inhibition of mild steel corrosion in hydrochloric solution by some newly synthesized diamine derivatives: Experimental and theoretical investigations. Corros Sci. **2010**, *52*, 3042.
[147] W. E. Ross, R. A. G. Ewig, K. W. Kohn. Differences between melphalan and nitrogen mustard in the formation and removal of DNA cross-links. Cancer Res. **1978**, *38*, 1502.
[148] M. R. Osborne, D. E. V. Wilman, P. D. Lawley. Alkylation of DNA by the Nitrogen Mustard Bis-(2-chloroethyl)methylamine. Chem Res Toxicol. **1995**, *8*, 316.
[149] J. Bjerrum, J. P. McReynolds, A. L. Oppegard, R. W. Parry. in *Inorg Synth* **2007**, pp. 216-221 (John Wiley & Sons, Inc.).
[150] I. Bernal, X. Xia, F. Somoza. The phenomenon of conglomerate crystallization. Part 44. The crystallization behavior of $[cis\text{-}Co(tren)(NO_2)_2]BF_4$ (I), [cis-

$Co(tren)(NO_2)_2]2SiF_6$ (II), the space group of [cis-$Co(tren)(NO_2)_2$]I (III) and some bio-inorganic observations derived from their stereochemistry. Inorg Chim Acta. **1996**, *252*, 391.
[151] B. P. Sullivan, D. J. Salmon, T. J. Meyer. Mixed phosphine 2,2'-bipyridine complexes of ruthenium. Inorg Chem. **1978**, *17*, 3334.
[152] M. K. Nazeeruddin, S. M. Zakeeruddin, R. Humphry-Baker, M. Jirousek, P. Liska, N. Vlachopoulos, et al. Acid-Base Equilibria of (2,2'-Bipyridyl-4,4'-dicarboxylic acid)ruthenium(II) Complexes and the Effect of Protonation on Charge-Transfer Sensitization of Nanocrystalline Titania. Inorg Chem. **1999**, *38*, 6298.
[153] B.-H. Ye, X.-M. Chen, T.-X. Zeng, L.-N. Ji. Syntheses, spectra and crystal structures of ruthenium(II) complexes with polypyridyl: [Ru(bipy)2(phen)](ClO4)2 · H2O and [Ru(bipy)2(Me-phen)](ClO4)2. Inorg Chim Acta. **1995**, *240*, 5.
[154] I. F. Eckhard, L. A. Summers. 4,5-Diazafluoren-9-one from the oxidation of 1,10-phenanthroline by permanganate. Aust J Chem. **1973**, *26*, 2727.
[155] M. R. Reddy, P. V. Reddy, Y. P. Kumar, A. Srishailam, N. Nambigari, S. Satyanarayana. Synthesis, Characterization, DNA Binding, Light Switch "On and Off", Docking Studies and Cytotoxicity, of Ruthenium(II) and Cobalt(III) Polypyridyl Complexes. J Fluoresc. **2014**, *24*, 803.
[156] M. Zhou, G. P. Robertson, J. Roovers. Comparative Study of Ruthenium(II) Tris(bipyridine) Derivatives for Electrochemiluminescence Application. Inorg Chem. **2005**, *44*, 8317.
[157] N. Garelli, P. Vierling. Synthesis of new amphiphilic perfluoroalkylated bipyridines. J Org Chem. **1992**, *57*, 3046.
[158] M. Braumueller, M. Schulz, D. Sorsche, M. Pfeffer, M. Schaub, J. Popp, et al. Synthesis and characterization of an immobilizable photochemical molecular device for H2-generation. Dalton Trans. **2015**, *44*, 5577.
[159] R. D. Schmidt, C. A. Kent, J. J. Concepcion, W. Lin, T. J. Meyer, M. D. E. Forbes. A little spin on the side: solvent and temperature dependent paramagnetism in $[RuII(bpy)_2(phendione)]^{2+}$. Dalton Trans. **2014**, *43*, 17729.
[160] J. C. Freys, J. M. Gardner, L. D'Amario, A. M. Brown, L. Hammarstroem. Ru-based donor-acceptor photosensitizer that retards charge recombination in a p-type dye-sensitized solar cell. Dalton Trans. **2012**, *41*, 13105.
[161] B. Gholamkhass, K. Koike, N. Negishi, H. Hori, T. Sano, K. Takeuchi. Adjacent- versus Remote-Site Electron Injection in TiO_2 Surfaces Modified with Binuclear Ruthenium Complexes. Inorg Chem. **2003**, *42*, 2919.
[162] O. Botezat, J. van Leusen, V. Ch. Kravtsov, A. Ellern, P. Kogerler, S. G. Baca. Iron(III) carboxylate/aminoalcohol coordination clusters with propeller-shaped Fe8 cores: approaching reasonable exchange energies. Dalton Trans. **2015**, *44*, 20753.
[163] C. Papatriantafyllopoulou, C. M. Kizas, M. J. Manos, A. Boudalis, Y. Sanakis, A. J. Tasiopoulos. Hexanuclear complexes from the use of a series of amino-alcohol ligands in Fe chemistry. Polyhedron. **2013**, *64*, 218.
[164] P. P. Pellegrini, J. R. Aldrich-Wright. Evidence for chiral discrimination of ruthenium(ii) polypyridyl complexes by DNA. Dalton Trans. **2003**, 176.
[165] W. K. Seok, J. M. Ran, N. Kim, H. Yun. Comparative Study of Ruthenium(II) and Ruthenium(III) Complexes with the Ligand dmbpy (dmbpy = 4,4'-Dimethyl-2,2'-bipyridine). Z Anorg Allg Chem. **2012**, *638*, 754.
[166] X.-H. Wu, S. Wang, Y. Guo, Z.-Y. Xie, L. Han, Z.-H. Jiang. Enhanced energy conversion efficiency of La^{3+}-modified nanoporous TiO_2 electrode sensitized with a ruthenium complex. Chin J Chem. **2008**, *26*, 1939.

[167] C. Herrero, A. Quaranta, R.-A. Fallahpour, W. Leibl, A. Aukauloo. Identification of the Different Mechanisms of Activation of a $[RuII(tpy)(bpy)(OH_2)]^{2+}$ Catalyst by Modified Ruthenium Sensitizers in Supramolecular Complexes. J Phys Chem C. **2013**, *117*, 9605.
[168] H. Xia, Y. Zhu, D. Lu, M. Li, C. Zhang, B. Yang, et al. Ruthenium(II) Complexes with the Mixed Ligands 2,2'-Bipyridine and 4,4'-Dialkyl Ester-2,2'-bipyridine as Pure Red Dopants for a Single-Layer Electrophosphorescent Device. J Phys Chem B. **2006**, *110*, 18718.
[169] C. M. Elliott, E. J. Hershenhart. Electrochemical and spectral investigations of ring-substituted bipyridine complexes of ruthenium. J Am Chem Soc. **1982**, *104*, 7519.
[170] Y. Wang. *N*-(2-Pyridylmethanimidamido)pyridine-2-carboximidamide. Acta Crystallogr, Sect E: Struct Rep Online. **2010**, *66*, o1515.
[171] Q. Ma, Q. Wang. Detection of double analytes by employing new luminescent lanthanide probe. J Mol Struct. **2015**, *1099*, 204.
[172] G. M. Sheldrick. SHELXT - Integrated space-group and crystal-structure determination. Acta Crystallogr, Sect A: Found Adv. **2015**, *71*, 3.
[173] G. M. Sheldrick. Crystal structure refinement with SHELXL. Acta Crystallogr, Sect C: Struct Chem. **2015**, *71*, 3.
[174] O. V. Dolomanov, L. J. Bourhis, R. J. Gildea, J. A. K. Howard, H. Puschmann. OLEX2: a complete structure solution, refinement and analysis program. J Appl Crystallogr. **2009**, *42*, 339.